

## Towards environmentally friendly catalysts for alkyd coatings

**Citation for published version (APA):**

Oyman, Z. O. (2005). *Towards environmentally friendly catalysts for alkyd coatings*. [Phd Thesis 1 (Research TU/e / Graduation TU/e), Chemical Engineering and Chemistry]. Technische Universiteit Eindhoven.  
<https://doi.org/10.6100/IR584358>

**DOI:**

[10.6100/IR584358](https://doi.org/10.6100/IR584358)

**Document status and date:**

Published: 01/01/2005

**Document Version:**

Publisher's PDF, also known as Version of Record (includes final page, issue and volume numbers)

**Please check the document version of this publication:**

- A submitted manuscript is the version of the article upon submission and before peer-review. There can be important differences between the submitted version and the official published version of record. People interested in the research are advised to contact the author for the final version of the publication, or visit the DOI to the publisher's website.
- The final author version and the galley proof are versions of the publication after peer review.
- The final published version features the final layout of the paper including the volume, issue and page numbers.

[Link to publication](#)

**General rights**

Copyright and moral rights for the publications made accessible in the public portal are retained by the authors and/or other copyright owners and it is a condition of accessing publications that users recognise and abide by the legal requirements associated with these rights.

- Users may download and print one copy of any publication from the public portal for the purpose of private study or research.
- You may not further distribute the material or use it for any profit-making activity or commercial gain
- You may freely distribute the URL identifying the publication in the public portal.

If the publication is distributed under the terms of Article 25fa of the Dutch Copyright Act, indicated by the "Taverne" license above, please follow below link for the End User Agreement:

[www.tue.nl/taverne](http://www.tue.nl/taverne)

**Take down policy**

If you believe that this document breaches copyright please contact us at:

[openaccess@tue.nl](mailto:openaccess@tue.nl)

providing details and we will investigate your claim.

**Towards Environmentally Friendly Catalysts  
For Alkyd Coatings**

**Z. Okan Oyman**

CIP-DATA LIBRARY TECHNISCHE UNIVERSITEIT EINDHOVEN

Oyman, Zahit Okan

Towards environmentally friendly catalysts for alkyd coatings / by Zahit Okan Oyman. – Eindhoven : Technische Universiteit Eindhoven, 2005.

Proefschrift. – ISBN 90-386-2916-8

NUR 913

Trefwoorden: deklagen ; chemische drogers / alkydharsen / katalytische oxidatie / katalysatoren ; mangaan / emulsies / olie ; lijnzaadolie / vetzuren ; esters / vernetting / duurzame chemie

Subject headings: coating materials ; driers / alkyd resins / catalytic oxidation / catalysts ; manganese / emulsions / oil ; linseed oil / fatty acids ; esters / cross linking / sustainable chemistry

© 2005, Z. Okan, Oyman

Printed by Printpartners Ipskamp, Enschede, The Netherlands, 2005.

Cover design/ Jan-Willem Luiten, JLW producties.

An electronic copy of this thesis is available at the site of the Eindhoven University Library in PDF format ([w3.tue.nl/en/services/library](http://w3.tue.nl/en/services/library)).

# **Towards Environmentally Friendly Catalysts For Alkyd Coatings**

PROEFSCHRIFT

ter verkrijging van de graad van doctor aan de  
Technische Universiteit Eindhoven, op gezag van de  
Rector Magnificus, prof.dr. R.A. van Santen, voor een  
commissie aangewezen door het College voor  
Promoties in het openbaar te verdedigen  
op maandag 28 februari 2005 om 16.00 uur

door

Zahit Okan Oyman

geboren te Silifke, Turkije

Dit proefschrift is goedgekeurd door de promotoren:

prof.dr. R. van der Linde  
en  
prof.dr. R.A.T.M. van Benthem

Copromotor:  
dr. W. Ming

This research has been financially supported by Innovation Oriented Research Program (IOP) on Heavy Metals (IOP Zware Metalen No. IZW99241b), sponsored by Netherlands Ministry of Economic Affairs.

*Aileme...*

## TABLE OF CONTENTS

<b>Chapter 1</b>	
<b>Introduction</b>	<b>11</b>
1.1. Background	12
1.2. Oils and alkyd resins	13
1.2.1 Plant oils	13
1.2.2 Alkyd resins	15
1.3. Driers	16
1.4. Objectives and the scope of the thesis	19
1.5. References	21
<b>Chapter 2</b>	
<b>Literature survey of chemical drying of alkyd coatings</b>	<b>25</b>
2.1. Autoxidation	26
2.2. Model compounds for alkyd coatings	28
2.3. Oxidation of (Z,Z)- and (E,E)-3,6-nonadiene	30
2.4. Hydroperoxide formation during the oxidation of oleic acid/esters	30
2.5. Hydroperoxide formation during the oxidation of linoleic acid/esters	33
2.6. Hydroperoxide formation during the oxidation of linolenic acid/esters	35
2.7. Decomposition of hydroperoxides and formation of cross-links	35
2.8. Oxidation of conjugated fatty acid/esters without hydroperoxide formation	35
2.9. Photo-oxidation	36
2.10. Effect of metal-based catalysts on the oxidation reactions	37
2.10.1. Role of cobalt compounds in the oxidation reactions of alkyd coatings	38
2.10.2. Active species involved in the catalytic cycle	39
2.10.3. Promising alternatives to cobalt catalysts used for alkyd coatings	40
2.11. Oxidation reactions not leading to cross-links	42
2.11.1. Formation of alcohols	42
2.11.2. $\beta$ -scission	42
2.11.3. Russell termination	42
2.12. References	43
<b>Chapter 3</b>	
<b>Oxidation of model compounds catalyzed by cobalt-based catalysts</b>	<b>47</b>
<b>3a. Oxidation of model compound emulsions for alkyd coatings catalyzed by a cobalt-based catalyst</b>	<b>47</b>
3a.1. Introduction	48
3a.2. Experimental	49
3a.2.1. Materials	49
3a.2.2. Emulsion preparation	49
3a.2.3. Characterizations	50
3a.3. Oxidation of model compound emulsions during water evaporation	50

3a.4. Oxidation of model compound emulsions after water evaporation monitored by Raman spectroscopy	54
3a.4.1. Oxidation of methyl oleate (MO) emulsions	55
3a.4.2. Oxidation of ethyl linoleate (EL) emulsions	57
3a.4.3. Oxidation of methyl linolenate (MLn) emulsions	59
3a.5. Oxidation after water evaporation monitored by ATR-FTIR	61
3a.5.1. Oxidation of MO emulsions	61
3a.5.2. Oxidation of EL emulsions	62
3a.5.3. Oxidation of MLn emulsions	63
3a.6. The extent of double bonds during the oxidation of model compounds	63
3a.7. Oxidation kinetics of model compound emulsions	65
3a.8. Conclusions	66
<b>3b. Oxidation of drying oils containing non-conjugated and conjugated double bonds in the presence of a cobalt catalyst</b>	<b>69</b>
3b.1. Introduction	70
3b.2. Experimental	71
3b.2.1. Materials	71
3b.2.2. Oxygen uptake	71
3b.2.3. Peroxide value	71
3b.2.4. Characterization techniques	72
3b.3. Chemical composition of linseed oil and tung oil	72
3b.4. Oxygen uptake and peroxide evolution during the oxidation of oils	73
3b.5. Chemical changes during the oxidation of drying oils	75
3b.6. Discussion	79
3b.7. Conclusions	81
References	82
<b>Chapter 4</b>	
<b>Effect of a dinuclear manganese complex (MnMeTACN) and polyamines on the oxidation of ethyl linoleate</b>	<b>85</b>
4.1. Introduction	86
4.2. Experimental	88
4.2.1. Materials	88
4.2.2. Emulsion preparation	88
4.2.3. Characterization techniques and methods	89
4.2.4. EL oxidation in solution	90
4.3. Chemical changes during the oxidation of EL from emulsions	91
4.4. Role of polyamines during the EL oxidation from emulsions	94
4.5. Oligomerization during EL oxidation from emulsions	97
4.6. EL oxidation in methanol solution	99
4.6.1. Catalytic activity of MnMeTACN	99
4.6.1.1. Oxidation of non-purified EL	99
4.6.1.2. Oxidation of purified EL	101
4.6.2. Formation of volatile byproducts during EL oxidation	102
4.7. Catalytic role of MnMeTACN during the EL oxidation	106
4.8. Conclusions	108
4.9. References	108



<b>Chapter 5</b>	
<b>Effect of Mn(acac)<sub>3</sub> and 2,2'-Bipyridine on the oxidation of ethyl linoleate</b>	<b>111</b>
5.1. Introduction	112
5.2. Experimental	113
5.2.1. Materials	113
5.2.2. Instrumentation and procedures	113
5.2.2.1. Raman spectroscopy	113
5.2.2.2. Oxygen uptake	113
5.2.2.3. Peroxide value	113
5.2.2.4. Size exclusion chromatography	114
5.2.2.5. Head-space gas chromatography-mass spectrometry	114
5.3. Chemical changes during the oxidation of EL	114
5.4. Oxygen uptake and evolution of peroxides during EL oxidation	116
5.5. Oligomerization during EL oxidation	119
5.6. Formation of volatile byproducts during EL oxidation	121
5.7. Discussion	123
5.8. Conclusions	127
5.9. References	127
<b>Chapter 6</b>	
<b>Oxidation of <sup>13</sup>C-labeled ethyl linoleate (<sup>13</sup>C-EL) in the presence of various catalysts monitored by <sup>13</sup>C-NMR</b>	<b>129</b>
6.1. Introduction	130
6.2. Experimental	131
6.2.1. Materials	131
6.2.2. Oxidation of <sup>13</sup> C-EL	131
6.2.3. Quantitative <sup>13</sup> C-NMR	131
6.3. Advantage of using <sup>13</sup> C-EL	131
6.4. Experimental set-up for quantitative <sup>13</sup> C-NMR analysis	134
6.5. Quantitative analysis during the oxidation of <sup>13</sup> C-EL	135
6.5.1. Evolution of hydroperoxides (ROOH) and peroxy links (ROOR)	135
6.5.2. C=C variations during the oxidation of <sup>13</sup> C-EL	138
6.5.3. Variation of allylic groups during the oxidation of <sup>13</sup> C-EL	140
6.5.4. Other oxidation products	142
6.6. Conclusions	142
6.7. References	143
<b>Chapter 7</b>	
<b>Oxidative drying of real alkyd coatings catalyzed by MnMeTACN</b>	<b>145</b>
7.1. Introduction	146
7.2. Experimental	147
7.2.1. Materials	147
7.2.2. Confocal Raman Microscopy (CRM) for depth profiling	147
7.2.3. Preparation of paint systems	148
7.2.4. Drying tests of alkyd resin-based paints	148
7.3. Effect of various catalysts on the drying of alkyd resins followed by CRM	148

7.3.1. Depth profiling during the drying of solvent-borne alkyd resins	149
7.3.2. Depth profiling during the drying of water-borne alkyd resins	153
7.3.3. Implications from surface versus deep-layer drying	155
7.4. Drying tests and film properties of alkyd coatings	156
7.4.1. Drying of solvent-borne alkyd paints	156
7.4.2. Drying of water-borne alkyd paints	158
7.5. Conclusions	159
7.6. References	159
<b>Chapter 8</b>	
<b>Epilogue</b>	<b>161</b>
<b>Appendix</b>	<b>163</b>
<b>Summary</b>	<b>173</b>
<b>Samenvatting</b>	<b>175</b>
<b>Özet</b>	<b>179</b>
<b>Acknowledgments</b>	<b>181</b>
<b>Curriculum Vitae</b>	<b>183</b>

*Table of Contents*

---

## **Chapter 1**

### **Introduction**

#### **Summary**

*A general introduction of the research in this thesis is described. The importance of coatings and their components are firstly reviewed in general then drying oils and alkyd resins used as binder materials are introduced. The definition of driers and their effect during the oxidative drying of alkyd coatings is discussed. The Chapter concludes with objectives and the scope of the thesis.*

## 1.1. Background

Today, paints/coatings are used almost everywhere in our daily life; such as on buildings, furniture, cabinets, refrigerators, wires of electrical motors, cassettes and videotapes, compact discs, inside and outside of cans, ships, aircrafts, steel bridges, storage tanks, cars. They are used for decoration purposes as well as for protecting surfaces against various environmental effects like UV-radiation, chemical invasion, and mechanical stresses<sup>1</sup>.

Paints are composed of a complex mixture of chemical substances. A typical conventional paint consists of binder, pigment, solvent, and additives. The polymeric binder material with a large extent of variations is responsible for the formation of a continuous film that adheres to the substrate and holds the other substances together in the paint. One of the other major components of the paint is pigment, which provides color, improves the film strength, and hides substrates. Pigment also enhances the protection against corrosion and modifies flow and application properties<sup>2,3</sup>. Organic solvents are the transient component and used to provide flow and leveling during processing and application of paints. Additives such as thickeners, anti-skinning agents, anti-foaming agents, antioxidants, emulsifiers, UV-absorbers, fungicides, matting agents, and driers are added in very small amounts in the paint. Despite the small amount, each additive has specific influence on the final properties of the paint systems<sup>4</sup>.

Newly developed objects are nowadays designed with different shapes and are made from various materials that demand new ways of protection and application techniques with the desired performance. In addition, the trend of using solvent-based paints has been greatly shifted to the more environmentally friendly alternatives due to the more stringent legislations on environmental aspects, especially on the emission of volatile organic compounds (VOC). Because of these concerns and demands, new paint systems such as water-based coatings, radiation (*i.e.*, UV and electron beam) curable coatings, high solids coatings, and powder coatings have been developed in the last few decades. As fundamental understanding of the roles of the materials played in paint systems increases, control over the ingredients of the paints has been much more sophisticated. In order to obtain the desired performance and to meet legislation requirements, new proprietary binders, additives and cross-linking technologies such as hybrid binders (alkyd-acrylic latexes)<sup>5</sup>, organic-inorganic hybrid systems<sup>6-8</sup>, tailor made binders<sup>9</sup>, telechelic polymers<sup>10,11</sup>, novel hyperbranched resins<sup>12-</sup>

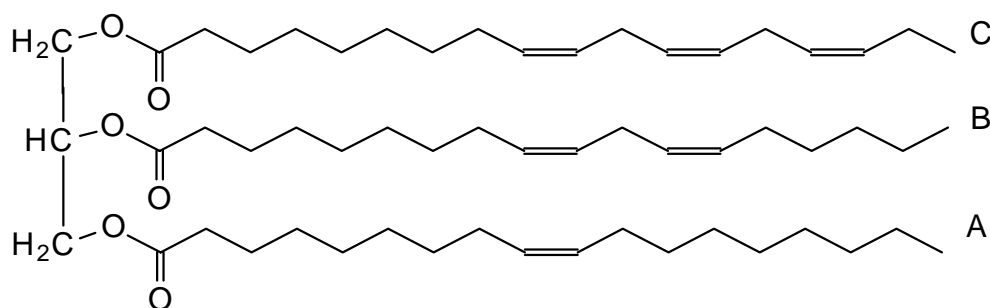
<sup>15</sup>, low surface energy films<sup>16-21</sup>, new chemistries for UV-curing systems<sup>22</sup>, chromate-free paints for metal substrates<sup>23</sup>, tin-free antifouling coatings<sup>24</sup>, and low temperature curing for powder coatings<sup>25-27</sup> have been extensively investigated.

New developments in the chemistry and technology in the coatings field however do not reduce the interest of conventional binder systems. Drying oils and alkyd resins for instance are one of the oldest and the cheapest coatings the chemical industry has been using<sup>28,29</sup>. Moreover, there is an increasing interest in using renewable resources, like plant oils for coating applications, because of the limited supply of petroleum-based products and their long-term effects to the environment. Although a few components (*i.e.*, polybasic acids and polyalcohols) of alkyd resins are still petroleum-based, it was recently shown that alkyd resins could be made from completely renewable resources<sup>30,31</sup>. Meanwhile, alkyd emulsions and high solid alkyd resins have shown a lot of success fulfilling the environmental demands. Moreover, life cycle analysis of alkyd emulsion paints showed less effect on the environment than those based on acrylic dispersions<sup>32</sup>. The possibility to obtain versatile, low cost, renewable, and low VOC emission products makes alkyd paints very attractive materials.

## 1.2. Oils and alkyd resins

### 1.2.1. Plant oils

Drying oils have been used in paints for many centuries<sup>1-3</sup>. They are obtained from plant seeds in the form of triglycerides. A typical structure is shown in Figure 1.1. Drying oils and fatty acids can be obtained naturally with a wide variety of unsaturation. This variation renders a wide range of film properties.



**Figure 1.1.** A typical structure of triglyceride containing (A) oleic, (B) linoleic (C) linolenic moieties<sup>33</sup>.

Plant oils are classified as drying oils that form solid films upon exposure to air, semi-drying oils that form tacky films, and non-drying oils that remain as low viscosity liquid even upon exposure to air. Oils can also be differentiated as non-conjugated and conjugated, depending on whether the double bonds are separated by methylene groups or not. Free fatty acids are also present, ~0.5-2% of the total weight, but it may be much higher, depending on the identity of the oil and how it is obtained<sup>34</sup>. A network is formed by a series of reactions of fatty acid chains of triglycerides upon exposure to air.

**Table 1.1.** Typical fatty acid compositions of selected drying oils<sup>33</sup>.

Oil	Fatty Acids (%)				
	Saturated <sup>(a)</sup>	Oleic(18:1)	Linoleic(18:2)	Linolenic(18:3)	Other
Linseed	10	22	16	52	
Safflower	11	13	75	1	
Soybean	15	25	51	9	
Sunflower, MN	13	26	61	Trace	
Sunflower, TX	11	51	38	Trace	
Tung	5	8	4	3	80 <sup>(b)</sup>
Tall oil fatty acid	8	46	41 <sup>(c)</sup>	3	2 <sup>(d)</sup>
Castor	3	7	3		87 <sup>(e)</sup>
Coconut	91	7	2		

*a: saturated fatty acids stearic (18:0), palmitic (16:0); coconut oil contains also (8:0, 10:0, 12:0, 14:0) groups.*

*b:  $\alpha$ -eleostearic acid (18:3 conjugated), c: linoleic plus geometric and conjugated isomers. d: Rosin. e: Ricinoleic acid (hydroxy fatty acid).*

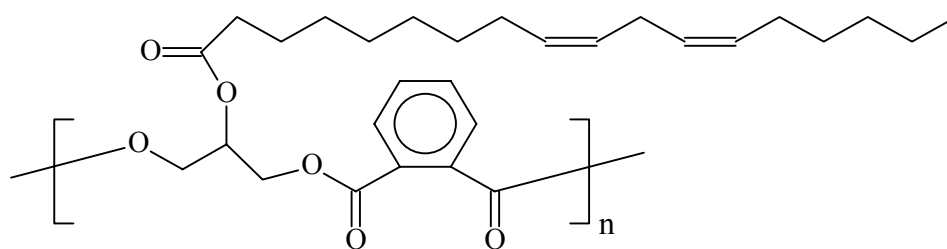
In general, the greater the unsaturation, the greater the drying ability and usually the darker the color of the coating is. The number of unsaturated double bonds in oils varies from stearic acid, which has no double bonds, to eleostearic, which has three conjugated double bonds. Natural oils contain varying amounts of these fatty acids. A few of them are listed in Table 1.1. Compositions alter slightly from year to year, depending on the natural conditions.

At the beginning of the 20<sup>th</sup> century drying oils were pre-polymerized to improve their drying properties. They were heated in the presence of air in a temperature range of 40 to 150 °C. If oil is heated with driers such as metal oxides, carbonates or acetates, then the oil is called “boiled oil”. If the oil is heated in the absence of driers, then the oil is called “blown oil”. Moreover “stand oils” were prepared by heating drying oils to higher temperatures from 270 to 310 °C in the absence of air and driers. However, from 1940s, the pre-polymerized drying oils could

not meet the increasing demand to obtain fast drying paints with excellent properties. This led to the partial replacement of drying oils with binders exhibiting specific properties such as alkyd resins. Most widely used drying oils for the production of air-drying alkyds are linseed oil, soybean oil, tung oil, safflower oil and dehydrated castor oil, and etc.<sup>35</sup>

### 1.2.2. Alkyd resins

Alkyd resins are based on polymeric resins developed in the 1920s<sup>35</sup>. The first alkyd resins sold commercially were made by General Electric Company under the name “Glyptal”. The term “alkyd” was joined from the “al” of alcohol, the “kyd” being representative of the last syllable of acid. The term “alkyd” today refers to polyesters modified with fatty acids.



**Figure 1.2.** Simplified structure of an alkyd made from phthalic acid anhydride, glycerol and linoleic acid.

Alkyds are prepared with the condensation polymerization of three types of monomers: polyalcohols (*i.e.*, glycerol, pentaerythritol, and etc.), polybasic acids (*i.e.*, phthalic anhydride, isophthalic acid, terephthalic acid, and etc.), and fatty acids or triglyceride oils (after alcoholysis) either by fusion or by solvent processes<sup>36</sup>. An example of a simplified alkyd resin structure made from phthalic acid, glycerol, and a fatty acid is shown in Figure 1.2.

Variations in the amounts and types of components give enormous varieties of resins with different properties. Alkyd resins are often classified with the oil type and the oil length<sup>37</sup>. The latter is defined as the weight percent of oil present in the resin. Alkyds can also be used in combination with other materials to obtain the desired properties. They are compatible with other materials because of the long chain fatty acid groups, which impart non-polar characteristics to the molecule, and promote



compatibility with other non-polar materials such as vinyl resins. Hydroxyl functional groups of the alkyd resin can react with acid and epoxy groups of the other resins. Moreover, unsaturated double bonds in the fatty acid chain can be used to graft conventional polymer chains such as polystyrene<sup>38</sup>.

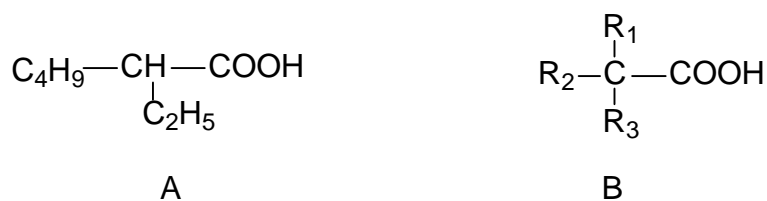
Though many newer resins have appeared, alkyd resins with such versatility still represent one of the most important and attractive binder systems produced for the coatings industry, particularly after the creation of the low VOC alkyd resins such as high solid alkyds and alkyd emulsions. They are produced up to 400.000 tons a year in Europe for decorative applications.

A lot of fundamental studies were performed in the past in order to understand mechanisms of the drying of oils and alkyd resins<sup>39,43</sup>. It is well known that chemical drying of alkyds occurs via the oxidation of the unsaturated fatty acid ester chains in the alkyd. These reactions are so slow that to accelerate them metal-based catalysts, known as “driers”, are the inevitable ingredients in typical alkyd paint formulations. A detailed review of the processes occurring during the chemical drying of alkyd resins is given in Chapter 2 of this thesis.

### 1.3. Driers

Driers (“siccatives” when in solution) are a group of metallic soaps or salts containing either alkaline-earth metals or heavy metals. They are added to air-drying coating systems to catalyze the oxidative cross-linking reactions<sup>39</sup>. Use of driers dates back to about 4000 years ago, when drying oils were already used. Various compounds of lead, iron, and manganese metals were used to form soaps with the fatty acids in the drying oils during the early Egyptian civilizations.

Already in the 1920s, a major advance in the drier technology was made with the preparation of metal naphthenates. The next step in the history of the drier development came with the introduction of “octoates” (monocarboxylic acids) such as 2-ethylhexanoic acids and neodecanoic acids (Figure 1.3). Most of the drier metals are in the oxidation state of +2 and usually dissolved in hydrocarbon solvents such as white spirit or aliphatic solvents.



**Figure 1.3.** (A) 2-ethylhexanoic acid, (B) neodecanoic acid, where the total carbon number in both compounds is 8. The metal salts of these are called “octoates”<sup>39</sup>.

Other synthetic acids such as isononanoic acid, heptanoic acid, and Versatic acid (Shell) also became available. They provide more uniform, paler color and have less odors than naphthenic acids.

Driers are often divided into two categories: primary and secondary driers. Primary driers promote rapid surface drying with limited through drying properties<sup>39</sup>. Also called “catalytic driers (surface or oxidative driers)”, cobalt, manganese, vanadium, cerium, and iron-based catalysts belong to this group. They promote oxygen uptake, peroxide formation and decomposition at ambient temperature. A complex oxidative or free radical chemistry is involved that leads to the formation of polymer-polymer cross-links (Chapter 2). During the reactions metal soaps, which exist in several oxidation states, undergo redox reactions. In addition Ali *et al.* recently examined organobismuth compounds as primary driers<sup>40</sup>. Secondary driers are also divided as “through” and “auxiliary driers”. They are not able to catalyze the oxidation reactions however they function to enhance the activity of primary driers. Lead, zirconium, aluminum, neodymium, bismuth, barium, and strontium are a few examples of “through driers”<sup>39</sup>. Metals in these compounds exist in a single oxidation state. “Auxiliary driers” are the other type of secondary driers such as calcium, potassium, lithium, and zinc-based compounds. Besides promoting the through drying by reacting with hydroxy and carboxyl groups in the binder and forming oxygen-metal-oxygen bridges, they improve the stability of the primary driers<sup>39</sup>. Most commonly used secondary driers are zirconium, calcium, barium, and zinc-based. Bismuth soaps combined with cobalt driers were found to shorten the drying times of alkyd paints particularly under adverse conditions such as low temperature and high humidity<sup>39,41</sup>. It has also been reported that combination of aluminum compounds with cobalt driers led to a significant increase in the hardness of the alkyd paint films<sup>42,43</sup>.

Turner *et al.* have proposed that their role is the formation of extra cross-links between alumina and polar groups in the oxidized alkyd network<sup>44</sup>.

Drier accelerators such as 2,2'-bipyridine (bpy) and 1,10-phenantroline are also extensively used. They function as chelating agents to form complexes with the primary driers. They apparently increase the activity of the metal towards decomposing peroxides<sup>39</sup>. Other chelating agents such as 2-aminomethylpyridine (amp) and 2-hydroxymethylpyridine (hmp) were recently reported in combination with manganese-based catalysts<sup>45</sup>. However, not many studies were demonstrated to understand their exact role during the metal-catalyzed oxidation of alkyd resins.

Currently, cobalt carboxylates (*e.g.*, Co(II)-2-ethylhexanoate) are the most effective, commercially available driers for alkyd coatings. Drying film often shows surface wrinkling and poor through drying when cobalt carboxylates are used alone. Cobalt-based driers are often used in combination with other metals such as zirconium and calcium to obtain uniform drying. However, precise mechanisms responsible for the catalyzing effect of the driers for alkyd resins or drying oils are not fully understood. Most of the published work has concentrated on the effects of the catalysts and not on the possible mechanisms. Nonetheless, a few possible mechanisms exist in the literature<sup>39</sup>. An overview of these mechanisms will be given in Chapter 2 of this thesis.

Moreover, traditional cobalt-based catalysts used in solvent-borne alkyd coatings are not suitable for alkyd emulsions. Water is one of the strongest complexing agents with  $\text{Co}^{3+}$ , leading to  $[\text{Co}(\text{H}_2\text{O})_6]^{3+}$  complex<sup>46</sup>. This complex has a weaker oxidation potential that results in the loss of catalytic capability for the cobalt catalysts. Proprietary ligands are used to pre-complex the drier to minimize this effect. Their main role is to obtain primary driers that are emulsifiable in water. They reduce the risk of the formation of the hydrate complexes and increase the catalytic activity. Nonetheless, higher drier concentrations are commonly used in water-based coatings.

Cobalt-based catalysts (*i.e.*, Cobalt carboxylates) were recently reported as potentially *carcinogenic* to tissues and lungs<sup>47-49</sup>. More stringent environmental legislations will lead to environmentally benign alternatives for the cobalt-based catalysts in the near future. Consequently, coatings containing cobalt catalysts are no longer accepted to hold the blue angel label in Germany.

#### 1.4. Objectives and the scope of the thesis

The objective of the study in this thesis is to obtain a more profound understanding of the catalytic activities and reaction mechanisms during the oxidative drying of alkyd coatings with the cobalt-based catalysts and with the potential environmentally-friendly catalysts.

Shining a light on the cobalt-catalyzed oxidation reactions will bring more insights on these reactions and provide the basis for further exploration of potential environmentally friendly catalytic systems for alkyd coatings. Promising manganese-based catalysts are investigated in this study, which may be applied as oxidation catalysts for both solvent-borne and water-borne alkyd coatings.

In order to examine the oxidation reactions, instead of alkyd resins, model compounds such as (m)ethyl esters of fatty acids and drying oils, are mostly used in this study. The outline of the thesis is given below.

**Chapter 2** gives an overview of the processes of the chemical drying of model compounds and/or alkyd resins. The generally recognized mechanism of oxidation reactions is described.

**Chapter 3** of the thesis describes our recently deeper understanding on the oxidation reactions of model compounds in the presence of cobalt-based catalysts. First, the oxidation reactions of model compounds in emulsions with varying number of non-conjugated unsaturated double bonds are studied in detail. Second, oxidation reactions of drying oils containing non-conjugated and conjugated double bonds are compared. The rationale of their mechanistic differences is examined.

In **Chapter 4**, an environmentally-friendly manganese complex containing 1,4,7-trimethyl-1,4,7-triazacyclononane (MnMeTACN) is described as a potential catalyst for water-borne and solvent-borne alkyd paints. The catalytic activity of MnMeTACN is demonstrated in model compound emulsions, especially in the presence of polyamines such as 1,1,4,7,10,10-hexamethyltriethylenetetramine, (HMTETA). The possible role of MnMeTACN and polyamines during the ethyl linoleate (EL) oxidation is discussed in detail.

The oxidation reactions of EL are examined in the presence of Mn(III)acetylacetonate (Mn(acac)<sub>3</sub>) as a promising catalyst and the possible role of 2,2'-bipyridine (bpy) ligand is discussed in **Chapter 5**.

In **Chapter 6**, the oxidation of <sup>13</sup>C-labeled ethyl linoleate, a model compound in the presence of cobalt- and manganese-based catalysts is investigated by <sup>13</sup>C-NMR

quantitatively. The reaction rate of the double bonds is examined. Moreover, major differences in the formation of hydroperoxides and peroxy links are studied.

The application of potential Mn-based catalysts in real coating formulations is demonstrated in **Chapter 7**. Depth profiling measurements were performed to examine the drying along the depth of the coatings.

The following papers have been published from the above investigations.

- Z.O. Oyman, W. Ming, R. van der Linde, Oxidation of model compound emulsions for alkyd paints under the influence of cobalt drier, *Prog. Org. Coat.* 48 (2003) 80.
- Z.O. Oyman, W. Ming, R. van der Linde, Drying of alkyd emulsions in the presence of a cobalt-free drier, Proceedings of XXVII FATIPEC Congress, Aix-en-Provence, France (2004) 607.
- Z.O. Oyman, W. Ming, R. van der Linde, A potential manganese-based catalyst for alkyd emulsion paints, *Polym. Prep.* 45(2) (2004) 213.
- Z.O. Oyman, W. Ming, F. Micciché, E. Oostveen, J. van Haveren, R. van der Linde, A promising environmentally friendly Mn-based catalyst for alkyd emulsion coatings, *Polymer* 45(22) (2004) 7431.
- Z.O. Oyman, W. Ming, R. van der Linde, R. van Gorkum, E. Bouwman, Effect of  $\text{Mn}(\text{acac})_3$  and its combination with 2,2'-bipyridine on the autoxidation and oligomerisation of ethyl linoleate, *Polymer* 46 (2005) in press.

The following manuscripts have been submitted for publication or in preparation.

- Z.O. Oyman, W. Ming, R. van der Linde, Jan ter Borg, Arno Schut, J.H. Bieleman, Oxidative drying of alkyd paints catalyzed by a dinuclear complex ( $\text{MnMeTACN}$ ), submitted to *Surf. Coat. Int.* (Dec. 2004).
- Z.O. Oyman, W. Ming, R. van der Linde, Oxidation of drying oils containing non-conjugated and conjugated double bonds in the presence of a cobalt catalyst, submitted to *Prog. Org. Coat.* (Jan. 2005).

- Z.O. Oyman, W. Ming, R. van der Linde, R. Hage, Catalytic activity of a dinuclear complex (MnMeTACN) on the oxidation of ethyl linoleate, in preparation.
- Z.O. Oyman, W. Ming, R. van der Linde, Oxidation of U-<sup>13</sup>C-18-labeled ethyl linoleate in the presence of various catalysts: A model study for the drying of alkyd coatings monitored by quantitative <sup>13</sup>C-NMR, in preparation.

## 1.5. References

1. Wicks Z.W., Jones F.N., Pappas S.P., “*Organic Coatings: Science and Technology Vol. I*”, John Wiley&Sons (1994).
2. Bentley J., Turner A., “*Introduction to Paint Chemistry and Principles of Paint technology*”, Chapman&Hall (1998).
3. Lambourne R., “*Paint and Surface Coatings*”, Ellis Horwood (1987).
4. Calbo L.J., “*Handbook of Coatings Additives*”, Marcel Dekker-Inc. (1987).
5. Hamersveld E.M.S., *Oil acrylic hybrid latexes*, thesis, TU Eindhoven (1999).
6. Posthumus W., *UV-curable acrylate metal oxide nanocomposites coatings*, thesis, TU Eindhoven (2004).
7. Frings S., *Organic-inorganic hybrid coatings: based on polyester resins and in situ formed silica*, thesis, TU Eindhoven (1999).
8. Soloukhin V.A., *Nanocomposite hybrid coatings on polycarbonate*, thesis, TU Eindhoven (2003).
9. Hillner K., Freytag A. E., *Farbe+ Lack* 106(4) (2000) 44.
10. Snijder A., *Telechelic polymers for moisture curable coatings by ATRP*, thesis, TU Eindhoven (2002).
11. Lima V., et al., *Polym. Prep.* 44(1) (2003) 812.
12. van Benthem R.A.T.M., et al., *Macromolecules* 34(11) (2001) 3559.
13. van Benthem R.A.T.M., et al., *Prog Org. Coat.* 40(1-4) (2000) 203.
14. Deng J., et al., *Eur. Polym. J.* 40(6) (2004) 1137.
15. Froehlich J., et al., *Polymer* 45(7) (2004) 2155.
16. Ming W., et al., *Macromolecules* 33(18) (2000) 6886.
17. van Ravenstein L., et al., *Macromolecules* 37(2) (2004) 408.
18. Ming W., et al., *Macromolecules* 35(18) (2002) 6920.
19. Patankar N.A., *Langmuir* 20(19) (2004) 8209.
20. Erbil Y.H., et al., *Science* 299(5611) (2003) 1377.

21. van de Grampel R.D., *Surfaces of fluorinated polymer systems*, thesis, TU Eindhoven (2002).
22. Decker C., et al., *Makrom. Chem.* 192(3) (1991) 507.
23. Bierwagen G., et al., *Polym. Pre.* 45(2) (2004) 144.
24. Omae I., *Chem. Rev.* 103(9) (2003) 3431.
25. Johansson M., et al., *J. Coat. Techn.* 72(906) (2000) 49.
26. Johansson M., et al., *J. Coat. Techn.* 70(884) (1998) 57.
27. Shah N.B., et al., *Paintindia* 53(8) (2003) 47.
28. Levesque C.L., “*Alkyd-Resin Technology*”, Offic. Digest, Federation of Paint and Varnish Production C. 278 (1948) 245.
29. Saatweber D., *Eur. Coat. J.* 11(20) (2003) 22.
30. Oostveen E.A., et al., (2003) WO 2003064477.
31. van Haveren J., et al., *Proceedings of XXVII FATIPEC congress*, Aix-en-Provence, France (2004) 907.
32. Beetsma J., Hofland A., *Surf. Coat. Int.* 81(10) (1998) 491.
33. Reference No. 1 of this Chapter, p. 259.
34. Tawn A.R.H., “*Solvents, Oils, Resins and Driers*” in paint technology manuals Vol. 2., Chapman and Hall, London (1969) 113.
35. Kienle R.H., *Ind. Eng. Chem.* 21 (1929) 349.
36. Martens C.R., “*Alkyd Resins*”, Reinhold Publishing Corp., New York (1961) 51.
37. Jones F.N., “*Alkyd Resins*”, in Ullman’s Encyclopedia of Industrial Chemistry, Vol. A1, 5<sup>th</sup> Ed., VCH, Weinheim (1985) 409.
38. Lin K.F., “*Alkyd Resins*”, in Kirk-Othmer Encyclopedia of Chemical Technology, Vol. 2, 4<sup>th</sup> Ed., Wiley, New York (1991) 53.
39. Bieleman J.H., “*Additives for Coatings*”, Wiley-VCH, Weinheim (2000) 203.
40. Ali M., et al., *App. Organomet. Chem.* 7 (1993) 137.
41. Middlemiss R.G., et al., *Am. Paint. Coat.* 78 (1993) 35.
42. Love D.J., *J. Oil. Col. Chem. Ass.* 60 (1977) 214.
43. Muizebelt W.J., et al., *J. Coat. Techn.* 70 (1998) 53.
44. Turner J.H.W., Womersley P., *Chem. Ind.* (1975) 203.
45. Wu J.-Z., et al., *Prog. Org. Coat.* 49 (2004) 103.
46. Hurley R., Buono F., *J. Coat. Techn.* 54(694) (1982) 55.
47. Lison D., et al., *Occup. Environ. Med.* 58 (2001) 619.

48. Bucher J.R., et al., *Toxicol. Sci.* 49 (1999) 56.
49. Danish EPA (2002). List of Dangerous Substances. 3<sup>rd</sup> June 2002. Available at <http://www.mst.dk>





## **Chapter 2**

### **Literature survey of chemical drying of alkyd coatings**

#### **Summary**

*General chemical drying processes of alkyd-based coatings are firstly reviewed in this Chapter. Then, the role of catalysts, represented by cobalt carboxylates, during the alkyd drying is described.*

## 2.1. Autoxidation

Autoxidation is a process in which atmospheric oxygen reacts spontaneously with unsaturated fatty acid chains of oils or alkyd resins. It has been the subject of many studies for biology<sup>1,2</sup>, food science<sup>3</sup>, pharmaceuticals<sup>4</sup>, cosmetics<sup>5</sup>, and coatings<sup>6</sup>. The autoxidation process is not desirable for the food industry; therefore, antioxidants are commonly added to prevent its occurrence<sup>7</sup>. In contrast, autoxidation is advantageous for the air-drying of alkyd coatings. It is generally accepted that as a result of a series of radical reactions (eqns. 2.1-2.19, where a substrate is represented as R-H), a cross-linked polymer network is formed that leads to an increase in the viscosity and eventually to the hardness of the paint films.

Autoxidation can be divided into 6 stages as shown below<sup>8</sup>.

1. Induction period
2. Initiation
3. Hydroperoxide formation
4. Hydroperoxide decomposition into free radicals
5. Cross-linking
6. Side reactions

*1. Induction period:* It exists due to the natural anti-oxidants such as  $\alpha$ - and  $\delta$ -tocopherols and  $\beta$ -carotene in the drying oils (therefore, also in alkyd coatings). The function of tocopherols (A-H, eqn. 2.1) is thought to be via radical trapping ( $P\bullet$  can be  $R\bullet$ ,  $RO\bullet$  or  $ROO\bullet$ , eqns. 2.1-2.2).



The rate of the H-atom abstraction (eqn. 2.1) was found to be around 4 times faster than the H-atom abstraction by  $ROO\bullet$  to create hydroperoxides ( $ROOH$ )<sup>7,9</sup>. Nevertheless, tocopherols also show pro-oxidant effect when they are used in excess amounts<sup>10</sup>.

$\beta$ -Carotene (C, also known as “pro-Vitamin A”) is proposed to have a different antioxidant function. It may inhibit oxidation reactions via quenching of singlet oxygen, as shown in eqn. 2.3<sup>11-13</sup>.



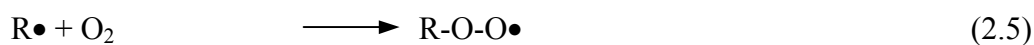
2. *Initiation*: This step is so far one of the least understood steps of autoxidation. The initiating free radical species is usually illustrated as  $X\bullet$  (eqn. 2.4). H-atom abstraction from the substrate (R-H) results in a  $R\bullet$ . As already indicated in eqns. 2.1-2.3, the initiation step can be inhibited by the presence of natural antioxidants, but it can also be accelerated by the addition of radical generating species such as peroxides<sup>14,15</sup> or metal-based catalysts (see section 2.10 of this Chapter).

#### *Initiation*



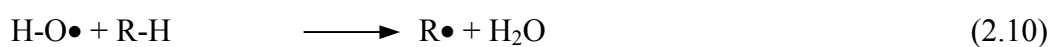
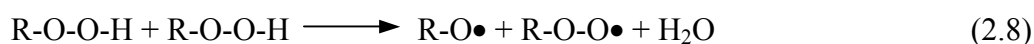
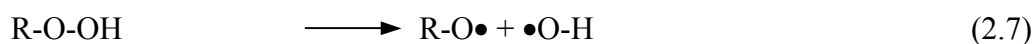
3. *Hydroperoxide formation*:  $R\bullet$  reacts instantaneously with the molecular oxygen to form  $ROO\bullet$  (eqn. 2.5).  $ROO\bullet$  forms hydroperoxides ( $ROOH$ , eqn. 2.6) by abstracting another H-atom from the substrate (R-H) such as an unsaturated fatty acid chain in the alkyd<sup>16</sup>.

#### *Formation of hydroperoxides*



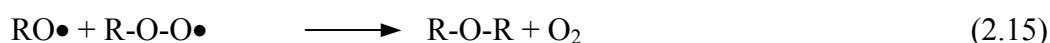
4. *Hydroperoxide decomposition and formation of free radicals*: In this stage, the formed  $ROOH$ s are decomposed and radicals such as  $R\bullet$ ,  $RO\bullet$ , and  $ROO\bullet$  are again created (eqns. 2.7-2.10)<sup>17,18</sup>. Reactions indicated in eqns. 2.7 and 2.8, are very slow processes. Catalysts, such as cobalt-based compounds, can catalyze this process, which is discussed in section 2.10 of this Chapter.

#### *Decomposition of hydroperoxides and formation of free radicals*



5. *Cross-linking*: The created radicals react by recombination to form cross-links. In this way, carbon-oxygen (C-O-C), carbon-oxygen-oxygen (C-O-O-C) and carbon-carbon (C-C) bonds are formed, which leads to an increase in the viscosity of the system (eqns. 2.11-2.16). Recombination reactions are not the only cross-linking mechanisms for alkyd-based coatings. Direct addition of radicals ( $R\bullet$ ,  $RO\bullet$ ,  $ROO\bullet$ ) to double bonds may also take place (eqns. 2.17-2.19)<sup>19,20</sup>.

*Formation of cross-links by recombination of radicals*



*Formation of cross-links by addition of radicals to carbon-carbon double bonds*

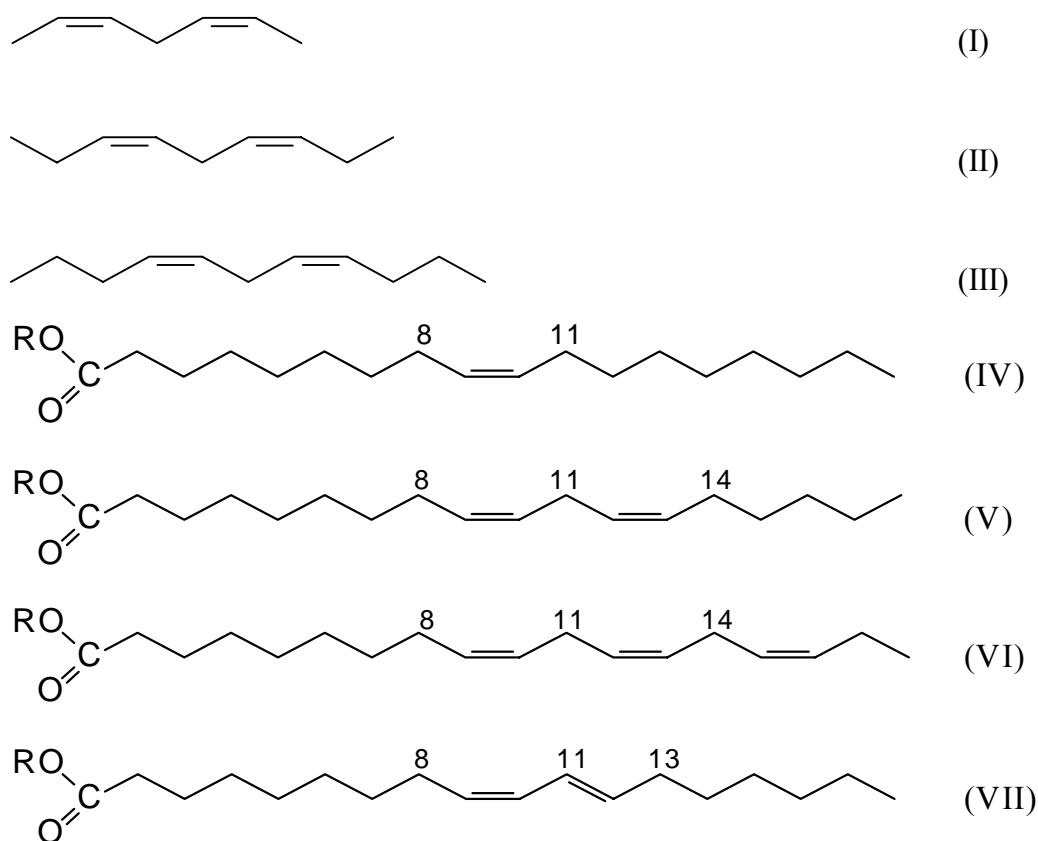


6. *Side reactions*: In addition to the formation of C-C, C-O-C, C-O-O-C cross-links, radical reactions, for instance  $\beta$ -scission (leading to volatile and non-volatile low molecular weight byproducts), and Russell termination (leading to the formation of ketones and alcohols) result in the formation of alcohols, aldehydes, ketones, carboxylic acids, epoxides, and endoperoxides. See section 2.11 for details.

## 2.2. Model compounds for alkyd coatings

The aforementioned oxidation reactions of alkyd coatings have been the subject of many studies. Chemical changes during the oxidation of alkyd resins were followed by analytical techniques such as FT-IR<sup>20-24</sup>, Raman spectroscopy<sup>25-27</sup>, and solid-state NMR<sup>28,29</sup>. Study on the oxidation reactions of alkyd resins is difficult due to their insolubility in organic solvents and the complex nature of the network formation. The chemistry of reactions involved in the oxidation is better studied by

using model compounds containing the same active sites, *i.e.*, allylic groups between two double bonds present in the fatty acid chain of alkyd resin. They can be dissolved in organic solvents so that oxidation reactions of these model compounds can be examined with many other analytical techniques such as solution NMR, mass spectrometry, liquid/gas chromatography, size exclusion chromatography, and etc. Drying oils such as linseed oil, tung oil, dehydrated castor oil, and safflower oil are commonly used as model compounds. In some cases, even drying oils create great characterization problems<sup>21</sup>.



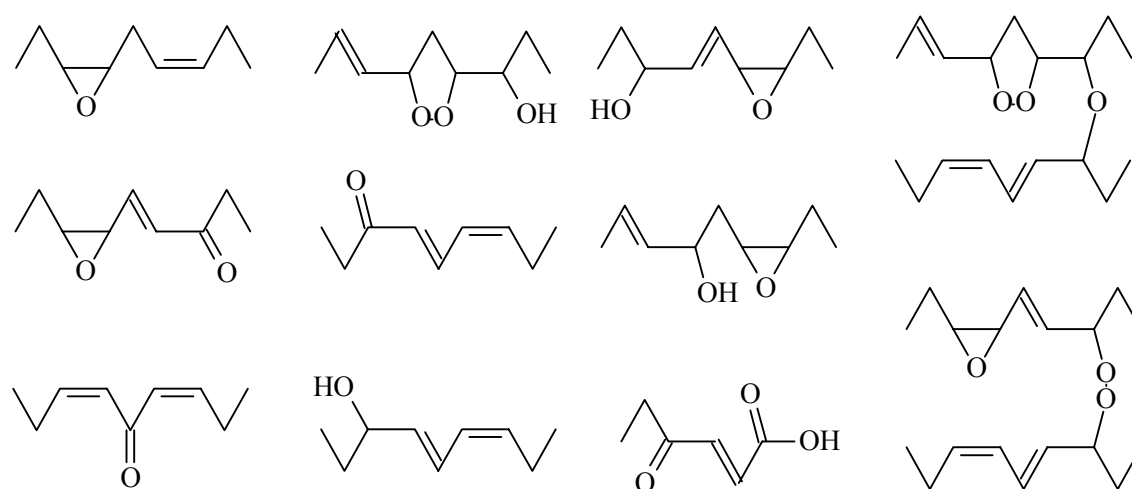
**Figure 2.1.** Chemical structures of the model compounds: *Z,Z*-2,5-heptadiene (I), *Z,Z*-3,6-nonadiene (II), *Z,Z*-4,7-undecadiene (III), esters of oleate (IV), linoleate (V), linolenate (VI), and conjugated linoleate (VII), where -R is either -CH<sub>3</sub> or -CH<sub>2</sub>CH<sub>3</sub>.

Consequently, model compounds having molar masses lower than drying oils are most commonly used, such as oleic acid<sup>30-32</sup>, linoleic acid<sup>33-36</sup>, conjugated linoleic acid<sup>21,37</sup>, and linolenic acid<sup>38</sup> or their (m)ethyl esters. Symmetrical model compounds even simpler than (m)ethyl esters are also used, such as 6,9-pentadecadiene<sup>39</sup>, 4,7 undecadiene<sup>40</sup>, 3,6-nonadiene<sup>41</sup>, and 2,5-heptadiene<sup>42</sup> to identify the primary and

secondary products of the oxidation reactions. Figure 2.1 illustrates the chemical structures of some model compounds examined in the oxidation reactions.

### 2.3. Oxidation of (Z,Z)- and (E,E)-3,6-nonadiene

Cobalt-catalyzed oxidation of (Z,Z or *cis-cis*)-3,6-nonadiene (structure given in Figure 2.1, II) and (E,E or *trans-trans*)-3,6-nonadiene was studied by Muizebelt *et al.*<sup>41</sup> These compounds were chosen due to their symmetry, which reduces the number of oxidation products compared to the non-symmetrical ones such as (m)ethyl linoleate. The most important oxidation products obtained in their study are shown in Figure 2.2.



**Figure 2.2.** Oxidation products of 3,6-nonadiene<sup>41</sup>.

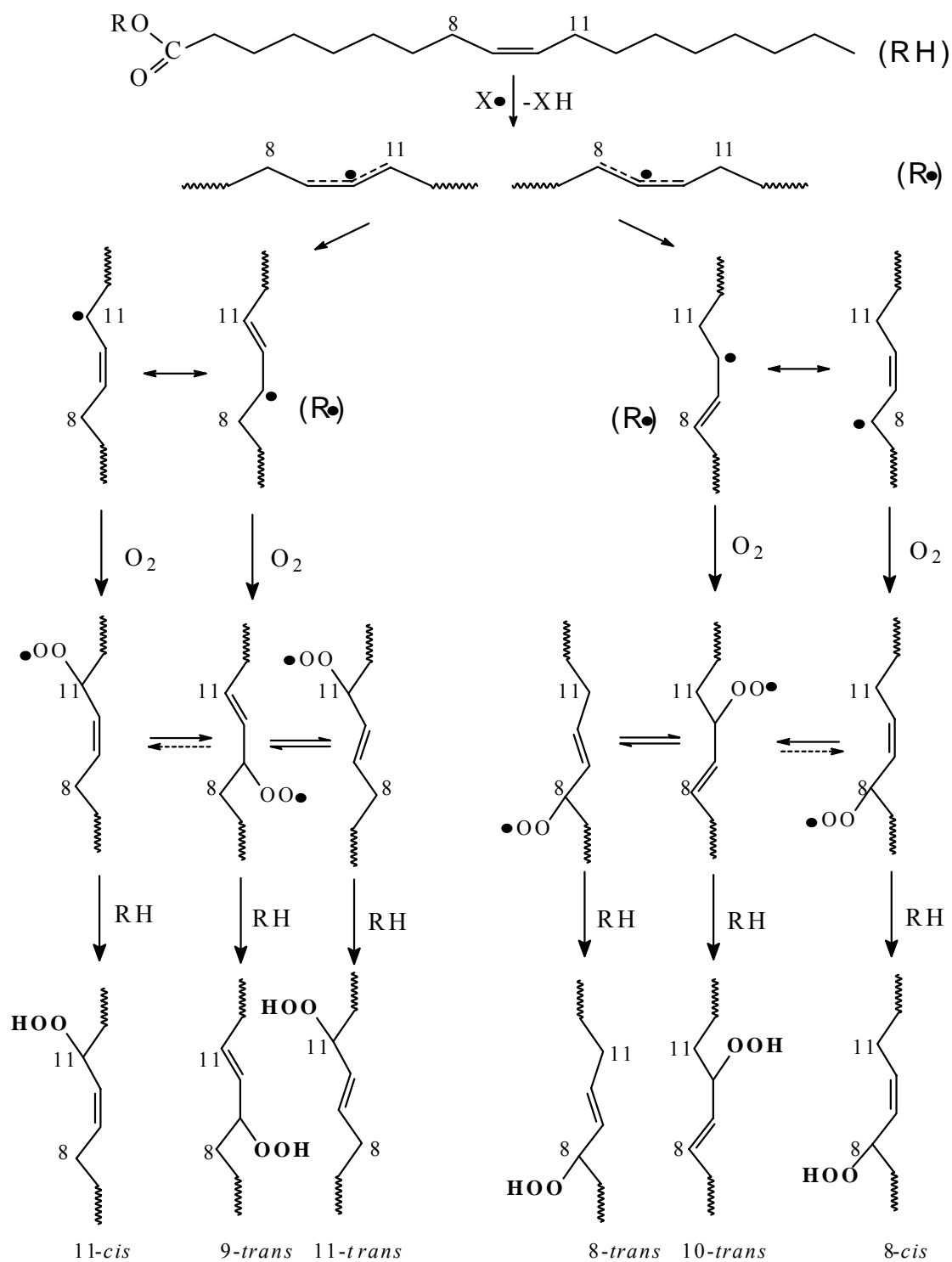
Other products such as endo-peroxides, epoxides, aldehydes, ketones, carboxylic acids, alcohols, and dimers were detected in the oxidation of 3,6-nonadiene. Formation of these products suggests that reactions follow three major reaction pathways: normal radical oxidation, photo-sensitized oxidation (reactions with  $^1\text{O}_2$ ) and epoxidation. Normal radical oxidation was concluded to be by far the most important mechanism while photo-sensitized oxidation and epoxidation were of minor importance<sup>41</sup>.

### 2.4. Hydroperoxide formation during the oxidation of oleic acid/esters.

Oxidation of oleic acid/esters was first studied in 1943<sup>43</sup>, and also later on it has been the subject of many studies<sup>30-32</sup>. Oxidation of oleate groups starts with the H-

atom abstraction from the mono-allylic sites (8-C-H or 11-C-H) that generates R•. The resonance structures include positions 8-C, 9-C, 10-C or 9-C, 10-C, 11-C in equal amounts<sup>32</sup>. The addition of oxygen molecules creates ROO•. It was reported that rearrangement of double bonds in the alkyl chain leads to 4 different hydroperoxide isomers. In 1977, Frankel *et al.*<sup>44</sup> showed that the amount of hydroperoxides formed at positions 8-C and 11-C is slightly higher than the amount of hydroperoxides at positions 9-C and 10-C. They also indicated that the oxidation temperature has an effect on the amount of different isomers. In 1984, these hydroperoxide isomers were quantified using GC-MS<sup>31</sup>. In a later study, Porter *et al.*<sup>45</sup> proposed another mechanism based on the oxidation products obtained, which is depicted in Figure 2.3. A peroxy radical rearrangement of 9-C-*trans* and 10-C-*trans* peroxy groups leads to the formation of 11-C-*trans* and 8-C-*trans* hydroperoxide isomers. In this respect, 6 different hydroperoxides were quantified during the oxidation of oleate at 30 °C. Product distribution was as follows: 11-C-*cis*, 13%; 9-C-*trans*, 21%; 11-C-*trans*, 16%; 8-C-*cis*, 13%; 10-C-*trans*, 21%; 8-C-*trans*, 16%.

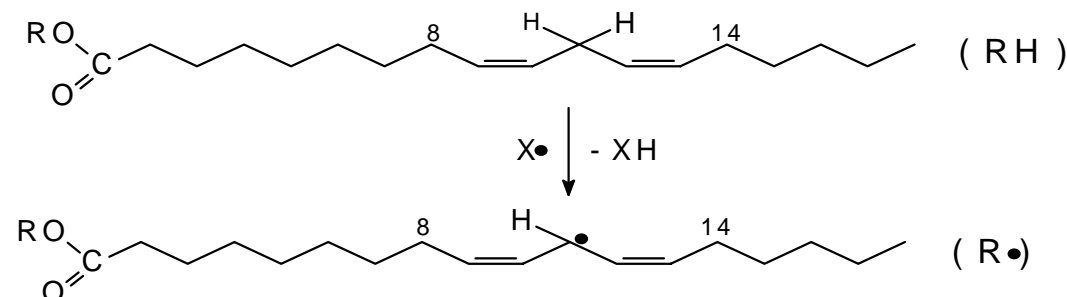




**Figure 2.3.** Proposed mechanism for oleate initiation and hydroperoxide formation, after Porter *et al.*<sup>45</sup>

## 2.5. Hydroperoxide formation during the oxidation of linoleic acids/esters

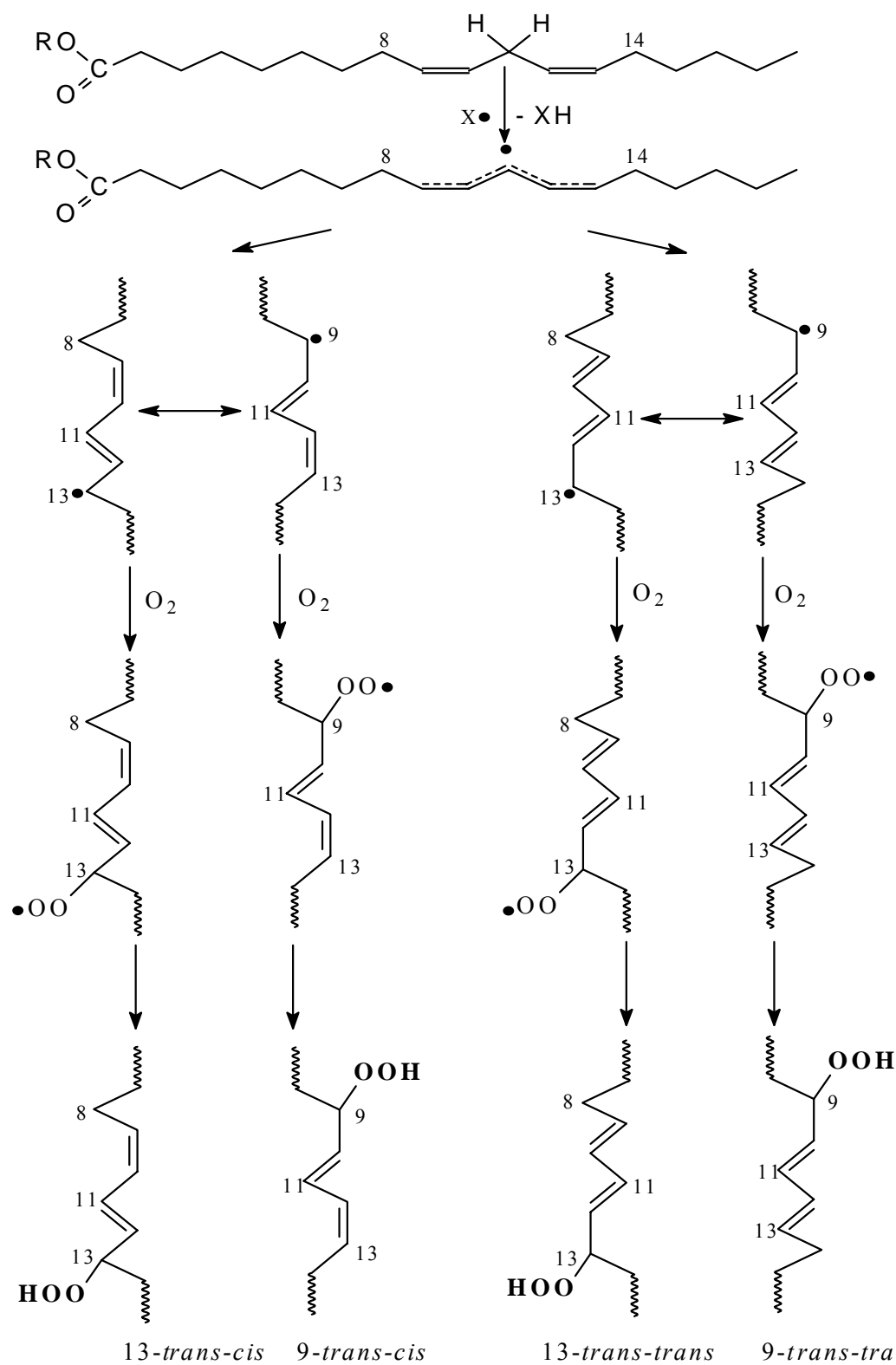
Oxidation of linoleic acids/esters has so far been the most extensively studied lipid system<sup>19-27,33-36</sup>. It is due to the fact that naturally occurring triglycerides used in the binders contain primarily the allylic group between two double bonds.



**Figure 2.4.** Formation of a radical in the linoleate ester oxidation.

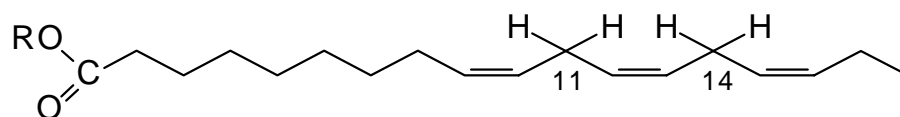
Initiation of linoleate oxidation is shown in Figure 2.4. H-atom is abstracted from double-allylic (11-C-H) position, which leads to the formation of a free radical ( $R\bullet$ ).  $R\bullet$  could also be created by mono-allylic H-atom abstraction at positions 8-C-H and 14-C-H. The latter however is energetically less favorable than the H atom abstraction from 11-C<sup>19</sup>. The generation of  $R\bullet$  at position 11-C leads to an instantaneous delocalization of this radical at positions 9-C, 10-C, 11-C, 12-C and 13-C, followed by the addition of oxygen molecules to form  $ROO\bullet$  and simultaneous formation of conjugated double bonds.  $ROO\bullet$  also abstracts H-atom from another 11-C position (RH) and hydroperoxide ( $ROOH$ ) is formed. The proposed mechanism of the formation of the primary products of the oxidation of linoleate is depicted in Figure 2.5. The 4 major hydroperoxides formed are: 9-C-*trans-cis*, 13-C-*trans-cis*, 9-C-*trans-trans*, 13-C-*trans-trans* hydroperoxides<sup>45</sup>. The product distribution was found to vary between 1 and 42% for these hydroperoxides<sup>36,45</sup>.

It should be noted that the final product distribution also depends on both the temperature and the concentration of linoleate (which acts as H-donor species). At higher temperatures, more *trans-trans* products are formed (thermodynamic control) and the increase in the amount of H-donor favors the formation of *trans-cis* species (kinetic control)<sup>45</sup>.



**Figure 2.5.** Proposed mechanisms for linoleate initiation and hydroperoxide formation, after Porter *et al.*<sup>45</sup>

## 2.6. Hydroperoxide formation during the oxidation of linolenic acids/esters



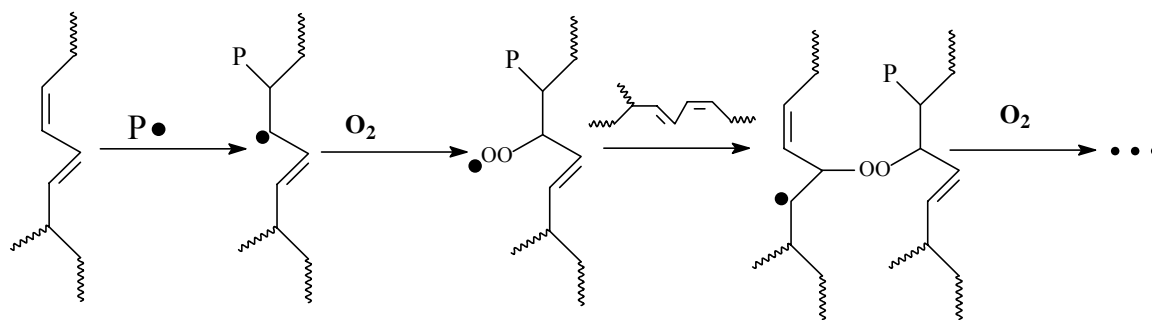
**Figure 2.6.** Structure of a linolenic acid ester.

As shown in Figure 2.6, linolenate group contains 4 double-allylic H-atoms at positions 11-C-H and 14-C-H that make the oxidation rate of linolenate about 3 times faster than linoleate<sup>46</sup>. Hydroperoxides are formed basically in the same way as for the linoleate group as described in the section 2.5 of this Chapter. During the oxidation of linolenate, however, 8 major hydroperoxide isomers were identified at positions 9-C, 12-C, 13-C, and 16-C with *cis-trans* and *trans-trans* isomers instead of 4<sup>46</sup>. It was found that 9-C and 16-C hydroperoxides were formed in larger quantities than the others<sup>47</sup>.

## 2.7. Decomposition of hydroperoxides and formation of cross-links

As shown in eqns. 2.7 and 2.8, the formed hydroperoxides are decomposed and radicals ( $R\bullet$ ,  $RO\bullet$ ,  $ROO\bullet$ ) are formed. Afterwards, termination occurs via recombination of the formed radicals and R-R, R-O-R, R-O-O-R cross-links are obtained, as already described in eqns. 2.11-2.16.

## 2.8. Oxidation of conjugated fatty acids/esters without hydroperoxide formation

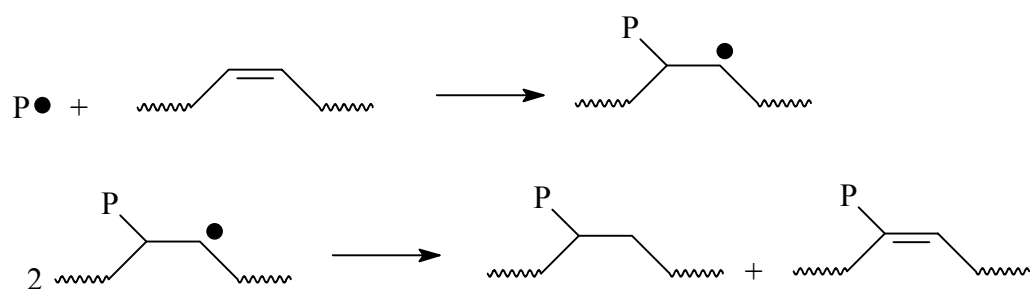


Radical addition to the double bonds

**Figure 2.7.** Oxidation pathway for conjugated double bonds and the formation of polyperoxides (where  $P\bullet = R\bullet, RO\bullet, ROO\bullet$ )<sup>19</sup>.

During the oxidation of fatty acids, the formed radicals ( $R\bullet$ ,  $RO\bullet$ ,  $ROO\bullet$ ) can also directly add to double bonds, conjugated ones in particular. Reactions between radicals and conjugated double bonds are proposed to occur with the loss of unsaturation (without any H-abstraction) in the unsaturated fatty acid chain, which leads to the formation of oligomeric free radicals, as already shown in eqns. 2.17-2.19 and also depicted in Figure 2.7.

As described by Muizebelt *et al.*<sup>48</sup>, these propagating radicals may be subsequently terminated by a disproportionation mechanism (Figure 2.8).



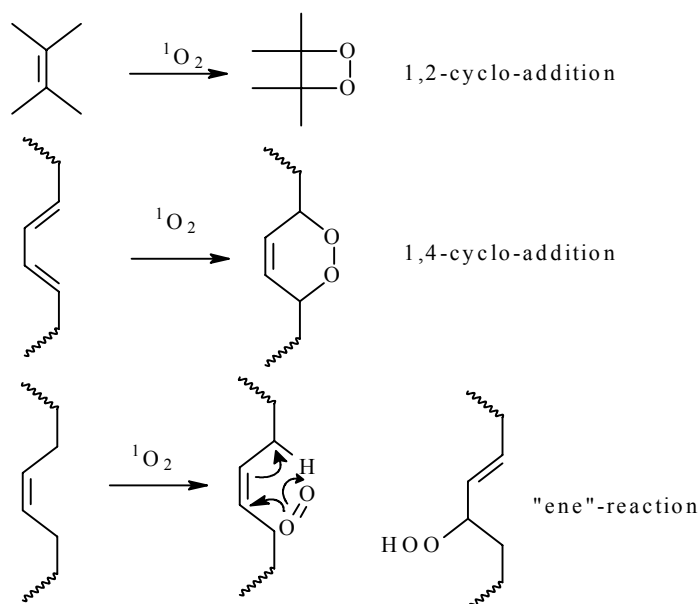
**Figure 2.8.** Termination of propagating radicals by disproportionation, where  $P\bullet = R\bullet$ ,  $RO\bullet$ , and  $ROO\bullet$ , after Muizebelt *et al.*<sup>48</sup>

## 2.9. Photo-oxidation

In the ground state molecular oxygen has a triplet spin configuration, whereas the double bonds of unsaturated fatty acids have a singlet configuration. The direct addition of oxygen molecules in the ground state to the double bonds of the fatty acids is therefore spin forbidden. Singlet oxygen can be formed from triplet oxygen by the help of photo-sensitizers. Upon absorption of light, a sensitizer is excited from the ground state to the excited singlet state. Once it is in the excited state, it reverts either to the ground state or to the triplet state. The latter process is more important in photo-oxidations. Sensitizers in the excited triplet state may relax to the ground state with the emission of light or may transfer their energy to oxygen. Then, oxygen is being excited to the singlet state, as shown in eqns. 2.20-2.22.



Muizebelt *et al.* reported the effect of photo-sensitizers such as rose bengal and methylene blue on the drying of alkyd coatings<sup>24</sup>. It was proposed that singlet oxygen could react with double bonds via “ene” reaction to form hydroperoxides (ROOH). Reactions between the double bonds and dioxygen in the singlet ground state may also form cyclic structures via either 1,2-cyclo-addition or 1,4-cyclo-addition to a substrate, as shown in Figure 2.9.



**Figure 2.9.** Reactions of singlet oxygen ( $^1\text{O}_2$ ) with substrate<sup>24</sup>.

## 2.10. Effect of metal-based catalysts on the oxidation reactions

Oxidation reactions of unsaturated fatty acids are slow processes without driers, particularly at 25 °C. For instance, it was reported that a thin film of a linseed oil forms a solid film in ~120 h while the same linseed oil in the presence of cobalt carboxylates forms a similar film within ~2.25 h<sup>49</sup>. As already described in Chapter 1 of this thesis, catalysts are a group of metal soaps or salts containing either alkaline-earth metals or heavy-metals. They are divided mainly into two groups: cobalt, manganese, vanadium, cerium, and iron-based catalysts belong to the first group known as “primary catalysts”, while lead, zirconium, aluminum, neodymium, bismuth, barium, strontium, calcium, potassium, lithium, and zinc-based catalysts belong to the second group known as “secondary catalysts”. The role played by secondary catalysts in the oxidation reactions is poorly understood and it is out of the scope of this thesis. In the next sections, we will describe the possible role of the primary catalysts played

in the oxidation of unsaturated fatty acids such as cobalt-based catalysts and other metal-based catalysts.

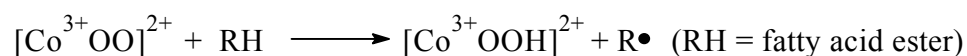
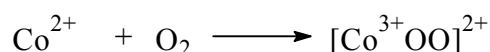
### **2.10.1. Role of cobalt compounds in the oxidation reactions of alkyd coatings**

Cobalt-based compounds are so far the most effective primary catalysts in the oxidation reactions at room temperature. Most of the studies have illustrated the effect of these catalysts during the oxidation of alkyds instead of the exact role played by them. Several mechanisms of the cobalt compounds in catalyzing the oxidation reactions were proposed<sup>8,50</sup>. Available information in the literature suggests that the role of the catalysts is:

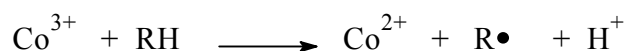
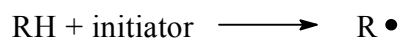
- a) Deactivation of natural antioxidants.
- b) Acceleration of oxygen absorption and peroxide formation by catalytic action.
- c) Cobalt catalysts react with molecular oxygen or hydroperoxides to form active species that catalyze oxidation reactions.
- d) Multivalent metals act as oxygen carriers because of their susceptibility to redox reactions. Hydroperoxides (ROOH) are decomposed into RO• and ROO• with this catalytic action.

Proposed reactions involved in the cobalt-catalyzed oxidation of alkyd-based coatings are depicted in Figure 2.10<sup>8</sup>.

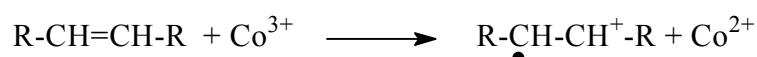
Oxygen absorption



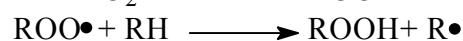
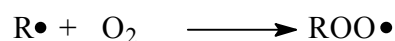
Hydrogen abstraction



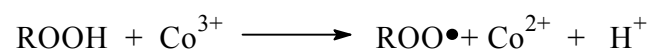
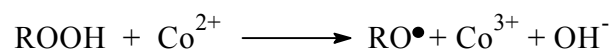
Direct activation of the double bond



Formation of hydroperoxides



Decomposition of hydroperoxides



**Figure 2.10.** Proposed reactions involved in the cobalt-catalyzed oxidation of alkyd-based coatings<sup>8</sup>.

### 2.10.2. Active species involved in the catalytic cycle

The exact active species responsible for catalyzing the oxidation reactions of alkyd paints is so far not exactly known. Based on X-ray crystallography results of cobalt carboxylates, a study suggested that unmodified cobalt carboxylates in hydrocarbon solvents would be polymeric<sup>51,52</sup>. Other studies proposed that cobalt carboxylates tend to form poly-nuclear complexes<sup>53,54</sup>. Lombard *et al.* proposed a dimeric cobalt(III) complex to take part in the catalyzed oxidation of  $\alpha$ -pinene<sup>55</sup>. Talsi *et al.* also suggested that cobalt compounds in benzene were present as the mixtures of dimers and trimers<sup>56</sup>.

Chavez *et al.* proposed the formation of ligand-Co(III)-OOR complexes as the active species during the oxidation reactions of hydrocarbons<sup>57</sup>. Depending on the ligand type, homolytic scission of either O-O or Co-O may create RO $\bullet$  and ROO $\bullet$ , which accelerate the oxidation reactions. No study so far, to the best of our



knowledge, is able to demonstrate the exact active species involved in the cobalt-catalyzed oxidations of alkyd resins.

### 2.10.3. Promising alternatives to cobalt catalysts used for alkyd paints

Due to the potential *carcinogenicity* of the cobalt compounds, their use in formulations of the next generation alkyd coatings should be avoided. Environmentally friendly and active catalysts should be developed, which can replace cobalt catalysts in both solvent-borne and water-borne alkyd coating formulations.

Pilemand *et al.* recently reported a study on the replacement of cobalt catalysts and methyl ethyl ketoxime for the oxidative drying systems<sup>58</sup>. Their basic conclusion was cobalt compounds are still catalytically more active than the alternatives they tested such as vanadium and manganese-based catalysts.

Steinert reported some new manganese-based alternatives to cobalt catalysts for the oxidatively drying ink systems<sup>59</sup>. He showed that manganese-based catalysts, especially in combination with organic accelerators, increase the rate of oxidation reactions.

Warzeska *et al.*<sup>60</sup> observed an increase in the catalytic activity of commercially available manganese-based catalysts when 2,2'-bipyridine (bpy) was *in-situ* added. Recently, other chelating agents such as 2-aminomethylpyridine (amp) and 2-hydroxymethylpyridine (hmp) were also reported in combination with a manganese complex based on 1,1,1,5,5,5-hexafluoroacetylacetonate for water-borne alkyd coatings<sup>61</sup>. The reason for using this complex was its good solubility in both water and the alkyd resin.

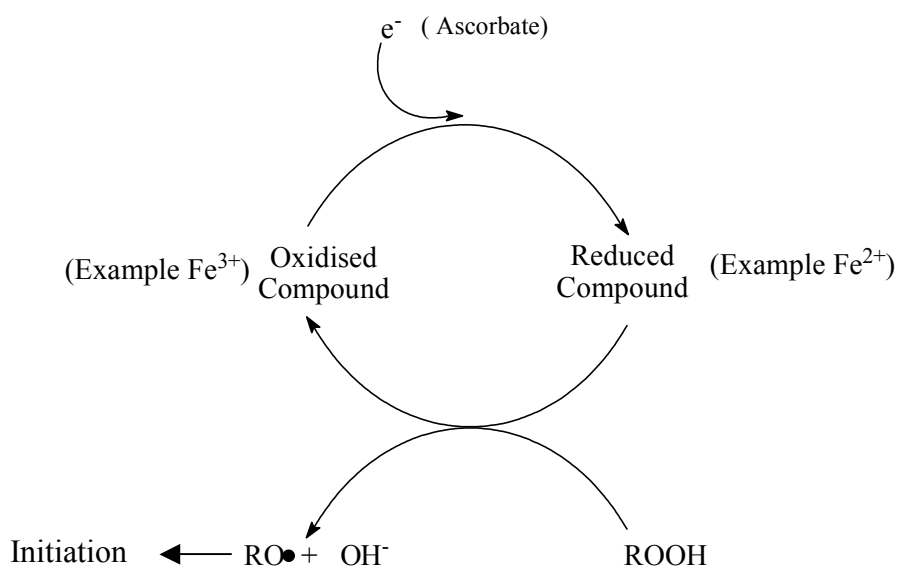
Vanadium salts such as vanadyl bis(acetylacetonate) were reported in a patent by Link *et al.* as primary catalysts<sup>62</sup>. The catalyst may contain polyvalent cations of vanadium or vanadium oxide and anionic organic acid groups. In the presence of their vanadium-based catalysts, fast-drying times (1.5-2.0 h) could be obtained with various alkyd resins.

In a more recent patent, Boomgaard *et al.* described new primary catalysts for alkyd-based coatings that are based on manganese, iron and other metal complexes substituted with salen-type ligands. Typical ligands consist of the condensation products of 1,2-diaminocyclohexane and 2-hydroxy-benzaldehyde with alkyl substituents. Their main action was to promote the solubility in apolar paint mixtures<sup>63</sup>.

Hage *et al.* demonstrated a dinuclear manganese-based complex (based on 1,4,7-trimethyl-1,4,7-triazacyclononane ligand) that was able to catalyze the oxidation of several alkenes to the corresponding epoxides<sup>66</sup>. More detailed description of this manganese-based complex and its effect on the oxidation of EL is given in Chapter 4 of this thesis.

Mn(III)acetylacetonate,  $\text{Mn}(\text{acac})_3$ , was recently reported as a promising primary catalyst for solvent-borne alkyd-based coatings by van Gorkum *et al.*<sup>64,65</sup> Oxidation of EL and the increasing catalytic effect of  $\text{Mn}(\text{acac})_3$  with the *in-situ* addition of 2,2'-bipyridine (bpy) was demonstrated. They proposed a radical initiation mechanism via a hydrogen atom abstraction pathway. In Chapter 5 of this thesis, we further examine the catalytic activity of  $\text{Mn}(\text{acac})_3$  and the effect of bpy *in-situ* added to  $\text{Mn}(\text{acac})_3$  on the oxidation reactions of EL.

Iron-based catalysts in combination with ascorbic acid (also known as "Vitamin C") or ascorbic acid-palmitate (its lipophilic derivative) were reported as primary catalysts in the oxidation of alkyd-based coatings<sup>69</sup>. Iron-based catalysts in combination with these reducing species are proposed to be good candidates for replacement of cobalt-based catalysts from alkyd coatings. A catalytic cycle involved in the hydroperoxide decomposition was proposed<sup>69</sup>, which is depicted in Figure 2.11.

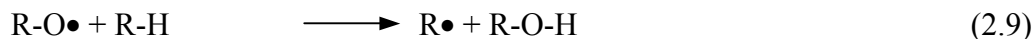


**Figure 2.11.** Proposed iron/ascorbate/peroxide catalytic cycle during the fatty acid oxidation<sup>69</sup>.

## 2.11. Oxidation reactions not leading to cross-links

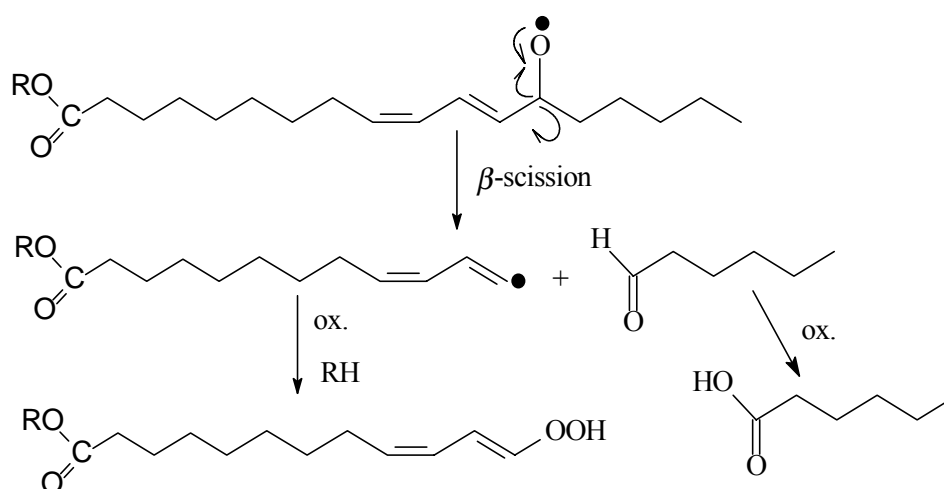
### 2.11.1. Formation of alcohols

Alcohols are formed from alkoxy (RO•) radicals, which react with fatty acid molecule, as shown below.



### 2.11.2. $\beta$ -scission

Studies on the reaction products of  $\beta$ -scission of unsaturated fatty acids showed that aldehydes, acids, alkanes<sup>41,70</sup>, CO<sub>2</sub><sup>71</sup> are formed. Most of the aldehydes produced from  $\beta$ -scission are volatile, such as propanal, pentanal, and hexanal, which give the characteristic sharp smell of alkyd-based coatings during drying. These reactions compete with the H-atom abstraction mechanisms depending on the temperature and the nature of H-donor species<sup>45</sup>. According to Muizebelt *et al.*<sup>19</sup>, during the cobalt-catalyzed oxidation of ethyl linoleate (EL), ~20% of the EL chains are cleaved by  $\beta$ -scission leading to the degradation of the material at ambient temperature. A tentative mechanism of the  $\beta$ -scission is depicted in Figure 2.12.

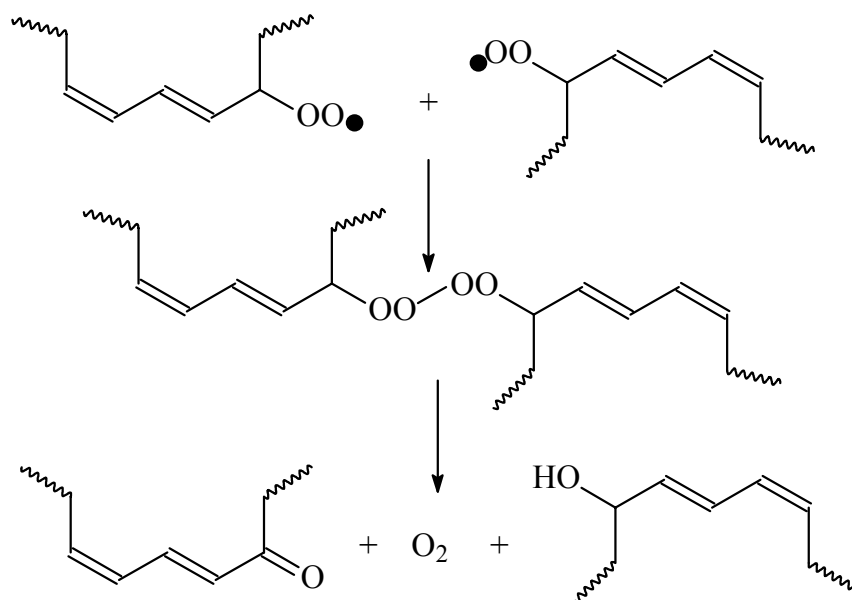


**Figure 2.12.**  $\beta$ -scission reactions during the oxidation of linoleate ester<sup>72,73</sup>.

### 2.11.3. Russell termination

Another reaction pathway for the peroxy radicals (ROO•) is *via* Russell termination mechanism<sup>74,75</sup>. As depicted in Figure 2.13, alcohols and ketones are mainly formed from ROO• intermediates. Similar to  $\beta$ -scission, Russell termination reactions compete with the ROOH formation (eqn. 2.6) and also cross-linking reactions (eqns. 2.14, 2.15 and 2.19). Alcohols and acids produced from these

reactions are thought to play an important role in through drying of the alkyd paints<sup>8</sup>. These groups may be coordinated with secondary driers and form additional cross-links in the network system. Nonetheless, these reactions are out of the scope of this thesis.



**Figure 2.13.** Russell termination mechanism during the oxidation of an unsaturated fatty acid<sup>74,75</sup>.

## 2.12. References

1. Medina-Navarro R., et al., *Clinica Chimica Acta* 337(1-2) (2003) 183.
2. Cabrera J., et al., *Pharmac. Toxic.* 89(5) (2001) 225.
3. Carlos F., Kusano B., *Revista de Nutricao* 11(1) (1998) 3.
4. Karbownik M., et al., *J. Cellul. Biochem.* 81(4) (2001) 693.
5. Carlotti M.E., et al., *J. Soc. Cosmet. Chem.* 42(5) (1991) 285.
6. Wicks Z.W., Jones F.N., Pappas S.P., “*Organic Coatings: Science and Technology Vol. I*”, John Wiley & Sons (1994) 259.
7. Mäkinen M., et al., *J. Am. Oil Chem. Soc.* 77(8) (2000) 801.
8. Bieleman J.H., “*Additives for Coatings*”, Wiley-VCH, Weinheim (2000) 203.
9. Al-Malaika S., Issenhuth S., *Polymer* 42 (2001) 2915.
10. Mukai K., et al., *Lipids* 28(8) (1993) 747.
11. Krinsky N.I., *Proc. Soc. Exp. Biol. Med.* 200 (1992) 248.
12. Krinsky N.I., *Free Rad. Biol. Med.* 7 (1989) 617.
13. Krinsky N.I., *Pure Appl. Chem.* 51 (1979) 649.

14. Courtneidge J.H., *Chem. Commun.* (1992) 1270.
15. Courtneidge J.H., *J. Chem. Soc., Perkin Trans. I* (1992) 1531.
16. Frankel E.N., *J. Sci. Food Agric.* 54 (1991) 495.
17. Bawn C.E.H., *J. Oil Col. Chem. Assoc.* 40 (1957) 1027.
18. Sheldon R.A., Kochi J.K., *Adv. Catal.* 25 (1976) 272.
19. Muizebelt W.J., et al., *J. Coat. Techn.* 70(876) (1998) 83.
20. Muizebelt W.J., Van Velde J.W., Van Wijk F.G.H., *Adv. Org. Coat. Sci. Techn. Ser.* 13 (1991) 57.
21. Muizebelt W.J., et al., *Prog. Org. Coat.* 40(1-4) (2000) 121.
22. Hartsthon J.H., *J. Coat. Techn.* 54(687) (1982) 53.
23. Mallégol J., et al., *Prog. Org. Coat.* 39(1-3) (2000) 107.
24. Muizebelt W.J., et al., *J. Coat. Techn.* 69(869) (1997) 59.
25. Davies J.E.D., et al., *J. Chem. Soc., Perkin Trans. 2*(11) (1972) 1557.
26. Agbenyega J.K., Claybourn M., Ellis G., *Spectrochimica Acta* 47A(9/10) (1991) 1375.
27. Ellis G., Claybourn M., *Spectrochimica Acta* 46A(2) (1990) 227.
28. Marshall G.L., et al., *Polymer* 29(8) (1988) 1501.
29. Marshall G.L., et al., *Polymer* 28(7) (1987) 1093.
30. Waldemar A. et al., *J. Photochem. Photobio. B: Bio.* 34(1) (1996) 51.
31. Frankel E.N., et al., *J. Chem. Soc., Perkins Trans. I* (1984) 2233.
32. Porter N.A., et al., *J. Am. Chem. Soc.* 116(15) (1994) 6690.
33. Chan H.W.-S., Levett G., *Lipids* 12(11) (1976) 99.
34. Porter N.A., et al., *J. Am. Chem. Soc.* 102 (1980) 5597.
35. Porter N.A., Wujek D.G., *J. Am. Chem. Soc.* 106 (1984) 2626.
36. Porter N.A., *Acc. Chem. Res.* 19 (1986) 262.
37. Hwan S.-S., et al., *Biosci. Biotechn. Biochem.* 63(11) (1999) 2009.
38. Neff W.E., et al., *Lipids* 16(6) (1981) 439.
39. Hancock R.A., Leeves N.J., *Prog. Org. Coat.* 17(3) (1989) 349.
40. Carless H.A.J., Batten R.J., *J. Chem. Soc., Perkin Trans. I* (1987) 1999.
41. Hubert J.C., et al., *Prog. Org. Coat.* 31(4) (1997) 331.
42. Frankel E.N., et al., *J. Chem. Soc., Perkin Trans. I* (1982) 2707.
43. Farmer E.H., et al., *J. Chem. Soc.* (1943) 541.
44. Frankel E.N., et al., *Lipids* 12(11) (1977) 901.
45. Porter N.A., et al., *Lipids* 30(4) (1995) 277.

46. Frankel E.N., "Analytical Methods Used in the Study of Autoxidation Processes", Plenum Press, New York (1980) 141.
47. Gunstone F.D., *J. Am. Oil Chem. Soc.* 61(2) (1984) 441.
48. Muizebelt W.J., Nielen M.W.F., *J. Mass. Spect.* 31 (1996) 545.
49. Menegetti S.M.P., et al., *Prog. Org. Coat.* 33 (1998) 219.
50. Love D.J., *Polym. Paint. Col. J.* 175 4146 (1985) 436.
51. Nakamoto K., "Infrared Spectra of Inorganic and Coordination Compounds" John Wiley & Sons, New York (1963) 197.
52. O'Neill L.A., Falla N.A.R., *Br. Polym. J.* 5 (1973) 115.
53. Denisov E.T., Emanuel N.M., *Russ. Chem. Rev.* 29 (1960) 645.
54. Lande S.S., Falk C.D., Kochi J.K., *J. Inorg. Nuc. Chem.* 33 (1971) 4101.
55. Lombard R., Rommert L., *Bull. Soc. Chim. Fr.* (1956) 36.
56. Talsi E.P., et al., *J. Molec. Cat.* 81 (1993) 215.
57. Chavez F.A., Mascharak P. K., *Acc. Chem. Res.* 33 (2000) 539.
58. Pilemand C., et al., *Proceedings of XXVII FATIPEC Congress, Aix-en-Provence, France* (2004) 649.
59. Steinart A., *Proceedings of XXVII FATIPEC Congress, Aix-en-Provence, France* (2004) 857.
60. Warzeska S.T., et al., *Prog. Org. Coat.* 44(3) (2002) 243.
61. Wu J.-Z., et al., *Prog. Org. Coat.* 49 (2004) 103.
62. Link G., et al., (1998) US6063841.
63. Boomgard R.E., et al., (2003) WO03029371.
64. van Gorkum R., et al., *Inorg. Chem.* 43 (2004) 2456-2458.
65. van Gorkum R., et al., (2004) EP1382648.
66. Brinksma J., et al., *Chem. Commun.* (2000) 537.
67. Hage R., et al., *Inorg. Chem.* 34 (1995) 4973.
68. Hage R., et al., *Nature* 369 (1994) 637.
69. Oostveen E.A., Micciché F., et al., (2003) WO2003093384.
70. Audouin-Jirackova L., Verdu J., *J. Polym. Sci., A Polym. Chem.* 25 (1987) 1205.
71. Christensen P.A., et al., *J. Mater. Sci.* 37 (2002) 3667.
72. Hancock R.A., Leeves N.J., *Prog. Org. Coat.* 17 (1989) 321.
73. Chang J.C.S., Guo Z., *Atmosph. Environ.* 32 (1998) 3581.
74. Russell G.A., *J. Am. Chem. Soc.* 78 (1956) 1047.

75. Russell G.A., *J. Am. Chem. Soc.* 79 (1957) 3871.

## Chapter 3

### Oxidation of model compounds catalyzed by cobalt-based catalysts

#### 3a. Oxidation of model compound emulsions for alkyd coatings catalyzed by a cobalt-based catalyst\*

##### Summary

*A systematic investigation on the oxidation of different model compounds (including methyl oleate, ethyl linoleate, and methyl linolenate) in emulsions in the presence of an emulsifiable cobalt catalyst is performed. Raman spectroscopy, attenuated total reflectance (ATR)-FTIR, and  $^1\text{H}$  NMR are used. Raman spectroscopy proves to be a powerful technique at following the oxidation of these model compounds in emulsions not only after but also during the water evaporation. Raman and ATR-FTIR ( $\text{D}_2\text{O}$  is used instead of  $\text{H}_2\text{O}$ ) investigations clearly demonstrate that there is essentially no observable chemical change during the water evaporation. The oxidation of model compounds in emulsions, after the water evaporation, is found to be similar to the oxidation of bulk/solvent-borne model compounds. The presence of an emulsifier (sodium dodecyl sulfate) and water does not show any significant effects on the oxidation of the model compounds. An increase in the intensity of conjugated double bonds and trans-double bonds is first observed, followed by a decrease. More than 90% of double bonds disappear for ethyl linoleate and methyl linolenate after 13 days of oxidation as examined by  $^1\text{H}$  NMR, which may be attributed to the addition of radicals to double bonds, especially conjugated double bonds and the  $\beta$ -scission of double-bond-containing radicals into byproducts. The oxidation of methyl oleate takes place much slower than that of ethyl linoleate and methyl linolenate. The number of double allylic group in the model compounds shows significant influence on the rate of oxidation for emulsions after water evaporation.*

---

\* Part of this Chapter has been published: Z.O. Oyman, W. Ming, R. van der Linde, *Prog. Org. Coat.*, 48 (2003) 80-91.



### 3a.1. Introduction

Currently for alkyd coatings, solvent-borne alkyd paints still dominate the market, but due to more stringent environmental concerns, environmentally friendlier alternatives have been sought after. Among them, alkyd emulsions have shown a lot of success. However, not much has been investigated in terms of the oxidation of alkyd emulsions despite numerous studies on the film formation and formulation of alkyd emulsions<sup>1-8</sup>. One reason is the presence of water. Many analytical techniques including FTIR fail to obtain sufficient chemical information when water is present.

Although similar oxidation reactions to solvent-borne alkyds are believed to occur in water-borne alkyds, there are some important differences that must be considered. It is generally recognized that water-borne alkyds dry slower than their solvent-borne counterparts probably due to the presence of water. Water is one of the strongest complexing agents with many metal ions including  $\text{Co}^{3+}$ . The formed  $[\text{Co}(\text{H}_2\text{O})_6]^{3+}$  hydrate complex will cause the loss of catalytic capability of cobalt-based catalysts. Therefore, catalysts used for solvent-borne alkyds may not be suitable for alkyd emulsions. In order to minimize this effect in alkyd emulsions, catalysts that are emulsifiable in water and soluble in white spirit were developed<sup>9</sup>. In addition, higher catalyst concentrations are needed to get a satisfactory drying performance<sup>10</sup>.

As already illustrated in Chapter 2, oxidation starts by the abstraction of an allylic hydrogen atom from fatty acid ester side chains by free radicals. The resulting radical reacts with the molecular oxygen to form hydroperoxides, with the conjugated double bonds being formed simultaneously. The hydroperoxides are decomposed into alkoxy ( $\text{RO}\bullet$ ) and peroxy ( $\text{ROO}\bullet$ ) radicals by metal-based catalysts. The radicals may then recombine one another to form carbon-carbon, ether, and peroxy cross-links that lead to the hardening of alkyd paints. The radicals can also initiate the propagation of double bonds to form higher oligomers, especially when conjugated double bonds are available. Beside these cross-linking reactions, radicals may undergo some side reactions ( $\beta$ -scission and Russell termination<sup>11-14</sup>) to generate byproducts, such as aldehydes, ketones, epoxides, and carboxylic acids<sup>15</sup>. Figure 2.12 (Chapter 2) illustrates  $\beta$ -scission of alkoxy radicals leading to the disappearance of double bonds.

Investigations of the oxidation reactions on alkyd emulsions with water-emulsifiable catalysts are still rare<sup>10</sup> and the oxidation mechanism needs to be further clarified. The effect of certain additives for water-borne alkyds (emulsifiers and

thickeners, etc.) on the oxidation is not yet known. It has been shown for solvent-borne alkyds that the oxidation rate increases as the number of double allylic groups (between two double bonds) increases<sup>16</sup>. However, no study has yet shown the effect of the number of double bonds on the oxidation rate from emulsions.

In this Chapter, three model compounds in emulsions are investigated to gain a better understanding of the oxidation reactions of alkyd emulsions in the presence of surfactants and emulsifiable cobalt catalysts. The oxidation of model compounds in emulsions during and after the water evaporation is monitored by Raman spectroscopy, attenuated total reflection (ATR)-FTIR, and <sup>1</sup>H NMR. Special attention is paid to the possible effects of water and emulsifier on the oxidation.

## **3a.2. Experimental**

### **3a.2.1. Materials**

Methyl oleate (MO, 60-70%, the remainder being saturated esters), ethyl linoleate (EL, 73%, the remainder being ethyl oleate and saturated esters), methyl linolenate (MLn, 70-80%, the remainder: methyl linoleate and saturated esters), and n-pentanol were obtained from Sigma-Aldrich Chemie B.V. (Zwijndrecht, The Netherlands). Model compounds contain small amounts of hydroperoxides<sup>17</sup>. Sodium dodecyl sulfate (SDS) was obtained from Merck B.V. (Amsterdam, The Netherlands). A cobalt-based catalyst (Nuodex Web-Co 6, a water emulsifiable catalyst containing 6 w% metal content) was obtained from Sasol Servo B.V. (Delden, The Netherlands). All chemicals were used without further purification.

### **3a.2.2. Emulsion preparation**

20% of the model compounds were emulsified in water containing 1% (w/w) of SDS and 0.01% (w/w) n-pentanol by dropwise addition of oil to water (o/w) using Branson type ultrasound sonifier for 10 min. Temperature of the emulsion reached up to 80 °C during the sonification. After cooling down 0.07% (metal/oil, w/w) catalyst was added to the prepared emulsion. Particle size was measured on a Coulter particle size analyzer (model LS 230). Typically, the average particle size was around 0.9 μm, and the change in particle size over a period of 2 days was negligible within the experimental error.

### 3a.2.3. Characterizations

The oxidation of model compound emulsions was *in-situ* followed by time-resolved ATR-FTIR on a Bio-Rad Excalibur FTS3000MX infrared spectrophotometer (30 scans per spectrum with a resolution of  $4\text{ cm}^{-1}$ ) equipped with an ATR diamond unit (Golden Gate), and by Raman spectroscopy on a Dilor-Jobin Yvon-Horiba confocal dispersive Raman spectrometer (633 nm excitation wavelength,  $1000\text{ }\mu\text{m}$  pinhole, and 8 mW laser intensity) with an Olympus MX40 microscope. The prepared emulsions were deposited on the diamond crystal of ATR unit for infrared analysis and on glass slides for Raman analysis. The thickness of wet films was kept around  $200\text{ }\mu\text{m}$ . Samples were withdrawn from films after the water evaporation and dissolved in  $\text{CDCl}_3$  (5 mg/mL) for  $^1\text{H}$  NMR analysis on a Varian 400 MHz spectrometer.

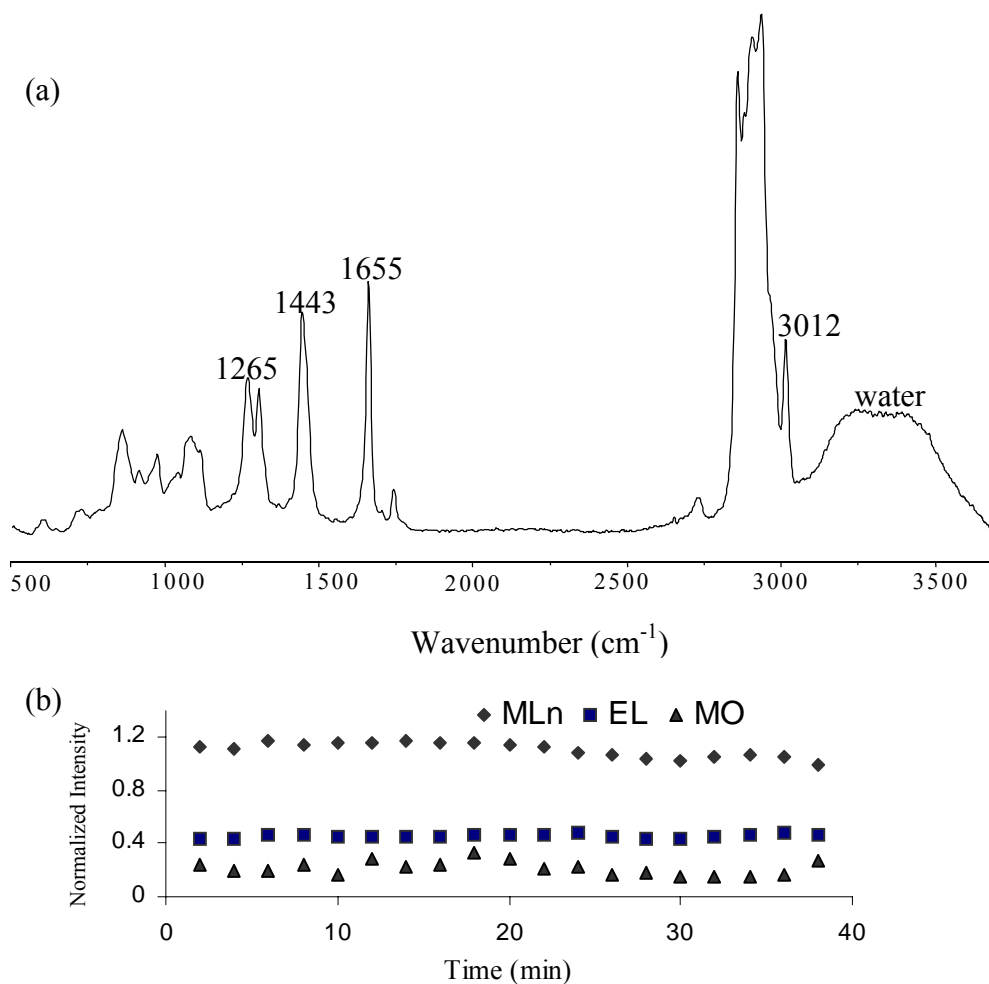
### 3a.3. Oxidation of model compound emulsions during water evaporation

It is generally accepted that the oxidation starts after the water evaporation for alkyd emulsions. However, no direct experimental evidence has been shown yet.

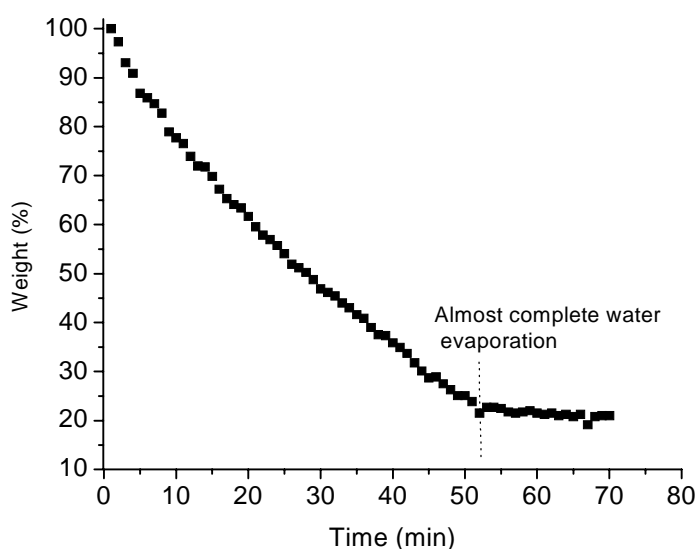
Raman spectroscopy is a very useful technique for the study of the oxidation behavior of model compound emulsions. It is quite advantageous to use Raman to monitor the variation of double bonds during the oxidation reactions since, in comparison with IR, double bonds demonstrate stronger Raman absorptions<sup>19</sup>. The *cis/trans*-double bond isomers can be easily identified. In addition, because water peak does not interfere with the major peaks of the model compounds, Raman spectroscopy allows us to take a closer look at what takes place during the water evaporation, even when the majority of water is still present.

Figure 3.1a shows the Raman spectrum of an EL emulsion at the very beginning of water evaporation. Although the broad water peak overlaps slightly with the C-H stretching peak at around  $2900\text{ cm}^{-1}$ , the peak at  $3012\text{ cm}^{-1}$  (corresponding to the antisymmetric stretching of *cis*-C=C-H) is clearly visible and can be used for further analysis. A decrease in the intensity of  $3012\text{ cm}^{-1}$  peak is an indication of the starting point of an oxidation reaction. Shown in Figure 3.1b is a plot of the  $3012\text{ cm}^{-1}$  peak intensity (normalized against -CH<sub>2</sub>- scissor deformation at  $1443\text{ cm}^{-1}$ ) for three model compound emulsions as a function of time during the water evaporation. Obviously the  $3012\text{ cm}^{-1}$  peak intensity remains essentially the same for all three

model compounds during the observation period (about 40 min). There is hardly any observable change for other double bond related peaks of the model compounds during the water evaporation. By using Raman it was clearly shown that, for the cobalt catalyst, essentially no oxidation takes place during water evaporation.



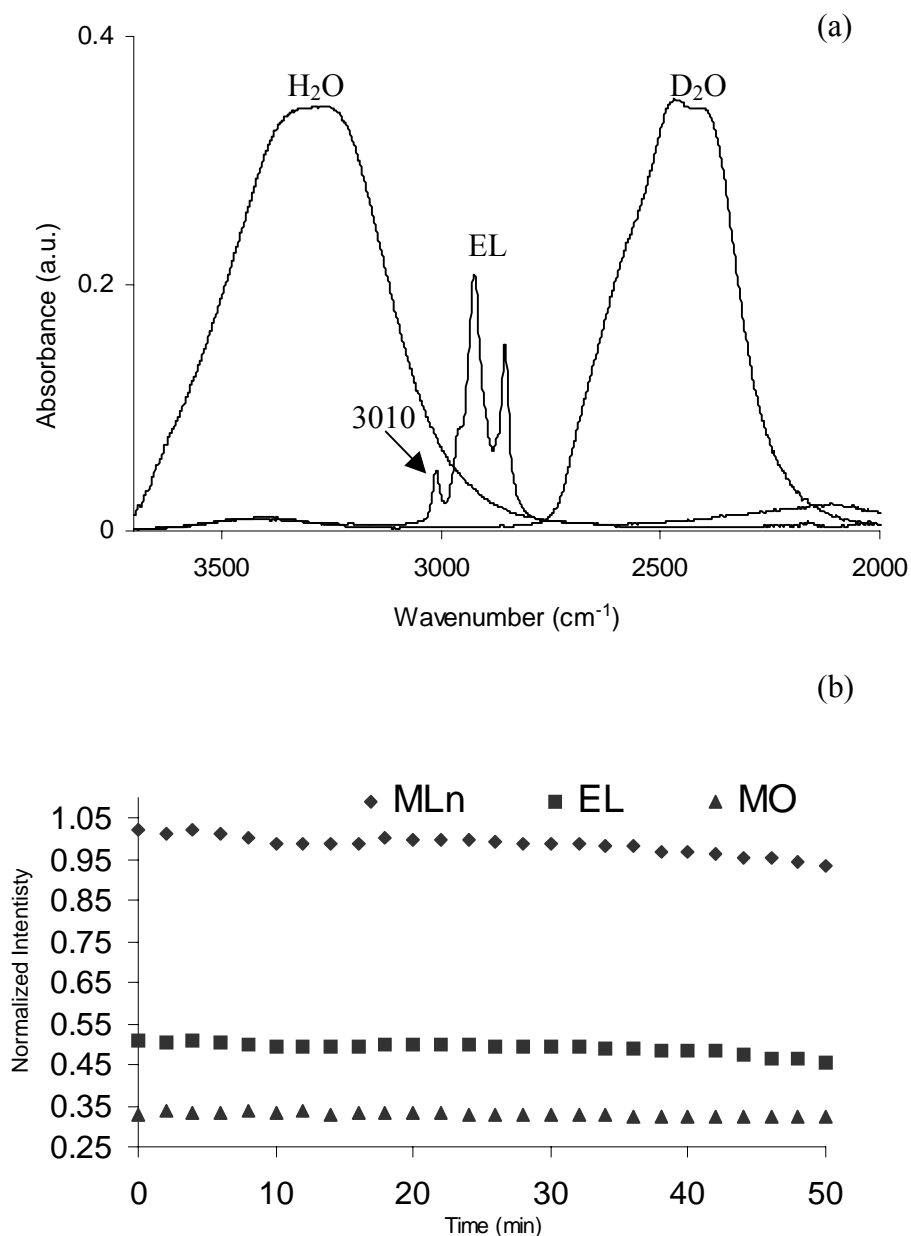
**Figure 3.1.** (a) Raman spectrum of EL emulsion at the very beginning of water evaporation, and (b) variation of the intensity of antisymmetric *cis*-C=C-H stretching peak at 3012 cm<sup>-1</sup> (Raman) for model compound emulsions during water evaporation (normalized against -CH<sub>2</sub>- scissor deformation at 1443 cm<sup>-1</sup>) as a function of time under the influence of 0.07% Nuodex Web-Co.



**Figure 3.2.** Weight loss of 20% EL emulsion during water evaporation at room temperature with  $\sim 200$   $\mu\text{m}$  wet film thickness.

In fact, water has to evaporate in order for the cobalt-based catalyst to have a catalytic effect. Figure 3.2 shows a typical weight loss curve for EL emulsion during the water evaporation. The weight loss experiment of a 20% EL emulsion was performed on a balance. 50  $\mu\text{L}$  of the emulsion (about 200  $\mu\text{m}$  in thickness) was applied on a glass slide. The weight of the wet film was recorded during the water evaporation. In this particular case, about 50 minutes are needed to reach complete water evaporation. As a matter of fact, a few parameters govern the evaporation rate of water even when the water amount is the same, including temperature, humidity, and sample thickness.

Since the water peak overlaps with peaks of interest in the model compounds, it was not possible to follow the initial stages of oxidation by FTIR. This problem is solved by replacing  $\text{H}_2\text{O}$  with  $\text{D}_2\text{O}$ . Figure 3.3a gives IR spectra of  $\text{D}_2\text{O}$ ,  $\text{H}_2\text{O}$ , and EL; clearly it is possible to monitor the  $3010\text{ cm}^{-1}$  peak in the presence of  $\text{D}_2\text{O}$ .



**Figure 3.3.** (a) Infrared spectra of H<sub>2</sub>O, D<sub>2</sub>O and EL (2000-3700 cm<sup>-1</sup>) and (b) variation of the intensity of symmetric *cis*-C=C-H stretching peak at 3010 cm<sup>-1</sup> (ATR-FTIR) for model compound emulsions during D<sub>2</sub>O evaporation (normalized against -O-CO- stretching at 1178 cm<sup>-1</sup>) as a function of time under the influence of 0.07% Nuodex Web-Co.

Similar to the Raman study on the oxidation of model compound emulsions described, the first 50-min oxidation of the model compound emulsions in D<sub>2</sub>O was monitored by ATR-FTIR. Figure 3.3b gives the intensity of the 3010 cm<sup>-1</sup> peak (the symmetric stretching of *cis*-C=C-H) against an internal standard (-O-CO- stretching

at 1178  $\text{cm}^{-1}$ ) as a function of time. Obviously, for the three model compounds studied, essentially no change in the 3010  $\text{cm}^{-1}$  peak intensity was observed. Therefore, FTIR also confirms that, for the cobalt-based catalyst, essentially no oxidation takes place when water is present.

Water reduces oxygen diffusion and therefore retards the oxidation process<sup>10</sup>. The oxidation starts as soon as water has evaporated. However, the oxidation reactions of model compounds, even with effective catalysts, are slow processes. Even after the water evaporation, some time is needed for oxygen to react with unsaturated fatty acids. The efficiency of catalyst also plays an important role for accelerating these oxidation reactions. Different catalysts may demonstrate different catalytic behaviours. For cobalt-based catalysts, catalytic capability becomes effective only after the water evaporation for the model compounds.

### 3a.4. Oxidation of model compound emulsions after water evaporation monitored by Raman spectroscopy

In the following, we will be focusing on the oxidation of model compounds after water evaporation by Raman spectroscopy. Raman peak assignments are given in Table 3.1

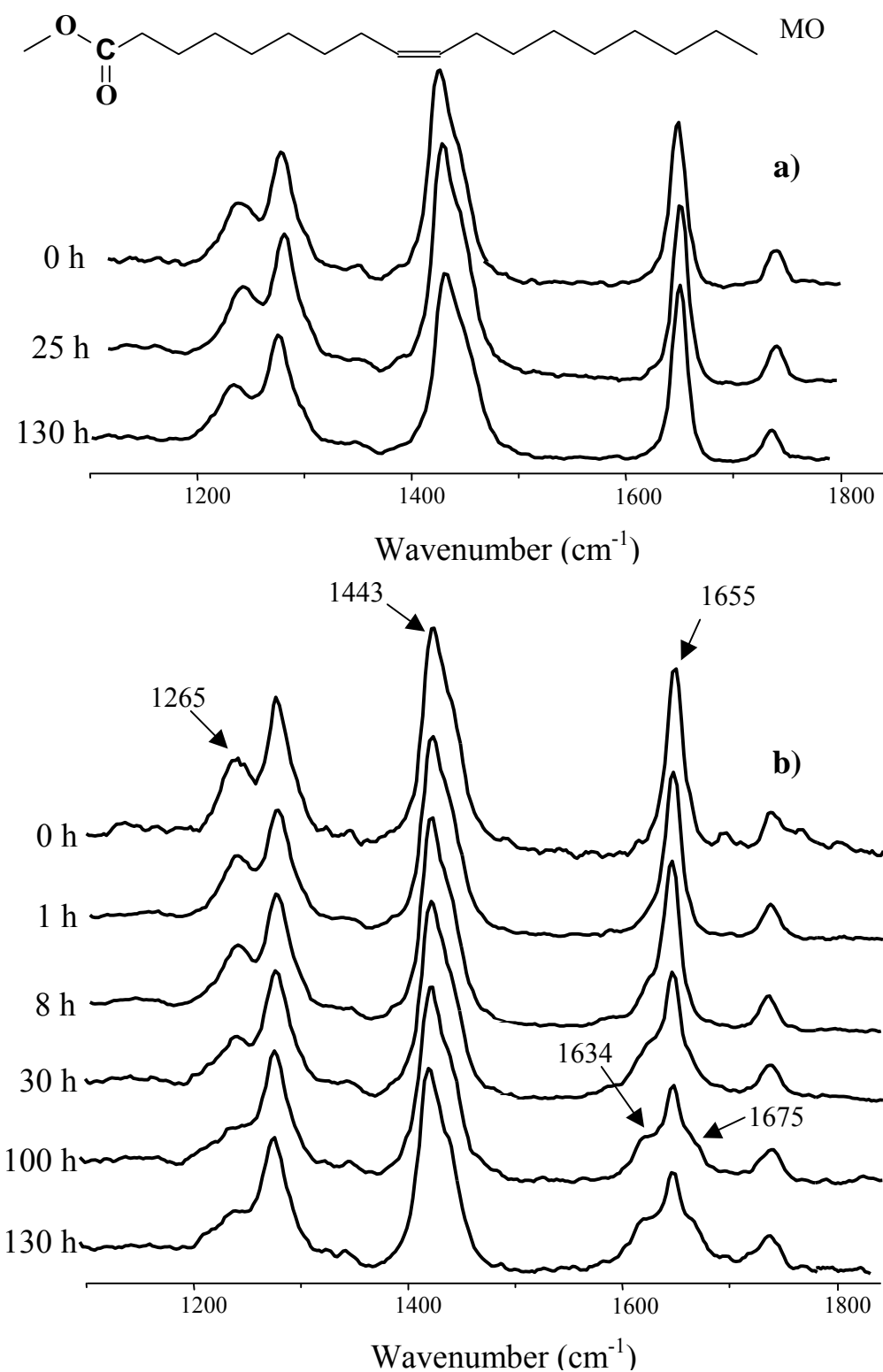
Table 3.1 Important Raman band assignments of model compounds<sup>18-20</sup>.

Bands	Assignments
1265 w	nonconjugated <i>cis</i> -C=C-H symmetric rock
1306 w	-CH <sub>2</sub> - in phase methylene twist
1320 w	nonconjugated <i>trans</i> -C=C-H symmetric rock
1443 s	-CH <sub>2</sub> - scissor deformation; $\delta(\text{CH}_2)$
1597 w	antisymmetric conjugated C=C stretching
1634 s	symmetric conjugated C=C stretching ( <i>cis-trans</i> and <i>trans-trans</i> ) and/or terminal C=C stretching
1655 s	symmetric <i>cis</i> -C=C stretching (nonconjugated)
1675 s	isolated <i>trans</i> -C=C stretching
1744 w	C=O stretching (ester)
2855-2893 vs-sh	CH <sub>2</sub> stretching (-CH <sub>2</sub> - asym), (-CH <sub>3</sub> asym)
2926-2955 vs-sh	CH <sub>2</sub> stretching (-CH <sub>2</sub> - sym), (-CH <sub>3</sub> sym)
3012 s	<i>cis</i> -C=C-H antisymmetric stretching

### 3a.4.1. Oxidation of methyl oleate (MO) emulsions

Figure 3.4 illustrates Raman spectra during the oxidation of MO from emulsions in the absence and presence of Nuodex Web-Co. When Nuodex Web-Co was not added (Figure 3.4a), no obvious change in Raman spectra was detected up to 130 h, indicating that there is almost no oxidation for MO. However, in the presence of Nuodex Web-Co observable changes could be identified after 8 h (Figure 3.4b), for instance, the decrease of the *cis*-C=C peak ( $1655\text{ cm}^{-1}$ ) and the *cis*-C=C-H symmetric rock peak ( $1265\text{ cm}^{-1}$ ). The appearance of *trans*-C=C peak ( $1675\text{ cm}^{-1}$ ) was also observed in the later stage. This is a clear indication that *cis*-C=C is converted into *trans*-C=C. The appearance of a shoulder at  $1634\text{ cm}^{-1}$  is noticeable after 8 h. Although this peak can be due to conjugated-C=C and/or terminal C=C, the exact assignment of this peak is still unclear. Since MO has only one double bond, the conjugation of double bonds is not possible (MO does not have EL impurities, as determined by GC-MS). Although the formation of terminal C=C was already reported for EL<sup>31</sup>, we do not have direct evidence for the formation of terminal double bonds in the case of MO. After 130-h oxidation of MO, *cis*- and *trans*-C=C peaks were still present due to the low oxidation rate of MO.

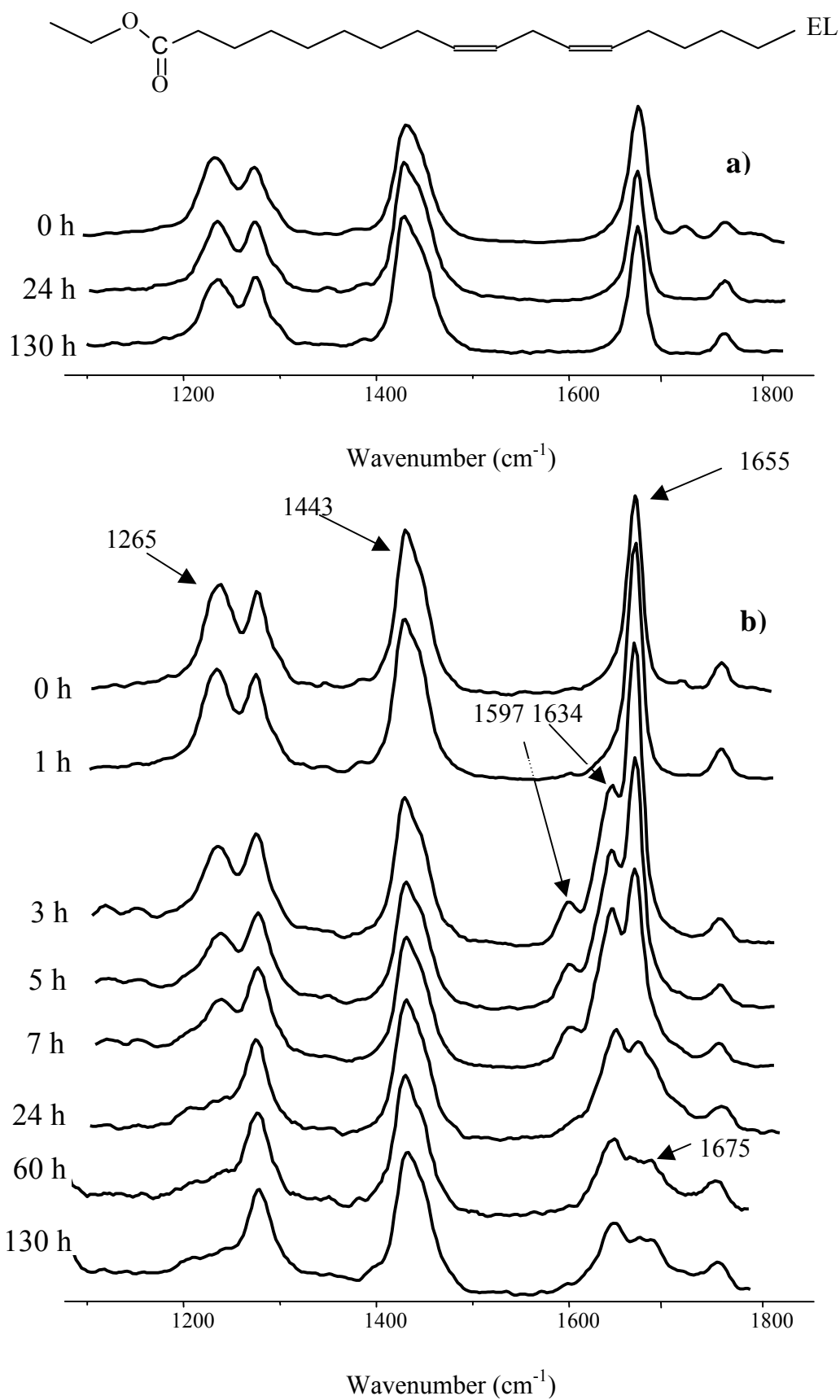




**Figure 3.4.** Raman spectra during the oxidation of MO emulsion at 1200-1800 cm<sup>-1</sup>: (a) without Nuodex Web-Co, and (b) with Nuodex Web-Co.

### 3a.4.2. Oxidation of ethyl linoleate (EL) emulsions

Figure 3.5 illustrates Raman spectra during the oxidation of EL from emulsions with and without Nuodex Web-Co. In the absence of the catalyst, similar to MO, only small changes were observed over a period of 130 h (Figure 3.5a), for instance, the slight decrease of the  $1265\text{ cm}^{-1}$  peak. In contrast, in the presence of Nuodex Web-Co, the chemical changes of double bonds are very obvious within 3 h (Figure 3.5b). The non-conjugated *cis*-C=C peak ( $1655\text{ cm}^{-1}$ ) significantly decreases, due to the conversion to conjugated C=C including both *cis-trans* and *trans-trans*-C=C, which are difficult to be differentiated. The decrease in the *cis*-C=C-H symmetric rock peak ( $1265\text{ cm}^{-1}$ ) is also obvious. The  $1634\text{ cm}^{-1}$  peak corresponds to the symmetric stretching of the conjugated double bonds, and the  $1597\text{ cm}^{-1}$  peak to the antisymmetric stretching. The intensity of the antisymmetric stretching is generally low in Raman<sup>20</sup>. After 24 h oxidation, a peak at  $1675\text{ cm}^{-1}$  (isolated *trans*-C=C) appears due to the consumption of neighboring double bonds. During the oxidation, the intensity of conjugated double bonds first increases in intensity, until reaching a maximum level. Afterwards, the intensity of the double bonds starts to decrease due to the addition of radicals to double bonds (especially after the formation of conjugated double bonds) and/or  $\beta$ -scission (Chapter 2).

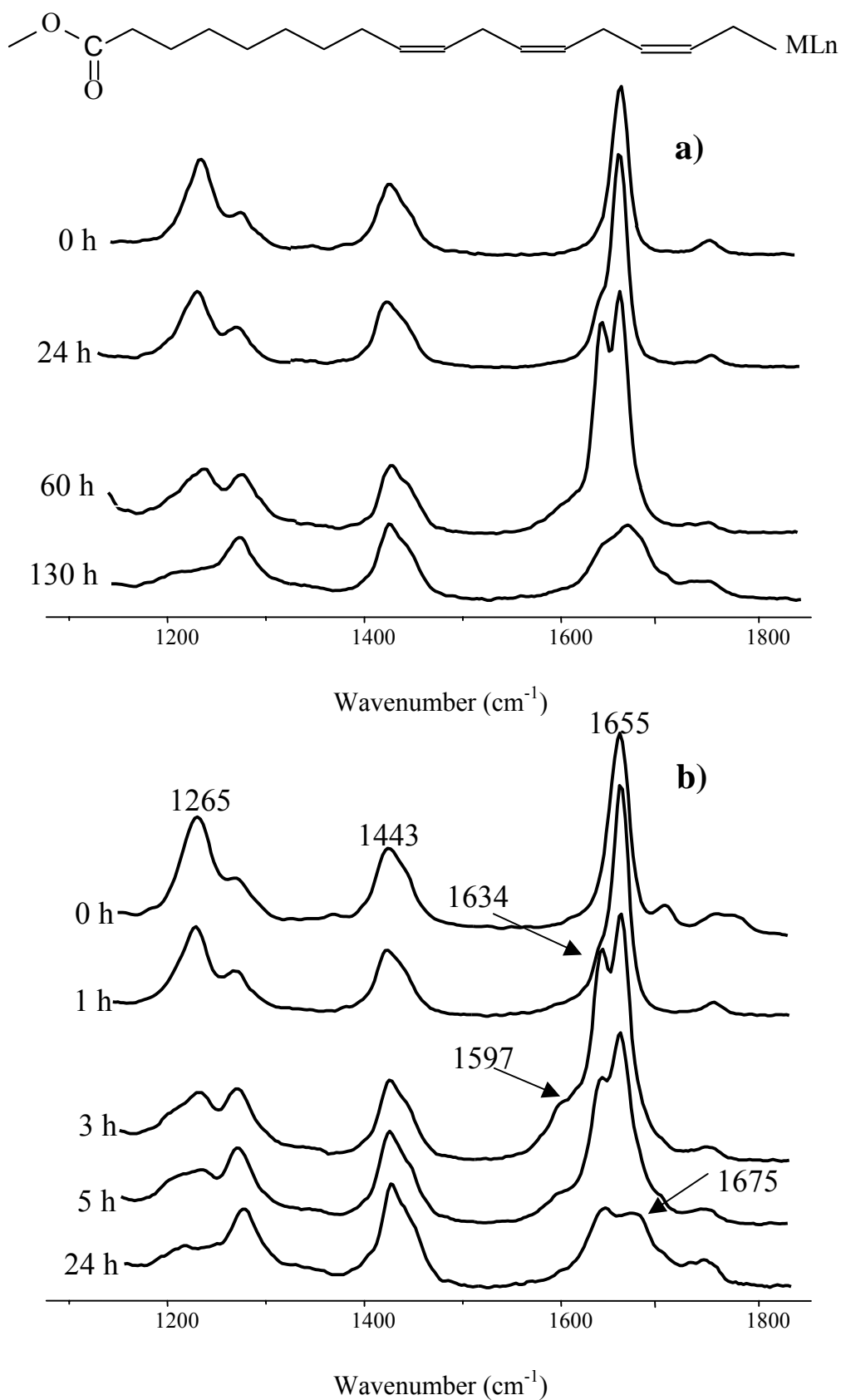


**Figure 3.5.** Raman spectra during the oxidation of EL emulsion at 1200-1800 cm<sup>-1</sup>: (a) without Nuodex Web-Co, (b) with Nuodex Web-Co.

### **3a.4.3. Oxidation of methyl linolenate (MLn) emulsions**

The Raman spectra of MLn emulsion during the oxidation in the absence and in the presence of Nuodex Web-Co are shown in Figure 3.6. As expected, in the beginning the intensities of C=C stretching ( $1597\text{-}1680\text{ cm}^{-1}$ ) and rock ( $1265\text{ cm}^{-1}$ ) peaks are much higher than in the case of EL and MO, and the CH<sub>2</sub> scissor peak ( $1443\text{ cm}^{-1}$ ) of the alkyl chain is much lower because of the presence of three non-conjugated double bonds. In the absence of Nuodex Web-Co, MLn demonstrates much faster oxidation than EL (Figure 3.6a). The appearance of conjugated peaks could be seen after 24 h oxidation, as indicated by a shoulder at around  $1634\text{ cm}^{-1}$ . After 130 h, the intensity of double bonds decreases substantially. The faster oxidation is due to the presence of two double allylic groups in MLn.

In the presence of Nuodex Web-Co, the same conversion of the double bonds is reached after 24 h (Figure 3.6b), instead of 130 h in the absence of a catalyst. MLn gets oxidized much more rapidly than MO and EL. The intensity of conjugated double bonds formed within 3 h was much higher than that of EL during the same period. Apparently, increasing the number of double bonds in the fatty acid chain increases the oxidation rate of model compounds from emulsions. This trend is similar to that observed in solvent-borne systems. Similar to EL, the intensity of conjugated and isolated C=C first increases and then decreases due to the consumption of double bonds.



**Figure 3.6.** Raman spectra during the oxidation of MLn emulsion at 1200-1800 cm<sup>-1</sup>: (a) without Nuodex Web-Co, (b) with Nuodex Web-Co.

### 3a.5. Oxidation after water evaporation monitored by ATR-FTIR

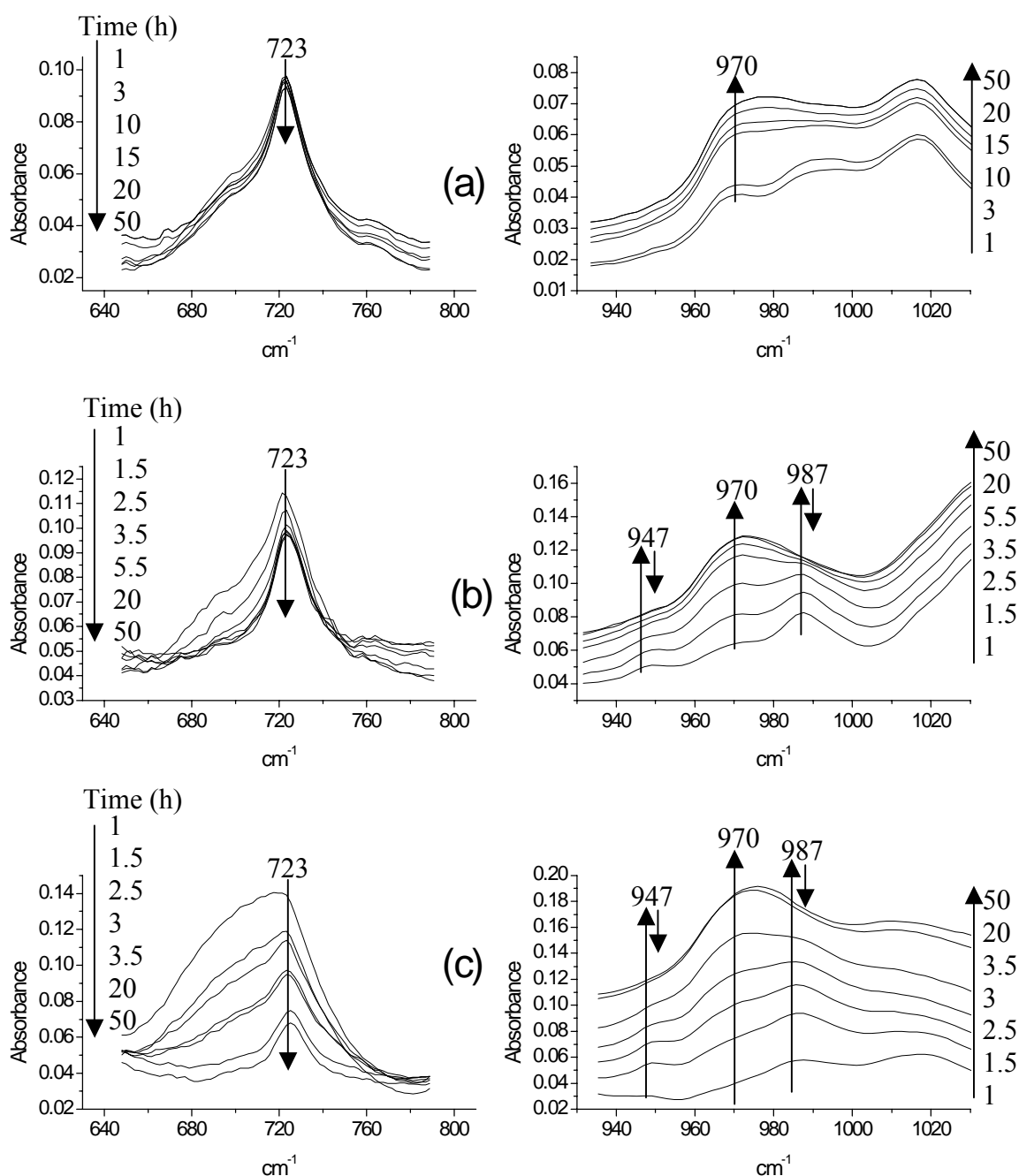
Although water interferes with the peak of interest, water evaporates almost completely after a certain period. After the evaporation of water, the oxidation of model compounds can be easily followed *in-situ* by time-resolved ATR-FTIR. We will demonstrate the oxidation of model compound emulsions after water evaporation. Assignments of infrared peaks are given in Table 3.2.

Table 3.2 Important infrared band assignments of model compounds<sup>18,20,21</sup>.

Bands	Assignments
723	C-C skeletal vibration of CH <sub>2</sub> chain
723 m	<i>cis</i> -C=C-H planar bending
987 m	<i>trans-trans</i> conjugated C=C-H wag
947 s and 987 s	<i>cis-trans</i> conjugated C=C-H wag
970 s	isolated <i>trans</i> -C=C-H wag
1370 m	CH <sub>2</sub> wagging
2855-2893 vs-sh	CH <sub>2</sub> stretching (-CH <sub>2</sub> - asym), (-CH <sub>3</sub> asym)
2926-2955 vs-sh	CH <sub>2</sub> stretching (-CH <sub>2</sub> - sym), (-CH <sub>3</sub> sym)
3010 w	<i>cis</i> -C=C-H symmetric stretching
3451-3600 m (broad)	O-H stretch (free-bonded)

#### 3a.5.1. Oxidation of MO emulsions

Figure 3.7a shows the infrared spectra during the oxidation of MO emulsion after water evaporation in the presence of Nuodex Web-Co over a period of 50 h at 650-1050 cm<sup>-1</sup> region. This region shows changes in the wagging of *cis*- and *trans*-C=C-H as reported previously for linseed oil<sup>21</sup>. The absorption at 660-780 cm<sup>-1</sup> is probably due to the combination of C-C alkane skeletal vibration and the wagging of *cis*-C=C-H. During the observation period, this peak becomes narrower due to the formation of isolated *trans*-C=C-H (970 cm<sup>-1</sup>).



**Figure 3.7.** ATR-FTIR spectra ( $700\text{-}1050\text{ cm}^{-1}$ ) during 50-h oxidation of model compound emulsions: (a) methyl oleate, (b) ethyl linoleate, (c) methyl linolenate.

### 3a.5.2 Oxidation of EL emulsions

Figure 3.7b shows infrared spectra ( $650\text{-}1050\text{ cm}^{-1}$  region) during the oxidation of the EL emulsion in the presence of Nuodex Web-Co over a period of 50 h. The decrease of the *cis*-C=C-H wagging peak at  $723\text{ cm}^{-1}$  is more obvious within 50 h. At the very beginning of the oxidation, three small peaks at 947, 970, and  $987\text{ cm}^{-1}$  are shown (EL already contains small amount of hydroperoxides<sup>17</sup>). These three

peaks correspond to C-H wagging of either conjugated or isolated *trans*-C=C-H bonds. Among them, peaks at 947 and 987  $\text{cm}^{-1}$  are likely due to conjugated double bonds while the peak at 970  $\text{cm}^{-1}$  is from isolated *trans*-double bonds (Table 3.2)<sup>20</sup>. As the oxidation proceeds, the intensity of these peaks increases. After reaching a maximum level, conjugated double bond peaks at 947 and 987  $\text{cm}^{-1}$  starts decreasing in intensity. The isolated *trans*-C=C-H (970  $\text{cm}^{-1}$ ) peak remains with the highest intensity within the observation period. The results are in good agreement with Raman results described in 3a.4.2.

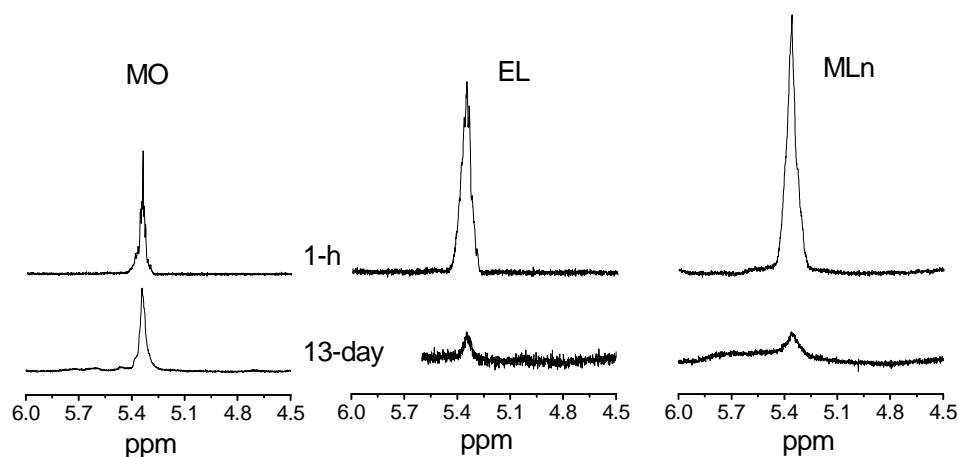
### 3a.5.3. Oxidation of MLn emulsion

Figure 3.7c illustrates the infrared spectra during the oxidation of the MLn emulsion with Nuodex Web-Co up to 50 h. The decrease in *cis*-C=C-H wagging peak is much faster than the other two model compounds. In the region of 930-995  $\text{cm}^{-1}$ , an increase in peak intensity due to the formation of conjugated and isolated *trans*-double bonds, followed by a steady decrease in conjugated double bonds, was again observed, very similar to the oxidation of EL. The isolated *trans*-C=C-H (970  $\text{cm}^{-1}$ ) wagging peak also remains with the highest intensity for MLn within the observation period. The assignments of MLn peaks during oxidation are more complicated than for EL due to the third double bond that, together with the other two, may form many isomers. The differentiation of these isomers is not attempted.

### 3a.6. The extent of double bonds during the oxidation of model compounds

The oxidation of model compounds from emulsions in the presence of Nuodex Web-Co was also examined by  $^1\text{H}$  NMR. The intensity of *cis*-C=CH (5.4 ppm) of 1-h and 13-day oxidized samples is shown in Figure 3.8. Previously, Raman and ATR-FTIR have already shown the great loss of double bonds over a period of 130-h oxidation. After samples were oxidized for 13 days, > 90% of double bonds have disappeared for EL and MLn. But MO shows only a slight decrease. It is already known that for MO hydrogen abstraction takes place from mono allylic groups, while hydrogen is abstracted from double allylic groups in EL and MLn. The latter is energetically more favourable. From this point of view, MO gets oxidized much slower than EL and MLn.



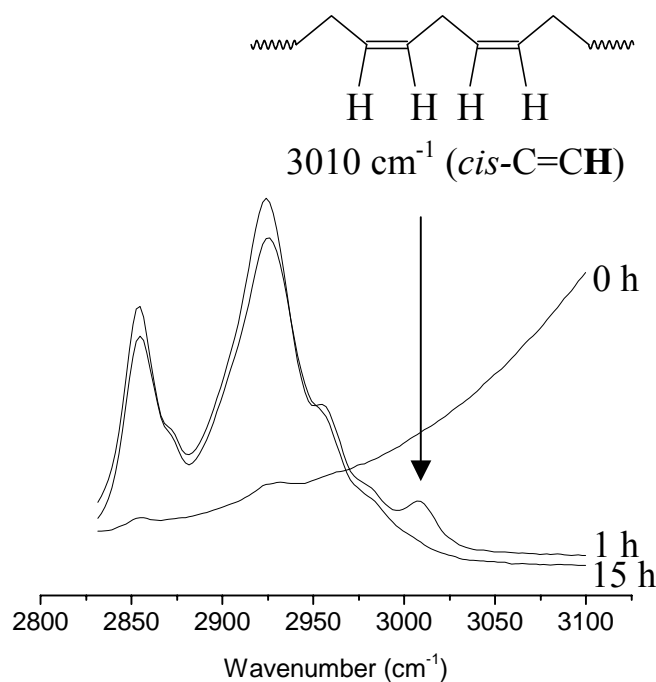


**Figure 3.8.** <sup>1</sup>H NMR intensity of CH=CH (5.4 ppm) for 1-h and 13-day oxidized model compound (MO, EL, MLn) emulsions in the presence of Nuodex Web-Co after water evaporation.

The above studies show that, in a short period of time, the intensities of all double bond-related peaks for EL and MLn decrease tremendously. The fast disappearance of double bonds further indicates that mechanisms other than recombination of radicals also play an important role. Muizebelt *et al.* suggested that for EL the recombination of radicals is the main route for the formation of higher oligomers, while for conjugated EL the addition of radicals to double bonds plays a major role for the consumption of the double bonds<sup>22</sup>. Other reactions like  $\beta$ -scission are already known to decrease the unsaturation, but the loss of unsaturation would not be so great. The recombination of free radicals does not affect the double bonds. In view of the enormous unsaturation loss in this study, it appears that even for EL and MLn (containing only non-conjugated double bonds) the addition of free radicals to double bonds also plays an important role in the disappearance of the double bonds. It is known that, during the formation of hydroperoxide, the non-conjugated double bonds are converted into conjugated bonds. Therefore, it is reasonable to attribute the great loss of double bonds, even in the case of model compounds containing non-conjugated double bonds, to the direct addition of free radicals ( $R\bullet$ ,  $RO\bullet$ ,  $ROO\bullet$ ) to the double bonds.

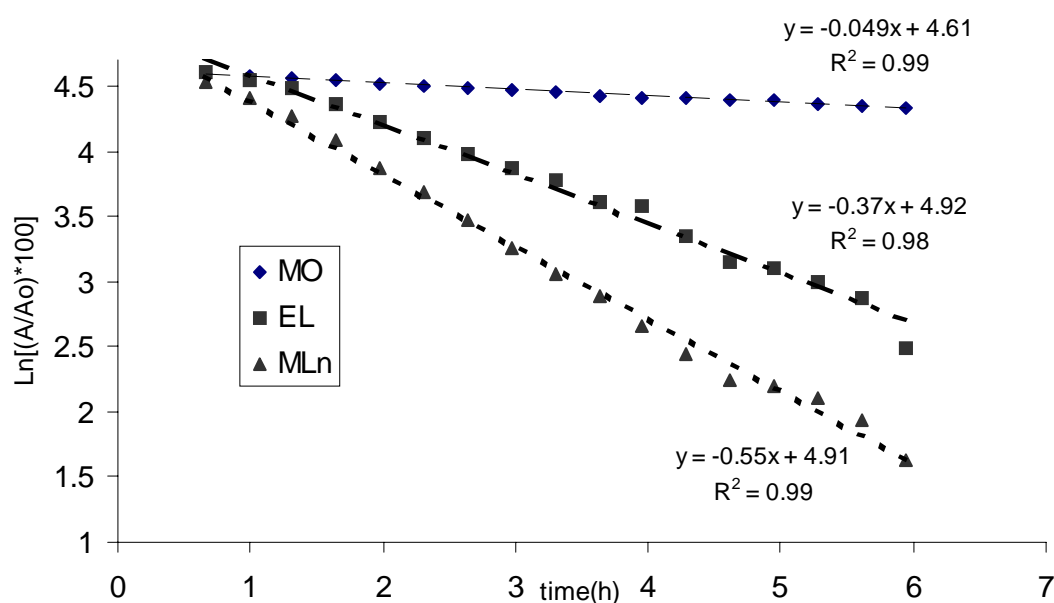
### 3a.7. Oxidation kinetics of model compound emulsions

The oxidation kinetics of model compounds can be followed *in-situ* via either the decrease in the *cis*-C=C-H symmetric stretch ( $3010\text{ cm}^{-1}$ ) by ATR-FTIR in Figure 3.9 or the decrease in the antisymmetric stretching of *cis*-C=C-H ( $3012\text{ cm}^{-1}$ , Figure 3.1a) by Raman. FTIR and Raman results are in good agreement. Here we only demonstrate the results on the basis of ATR-FTIR measurements.



**Figure 3.9.** ATR-FTIR spectra of EL emulsion showing the variation of *cis*-C=C-H symmetric stretch peak during the oxidation under the influence of Nuodex Web-Co.

The kinetic plots (natural logarithm of the peak height (normalized values) versus time) of the oxidation of three model compounds are depicted in Figure 3.10. The slopes indicate different oxidation rates. The oxidation rates of model compounds are similar to the reported values for solvent-borne/bulk systems<sup>16,23</sup>. Therefore, the oxidation kinetics of model compound emulsions after water evaporation appears to be similar to the solvent-borne/bulk systems. The presence of SDS does not show any obvious effect on the oxidation of model compounds. It can be seen in Figure 3.10 that the oxidation rate of model compounds in the presence of Nuodex Web-Co also increases with the increasing number of allylic groups between two double bonds. It means that, beside the catalyst capability, the unsaturation number of the alkyd resin in emulsion is also very important to get an optimum drying performance.



**Figure 3.10.** The oxidation kinetics of model compound emulsions obtained by the decrease in *cis*-C=C-H symmetric stretch peak at  $3010\text{ cm}^{-1}$  (after water evaporation) under the influence of Nuodex Web-Co (pseudo-first order rates calculated from the graph are indicated).

### 3a.8. Conclusions

Raman spectroscopy has been demonstrated to be a suitable technique for the study of the oxidation of model compounds (MO, EL, and MLn) in emulsions. From Raman and ATR-FTIR investigation, it has been clearly shown that essentially no oxidation takes place during water evaporation of three model compound emulsions. After water evaporation, the oxidation reactions start in a manner similar to the bulk/solvent-borne systems. In the case of EL and MLn, as the oxidation proceeds, the *cis*-C=C is converted into *trans*-C=C and conjugated C=C, and their intensities reached a maximum level. These double bonds start to disappear afterwards, and conjugated double bonds decrease much faster than isolated *trans*-C=C. This is probably due to the direct addition of radicals ( $R\bullet$ ,  $RO\bullet$ ,  $ROO\bullet$ ) to the double bonds (conjugated double bonds in particular; they are formed during the oxidation); which might be the main reason of the great loss of double bonds. The number of double allylic group in the model compounds also shows significant influence on the rate of oxidation: the greater the unsaturation number, the faster the oxidation. The kinetic study reveals that the presence of water and surfactant in the emulsion does not show

observable effects on the oxidation of model compounds. It can be concluded that the oxidation of model compounds in emulsions takes place in a way comparable to their counterparts in solvent-borne/bulk systems.



## Chapter 3

### Oxidation of model compounds catalyzed by cobalt-based catalysts

#### 3b. Oxidation of drying oils containing non-conjugated and conjugated double bonds in the presence of a cobalt catalyst\*

##### Summary

*The oxidation of drying oils containing non-conjugated (linseed oil) and conjugated (tung oil) double bonds catalyzed by Co(II)-2-ethylhexanoate (Co-EH) is investigated. There is distinctive difference in the oxidation mechanism between the two model oils. For the non-conjugated linseed oil, H-abstraction occurs via the most susceptible double allylic H atom. A large amount of oxygen is taken up, leading to the formation of hydroperoxides; the hydroperoxides are then decomposed into alkoxy and peroxy free radicals, followed by the formation of cross-links and byproducts. In contrast, for the mainly conjugated tung oil, the oxidation has to start with H-abstraction from the monoallylic position. In comparison with linseed oil, a lower amount of oxygen is consumed; much less hydroperoxides and byproducts are formed. It indicates that, once free radicals are formed, they tend to directly add to a conjugated double bond, instead of abstracting a monoallylic H atom. A tentative explanation is given in terms of bond dissociation energy of related bonds.*

---

\* Part of this Chapter has been submitted for publication: Z.O. Oyman, W. Ming, R. van der Linde, submitted to *Prog. Org. Coat.* (Jan. 2005).

### 3b.1. Introduction

Fundamental understanding of the chemical drying processes of alkyd coatings is very important to formulate and design new types of paints with desirable properties. Alkyd coatings are used in a wide variety of applications resulting in a wide range of film properties. This variation is largely due to the type and the amount of unsaturated fatty acid used during the alkyd synthesis<sup>24</sup>. Drying oils and fatty acids used for alkyd preparation can be obtained naturally with a wide variety of unsaturation. It is known that the number of double allylic groups in the unsaturated fatty chain has great influence on the rate of oxidation (Figure 3.10)<sup>16</sup>.

Oxidation of an alkyd resin starts by the formation of hydroperoxides via H-abstraction from either double allylic hydrogen atom. These hydroperoxides are then decomposed into alkoxy and peroxy free radicals, usually catalyzed by a metal compound such as Co(II)-2-ethylhexanoate (Co-EH). Once these free radicals are formed, there is a four-way competition: (1) further H-abstraction (from double allylic H in the early stage and from monoallylic H in the late stage), leading to the buildup of hydroperoxide; (2) recombination of free radicals to form C-C, C-O-C, and C-O-O-C cross-links; (3) the addition of free radicals to double bonds (especially conjugated double bonds), and (4) formation of byproducts via, for instance,  $\beta$ -scission and Russell termination.

The general oxidation mechanism for non-conjugated fatty acid has been described in detail in Chapter 2. On the other hand, alkyd resins having conjugated fatty acid side chains appear to follow a different mechanism. Muizebelt *et al.* investigated the reaction mechanisms of conjugated ethyl linoleate (conj-EL) as the model compound<sup>23,25</sup>. For conj-EL, beside radical recombination, cross-linking reactions also occur via a direct addition of free radicals to the conjugated double bonds. This mechanism often leads to higher molecular-weight oligomers<sup>3,17</sup>.

Despite the numerous studies, a comprehensive study is still needed to further clarify the difference in the oxidation reactions between unsaturated fatty acids containing non-conjugated and conjugated double bonds. Therefore, in this work drying oils containing non-conjugated (linseed oil, 18:3) and conjugated (tung oil, 18:3) double bonds are chosen as model compounds. Raman spectroscopy and ATR-FTIR are used to study the chemical changes (*i.e.*, variation of double bonds) of drying oils during oxidation. Oxygen uptake and the evolution of peroxides during the

Co-EH catalyzed oxidation of drying oils are monitored. The possible explanations for the differences in the oxidation mechanisms between these drying oils will be given from a viewpoint of bond dissociation energy.

### 3b.2. Experimental

#### 3b.2.1. Materials

Linseed oil and tung oil (Table 3.3) were kindly provided by DSM Coating Resins, Zwolle, The Netherlands. Drying oils contain small amounts of hydroperoxides (Linseed oil: ~5 mmol/kg, tung oil: ~2 mmol/kg). Co(II)-2-ethylhexanoate (Co-EH), 65% (w/w) in white spirit, was purchased from Sigma-Aldrich. Chemicals were used without further purification.

Table 3.3. Fatty acid composition of oils<sup>26</sup>.

Oil	Fatty Acids (wt %)				
	<i>Saturated<sup>a</sup></i>	<i>Oleic(18:1)</i>	<i>Linoleic(18:2)</i>	<i>Linolenic(18:3)</i>	<i>Conjugated</i>
Linseed	10	22	16	52	-
Tung	5	8	4	3	80 <sup>b</sup>

<sup>a</sup>saturated fatty acids: stearic (18:0), palmitic (16:0)

<sup>b</sup> $\alpha$ -eleostearic acid (*cis,trans,trans*-triple conjugated)

#### 3b.2.2. Oxygen uptake

A Fibox fiber-optic oxygen meter (Precision Sensing GmbH) was used to measure the oxygen uptake during the oxidation of drying oils<sup>27</sup>. More information about the principle of the oxygen meter is given in the Appendix.

For the oxygen uptake measurement at room temperature, 4 g of drying oil, premixed with 0.1% (w/w) of the Co-EH catalyst, was placed into a 6-L sealed container, equipped with oxygen and temperature sensors inside. The oxygen consumed is expressed as mmol O<sub>2</sub> per g of oil.

#### 3b.2.3. Peroxide value

An American Oil Chemists' Society (AOCS) method for determining peroxide value was used with some modifications<sup>28</sup>. Details are given in the Appendix.



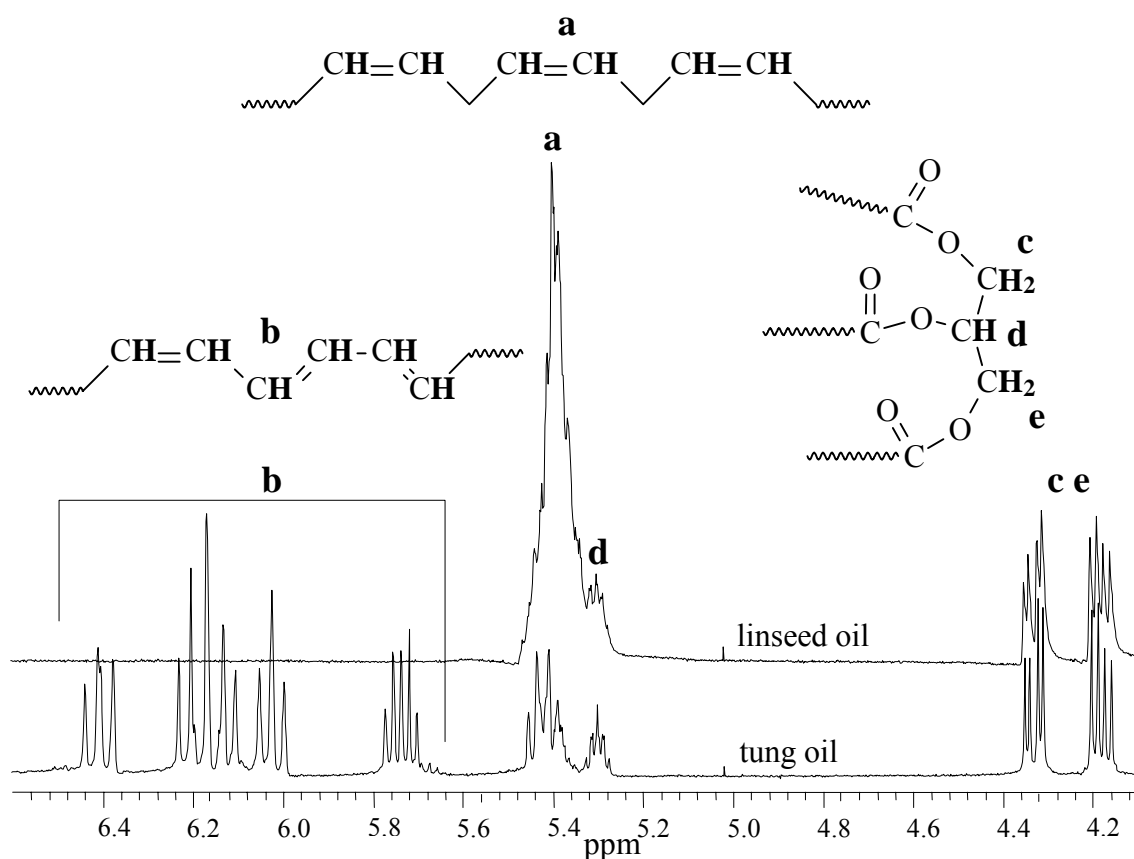
### 3.2.4. Characterization techniques

The oxidation of drying oils was followed by Raman spectroscopy on a Dilor-Jobin Yvon-Horiba confocal dispersive Raman spectrometer (633 nm excitation wavelength, 1000  $\mu\text{m}$  pinhole, and 8 mW laser intensity) with an Olympus MX40 microscope and by ATR-FTIR on a Bio-Rad Excalibur FTS3000MX infrared spectrophotometer (30 scans per spectrum with a resolution of 4  $\text{cm}^{-1}$ ) equipped with an ATR diamond unit (Golden Gate). Drying oils premixed with 0.1% (w/w) of the Co-EH catalyst were deposited onto glass slides ( $\sim 30 \mu\text{m}$ ) for *in-situ* Raman analysis and on the diamond crystal of ATR unit ( $\sim 30 \mu\text{m}$ ) for infrared analysis by using a roller blade. Linseed oil and tung oil were separately dissolved in  $\text{CDCl}_3$  (10 mg/mL) for  $^1\text{H}$  NMR analysis on a Varian 500 MHz spectrometer. Details are given in the Appendix.

### 3b.3. Chemical composition of linseed oil and tung oil

As shown in Table 3.3, the fatty acid compositions of drying oils are quite different. Linseed oil contains around 68% of non-conjugated double bonds. On the other hand, tung oil contains 80% conjugated double bonds.

Figure 3.11 illustrates  $^1\text{H}$  NMR spectra of linseed oil and tung oil. It is clearly shown that linseed oil contains a large amount of non-conjugated *cis*- $\text{CH}=\text{CH}$  at  $\sim 5.4$  ppm. In contrast, in tung oil the majority of the double bonds are conjugated  $\text{CH}=\text{CH}$ , appearing at 5.6-6.5 ppm. There is a small amount of non-conjugated double bonds in tung oil, in agreement with the chemical composition in Table 3.3.

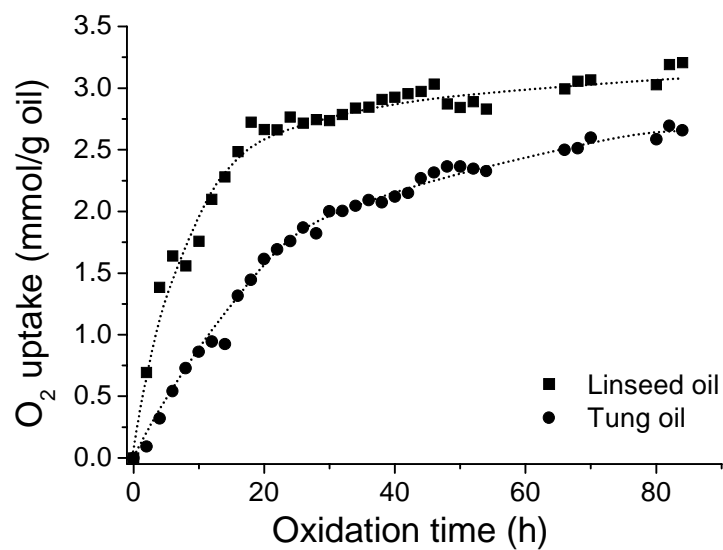


**Figure 3.11.**  $^1\text{H}$  NMR spectra of linseed oil and tung oil.

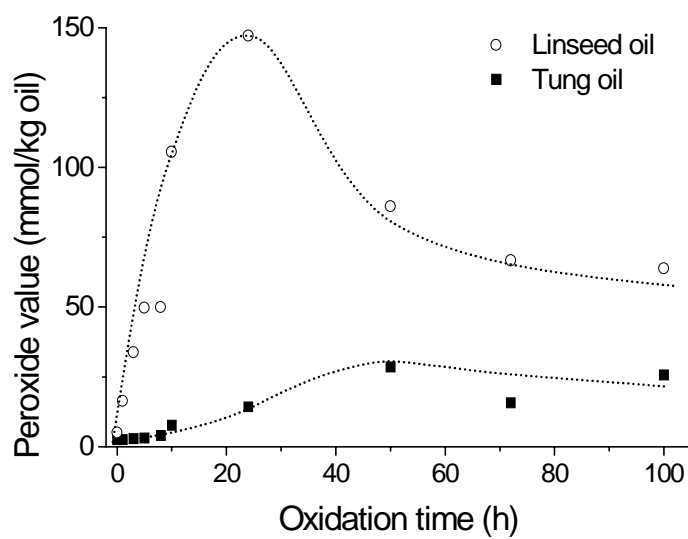
### 3b.4. Oxygen uptake and peroxide evolution during the oxidation of oils

The oxygen uptake during the oxidation of the oils in the presence of Co-EH is shown in Figure 3.12. During the early stage of oxidation (the first 20 h), the amount of  $\text{O}_2$  taken up by linseed oil is significantly larger than by tung oil, and the rate of the  $\text{O}_2$  uptake is also higher. At the end of the observation period (about 85 h), about 3.2 mmol/g  $\text{O}_2$  was consumed by linseed oil, compared to about 2.6 mmol/g for tung oil.

We also measured the peroxide amount during the oxidation of these oils catalyzed by Co-EH, as shown in Figure 3.13. For linseed oil, there is a strong buildup of peroxide during the first about 25 h, amounting to a level of about 150 mmol/kg oil. Afterwards, the peroxide amount decreases drastically to a level of 70 mmol/kg. In a sharp contrast, tung oil demonstrates a completely different picture. First, during the early stage of oxidation, there is a very slow buildup of peroxides; second, the maximum peroxide level, about 25 mmol/kg, is remarkably lower than that of linseed oil.



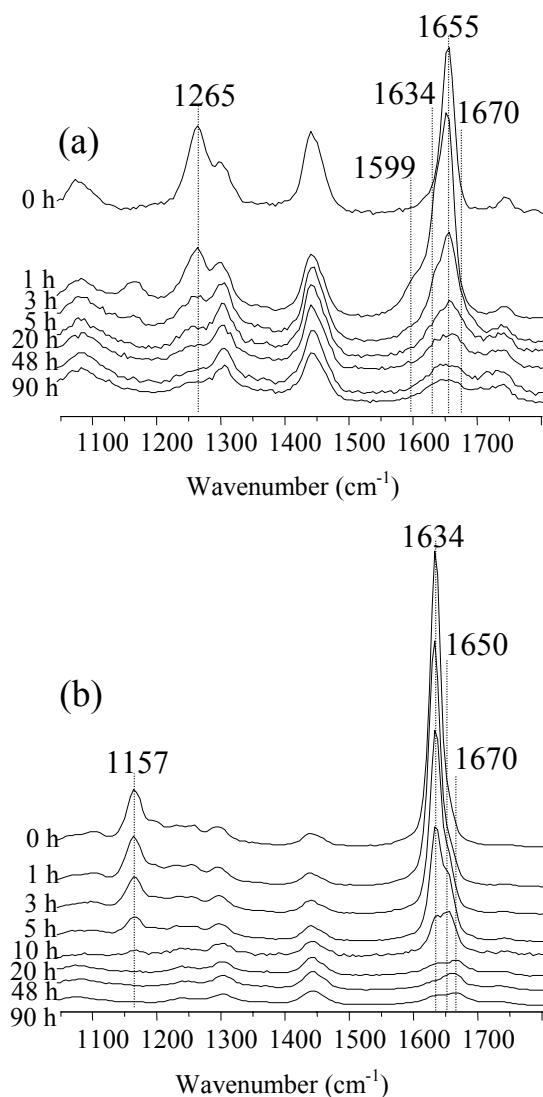
**Figure 3.12.** O<sub>2</sub> uptake during the oxidation of linseed and tung oil catalyzed by Co-EH.



**Figure 3.13.** Evolution of peroxide amount during the oxidation of linseed and tung oil catalyzed by Co-EH.

### 3b.5. Chemical changes during the oxidation of drying oils

In-situ chemical changes during the oxidation of oils were followed by Raman spectroscopy and ATR-FTIR.

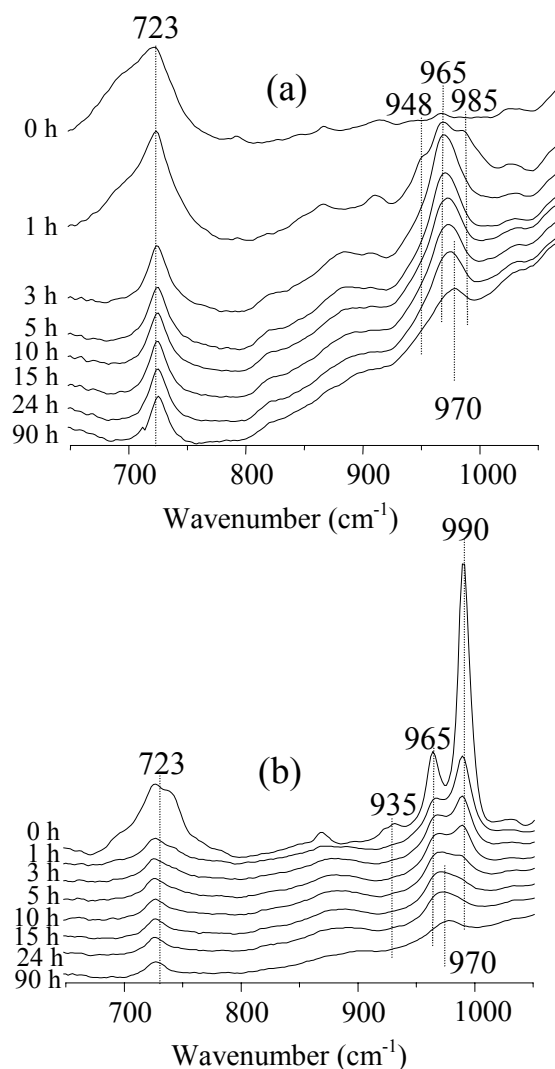


**Figure 3.14.** In-situ Raman spectra ( $1050\text{--}1800\text{ cm}^{-1}$ ) during the oxidation of (a) linseed oil and (b) tung oil.

The strong Raman absorbance from double bonds allows us to follow the variation of C=C during the oxidation. The following peaks are discernible during the oxidation of linseed oil: non-conjugated *cis*-C=C stretching peak at  $1655\text{ cm}^{-1}$ , *cis*-CH=CH wagging at  $1265\text{ cm}^{-1}$ , conjugated C=C stretching at  $1599$  and  $1634\text{ cm}^{-1}$ , and isolated *trans*-C=C stretching at  $1670\text{ cm}^{-1}$ <sup>18,29</sup>, as shown in Figure 3.14a. At the beginning of oxidation, only peaks at  $1655$  and  $1265\text{ cm}^{-1}$  due to non-conjugated *cis*-

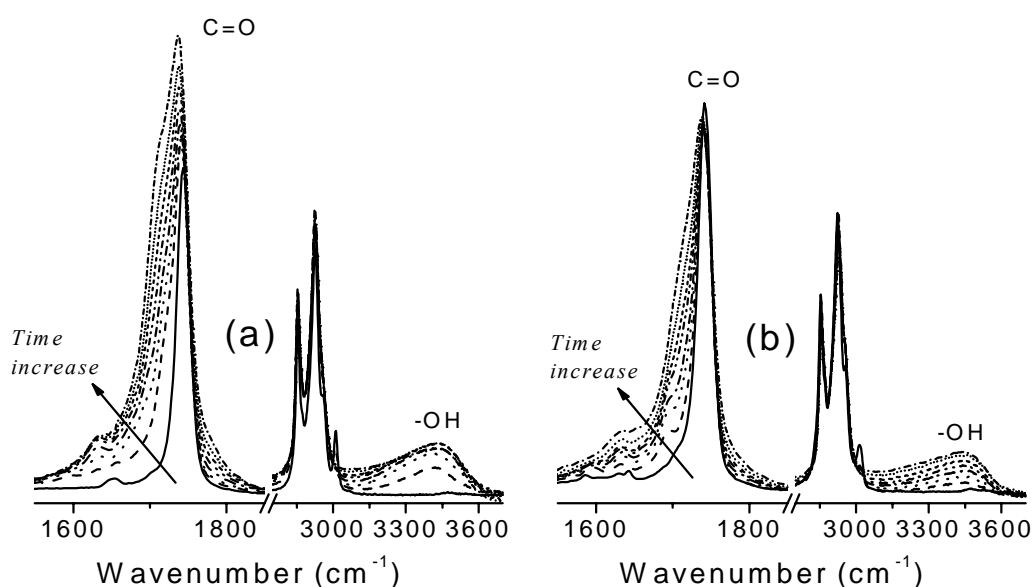
C=C bonds were observed. As the oxidation proceeds new peaks at 1599 and 1634  $\text{cm}^{-1}$  emerge, due to the formation of conjugated double bonds, while the intensity of peaks at 1655 and 1265  $\text{cm}^{-1}$  decreases. As the oxidation continues, all the peaks related to double bonds decrease substantially; after 90 h, only a small peak, likely from conjugated and isolated *trans*-C=C (1670  $\text{cm}^{-1}$ ), is visible.

In the case of tung oil, only peaks due to conjugated double bonds, 1634  $\text{cm}^{-1}$  and 1157  $\text{cm}^{-1}$  (conjugated C=C-H wagging), are shown at the beginning of oxidation (Figure 3.15b). During the course of oxidation, these two peaks decrease steadily; eventually, similar to linseed oil, only a small peak due to conjugated and isolated *trans*-C=C is left after 90 h.



**Figure 3.15.** In-situ ATR-FTIR spectra (650-1050  $\text{cm}^{-1}$ ) during the oxidation of (a) linseed oil and (b) tung oil.

In-situ IR spectra (Figure 3.15) during the oxidation of these two oils reflect chemical changes similar to Raman spectra. For linseed oil, there is only one peak (*cis*-C=C-H bending at  $723\text{ cm}^{-1}$ ; this peak is also from  $\text{CH}_2$  skeletal vibration<sup>29</sup> at  $t = 0$ , while for tung oil several peaks related to conjugated double bonds are visible. During the oxidation, the IR absorptions undergo transitions (peak assignments are referred to in **3a.5**) similar to what have been observed by Raman spectroscopy. At the end of the observation period (90 h), for both oils only a small peak at  $970\text{ cm}^{-1}$  (isolated *trans*-C=C-H) is left.

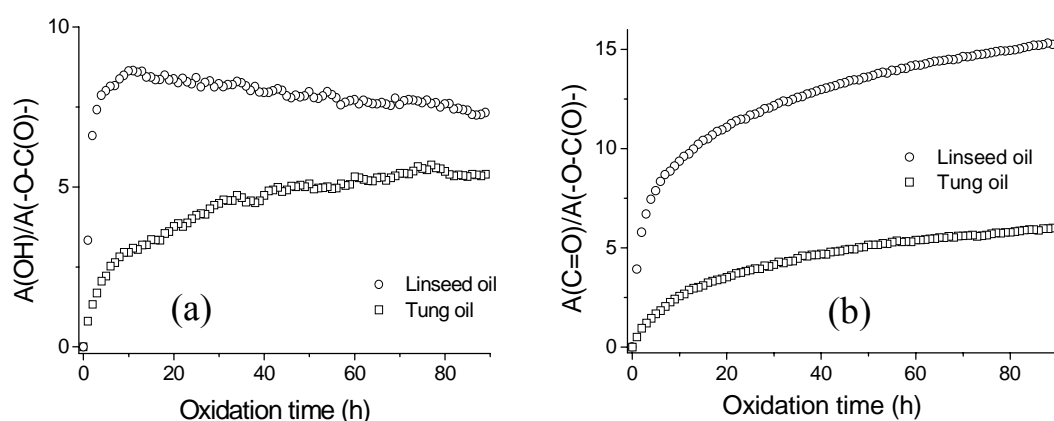


**Figure 3.16.** ATR-FTIR spectra ( $1500\text{--}3700\text{ cm}^{-1}$ ) during the oxidation of (a) linseed oil and (b) tung oil in the presence of Co-EH. Spectra were collected at time = 0, 1, 3, 5, 10, 20, 48, and 90 h.

In addition to the variation of double bonds, ATR-FTIR allows us to follow quantitatively the formation of nonvolatile byproducts, including C=O and OH containing species. Figure 3.16 shows the ATR-FTIR spectra ( $1500\text{--}3700\text{ cm}^{-1}$ ) for linseed oil and tung oil during the oxidation. The emergence of a broad peak in the range of  $3100\text{--}3600\text{ cm}^{-1}$  indicates the formation of hydroperoxides, alcohols, and acids. Meanwhile, the peak centered at  $1720\text{ cm}^{-1}$  corresponding to C=O absorption broadens significantly during the oxidation, implying the formation of carbonyl-containing species, such as aldehydes, ketones, and carboxylic acids. All these changes are in agreement with generally accepted oxidation mechanisms.

On the other hand, there is also noticeable difference in the formation of C=O and OH containing species between linseed and tung oil. For instance, the carbonyl peak appears to broaden to a larger extent for linseed oil than for tung oil. Besides, with careful examination, we notice that for linseed oil the intensity of the broad peak ( $3100\text{-}3600\text{ cm}^{-1}$ ) increases during the first about 10 h of oxidation, followed by a gradual decrease. These peaks are quantified against an internal standard (a peak corresponding to  $\text{-C(O)-O-}$  ester peak at  $1178\text{ cm}^{-1}$ ), and results are given in Figure 3.17.

For linseed oil, the peak area for OH-containing species increases very rapidly during the first 10 h; this is a clear indication that the formation of hydroperoxides is predominant during this period. After reaching a maximum, this peak intensity decreases gradually due to decomposition of formed hydroperoxides. This decrease is, however, not as sharp as the decrease we observed in the peroxide evolution (Figure 3.13). It is reasonable that the formation of carboxylic acids and alcohols during this period would compensate the intensity decrease due to the decomposition of hydroperoxides, leading to an overall gradual decrease in the OH containing species up to 90 h. On the other hand, for tung oil, a different trend was observed: the amount of OH containing species formed during the early stage of oxidation is much lower than in the case of linseed oil, and its level keeps increasing throughout the observation period. This observation suggests that, in comparison with linseed oil, a much lower amount of hydroperoxides is formed during the oxidation of tung oil.

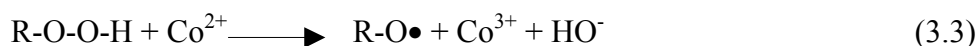


**Figure 3.17.** (a) The intensity of OH containing species and (b) the intensity of C=O containing species formed during the oxidation of linseed oil and tung oil as a function of oxidation time (peak area normalized against the ester  $\text{-O-C(O)-}$  stretching peak at  $1178\text{ cm}^{-1}$ ).

The amount of C=O containing species formed during the oxidation for both linseed and tung oil increases as a function of oxidation time, as depicted in Figure 3.17b. The nonvolatile C=O containing species are the products of some side reactions such as  $\beta$ -scission<sup>11,12</sup> and Russell termination<sup>13,14</sup>. The larger amount of the formed C=O containing species for linseed oil is very likely due to the higher amount of hydroperoxides formed (see Figure 3.13) during the course of oxidation, which in turn leads to a higher amount of free radicals.

### 3b.6. Discussion

The aforementioned results clearly indicate that there is a significant difference in the oxidation behavior between linseed oil and tung oil. For linseed oil, the significant O<sub>2</sub> uptake, together with a strong buildup of the peroxide amount, indicates that the formation of ROOH (eqns. 3.1 and 3.2) is dominant during the early stage of the oxidation. After that period, the decrease in the amount of peroxides indicates that decomposition of ROOHs, catalyzed by the Co catalyst, as shown in eqns. 3.3 and 3.4 takes place much faster than the ROOH formation.



From Figure 3.12 it is obvious that the oxygen uptake slows down after the first 20 h, probably due to the fact that at this point most of the double allylic hydrogen atoms have been abstracted. The H-abstraction from a monoallylic group is very likely much slower than from a double allylic site, resulting in a slower ROOH formation. Meanwhile, since ROOH decomposition does not depend on the concentration of double allylic C-H bonds, the reactions shown in eqns. 3.3 and 3.4 become more favorable than reactions in eqns 3.1 and 3.2, as evidenced by the significant decrease in the amount of peroxides (Figure 3.13) after around 20 h. Once RO• and ROO• are formed (via eqns. 3.3 & 3.4), the occurrence of  $\beta$ -scission and Russell termination (Chapter 2) is inevitable, clearly indicated by the substantial broadening of the C=O peak (Figure 3.17b) due to the formation of non-volatile



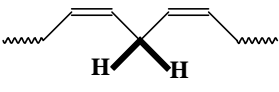

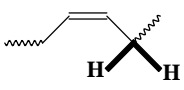
aldehydes, carboxylic acids, and ketones, even during the very early stage (first 10 h) of oxidation. During the early stage of oxidation, the concentrations of R•, RO•, ROO• are most probably not very high; as a consequence, termination by radical-radical recombination (eqns. 2.11-2.16 in Chapter 2) may be less favorable than the  $\beta$ -scission reactions. In other words, the probability of the two radicals finding each other is much less than  $\beta$ -scission. As the amount of radicals increases, the chance for the termination by radical-radical recombination increases, leading to oligomerization. The oligomerization can be also partially ascribed to the addition of free radicals to the conjugated double bonds that are formed at the same time of hydroperoxides being generated.

A different trend is observed when tung oil is oxidized. The low peroxide amount throughout the oxidation, coupled with the lower oxygen consumption in comparison with linseed oil, suggests that the reaction 3.2 (H-abstraction from a monoallylic position) is not favorable during the oxidation of tung oil. As a consequence, reactions 3.3 and 3.4 also take place to a lesser extent. Instead of the reaction 3.2, the radical addition to the conjugated double bonds (eqn. 3.5) is probably the most favorable reaction during the oxidation of tung oil, which is indicated by the sharp decrease in the conjugated double bonds (e.g. 1634  $\text{cm}^{-1}$  in Figure 3.14b).



As the consequence of the low buildup of ROOH for tung oil, the formation of RO• and ROO• (eqns. 3.3 and 3.4) is supposed to be less than in the case of linseed oil. The formation of C=O and OH containing species via  $\beta$ -scission and/or Russell terminations is, therefore, much less during the oxidation of tung oil (Figure 3.17). Nevertheless, RO• can still form in low amounts from the decomposition of RO-OR or decomposition of ROOH (formed via H-abstraction of monoallylic groups). It is very likely that, for tung oil, a major portion of free radicals will directly add to (conjugated) double bonds, which leads to higher oligomers (also see eqns 2.17-2.19)<sup>23</sup> as compared to the radical-radical recombination mechanism.

Table 3.4. Bond dissociation energies (BDE) of several bonds (in bold) present during the oxidation of unsaturated fatty acid chain<sup>30</sup>.

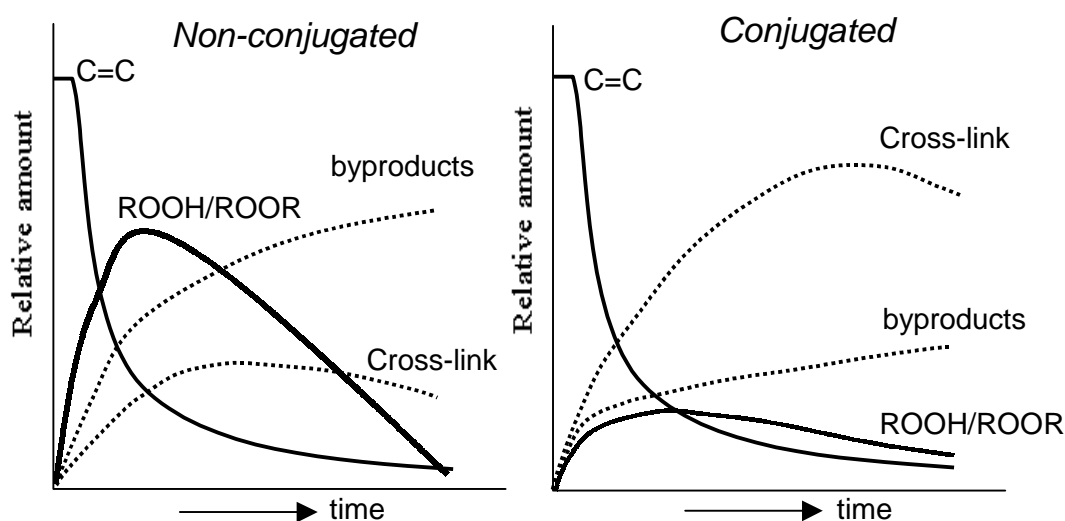
Bond type	BDE (kJ/mol)
RO-OH	104-167
	272
 ( $\pi$ -bond)	284
	322

We attempt to interpret the difference in the oxidation mechanism between linseed oil and tung oil in terms of bond dissociation energy (BDE). The BDEs of relevant bonds during the oxidation are listed in Table 3.4. It is known that the lower the BDE of a bond, the easier the dissociation of the bond. Among the bonds that are present during the oxidation of unsaturated fatty acids, RO-OH has the lowest BDE, indicating that this O-O bond can be readily broken down as soon as ROOH is formed, resulting in alkoxy free radicals. After the formation of the free radicals, they can abstract a hydrogen atom from either a double allylic or a monoallylic group, or add to a double bond. From Table 3.4, it is obvious that as long as there are nonconjugated double bonds available, the H-abstraction from the double allylic group is the most favorable reaction; this is why a strong buildup of hydroperoxide is observed during the oxidation of linseed oil. On the other hand, for tung oil, there is almost no double allylic group available, and the preferred reaction pathway for a free radical is to add to a (conjugated) double bond (BDE of the  $\pi$ -bond: 284 kJ/mol), other than abstracting a monoallylic H atom (BDE of the monoallylic C-H: 322 kJ/mol).

### 3b.7. Conclusions

With respect to the results obtained, Figure 3.18 summarizes the oxidation processes during the oxidation of unsaturated fatty acids containing non-conjugated and conjugated double bonds. During the oxidation for fatty acids containing non-conjugated double bonds, there is a strong buildup of hydroperoxides; in the meantime, non-conjugated double bonds are converted into conjugated double bonds.

The hydroperoxides are then decomposed into free radicals. These radicals form either cross-links via mainly radical recombination and partially addition to conjugated double bonds, or form byproducts (Figure 3.18). On the other hand, for conjugated systems, the oxidation takes place in a different way even though oxidation products appear to be similar. The buildup of hydroperoxides is much less due to the direct radical addition to (conjugated) double bonds, consequently leading to the formation of a higher amount of cross-links and a lower amount of byproducts.



**Figure 3.18.** Summary of oxidation processes during the oxidation of unsaturated fatty acids containing non-conjugated and conjugated double bonds.

### References

1. Weissenborn P.K., et al., *J. Coat. Techn.* 72(906) (2000) 65.
2. Ostberg G., Hulden M., *Prog. Org. Coat.* 24 (1994) 281.
3. Hurley R., Buono F., *J. Coat. Techn.* 54(694) (1982) 55.
4. Weissenborn P.K., et al., *Prog. Org. Coat.* 40(1-4) (2000) 253.
5. Ciampi E., et al., *Langmuir* 16(3) (2000) 1057.
6. Wang C., Jones F.N., *J. Appl. Polym. Sci.* 78(9) (2000) 1698.
7. Beetsma J., *Pigment Resin Techn.* 27(11) (1998) 12.
8. Beetsma J., Hofland A., *Surface Coat. Intern.* 81(10) (1998) 491.
9. Bieleman J., "Additives for Coatings", Wiley/VCH, Weinheim (2000) Chp. 7.
10. Hurley R., Buono F., *J. Coat. Techn.* 54(694) (1982) 55.
11. Hancock R.A., Leves N.J., *Prog. Org. Coat.* 17 (1989) 321.

12. Chang J.C.S., Guo Z., *Atmosph. Environ.* 32 (1998) 3581.
13. Russell G.A., *J. Am. Chem. Soc.* 78 (1956) 1047.
14. Russell G.A., *J. Am. Chem. Soc.* 79 (1957) 3871.
15. Muizebelt W.J., et al., *J. Coat. Techn.* 70(876) (1998) 83.
16. Roginskii V.A., *Kinetics and Catalysis* 31(3) (1990) 475.
17. van Gorkum R., et al., *Inorg. Chem.* 43 (2004) 2456.
18. Agbenyega J.K., Claybourn M., Ellis G., *Spectrochimica Acta* 47A(9/10) (1991) 1375.
19. Ellis G., Claybourn M., *Spectrochimica Acta* 46A(2) (1990) 227.
20. Colthup B., et al., “*The Handbook of Infrared and Raman Characteristic Frequencies of Organic Molecules*”, Academic Press (1993) 82.
21. Mallécol J., et al., *Prog. Org. Coat.* 39(1-3) (2000) 107.
22. Muizebelt W.J., Nielen W.F., *J. Mass. Spec.* 31 (1996) 545.
23. Muizebelt W.J., Hubert J.C., Nielen M.W.F., Klaasen R.P., Zabel K.H., *Prog. Org. Coat.* 40(1-4) (2000) 121.
24. Martens C.R., “*Alkyd Resins*”, Reinhold Publ., New York, (1961) 34.
25. Frankel E.N., Garwood R.F., Vinson J.R., Weedon B.S.L., *J. Chem. Soc., Perkin Trans. I* (1982) 2707.
26. Wicks Z.W., Jones F.N., Pappas S.P., “*Organic Coatings Science and Technology*”, Wiley/VCH (1999) 39.
27. [www.presens.de](http://www.presens.de)
28. American Oil Chemists’ Society, Cd 8b-53.
29. Oyman Z.O., Ming W., van der Linde R., *Prog. Org. Coat.* 48(1) (2003) 80.
30. Fossey J., Lefort. D., Sorba J., “*Free Radicals in Organic Chemistry*”, Wiley (1995) 33, 276.
31. Muizebelt W.J., van Velde J.W., et al., *Adv. Org. Coat. Sci. Techn. Ser.* 13 (1991) 57.



## Chapter 4

### Effect of a dinuclear manganese complex (MnMeTACN) and polyamines on the oxidation of ethyl linoleate \*

#### Summary

The catalytic activity of a dinuclear manganese-based complex,  $[Mn^{IV}_2(\mu-O)_3L_2](PF_6)_2$  (MnMeTACN) ( $L = 1,4,7$ -trimethyl-1,4,7-triazacyclononane), and the effect of polyamines are investigated on the oxidation of ethyl linoleate. MnMeTACN in combination with polyamines demonstrates higher catalytic activity than a commercially available Mn-based catalyst (Nuodex Web-Mn) and comparable activity to a Co-based catalyst (Nuodex Web-Co) during the oxidation of EL from emulsions in spite of a certain induction period. When MnMeTACN is molecularly mixed with EL in a co-solvent (methanol), MnMeTACN alone is found to be a very active catalyst for EL oxidation similar to the catalytic activity of a Co-based catalyst. The main role of polyamines is proposed as increasing the miscibility between MnMeTACN and EL, and decomposing the formed hydroperoxides. However, an excessive amount of polyamines would not contribute to the formation of oligomers during oxidation. In the presence of MnMeTACN/polyamine, a larger amount of volatile byproducts is formed due to the accelerated  $\beta$ -scission side reactions. MnMeTACN and MnMeTACN/polyamines appear to be potential alternatives for commercial Co- and Mn-based driers for alkyd coatings.

---

\* Part of this Chapter has been published: Z.O. Oyman, W. Ming, F. Micciché, E. Oostveen, J. van Haveren, R. van der Linde, *Polymer*, 45 (2004) 7431-7436, and presented at 228<sup>th</sup> ACS Meeting (Aug. 2004, Philadelphia): Z.O. Oyman, W. Ming, R. van der Linde, *Polym. Prep.* 45(2) (2004), 213-214.

#### 4.1. Introduction

Cobalt-based catalysts (*e.g.*, cobalt carboxylates), which are currently widely used in alkyd coatings to promote the oxidative drying, were recently reported as potentially *carcinogenic* to tissues and lungs<sup>1-3</sup>. In the near future, more stringent environmental legislations will force the coatings industry to search for environmentally benign alternatives for cobalt-based catalysts. Manganese and iron complexes are generally recognized as more environmentally benign than cobalt-based compounds<sup>3</sup>. Commercially available manganese-based catalysts, such as manganese octoate derivatives, however, are much less effective than cobalt-based ones.

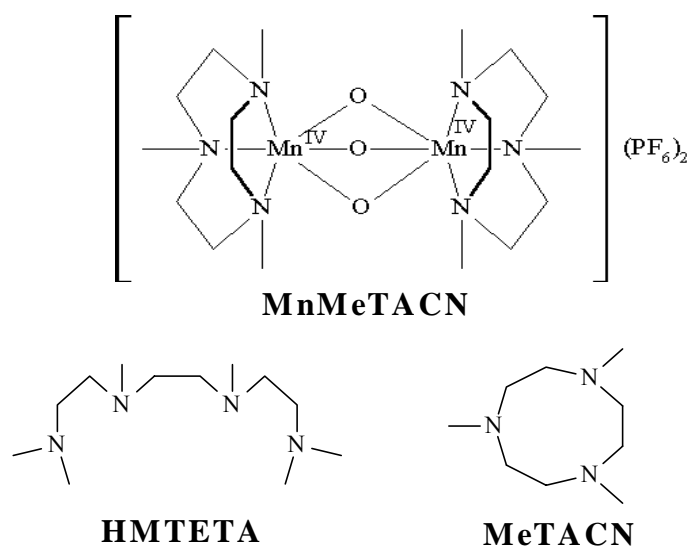
Due to strict legislations on emissions of the volatile organic compounds (VOC), solvent-borne alkyds will be greatly shifted to the more environmentally friendly alternatives, such as water-borne alkyd coatings. Conventional cobalt-based catalysts used in solvent-borne alkyds, however, are not suitable for their water-borne counterparts<sup>4</sup>. Water is one of the strongest complexing agents with  $\text{Co}^{3+}$ , leading to the formation of  $[\text{Co}(\text{H}_2\text{O})_6]^{3+}$  complex<sup>5</sup>. This complex has a weaker oxidation potential that results in the loss of catalytic capability of the cobalt-based catalysts. Proprietary ligands are used to minimize this effect by pre-complexing cobalt-based catalysts<sup>6</sup>. Their main role is to make catalysts emulsifiable in water so that the risk of the formation of cobalt-hydrate complexes is reduced. Even though the effect of water on the catalyst is reduced, the concentration of emulsifiable catalysts for a similar drying effect is usually higher than in solvent-borne alkyds.

Ethyl linoleate (EL) has been widely used as a model compound due to the complex nature of alkyds during the network formation<sup>7-12</sup>. Warzeska *et al.* observed a promising catalytic activity of a commercial Mn-based catalyst containing chelating ligands such as 2,2'-bipyridine (bpy) on the oxidation of EL<sup>13,14</sup>. Wu *et al.* recently reported a manganese-based complex based on 1,1,1,5,5,5-hexafluoroacetylacetonate and effect of 2-aminomethylpyridine and 2-hydroxymethylpyridine chelating agents on the drying of solvent-borne and water-borne alkyd coatings<sup>15</sup>.

In this Chapter we demonstrate a dinuclear manganese-based complex,  $[\text{Mn}^{\text{IV}}_2(\mu\text{-O})_3\text{L}_2](\text{PF}_6)_2$  (MnMeTACN) ( $\text{L} = 1,4,7$ -trimethyl-1,4,7-triazacyclononane), which may be a potential alternative for cobalt-based catalysts for alkyd coatings. MnMeTACN (Figure 4.1) was originally designed to catalyze low temperature

bleaching of stains<sup>16-18</sup> and it was shown that MnMeTACN and its derivatives act as highly effective catalysts during the oxidation of organic molecules<sup>19-21</sup>. Chemical bleaching consists of oxidative/reductive decomposition of double bonds present in the chromophoric groups<sup>22</sup>. Similarly, chemical drying of alkyd coatings involves the oxidation of unsaturated fatty acid chains in the alkyd<sup>7-14</sup>. Hage *et al.* showed that MnMeTACN also catalyzes epoxidation of alkenes at room temperature and oxidation of polyphenolic substrates in the presence of hydrogen peroxide<sup>19</sup>.

Some polyamines such as 1,1,4,7,10,10-hexamethyltriethylenetetramine (HMTETA) (Figure 4.1) were recently used as ligands in Cu-mediated atom transfer radical polymerizations (ATRP)<sup>23,24</sup>. Polymerization rates in the presence of polyamines were found to be higher than the rates with bpy derivatives. Tertiary amines were also used as accelerators in the curing of unsaturated polyester compositions<sup>25</sup>. These results inspired us to use polyamines to possibly increase the catalytic activity of MnMeTACN on the oxidation of EL.



**Figure 4.1.** Chemical structures of MnMeTACN and polyamines. Detailed study on the electrochemistry and geometry of MnMeTACN was given elsewhere<sup>18,26</sup>.

In this Chapter we monitor the catalytic activity of MnMeTACN and effects of polyamines on the oxidation reactions of EL. We demonstrate the kinetics of oxidation of EL by attenuated total reflectance (ATR)-infrared spectroscopy. We use Raman spectroscopy to study the effects of MnMeTACN/polyamines on the variation and disappearance of the double bonds of EL. The effects of catalysts on the oxygen uptake of EL and the evolution of peroxides are examined. Size exclusion



chromatography (SEC) is used to bring in more insights on the oligomerization of EL in the presence of MnMeTACN and polyamines. The formation of volatile byproducts is demonstrated using head-space GC-MS. Using a co-solvent, we further examine the catalytic activity of MnMeTACN on the oxidation of EL. The catalytic cycle of MnMeTACN during the oxidation of EL is proposed and the possible role of polyamines is discussed.

## 4.2. Experimental

### 4.2.1. Materials

Ethyl linoleate (EL, 98%) and technical grade EL, containing 73% EL, 19% ethyl oleate, 6% ethyl palmitate, and 2% ethyl stearate as determined by GC-MS, were obtained from Fluka. Co(II)-2-ethylhexanoate (65% w/w solution in white spirits), 1,4,7-trimethyl-1,4,7-triazacyclononane (MeTACN, ~97.7%), 1,1,4,7,10,10-hexamethyl triethylenetetramine (HMTETA, ~97%) and *tert*-butyl hydroperoxide (5.0-6.0 M in decane solution, TBH) were obtained from Sigma-Aldrich Chemie B.V. (Zwijndrecht, The Netherlands). Sodium dodecyl sulphate (SDS, 99%) was obtained from Merck B.V. (Amsterdam, The Netherlands). Nuodex Web-Co (an emulsifiable drier containing 6 w% Co) and Nuodex Web-Mn (an emulsifiable drier containing 9 w% Mn) were obtained from Sasol Servo B.V. (Delden, The Netherlands). MnMeTACN was a gift from Unilever R&D, Vlaardingen, The Netherlands. Chemicals were used without further purification unless otherwise stated.

### 4.2.2. Emulsion preparation

Under magnetic stirring, EL was emulsified by dropwise addition of a mixture of water and surfactant (containing 1 w% SDS). First, a W/O (water-in-oil) emulsion was obtained, and then phase-inverted into an O/W (oil-in-water) emulsion after > 50% of water and surfactant mixture was added. A Branson type ultrasound sonifier was used for 5 min, with the emulsion temperature reaching ~80 °C. In the emulsion, the amount of EL was kept at 37 w%. After cooling down to room temperature, various catalysts (0.07% metal/oil, w/w) were added. When polyamines were used, they were added directly to the emulsion before the addition of catalyst with molar ratios of 1/1, 1/3, and 1/6 (Mn complex/polyamine). Change in particle size of emulsions was measured on a Coulter particle size analyzer (model LS 230).

Typically, the average particle size was around 0.95  $\mu\text{m}$ , and the change in particle size over a period of 2 days was negligible within the experimental error.

#### **4.2.3. Characterization techniques and methods**

Detailed description of techniques and methods is given in the Appendix.

Oxidation of EL emulsions in the presence of catalysts was followed *in-situ* by time-resolved ATR-FTIR. EL emulsions were deposited ( $\sim 100 \mu\text{m}$ ) onto the diamond crystal in the ATR unit of IR spectrometer. Then, spectra were collected each 20 min for a period of  $\sim 15$  h. The first spectrum was discarded due to the high interference of water with EL.

EL emulsions in the presence of different catalysts were deposited ( $\sim 100 \mu\text{m}$ ) onto glass slides for time-resolved Raman spectroscopy.

A fiber-optic oxygen meter was used to measure the oxygen uptake of EL (4 g) from emulsions. EL in emulsion was placed in a 6-L container.  $\text{N}_2$  was purged into the flask to accelerate the water evaporation, which took about 40-50 min. During water evaporation virtually no oxidation took place (Chapter 3). After water evaporation, air was purged for 1 min and the container was sealed and the oxygen amount in the gas phase was monitored at room temperature. The oxygen concentration was expressed as mol  $\text{O}_2$  consumed per mol of EL in the presence of various catalysts.

EL emulsions (40 g) (50 w% in EL) were placed in Petri dishes ( $\sim 20$  cm radius). 1 g of EL was withdrawn at different time intervals for peroxide value determination during the oxidation. The peroxide amount during EL oxidation was determined according to an American Oil Chemists' Society (AOCS) method<sup>27</sup>. Duplicate measurements were performed for each sample and average values were taken.

Oligomerization of EL was followed by size exclusion chromatography (SEC) on a Waters GPC instrument equipped with a Waters model 510 pump, a model 410 differential refractometer (40  $^\circ\text{C}$ ), and a low molar mass column. THF was used as the eluent. EL was dissolved in THF ( $\sim 1$  mg/mL) for SEC analysis.

Electrospray ionisation-mass spectrometry (ESI-MS) analysis was carried out on an Agilent Technologies 1100 series system, using a G1313A autosampler, a G1315B UV-DAD detector at 254 nm and an Agilent MDS type SL G1946D mass

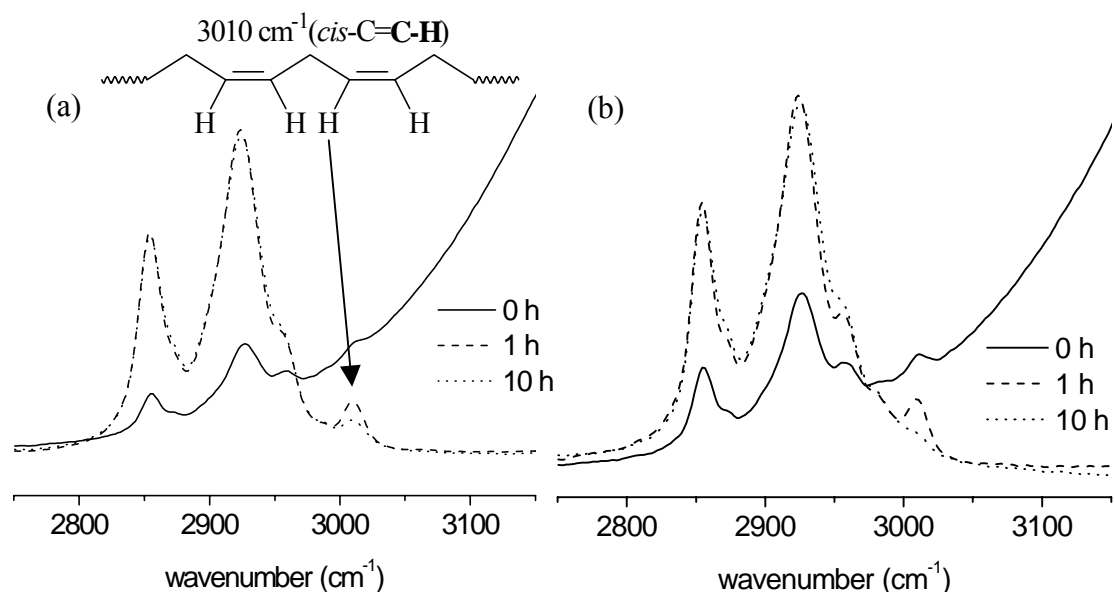
spectrometer with atmospheric pressure electrospray ionisation. All data were processed with HP chemstation software. Samples were dissolved in methanol (10 mg/mL), which was used as received for ESI-MS analysis. Typical injection volumes were 10  $\mu$ L.

#### 4.2.4. EL oxidation in solution

Using a co-solvent (methanol) a homogeneous solution of MnMeTACN and EL (98% pure) was obtained. 0.07% (w/w, metal/EL) of catalysts were dissolved in 1 g of methanol then 1 g of EL was added to the solution to obtain 50% (w/w) EL solution in methanol. The prepared solution was immediately placed in a 1-L sealed flask. Under continuous stirring, EL was oxidized at room temperature. During EL oxidation, several samples were withdrawn at different time intervals and dissolved in  $\text{CDCl}_3$  (10 mg/mL) for  $^1\text{H}$  NMR analysis. When purified EL was used, existing hydroperoxides in EL were removed by eluting over a basic  $\text{Al}_2\text{O}_3$  column.

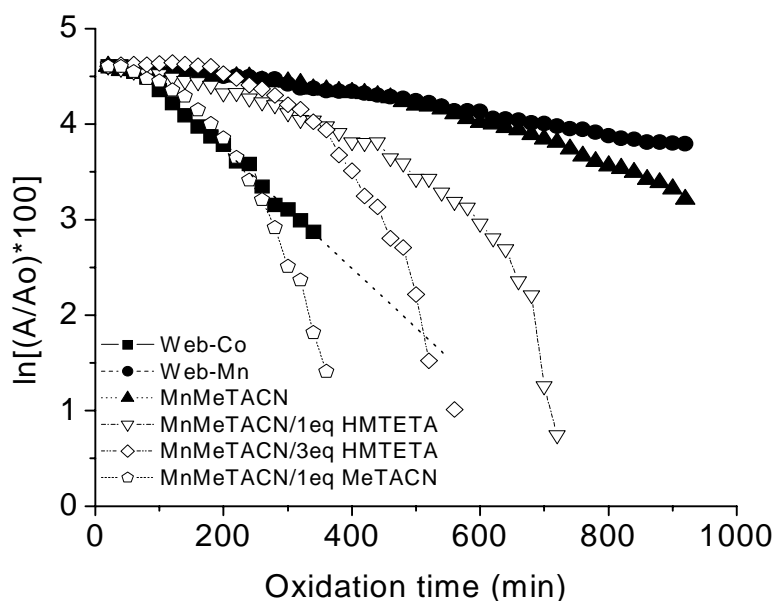
Volatile byproducts were determined by head-space GC-MS. 0.07% (metal/EL, w/w) MnMeTACN was dissolved in methanol. Afterwards, EL was added (70% w/w EL solution was prepared). An aliquot of 10 mg of EL was placed in a 20 mL head-space vial for each measurement, followed by the addition of 1  $\mu$ L cyclohexane solution (0.37 M in xylene) as an internal standard. Further experimental details for head-space GC-MS are given in the Appendix.

### 4.3. Chemical changes during the oxidation of EL from emulsions



**Figure 4.2.** ATR-FTIR spectra of EL from emulsions showing the variation of *cis*-C=C-H symmetric stretch peak during the oxidation in the presence of (a) 0.07% MnMeTACN and (b) 0.07% MnMeTACN/3 eq. HMTETA.

Chemical changes during the oxidation of EL from emulsions are investigated by ATR-FTIR. The decrease in the intensity of the symmetric *cis*-C=C-H stretch peak ( $3010\text{ cm}^{-1}$ ) indicates the oxidation of EL. As shown in Figure 4.2, water peak at 0 h interferes with the peaks of interest in EL. After the evaporation of water, oxidation rates in the presence of different catalysts can be derived from the kinetic plots, *i.e.*, the natural logarithm of *cis*-C=C-H stretch peak intensity (normalized against the ester peak (C-O) at  $1178\text{ cm}^{-1}$ ) versus time.



**Figure 4.3.** Plots of natural logarithm of the peak intensity (normalized values) of the symmetric *cis*-C=C-H stretch peak ( $3010\text{ cm}^{-1}$ ) of EL versus time followed by ATR-FTIR. The metal content was 0.07 w% on the basis of EL. Lines were added to aid the eye.

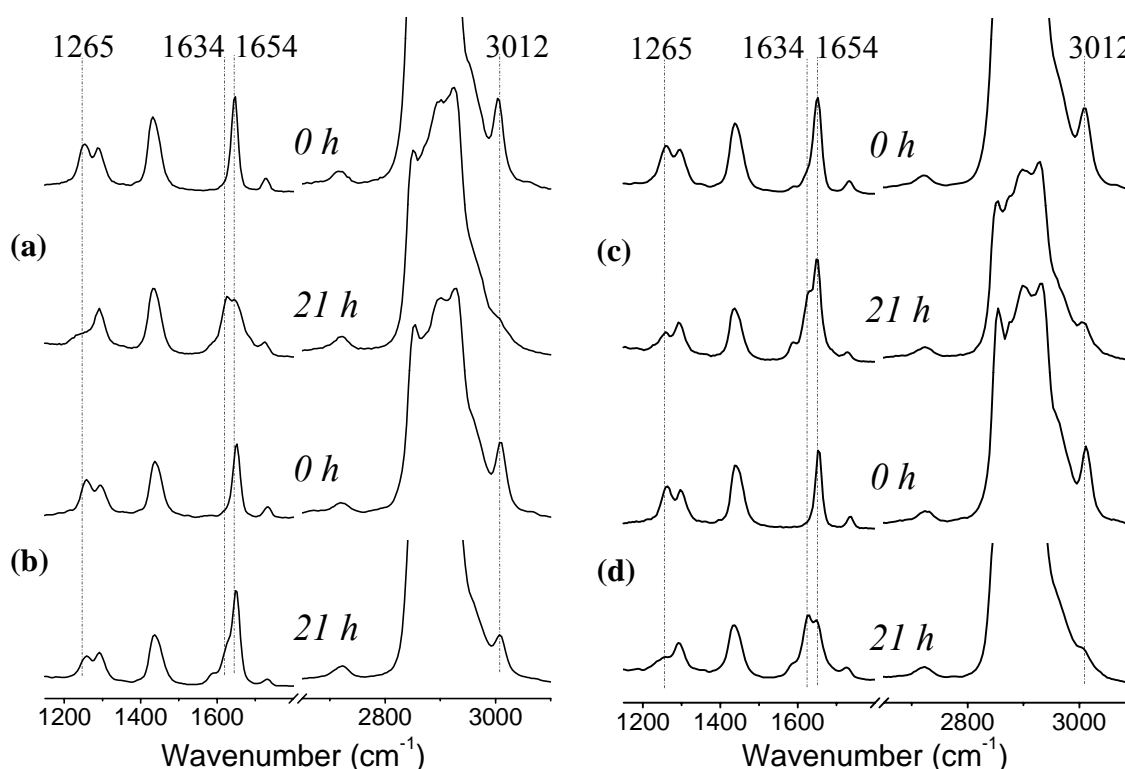
As shown in Figure 4.3, the catalytic activity of MnMeTACN is slightly higher than that of a commercial Mn-based catalyst (Nuodex Web-Mn), but much lower than a commercial Co-based catalyst (Nuodex Web-Co). When 1 equiv. HMTETA is combined with MnMeTACN, the conversion of *cis*-C=C-H is significantly accelerated. This effect is more pronounced upon the addition of 3 equiv. HMTETA. Although a 200-min “induction” period is still observed for the MnMeTACN/3 eq. HMTETA combination, an extent of reaction similar to the Web-Co-catalyzed system would be reached after about 9 h of oxidation. We also combined MnMeTACN with 1 equiv. of MeTACN, a cyclic polyamine and the ligand in the MnMeTACN complex (Figure 4.1), for the oxidation of EL. With MnMeTACN /1 eq. MeTACN combination, the “induction” period is decreased to about 1 h during EL oxidation and much faster conversion is obtained than with Web-Co. HMTETA was also combined with Web-Mn, but the increase in catalytic activity is much less significant (data not shown).

Chemical changes during the oxidation of EL from emulsions are also investigated by Raman spectroscopy. Raman spectroscopy previously proved to be a suitable technique to differentiate the formation of various C=C double bonds with

high intensities at  $1599\text{-}1680\text{ cm}^{-1}$ <sup>28</sup>. Moreover, existence of water at the beginning of the oxidation does not interfere with Raman spectra of EL.

As shown in Figure 4.4, Raman spectra of EL indicate significant changes of C=C related peaks during oxidation in the presence of catalysts. The *cis*-C=C-H asymmetric stretch ( $3012\text{ cm}^{-1}$ ) and rock ( $1265\text{ cm}^{-1}$ ) peaks of EL have nearly disappeared after 21-h reaction in the presence of Web-Co (Figure 4.4a) and MnMeTACN /3 eq. HMTETA combination (Figure 4.4d). The decrease in *cis*-C=C stretch peak ( $1654\text{ cm}^{-1}$ ) and the appearance of conjugated C=C peak ( $1634\text{ cm}^{-1}$ ) were also clearly observed<sup>29,30</sup>.

Although the peaks at  $3012$  and  $1265\text{ cm}^{-1}$  in the presence of Web-Mn and MnMeTACN also decrease after 21 h (Figure 4.4b&c), the decrease is much less significant than those catalyzed by Web-Co and MnMeTACN/3 eq. HMTETA. In the latter two cases, the peak intensity ratio of  $1634\text{ cm}^{-1}$  (conjugated C=C) over  $1654\text{ cm}^{-1}$  (non-conjugated *cis*-C=C) is much greater after 21-h of reaction, indicating much greater extent of oxidation of EL.

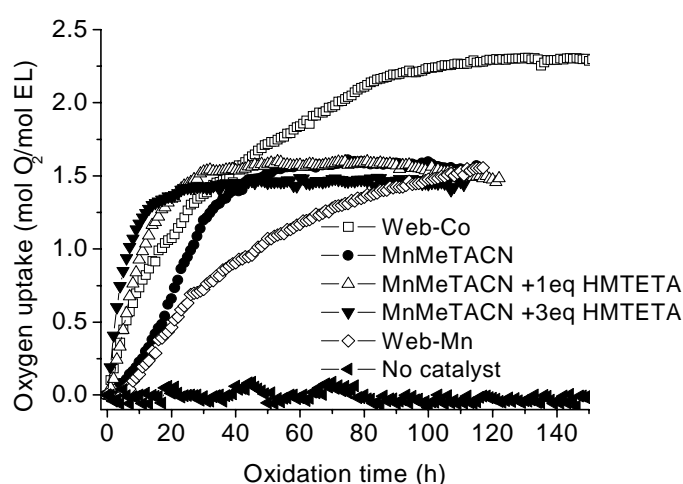


**Figure 4.4.** Raman spectra of EL from emulsions during the oxidation (after 0 and 21 h) in the presence of (a) Web-Co, (b) Web-Mn, (c) MnMeTACN, and (d) MnMeTACN/3 eq. HMTETA. The metal content was 0.07 w% on the basis of EL.

#### 4.4. Role of polyamines during the EL oxidation from emulsions

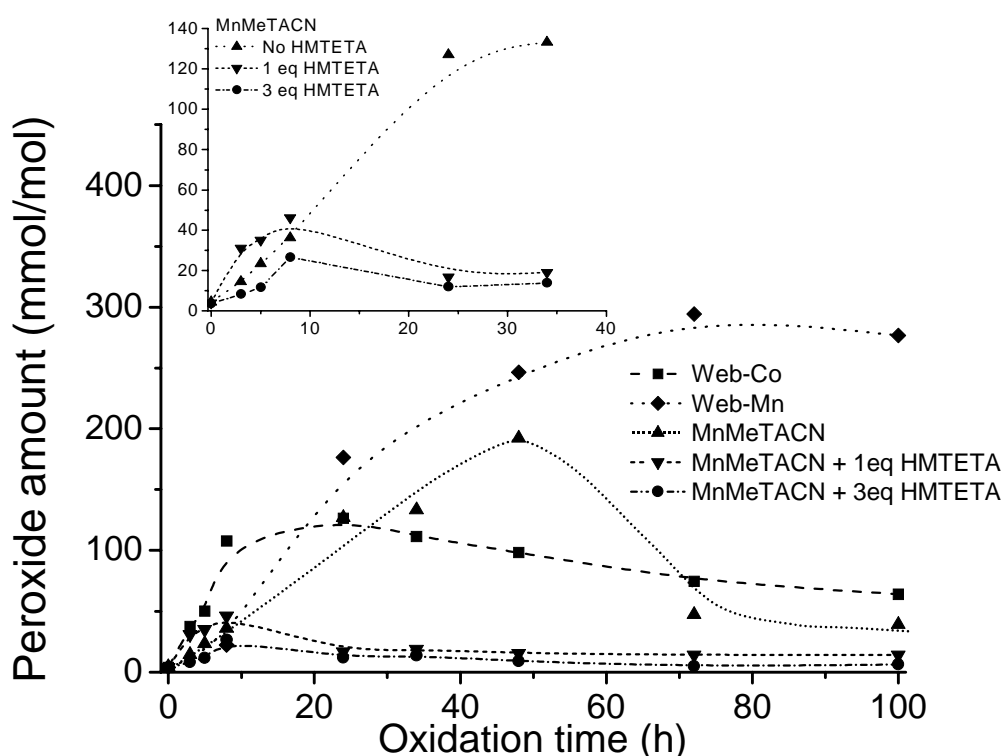
In order to find out the role played by polyamines (*e.g.*, HMTETA) during the oxidation of EL, we used electrospray ionization mass spectrometry (ESI-MS) and  $^1\text{H-NMR}$  to check, in the mixture of MnMeTACN and HMTETA in an aqueous solution, whether a new complex containing HMTETA was formed or not. We did not detect any evidence of the exchanging of HMTETA and MeTACN (data not shown). To illustrate the role of polyamines, oxygen uptake and peroxide amounts were monitored during the oxidation of EL.

Figure 4.5 illustrates the  $\text{O}_2$  uptake results for EL without any catalyst as well as in the presence of various catalysts. In the absence of a catalyst, virtually no oxygen is taken up by EL during the observation period of time (150 h). In the presence of Web-Co, EL takes up a significant amount of  $\text{O}_2$ ; the  $\text{O}_2$  consumption amounts to 2.25 mol per mol of EL after 150 h. Less  $\text{O}_2$  ( $\sim 1.50$  mol/mol EL after 120 h) is consumed when Web-Mn is present as a catalyst. When the MnMeTACN complex was used as a catalyst, although the  $\text{O}_2$  uptake amount is comparable to Web-Mn after 120 h, the pace of the  $\text{O}_2$  uptake is sped up during the early stage (a plateau was reached after about 50 h). The addition of 1 and 3 equiv. HMTETA further accelerates the rate of the  $\text{O}_2$  uptake during the early stage of the EL oxidation. It is clear that, compared to the Web-Mn catalyst, MnMeTACN itself can better enhance the  $\text{O}_2$  uptake of EL, but much faster  $\text{O}_2$  uptake is achieved in the presence of HMTETA.



**Figure 4.5.**  $\text{O}_2$  uptake during the oxidation of EL from emulsions without catalyst as well as in the presence of various catalysts.

It is well established that hydroperoxides (ROOHs) have a crucial role during the oxidation of alkyd resins<sup>8,31,32</sup>. ROOHs are formed and then decomposed to form free radicals (*i.e.*, RO•, ROO•). This sequential formation and decomposition of ROOHs can be greatly enhanced by an appropriate catalyst. An effective catalyst catalyzes both the formation of ROOHs and the decomposition of the formed ROOHs. ROOHs also form and then decompose in the absence of a catalyst; however, this process is very slow without a catalyst<sup>29,31,32</sup>.



**Figure 4.6.** The evolution of peroxide amount during the oxidation of EL under the influence of various catalysts. Lines are added to aid the eye.

We measured the peroxide amounts during the EL oxidation in the presence of various catalysts, as shown in Figure 4.6. The EL we used contains around 4 mmol/mol preformed ROOHs. In the presence of Web-Co, the amount of peroxide increases rapidly to about 50 mmol/mol in 5 h, and reaches a maximum at about 125 mmol/mol after about 20-h oxidation; after that, the peroxide value decreases steadily to 65 mmol/mol after 100 h (some peroxy links exist for oxidized alkyds<sup>9-11</sup>). This observation is in agreement with what was found by Mallegol *et al.*<sup>31</sup>: the Co-catalyst



accelerates the formation and then the decomposition of ROOHs. When Web-Mn is used, a completely different scenario occurs: in the beginning of the EL oxidation, the peroxide amount increases at a slow pace; but it keeps increasing till reaching a maximum at about 300 mmol/mol after about 80 h. This maximum amount of peroxide is much larger than that in the presence of Web-Co, even though the total amount of oxygen consumed in the latter case is much higher (Figure 4.5). This is a clear indication that, in comparison with Web-Co, Web-Mn is a much less effective catalyst in catalyzing both the formation of ROOHs and the decomposition of the formed ROOHs.

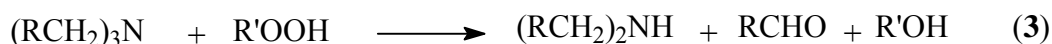
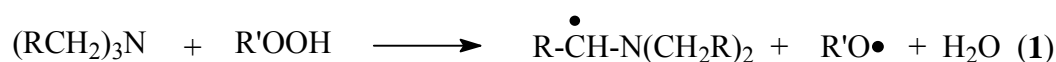
In the presence of MnMeTACN, the amount of peroxides also increases significantly during the EL oxidation. The maximum peroxide amount, 190 mmol/mol (much higher than in the presence of Web-Co), is reached after about 50 h; afterwards, the peroxide amount decreases to about 50 mmol/mol (Figure 4.6). Apparently, the catalytic activity of MnMeTACN falls in between Web-Co and Web-Mn. On the other hand, when MnMeTACN is combined with HMTETA (1 or 3 equiv. to Mn complex), a dramatic effect on the peroxide evolution is observed (Figure 4.6 and its inset). The maximum peroxide amount is much lower than in other cases: 45 mmol/mol for MnMeTACN/1 eq. HMTETA combination, and 25 mmol/mol for MnMeTACN/3 eq. HMTETA combination, respectively. Afterwards, the overall peroxide amount decreases to 20 mmol/mol for MnMeTACN/1 eq. HMTETA combination and 15 mmol/mol for MnMeTACN/3 eq. HMTETA combination, respectively. Possible influence of polyamines on the titration method was checked using an excess amount of polyamines, *e.g.*, HMTETA. We found that polyamines do not interfere with the reactions during the titration.

It has been previously shown (Figure 4.5) that the total oxygen consumption in the case of MnMeTACN/HMTETA combination is comparable to the systems catalyzed by Web-Mn or MnMeTACN alone. In the presence of the MnMeTACN/HMTETA combination, the formation and decomposition of ROOHs takes place almost simultaneously (Figure 4.6), leading to the very low overall peroxide levels. Therefore, the MnMeTACN/HMTETA combination is very effective in catalyzing the decomposition of peroxides.

If the main role of a polyamine (like HMTETA) is to assist MnMeTACN in decomposing the formed hydroperoxides during the oxidation of EL, other polyamines with a similar structure should function in a similar way. Our FTIR study

(Figure 4.3) suggests that, as expected, the oxidation of EL is also significantly accelerated with the MnMeTACN/MeTACN combination.

Reactions between hydroperoxides (ROOH) and tertiary amines have been the subject of a few studies<sup>33-36</sup>. Formation of alkoxy (RO•) free radical intermediates was proposed by De La Mare<sup>33</sup>. Later on, Coppinger *et al.*<sup>34</sup> also described the reactions of tertiary amines with ROOHs. Possible reactions of tertiary amines with fatty acid hydroperoxides are depicted in Figure 4.7. ROOHs are decomposed by tertiary amines and R-O• free radical intermediates are formed. R-O• free radical intermediates may further react with ROOHs that lead to peroxy free radicals (ROO•). As a result, these free radicals facilitate the oxidation of fatty acids. However, R-O• may also lead to the degradation of the material via  $\beta$ -scission reactions (see 4.6.2). The other alternative route proposed by Coppinger *et al.*<sup>34</sup> is that tertiary amines react with hydroperoxides that lead to non-free radical byproducts such as alcohols and aldehydes, as shown in eqn. 3. of Figure 4.7.



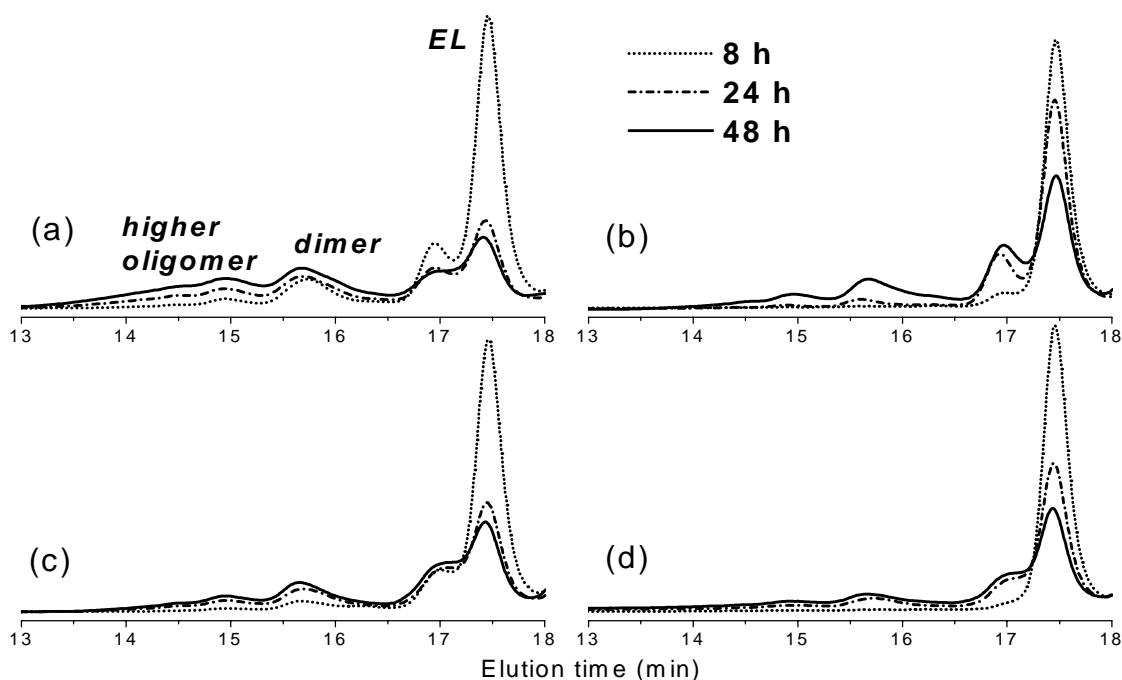
**Figure 4.7.** Possible reactions of tertiary amines with fatty acid hydroperoxides (ROOHs), after De La Mare and Coppinger *et al.*<sup>33,34</sup>

#### 4.5. Oligomerization during EL oxidation from emulsions

The oxidation of EL generally leads to the formation of oligomers, which is pivotal for the hardening of alkyd coatings. Figure 4.8 gives SEC chromatograms of EL after various periods of oxidation catalyzed by Web-Co and MnMeTACN/HMTETA. In the presence of Web-Co, some dimers and higher oligomers have already formed after 8-h oxidation (Figure 4.8a). The shoulder at 17 min is likely due to the EL hydroperoxide<sup>9-11,37</sup> and other EL derivatives (for example, epoxy<sup>11</sup>). As the oxidation proceeds (24 and 48 h), more oligomers are formed.

When MnMeTACN is used alone, almost no oligomer is formed after 8 h; a very small amount of dimer is observed after 24 h (Figure 4.8b). It is until 48 h that a considerable amount of oligomers appears. When 1 equiv. of HMTETA is combined

with MnMeTACN, the formation of oligomers is apparently accelerated (Figure 4.8c). A higher amount of HMTETA (for instance, 3 equiv. of Mn) leads to a slightly less amount of oligomers after 24 h (data not shown). On the other hand, if too much HMTETA (*e.g.*, 6 equiv.) is added, there is no oligomer formation at all after 8-h oxidation (Figure 4.8d); even after 48 h, less oligomers are formed than those with only 1 equiv. HMTETA or no HMTETA. This clearly suggests that an excessive amount of HMTETA could impose an adversary effect on the EL oxidation. We assume that this is due to: (1) a large amount of polyamine would lead to the formation of non-free-radical byproducts<sup>33</sup> that would not contribute to the formation of oligomers during the oxidation of EL (see 4.4); or (2) formation of alkoxy radicals that leads to volatile byproducts (see 4.6.2).



**Figure 4.8.** Size exclusion chromatograms of EL after different periods of oxidation in the presence of various catalysts: (a) Web-Co, (b) MnMeTACN, (c) MnMeTACN/1 eq. HMTETA, and (d) MnMeTACN/6 eq. HMTETA. The metal content was 0.07 w% on the basis of EL.

## 4.6. EL oxidation in methanol solution

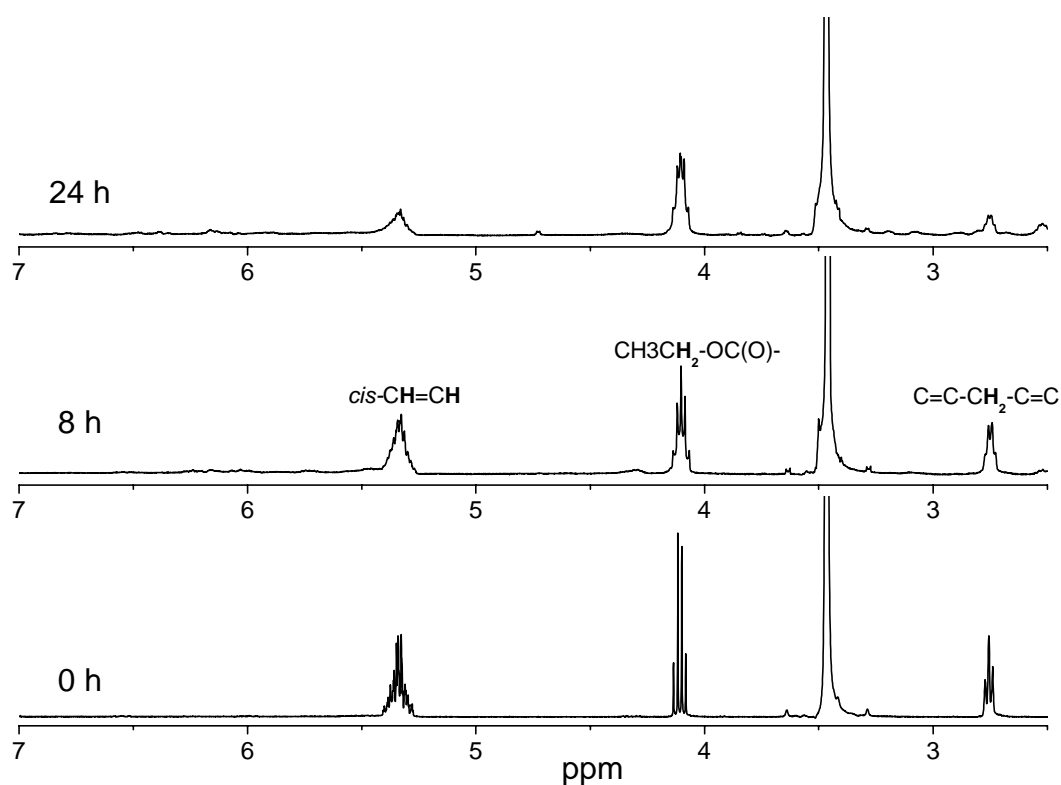
### 4.6.1. Catalytic activity of MnMeTACN

#### 4.6.1.1. Oxidation of non-purified EL

We have demonstrated that the combination of MnMeTACN/polyamine can significantly accelerate the oxidation of EL from emulsions. The catalytic activity of MnMeTACN alone is slightly higher than the commercial manganese-based catalyst (Nuodex Web-Mn, Figure 4.3) indicating that MnMeTACN is an active catalyst for the oxidation of EL. On the other hand, due to the fact that MnMeTACN is not soluble in EL, in the EL emulsion systems there is only a very small amount of MnMeTACN existing in the oil (EL) phase owing to partitioning, therefore we dealt essentially with a heterogeneous catalytic system, which makes it very difficult to have a full understanding on the catalytic capability of MnMeTACN.

We attempted to prepare a solution of both MnMeTACN and EL, and it turned out that, among the common solvents we tested, methanol is the only good solvent for both EL and MnMeTACN. In order to illustrate the effects of polyamine and hydroperoxide, both unpurified and purified EL was used.

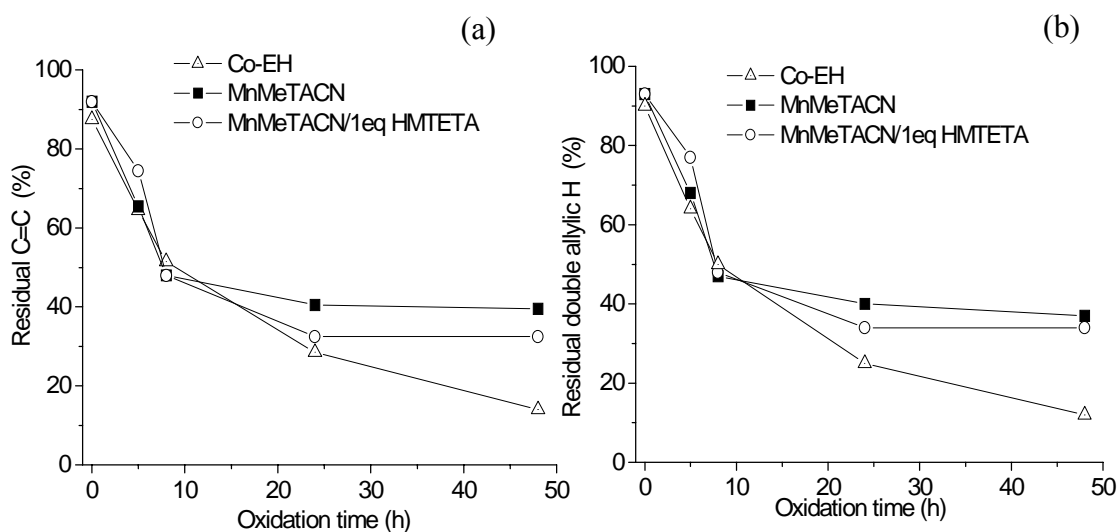
$^1\text{H}$  NMR was used to monitor the chemical changes during the oxidation of EL in methanol solution (see section 4.2.4 for details). A typical example on the variation of NMR spectra of the purified EL in the presence of MnMeTACN is given in Figure 4.9. During the course of oxidation, the peaks at 5.35 ppm (*cis*- $\text{CH}=\text{CH}$ ) and at 2.75 ppm ( $\text{C}=\text{C}-\text{CH}_2-\text{C}=\text{C}$ , double allylic H) gradually decrease, indicating the disappearance of *cis* double bonds. The peak at 4.11 ppm, corresponding to  $\text{CH}_3\text{CH}_2-\text{OC}(\text{O})-$ , is supposed to remain unchanged, and is therefore taken as an internal standard for quantitative analysis.



**Figure 4.9.** <sup>1</sup>H-NMR spectra for the purified EL during its oxidation catalyzed by MnMeTACN in methanol.

The amount of residual *cis*-C=C-related peaks for the unpurified EL oxidized by different catalyst is shown in Figure 4.10. The initial conversion of about 8% at the beginning of the experiment is due to the fact that some *cis*-C=C already reacted in the unpurified EL during storage. It is obvious from Figure 4.10 that, during the first about 10 h of oxidation, the conversion of *cis*-C=C and double allylic H takes place in a similar rate, regardless of the catalyst system used. In the absence of HMTETA, MnMeTACN appears to be a very active catalyst for the oxidation of EL during the early stage. The existence of HMTETA does not seem to make much difference. This is in a sharp contrast to what has been found for the oxidation of EL emulsions, where the addition of HMTETA to the system plays a vital role in both shortening the induction period and accelerating the disappearance of EL. We believe that, in the emulsion systems, the slow oxidation of EL in the presence of only MnMeTACN is the consequence of the poor solubility of MnMeTACN in EL. The role of HMTETA

may be twofold: to accelerate the decomposition of the formed hydroperoxides<sup>30</sup>, and to promote the partitioning of MnMeTACN in the EL phase.



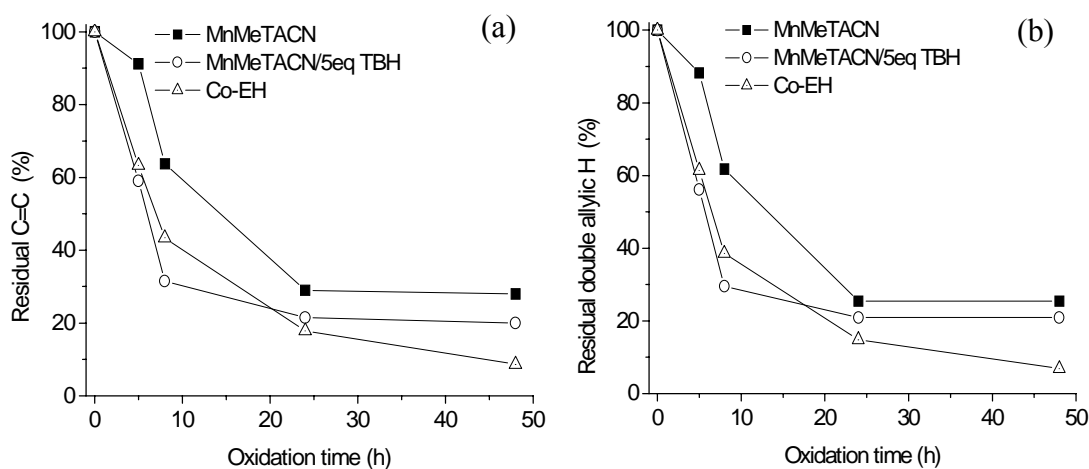
**Figure 4.10.** The amount of residual peaks of (a) *cis*-CH=CH, 5.35 ppm, and (b) C=C-CH<sub>2</sub>-C=C, 2.75 ppm, during the oxidation of unpurified EL (98%) in methanol, normalized against -CH<sub>2</sub>-OC(O)- at 4.11 ppm in the presence of different catalysts.

From the current NMR analysis in methanol solution, it is clear that MnMeTACN itself is a very effective catalyst for EL oxidation when MnMeTACN is molecularly mixed with EL. The induction period that is observed for EL emulsions disappears completely. Nonetheless, a higher degree of conversion of *cis*-C=C conversion is observed for the EL catalyzed by Co-EH after 20-h oxidation.

#### 4.6.1.2. Oxidation of purified EL

It is well established that hydroperoxides (ROOHs) have a crucial role during the oxidation of alkyd resins<sup>8,31,32</sup>. The unpurified EL we used contains around 4 mmol/mol hydroperoxides. These preformed ROOHs may have great influence on the oxidation of EL in the presence of various catalysts. In order to find out the possible role played by a hydroperoxide, purified EL (98%) (See 4.2.4 for details of purification) with or without TBH was also employed for <sup>1</sup>H-NMR analysis. When only MnMeTACN is used, the conversion of *cis*-C=C or double allylic H is only 10% after 5 h, as shown in Figure 4.11; meanwhile, about 40% conversion is already reached in the presence of Co-EH or the combination of MnMeTACN/5eq TBH

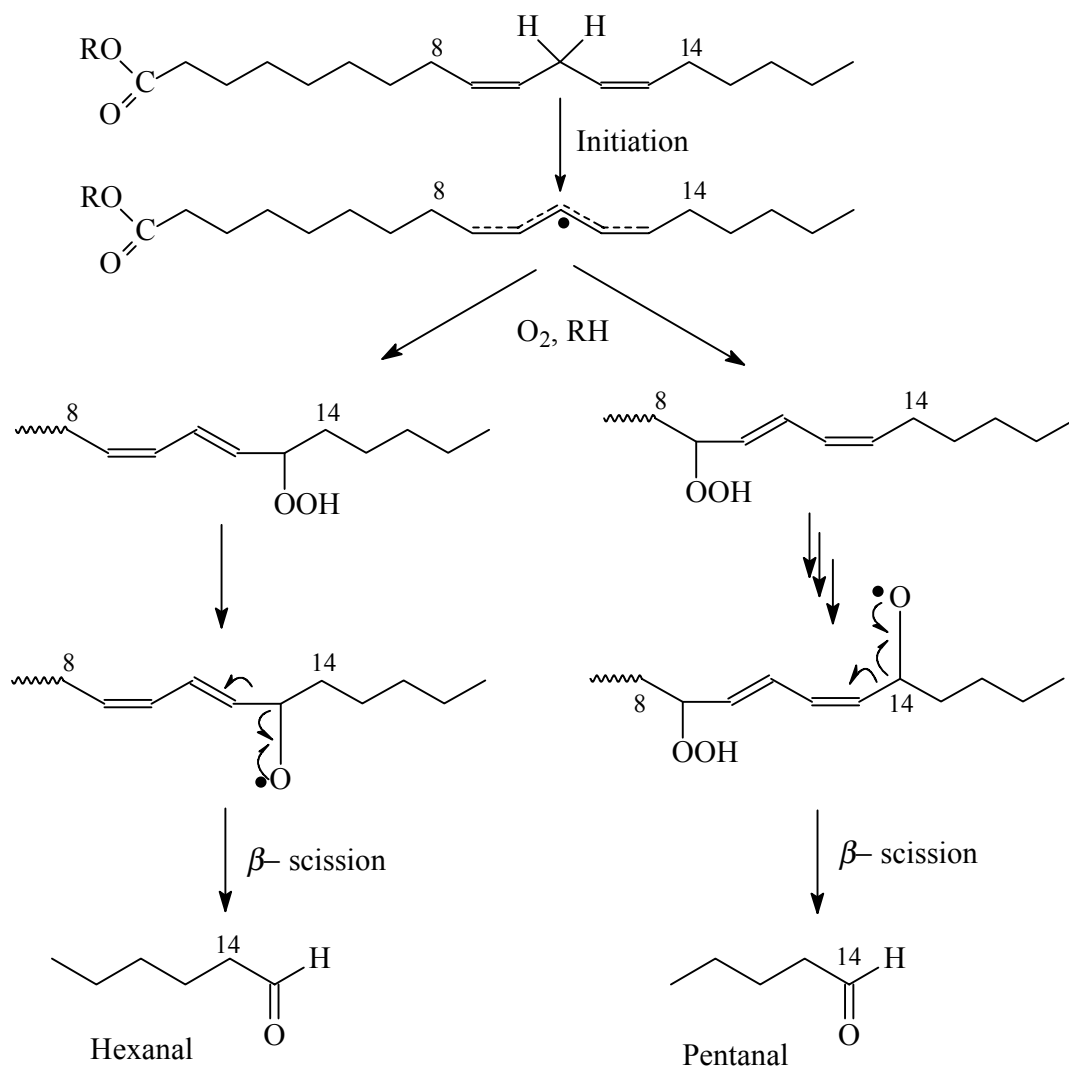
(corresponding to 13.5 mmol hydroperoxide per mole EL) at this point. MnMeTACN appears to be less effective in the absence of the hydroperoxide. Despite its lower catalytic activity in the early stages, a *cis*-C=C conversion of about 70% is also achieved with MnMeTACN after 24 h, reaching a similar level of conversion obtained with unpurified EL. It implies that once hydroperoxides are formed (the initiation step is complete), MnMeTACN can effectively catalyze the oxidation reactions. For the MnMeTACN catalyst, the presence of some hydroperoxides effectively starts the initiation of the oxidation of EL.



**Figure 4.11.** The amount of residual peaks of (a) *cis*-CH=CH, 5.35 ppm, and (b) C=C-CH<sub>2</sub>-C=C, 2.75 ppm, during the oxidation of purified EL (98%) in methanol, normalized against -CH<sub>2</sub>-OC=O at 4.11 ppm in the presence of various catalysts.

#### 4.6.2. Formation of volatile byproducts during EL oxidation

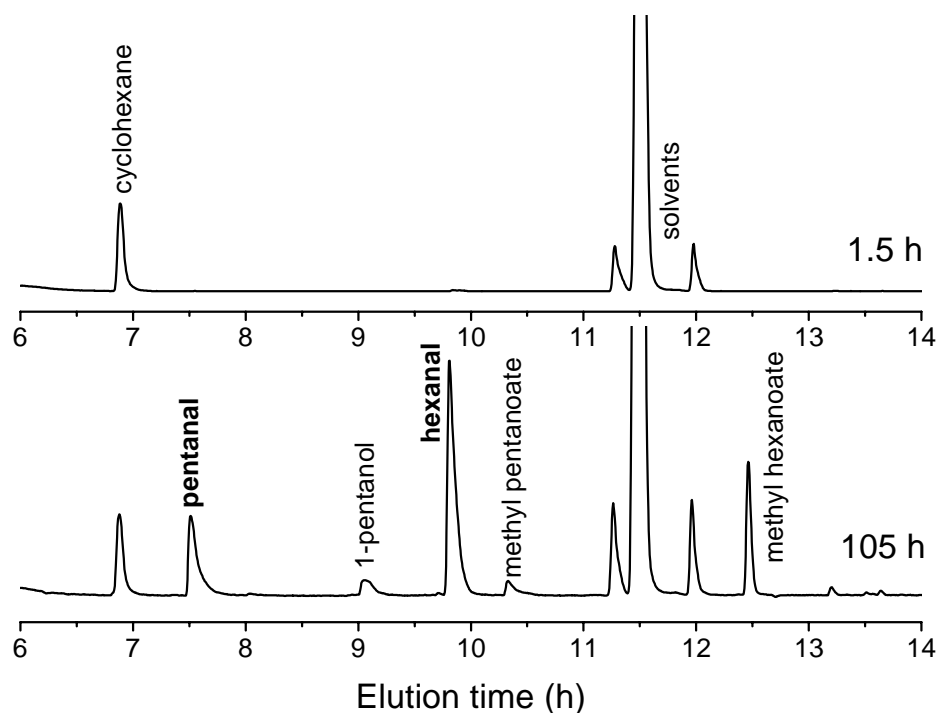
It is well known that air drying of alkyd coatings gives off a characteristic sharp smell due to the formation of volatile byproducts such as aldehydes, among which hexanal and pentanal are the major compounds via  $\beta$ -scission reactions of alkoxy free radicals<sup>38,39</sup>. The formation of hexanal and pentanal is schematically shown in Figure 4.12.



**Figure 4.12.** Schematic illustration on the formation of byproducts hexanal and pentanal via  $\beta$ -scission.

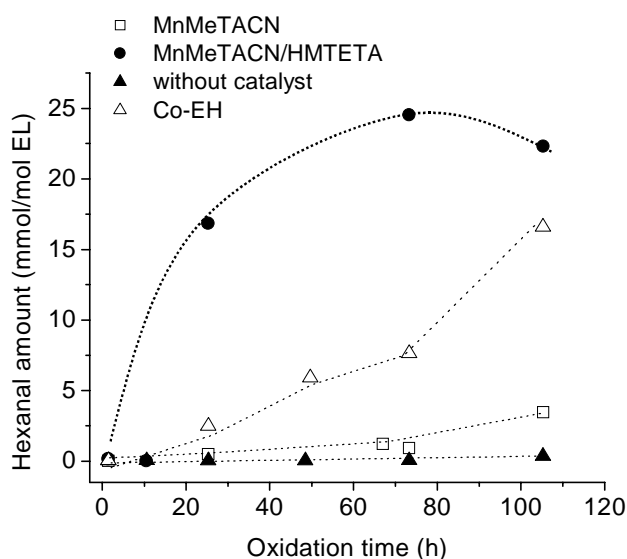
A typical head-space GC chromatogram is shown in Figure 4.13 for the oxidation of unpurified EL catalyzed by MnMeTACN/1 eq HMTETA, in which the major byproducts formed during the oxidation of EL are indicated. Apparently, hexanal is the volatile byproduct with the highest intensity after 105 h of oxidation, in agreement with the general  $\beta$ -scission mechanism. Pentanal and methyl hexanoate are the other two volatile compounds having relatively high intensities. The methyl hexanoate is the oxidation product of the formed hexanal followed by the esterification with methanol, the solvent used in this study. The formation of methyl pentanoate is probably due to the same reason.





**Figure 4.13.** Head-space GC (total ion) chromatograms showing the major volatile oxidation products of EL in methanol solution in the presence of MnMeTACN/1 eq. HMTETA after 1.5 h and 105 h of oxidation.

We quantified the amount of hexanal produced during the oxidation of EL by using cyclohexane as an internal standard because the amount of hexanal gives a direct indication of the extent of  $\beta$ -scission reactions in the presence of various catalysts. As shown in Figure 4.14, after 105 h of oxidation catalyzed by Co-EH, the amount of hexanal is about 16 mmol/mol EL. The amount of hexanal gradually increases under the influence of MnMeTACN and reaches up to 3.5 mmol/mol EL after 105 h of oxidation. When 1 equiv. HMTETA is combined with MnMeTACN, a dramatic increase in the amount of hexanal is observed. About 17 mmol of hexanal per mol of EL is obtained after only 25 h and reaches up to 24.5 mmol/mol EL after 73 h of oxidation. After reaching a maximum at 73 h, the amount of hexanal slightly decreases to 22.5 mmol/mol EL. This decrease is probably due to the further oxidation of hexanal into hexanoic acid and, subsequently, methyl hexanoate following the reaction between methanol and hexanoic acid.



**Figure 4.14.** Amount of hexanal formed during the oxidation of EL in the presence of MnMeTACN, MnMeTACN/1 eq. HMTETA, Co-EH, and in the absence of a catalyst.

We have previously demonstrated that HMTETA facilitates the decomposition of hydroperoxides into alkoxy free radicals ( $\text{RO}\bullet$ ). The high hexanal amount indicates the amount of  $\text{RO}\bullet$  produced in the presence of MnMeTACN/ 1 eq. HMTETA is much higher than in the presence of only MnMeTACN or Co-EH. This is in perfect agreement with what has been found in our previous study: the addition of HMTETA leads to the overall very low amounts of peroxides. The formation of a large amount of hexanal further corroborates that polyamines (*e.g.*, HMTETA) facilitate the decomposition of ROOH into alkoxy free radicals, which in turn result in a high level of volatile byproducts.

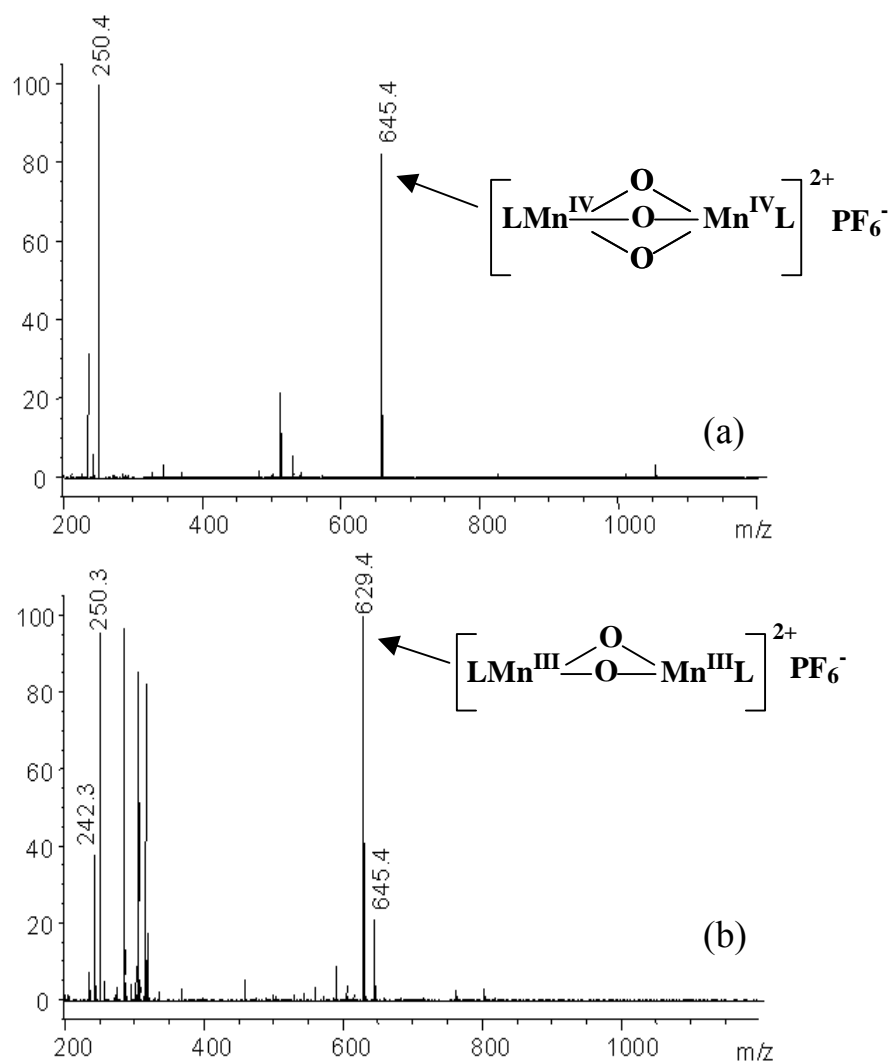
We also found from SEC (Figure 4.8) investigations that, in the presence of MnMeTACN/HMTETA, even though the disappearance of EL is faster, the formation of oligomers is less than the EL catalyzed by MnMeTACN alone. A large fraction of the consumed EL apparently contributes to the formation of volatile aldehydes and other byproducts. By combining the data from SEC and the formation of volatile byproducts, it becomes clear that a good oxidative drying is based on a proper balance between the fast oxidation (formation of hydroperoxides and their subsequent decomposition into free radicals) and the effective formation of higher oligomers.

#### 4.7. Catalytic role of MnMeTACN during the EL oxidation

The MnMeTACN complex has been the subject of many studies as an oxidation catalyst. Electrochemistry and geometry of the complex were extensively studied by Wieghart *et al.*<sup>26</sup> and Hage *et al.*<sup>18</sup> It has also been shown that MnMeTACN effectively catalyzes low temperature bleaching<sup>16</sup> and hydrocarbon oxidations<sup>21</sup>.

First we used ESI-MS and <sup>1</sup>H-NMR to check, in the mixture of MnMeTACN and HMTETA in an aqueous or methanol solution, whether a new complex containing HMTETA was formed or not. We did not detect any evidence of the exchanging of HMTETA and MeTACN (data not shown). It can be reasonably concluded that the role of a polyamine like HMTETA is to help decompose the formed hydroperoxides and, in the case of emulsion systems, to promote the partitioning of MnMeTACN in the EL phase.

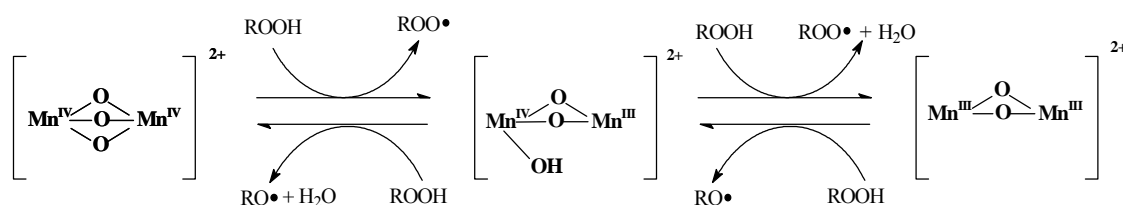
Since it has been shown in 4.6.1.2 that for the purified EL the existence of hydroperoxide is necessary to rapidly initiate the oxidation, we then decided to check the mixture of MnMeTACN and TBH in methanol solution by ESI-MS. Right after 5 equiv. of TBH was mixed with MnMeTACN in methanol solution, an ESI mass spectrum was collected, as shown in Figure 4.15a. We observed the typical fragments from MnMeTACN complex:  $[\text{Mn}^{\text{IV}}_2(\mu\text{-O})_3\text{L}_2]^{2+} (\text{PF}_6)^-$  ( $m/z = 645.4$ ) and  $[\text{Mn}^{\text{IV}}_2(\mu\text{-O})_3\text{L}_2]^{2+}$  ( $m/z = 250.4$ ). After 24 h of storage at room temperature, the mixture solution was checked by ESI-MS again. The peak at  $m/z = 645.4$  decreases substantially (Figure 8b); meanwhile, a new peak emerges at  $m/z = 629.4$ , which corresponds to the structure,  $[\text{Mn}^{\text{III}}_2(\mu\text{-O})_2\text{L}_2]^{2+} (\text{PF}_6)^-$ . Besides, a smaller peak appeared at  $m/z = 242.3$ , which is very likely to due to  $[\text{Mn}^{\text{III}}_2(\mu\text{-O})_2\text{L}_2]^{2+}$ . If a lower amount of TBH (1-2 equiv.) is mixed with MnMeTACN, the formation of the species  $[\text{Mn}^{\text{III}}_2(\mu\text{-O})_2\text{L}_2]^{2+}$  appears to be at a much lower rate.



**Figure 4.15.** ESI-MS spectra of a mixture of MnMeTACN + 5 eq. TBH in methanol solution, after (a) 0 h and (b) 24 h.

According to the species identified by ESI-MS, a tentative catalytic cycle for MnMeTACN on the decomposition of hydroperoxides during the oxidation of EL is proposed in Figure 4.16. MnMeTACN gets protonated in the presence of ROOH, leading to the formation of an intermediate  $[\text{Mn}^{\text{IV}}\text{Mn}^{\text{III}}(\mu\text{-O})_2(\mu\text{-OH})]^{2+}$  and  $\text{ROO}\bullet$ . This protonated species is likely not stable enough to be detected by ESI-MS. The species  $[\text{Mn}_2(\mu\text{-O})_2(\mu\text{-OH})]^{2+}$  has been proposed by adding perchloric acid to MnMeTACN in a solution<sup>18</sup>. ROOH can further react with the intermediate, resulting in a relatively stable species  $[\text{Mn}^{\text{III}}_2(\mu\text{-O})_2\text{L}_2]^{2+}$  (Figure 4.16), which is stable enough

to be detected by ESI-MS. These reactions are reversible in the presence of an excessive amount of ROOHs, leading to the formation of RO• radicals.



**Figure 4.16.** A tentative catalytic cycle for MnMeTACN in the presence of a hydroperoxide. The ligand L is skipped here for the sake of simplicity.

#### 4.8. Conclusions

In summary, MnMeTACN alone has proven to be an active catalyst for the oxidation of EL as long as it is molecularly mixed with EL in a co-solvent. A tentative catalytic cycle for MnMeTACN on the decomposition of hydroperoxides has been proposed, which is based on the reversible transition between Mn(IV) and Mn(III). It has been shown that hydroperoxides are necessary for the fast initiation of the catalytic cycle for MnMeTACN. The existence of HMTETA can accelerate the decomposition of the formed hydroperoxides into alkoxy free radicals, which in turn leads to a high level of volatile aldehyde byproducts due to  $\beta$ -scission side reactions. It becomes clear that a good oxidative drying is based on a proper balance between the fast oxidation (formation of hydroperoxides and their subsequent decomposition into free radicals) and the effective formation of higher oligomers.

#### 4.9. References

1. Lison D., et al., *Occup. Environ. Med.* 58 (2001) 619.
2. Bucher J.R., et al., *Toxicol. Sci.* 49 (1999) 56.
3. Danish EPA (2002). List of Dangerous Substances. 3<sup>rd</sup> June 2002. Available at <http://www.mst.dk>
4. Chapter 3 of this thesis.
5. Hurley R., Buono F., *J. Coat. Techn.* 54(694) (1982) 55.
6. Bieleman J., “*Additives for Coatings*”, Weinheim, Wiley-VCH, Germany (2000) Chp. 7.
7. Muizebelt W.J., et al., *J. Coat. Techn.* 69(869) (1997) 59.

8. Porter N.A., *Acc. Chem. Res.* 19 (1986) 262.
9. Muizebelt W.J., Hubert J.C., et al., *Prog. Org. Coat.* 24 (1994) 263.
10. Muizebelt W.J., Hubert J.C., et al., *Prog. Org. Coat.* 40 (2000) 121.
11. Muizebelt W.J., et al., *J. Coat. Techn.* 70(876) (1998) 83.
12. Agbenyega J.K., Claybourn M., Ellis G., *Spectrochimica Acta* 47A (1991) 1375.
13. Warzeska S.T., van Gorkum R., Bouwman E., et al., *Prog. Org. Coat.* 44 (2002) 243.
14. van Gorkum R., Bouwman E., Reedijk J., *Inorg. Chem.* 43 (2004) 2456.
15. Wu J.-Z., et al., *Prog. Org. Coat.* 49 (2004) 103.
16. Hage R., Iburg J.E., et al., *Nature* 369 (1994) 637.
17. Favre T.L.F., Hage R., et al., (1991) EP 458397.
18. Hage R., Krijnen L.B., et al., *Inorg. Chem.* 34 (1995) 4973.
19. Brinksma J., Hage R., et al., *Chem. Commun.* (2000) 537.
20. Zondervan C., Hage R., Feringa B.L., *Chem. Commun.* (1997) 419.
21. Grenz A., Ceccarelli S., Bolm C., *Chem. Commun.* (2001) 1726.
22. Smulders E., "Laundry Detergents", Wiley-VCH, Weinheim, Germany (2002).
23. Matyjaszewski K., Xia J., *Chem. Rev.* 101 (2001) 2921.
24. Liu S., Armes S.P., *J. Am. Chem. Soc.* 123 (2001) 9910.
25. Lou J. et al., (2003) EP1342739 A1.
26. Wieghart K., et al., *J. Am. Chem. Soc.* 110 (1988) 7398.
27. American Oil Chemists' Society, Cd 8b-53 1990.
28. Chapter 3a of this thesis, p. 54.
29. Oyman Z.O., Ming W., van der Linde R., *Prog. Org. Coat.* 48 (2003) 80.
30. Oyman Z.O., Ming W., van der Linde R., et al., *Polymer* 45 (2004) 7431.
31. Mallégol J., et al., *Prog. Org. Coat.* 39 (2000) 107.
32. Mallégol J., et al., *Prog. Org. Coat.* 41 (2001) 171.
33. De La Mare H.E., *J. Org. Chem.* 25 (1960) 2114.
34. Coppinger G.M., Swalen J.D., *J. Am. Chem. Soc.* 83 (1961) 4900.
35. Sheng M.N., Zajacek J.G., *J. Org. Chem.* 33(2) (1968) 588.
36. Oswald A.A., et al., *J. Org. Chem.* 26 (1961) 3969.
37. Tanase S., Bouwman E., Reedijk J., *Inorg. Chem.* 43 (2004) 2456.
38. Hancock R.A., Leves N.J., *Prog. Org. Coat.* 17 (1989) 321.

39. Chang J.C.S., Guo Z., *Atmos. Environ.* 32 (1998) 3581.

## **Chapter 5**

# **Effect of Mn(acac)<sub>3</sub> and 2,2'-Bipyridine on the oxidation of ethyl linoleate\***

### **Summary**

*In this Chapter we investigate the oxidation of ethyl linoleate (EL) catalyzed by Mn(acac)<sub>3</sub> (acac = acetylacetonate) and its combination with 2,2'-bipyridine (bpy), in comparison with the EL catalyzed by Co(II) 2-ethylhexanoate (Co-EH). Mn(acac)<sub>3</sub> and the Mn(acac)<sub>3</sub>/bpy combination are potential new drying catalysts. The oxidation of EL is studied through time-resolved Raman spectroscopy, oxygen uptake measurements, and peroxide amount determination. To follow the oligomerization of EL in time, size exclusion chromatography is used. Head-space GC-MS measurements is performed to determine the amounts of hexanal and pentanal that are formed as volatile byproducts during the oxidation of EL. When bpy is combined with Mn(acac)<sub>3</sub>, the conversion of non-conjugated cis-double bonds of EL is slightly faster than in the presence of Co(II)-2-ethylhexanoate, while much slower in the presence of Mn(acac)<sub>3</sub> alone, as demonstrated by Raman spectroscopy. The extent of EL oligomerization is much higher for Mn(acac)<sub>3</sub> compared to the other catalysts. Different mechanisms is proposed for the mode of action for each of the catalysts: Co-EH is primarily a hydroperoxide decomposition catalyst, as is Mn(acac)<sub>3</sub>, only less active. The Mn(acac)<sub>3</sub>/bpy combination probably forms the very reactive complexes  $[Mn(III)(acac)_2(bpy)]^+$  and  $[Mn(II)(acac)_2(bpy)]$ , which are responsible for a very high oxidation rate, but also for significant degradation of the formed EL oligomers via  $\beta$ -scission reactions due to the promotion of alkoxy radical formation.*

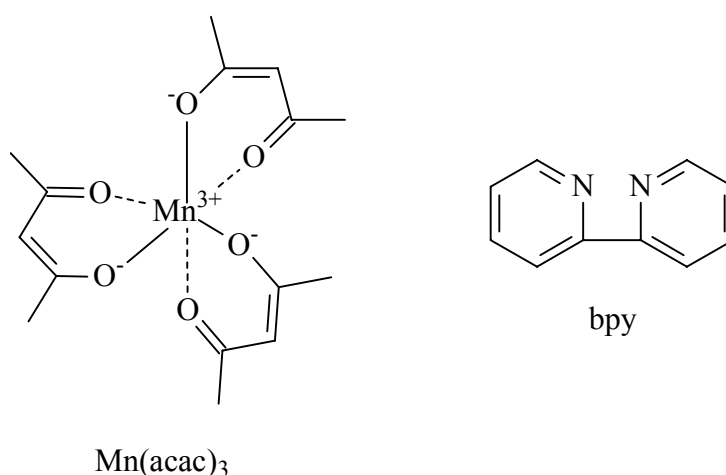
---

\* Part of this Chapter has been published: Z.O. Oyman, W. Ming, R. van der Linde, R. van Gorkum, E. Bouwman, *Polymer* 46 (2005), available at [www.sciencedirect.com](http://www.sciencedirect.com).



### 5.1. Introduction

Various types of metal-based catalysts based on acetylacetonates have been recently investigated as the potential alternatives for cobalt-based catalysts used for the drying of alkyd coatings<sup>1-4</sup>. In a recent patent, Link *et al.* reported that vanadium acetylacetonates were efficient catalysts for the drying of varnishes<sup>1</sup>. Wu *et al.* also studied a manganese complex based on 1,1,1,5,5,5-hexafluoroacetylacetonate ( $\text{Mn}(\text{hfac})_2$ )<sup>2</sup>. It was found that chelating agents such as 2-aminomethylpyridine (amp) and 2-hydroxymethylpyridine (hmp) increased the catalytic activity of  $\text{Mn}(\text{hfac})_2$  on the oxidation of ethyl linoleate (EL)<sup>2</sup>, a model compound for alkyd resins<sup>5-7</sup>. Recently, high catalytic activity of tris(acetylacetonato) manganese(III),  $\text{Mn}(\text{acac})_3$  was also reported<sup>3,4</sup>. It was found that the oxidation of EL catalyzed by  $\text{Mn}(\text{acac})_3$  was further accelerated by the addition of 2,2'-bipyridine (bpy)<sup>3,7</sup>. Chemical structures of  $\text{Mn}(\text{acac})_3$  and bpy are depicted in Figure 5.1.



**Figure 5.1.** Chemical structures of  $\text{Mn}(\text{acac})_3$  and 2,2'-bipyridine (bpy)

In this Chapter, the catalytic activity of  $\text{Mn}(\text{acac})_3$  and its combination with bpy for the oxidation of EL is further examined, in comparison with the catalytic activity of  $\text{Co}(\text{II})$ -2-ethylhexanoate. Raman spectroscopy is used to monitor the variation of double bonds of EL during oxidation in the presence of different catalysts. Oxygen uptake and peroxide value measurements are performed to investigate the catalytic effect of catalysts on the oxidation of EL. Oligomerization of EL is monitored by size exclusion chromatography (SEC). Volatile byproducts

formed during the oxidation is quantitatively measured and identified by head-space gas chromatography–mass spectrometry (GC-MS).

## **5.2. Experimental**

### **5.2.1. Materials**

Technical grade ethyl linoleate (EL), containing 73% EL, 19% ethyl oleate, 6% ethyl palmitate, and 2% ethyl stearate as determined by GC-MS, and Mn(III)acetylacetonate, Mn(acac)<sub>3</sub>, were obtained from Fluka. 2,2'-bipyridine (bpy) and Co(II)-2-ethylhexanoate (Co-EH, 65% w/w solution in white spirit) were obtained from Sigma-Aldrich. Chemicals were used as received unless otherwise stated.

### **5.2.2. Instrumentation and procedures**

#### **5.2.2.1. Raman spectroscopy**

The oxidation of EL was followed by Raman spectroscopy on a Dilor-Jobin Yvon-Horiba confocal dispersive Raman spectrometer. Details on the instrumentation can be found in the Appendix of this thesis. EL containing 0.07 w% (based on EL) of different catalysts was deposited (~200 μm) onto glass slides for *in-situ* Raman analysis. In the experiments involving bpy, 3 molar equivalents of bpy were added relative to Mn(acac)<sub>3</sub>.

#### **5.2.2.2 Oxygen uptake**

A Fibox fiber-optic oxygen meter (Precision Sensing GmbH) was used to measure the oxygen uptake of EL in the presence of various catalysts. Details about this technique can be found in the Appendix.

For oxygen uptake measurement at room temperature (~21 °C), 4 g of EL, premixed with a 0.07 w% catalyst (based on EL), was placed into a 6-L sealed container filled with air at a normal atmospheric pressure, equipped with oxygen and temperature sensors inside. When Mn(acac)<sub>3</sub> was used, it was first dissolved in a small amount of toluene. The consumed oxygen concentration was expressed as mol oxygen per mol of EL.

#### **5.2.2.3. Peroxide value**

An American Oil Chemists' Society (AOCS)-approved method for determining peroxide value (PV; Cd 8b-53)<sup>8</sup> was used with some modifications. EL

(40 g) was mixed with a catalyst (0.07 w%) and placed in a Petri dish (~20 cm radius) for oxidation at room temperature (21 °C, 50% RH). About 2 g of EL was withdrawn from Petri dishes for PV measurements. Details of the procedure can be found in the Appendix.

#### 5.2.2.4. Size exclusion chromatography

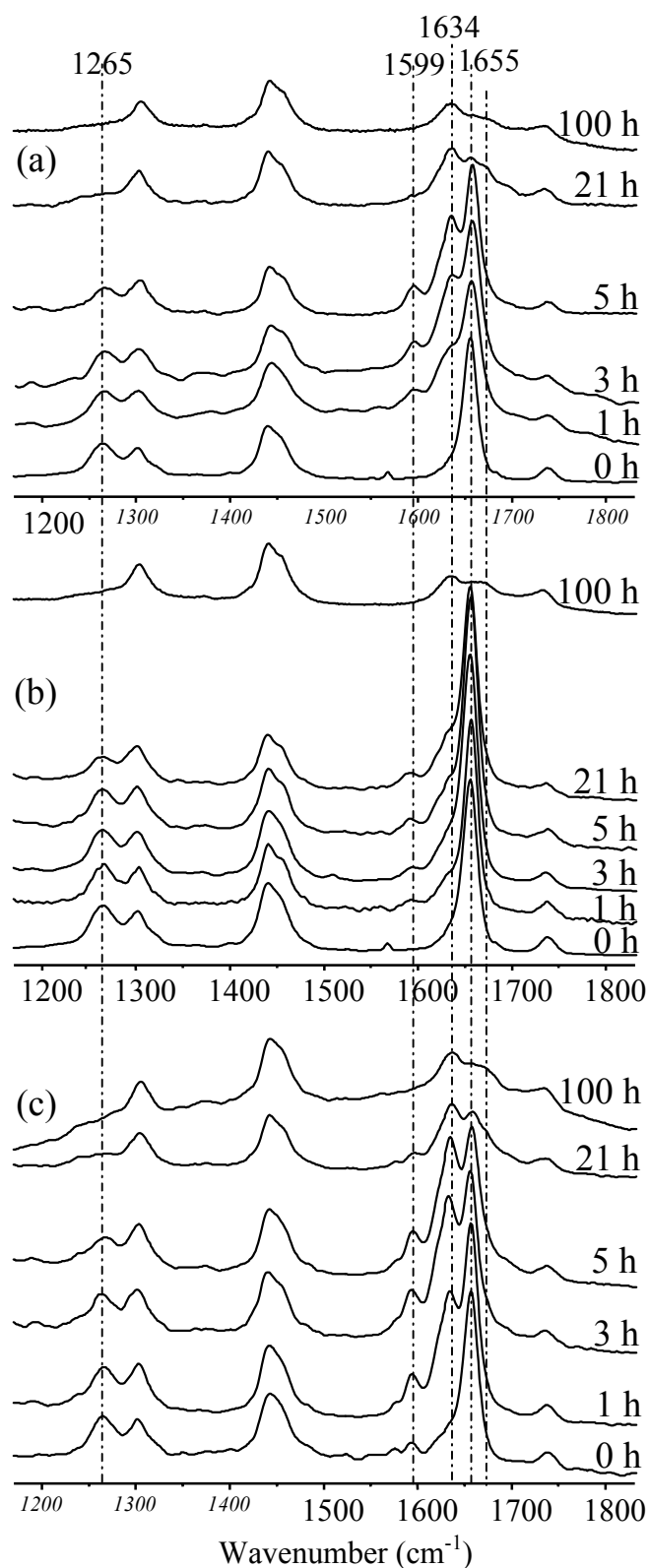
The oligomerization of EL was followed by size exclusion chromatography (SEC) on a Waters GPC instrument equipped with a Waters model 510 pump and a model 410 differential refractometer (40 °C); THF was used as the eluent. Samples were withdrawn from Petri dishes and dissolved in THF (1 mg/mL).

#### 5.2.2.5. Head-space gas chromatography – mass spectrometry (HSGC-MS)

EL (1 g) was first mixed with different catalysts (0.07 w%). An aliquot of 10 mg of EL was placed in a 20-mL head-space vial for each measurement, followed by the addition of 1  $\mu$ L of cyclohexane solution (0.37 M in xylene) as an internal standard. Detailed information on the setup of the instrument and experimental procedure can be found in the Appendix.

### 5.3. Chemical changes during the oxidation of EL

The variation of the double bonds during the oxidation of EL was followed by Raman spectroscopy in the presence of different catalysts. Raman spectroscopy proves to be a very suitable technique to detect the changes in double bonds<sup>9-12</sup>, due to their high Raman absorbance. In addition, conjugated (1599, 1634  $\text{cm}^{-1}$ ) C=C, non-conjugated (1655  $\text{cm}^{-1}$ ) *cis*-C=C, and isolated *trans*-C=C (1670  $\text{cm}^{-1}$ ) bonds can be easily differentiated<sup>9-12</sup>.



**Figure 5.2.** Raman spectra (1200-1800  $cm^{-1}$ ) during the oxidation of EL in the presence of (a) Co(II)-2-ethylhexanoate, (b)  $Mn(acac)_3$ , and (c)  $Mn(acac)_3/bpy$ .

In the absence of a catalyst, peaks of EL due to double bonds do not change even after 130 h<sup>10,12</sup>. In the presence of Co-EH, as illustrated in Figure 5.2a, C=C-related peaks of EL showed significant changes within 1 h. Non-conjugated *cis*-C=C bonds are partially converted into conjugated-double bonds (1599, 1634 cm<sup>-1</sup>, mainly *cis-trans* combination). As a result of this conversion, after 1-h oxidation, the non-conjugated *cis*-C=C peak (1655 cm<sup>-1</sup>) and the *cis*-C=CH rock peak (1265 cm<sup>-1</sup>) start to decrease while the conjugated-C=C (1599, 1634 cm<sup>-1</sup>) peaks start to form. After a few hours of reaction, the amount of the conjugated-C=C reached maximum levels. After that, both the non-conjugated *cis*-C=C and conjugated-C=C peaks of EL decreased substantially, and eventually end up with fairly low amounts of C=C (including isolated *trans*-C=C at 1670 cm<sup>-1</sup> and some conjugated C=C) after 100 h.

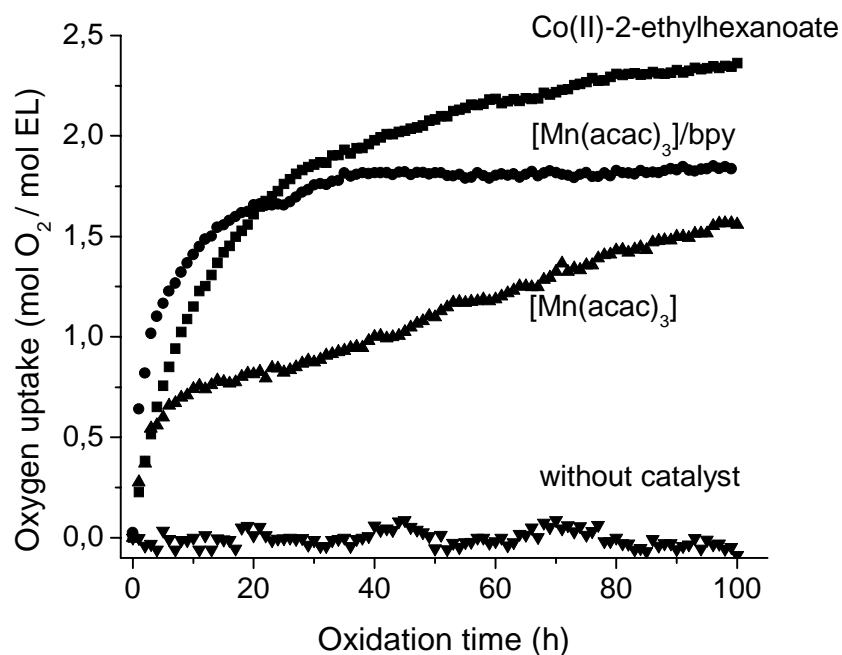
The C=C related peaks of EL in the presence of Mn(acac)<sub>3</sub> have shown similar variations (Figure 5.2b), however, the conversion appeared to be at a much slower rate compared to that in the presence of Co-EH. For instance, after 21-h oxidation, the intensity of the non-conjugated *cis*-C=C (1655 cm<sup>-1</sup>) peak is still relatively high.

The catalytic capability of Mn(acac)<sub>3</sub> is greatly enhanced by the addition of bpy, which has been shown previously by FT-IR<sup>3</sup>. As shown in Figure 5.2c, conjugated-C=C Raman peaks (1599, 1634 cm<sup>-1</sup>) of EL have already formed after 1 h when bpy is added, and at the same time, *cis*-C=C related peaks decreased. The time-evolution of C=C-related peaks appears to proceed in a very similar manner to the Co-EH-catalyzed system. Careful examinations revealed that, in the early stage of oxidation (1–3 h), the intensity of conjugated peaks is slightly higher under Mn(acac)<sub>3</sub>/bpy than under Co-EH, indicating an even faster reaction in the presence of Mn(acac)<sub>3</sub>/bpy.

#### 5.4. Oxygen uptake and evolution of peroxides during EL oxidation

Figure 5.3 illustrates the O<sub>2</sub> uptake results for EL without any catalyst as well as in the presence of the catalysts Co-EH, Mn(acac)<sub>3</sub>, and Mn(acac)<sub>3</sub>/bpy. In the absence of a catalyst, virtually no oxygen is taken up by EL during the observation period of time (100 h). In the presence of Co-EH, EL takes up a significant amount of O<sub>2</sub> (about 2.35 mol/mol EL after 100 h). A noticeably smaller amount of O<sub>2</sub> (1.55 mol/mol EL) is consumed when only Mn(acac)<sub>3</sub> is used as a catalyst. The uptake of O<sub>2</sub> by EL is enhanced when bpy is combined with Mn(acac)<sub>3</sub>: not only is a larger amount of oxygen (1.85 mol/mol EL) taken up than in the presence of Mn(acac)<sub>3</sub>, but

also the rate of  $O_2$  uptake is considerably higher. Interestingly, a plateau level of the  $O_2$  consumption is reached after about 35 h when  $Mn(acac)_3/bpy$  is used, whereas in the case of Co-EH and  $Mn(acac)_3$  no plateau has yet been reached after 100-h oxidation.

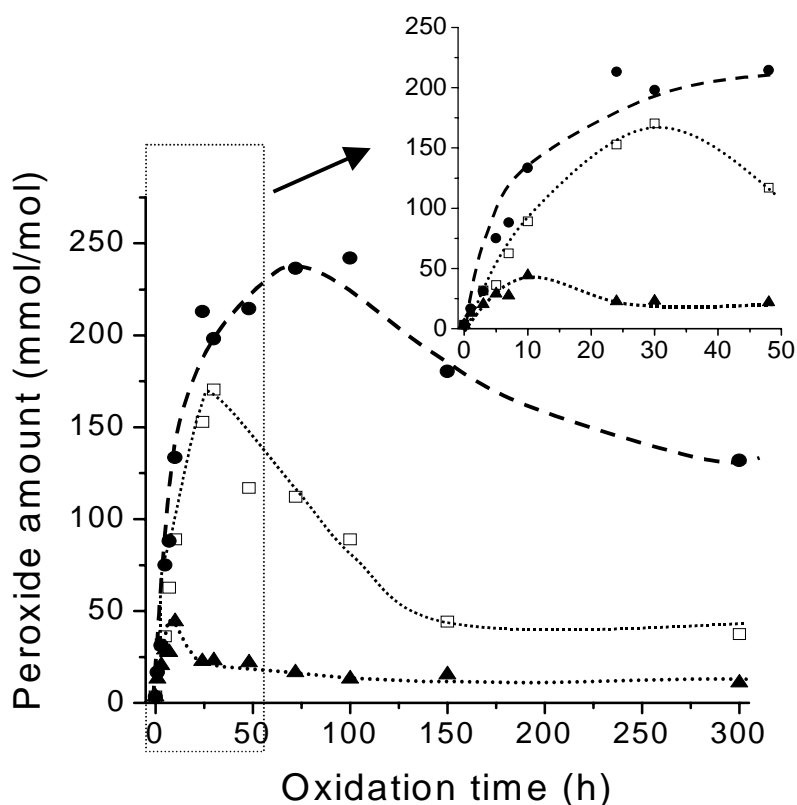


**Figure 5.3.**  $O_2$  uptake during the EL oxidation in the presence of various catalysts.

Hydroperoxides (ROOHs) have a crucial role during the oxidation reactions of alkyd resins. ROOHs are formed and then decomposed to form free radicals (*i.e.*,  $R\bullet$ ,  $RO\bullet$ ,  $ROO\bullet$ ) and these radicals are recombined to form R-R, R-O-R, R-O-O-R cross-links<sup>13-16</sup>. These free radicals can also directly add to (conjugated) double bonds<sup>5,13</sup>. The sequential formation and decomposition of ROOHs can be greatly enhanced by an appropriate catalyst. An effective catalyst accelerates both the formation of ROOHs and the decomposition of the formed ROOHs. ROOHs can also be formed and then thermally decomposed in the absence of a catalyst, however, this process is very slow at room temperature<sup>10</sup>.

The concentration of peroxides was monitored in time for the oxidation of EL in the presence of various catalysts, and the results are shown in Figure 5.4. The peroxide value for the unreacted EL, straight from the bottle received from the supplier, is determined to be 4 mmol/mol EL. In the presence of Co-EH, the peroxide

amount reaches about 50 mmol/mol after 5 h. As the oxidation of EL proceeds, the peroxide amount increases continuously and reaches a maximum level (about 170 mmol/mol) after about 30 h. Then, the peroxide value decreases very rapidly to a level of approximately 40 mmol/mol. These observations are in accordance with EL oxidation studies reported by Mallegol *et al.*<sup>14,17</sup>



**Figure 5.4.** The evolution of peroxide amounts during the oxidation of EL in the presence of various catalysts. Lines are added to aid the eye.

In the presence of  $\text{Mn}(\text{acac})_3$ , a much higher concentration of peroxides (240 mmol/mol) is reached after a much longer reaction time of 100 h. The rate-of-decrease of the peroxide value after attaining the maximum is much lower than for the oxidation with Co-EH. Even after 300 h a significant amount of peroxides of 130 mmol/mol still remains.

When bpy is added to  $\text{Mn}(\text{acac})_3$ , a totally different scenario is observed (Figure 5.4). The concentration of peroxides is, at all times, much lower than for the other two cases: a maximum amount is reached of about 45 mmol/mol in just after 10

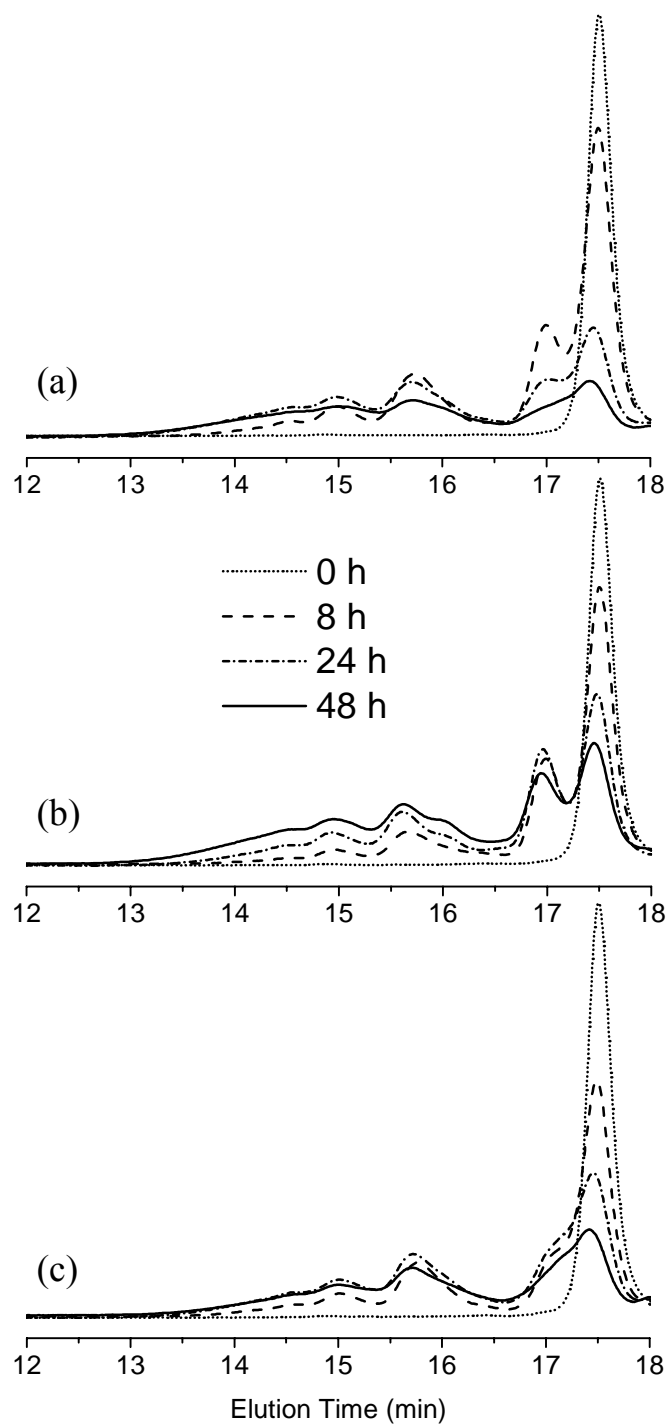
h of reaction time. The amount of peroxides then decreases to a very low level of about 10 mmol/mol over the course of the experiment (up to 300 h).

### **5.5. Oligomerization during EL oxidation**

The oxidation reactions of EL generally lead to the formation of oligomers, which is pivotal for the hardening of real alkyd coatings. Figure 5.5 illustrates SEC chromatograms of EL after various periods of oxidation catalyzed by Co-EH, Mn(acac)<sub>3</sub>, and Mn(acac)<sub>3</sub>/bpy.

After oxidation of EL for 8 h catalyzed by Co-EH, dimers (the peak at an elution time of 15.7 min), trimers (at 15 min) and higher oligomers (13-14.5 min) have been formed (Figure 5.5a)<sup>6</sup>. As the oxidation proceeded for 24 h, more trimers and higher oligomers are formed. After 48 h, both the dimer and trimer peaks have decreased relative to their levels after 24h, probably due to the formation of higher oligomers and due to oxidative degradation of the fatty acid chains (see also the HSGC-MS results in the next section). The EL peak does not disappear completely even after 48 h, which is most likely due to the presence of about 27% of non-reactive saturated esters and less reactive ethyl oleate<sup>10,11</sup> present in the technical grade EL. The peak appearing at 17 min is likely due to the EL hydroperoxides<sup>5-7,13,18</sup> and other oxygen-containing EL derivatives (for example, epoxy<sup>13</sup>). The amount of hydroperoxides first increases and then significantly decreases during the oxidation (Figure 5.5a), in agreement with the results obtained for the peroxide value determination.





**Figure 5.5.** Size exclusion chromatograms of EL after different periods of oxidation in the presence of various catalysts: (a) Co(II)-2-ethylhexanoate, (b) Mn(acac)<sub>3</sub>, and (c) Mn(acac)<sub>3</sub>/bpy.

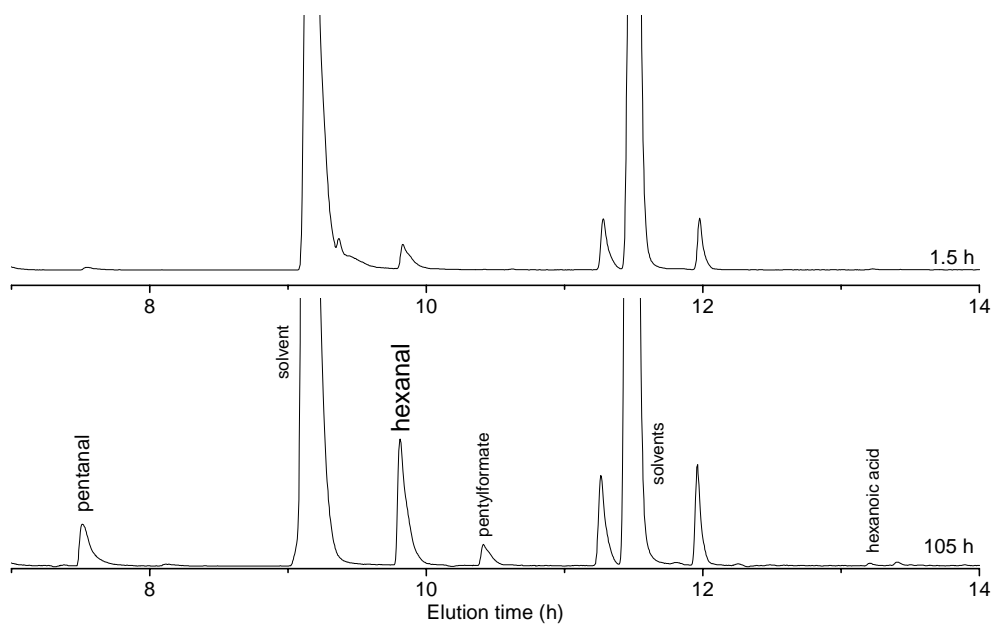
In the oxidation of EL with Mn(acac)<sub>3</sub>, the same observations can be made after 8 h as for the oxidation with Co-EH, dimers and trimers are formed although to a lesser extent than for the Co-EH catalyzed reaction. In contrast to the oxidation with Co-EH, however, the amount of (higher) oligomers only increases with prolonged reaction times, indicating little degradation of higher oligomers. The peak due to hydroperoxides remains significant for the entire duration of the experiment (48 h), again in agreement with the results obtained for the peroxide value determination for the oxidation with Mn(acac)<sub>3</sub>. The peak due to the EL-monomer also remains considerable, which is in perfect agreement with the difference in EL oxidation rates as were found for Co-EH and Mn(acac)<sub>3</sub>, using Raman (section 5.3) and FT-IR<sup>3</sup>.

In the oligomerization of EL with Mn(acac)<sub>3</sub> and bpy, the same trends in the formation of dimer, trimer and higher oligomers can be seen as for the oxidation with Co-EH (Figure 5.5c). Here, the peroxide peak is rather low in intensity at all times, in accordance with the observations made in the peroxide value determination (Figure 5.4).

## **5.6. Formation of volatile byproducts during EL oxidation**

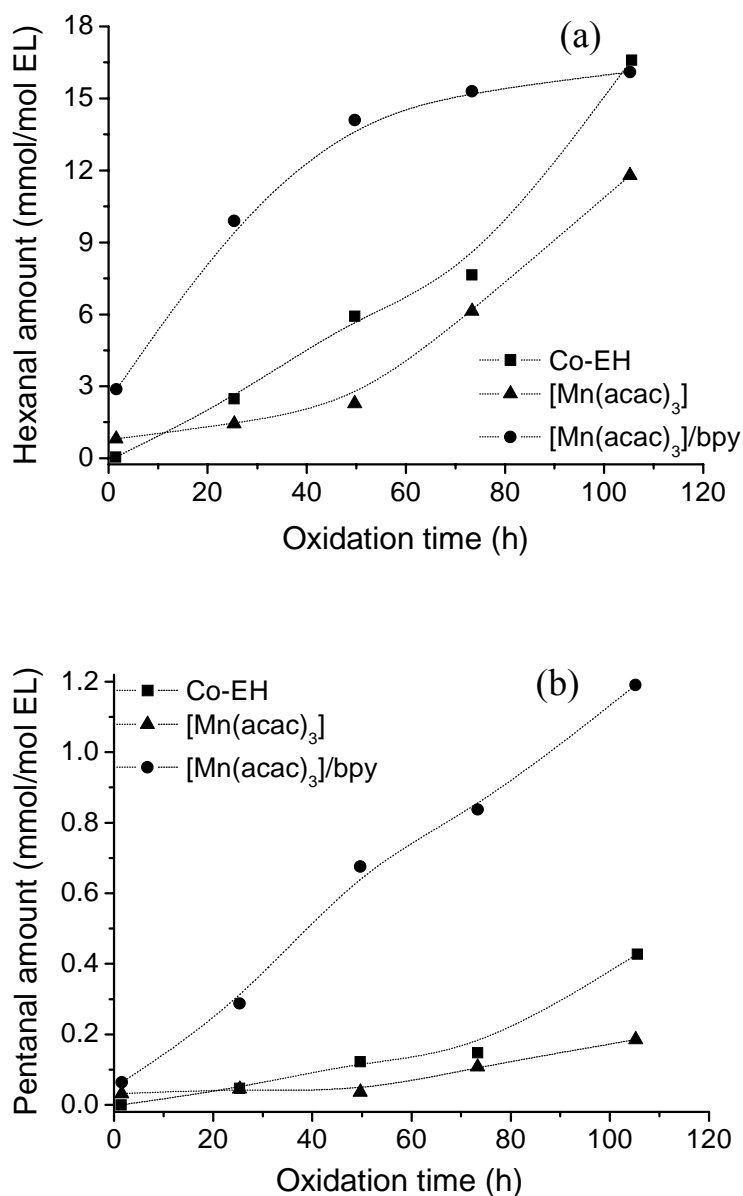
The characteristic odour during the air-drying of alkyd paints is due to the formation of volatile aldehydes, typically hexanal and pentanal. These aldehydes are major volatile byproducts formed through  $\beta$ -scission reactions of alkoxy radicals (RO•)<sup>19,20,21</sup>. The formation of hexanal and pentanal is schematically shown in Figure 4.12.

Hexanal and pentanal are also the major volatile oxidation products of EL in the presence of Mn(acac)<sub>3</sub>/bpy, as illustrated by the total ion chromatograms of the head-space GC in Figure 5.6. It is clear that hexanal and pentanal have already been formed after 1.5 h of oxidation, indicating that  $\beta$ -scission reactions start during the early stages of the oxidation.



**Figure 5.6.** Head-space GC (total ion) chromatograms showing the major volatile oxidation products of EL in the presence of  $\text{Mn}(\text{acac})_3/\text{bpy}$  after 1.5 h and 105 h of oxidation.

The amount of hexanal and pentanal formed during the oxidation of EL in the presence of Co-EH,  $\text{Mn}(\text{acac})_3$ , and  $\text{Mn}(\text{acac})_3/\text{bpy}$  is quantified by head-space GC-MS, as shown in Figure 5.7. In the reaction catalyzed by Co-EH, the amount of hexanal and pentanal increases steadily over the course of the reaction (105 h), reaching 16.6 and 0.4 mmol/mol EL, respectively. During the first 50 h of the oxidation with the  $\text{Mn}(\text{acac})_3/\text{bpy}$  system much more hexanal is generated than when Co-EH is used (Figure 5.7a). However, after 100 h the hexanal levels for both catalysts are found to be at a similar level. The amount of pentanal that is generated with the  $\text{Mn}(\text{acac})_3/\text{bpy}$  catalyst is significantly higher (about 1.2 mmol/mol EL after 105 h). In the oxidation with only  $\text{Mn}(\text{acac})_3$  as a catalyst, lower amounts of both hexanal and pentanal are formed compared to the reactions with Co-EH or  $\text{Mn}(\text{acac})_3/\text{bpy}$ .



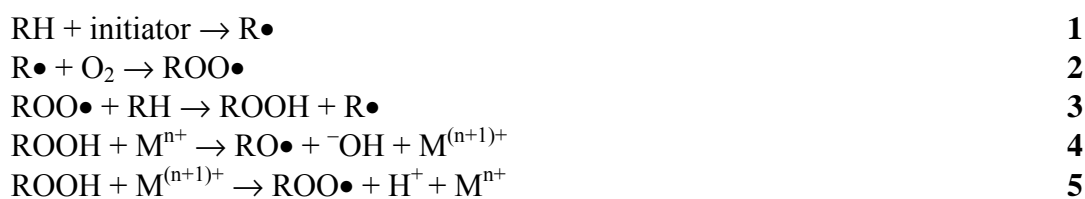
**Figure 5.7.** Formation of volatile byproducts (a) hexanal and (b) pentanal during the oxidation of EL in the presence of different catalysts. Lines are added to aid the eye.

### 5.7. Discussion

The Raman results (Section 5.3) and the FTIR results<sup>3</sup> have shown that  $Mn(acac)_3$  can oxidize EL at a reasonable rate, although this rate is lower than for the oxidation with Co-EH. The addition of bpy to  $Mn(acac)_3$  significantly enhances the oxidation rate. The Raman spectra and the rate of oxygen uptake for the catalysts Co-EH and  $Mn(acac)_3/bpy$  clearly show that the rate of oxidation of EL is higher for the  $Mn(acac)_3/bpy$  system, particularly during the first 20-h oxidation. From the data of

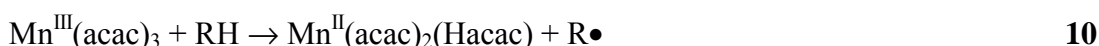
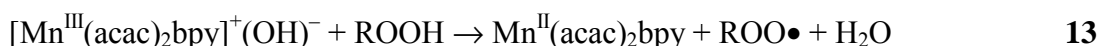
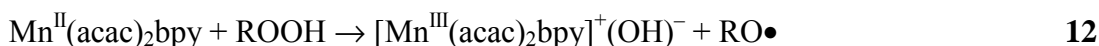
the peroxide amounts, it becomes clear that the high oxidation activity for the  $\text{Mn}(\text{acac})_3/\text{bpy}$  system might be attributed to its extremely efficient capability of hydroperoxide decomposition.

Scheme 5.1 shows the set of radical reactions that are often proposed for hydroperoxide (ROOH) build-up and decomposition in metal-catalyzed oxidation reactions<sup>5,6,17,18</sup>. The hydroperoxide concentration, at a given time, depends on the ratio of the rates for hydroperoxide decomposition vs hydroperoxide formation<sup>22</sup>. According to the reactions in Scheme 5.1, the higher the rate for reactions **4** and **5**, the lower the hydroperoxide concentration will be. It appears that reactions of **4** and **5** in the presence of  $\text{Mn}(\text{acac})_3$  occur in a much slower pace than in the presence of Co-EH and  $\text{Mn}(\text{acac})_3/\text{bpy}$  catalysts.  $\text{Mn}(\text{acac})_3/\text{bpy}$  in particular is able to decompose ROOH almost as soon as it is formed, thus attaining a very low ROOH concentration.



**Scheme 5.1.** Hydroperoxide formation and decomposition reactions<sup>16-18</sup>.

In Scheme 5.2, a tentative overview is given for the metal-catalyzed (hydro) peroxide decomposition reactions for each catalyst used in the present study. The Co-EH is known to be a robust peroxide decomposition catalyst, where reactions **6** and **7** take place. It is clear that from Figure 5.4, where the ROOH concentration decreases steadily after the maximum has been reached, that the cobalt catalyst retains its decomposition activity for at least 150 h. The oxygen uptake data for Co-EH-catalyzed EL shows that significant oxidation of EL takes place (oxygen uptake higher than 1 mol  $\text{O}_2/\text{mol}$  EL). The most common pathways during the oxidation are: through recombination of free radicals to form cross-links or through direct addition of free radicals ( $\text{R}\bullet$ ,  $\text{RO}\bullet$ ,  $\text{ROO}\bullet$ ) to conjugated double bonds, generating a new carbon-centered radical which can again react with dioxygen<sup>13,21</sup>. Moreover, substrate degradation via  $\beta$ -scission reaction of alkoxy radicals ( $\text{RO}\bullet$ ) also takes place, as evidenced by head-space GC-MS analysis.

**Cobalt-based catalyst****Mn(acac)<sub>3</sub> catalyst****Mn(acac)<sub>3</sub> + bpy catalyst**

**Scheme 5.2.** Proposed role of catalysts during the oxidation of unsaturated fatty acids.

Reactions **8** and **9** in Scheme 5.2 are the proposed ROOH decomposition reactions for the catalyst  $Mn(acac)_3$ . The most important difference for the activity of  $Mn(acac)_3$  compared to Co-EH is the rate at which reactions **8** and especially **9** proceed (apparent from the Raman data and the rate for oxygen uptake). A lower rate for these reactions can explain the significantly higher hydroperoxide concentration that is attained through reactions **10**, **2** and **3** in Scheme 5.1 and 5.2.

The amounts of hexanal and pentanal that are formed (Figure 5.7) are lower in the presence of  $Mn(acac)_3$  but follow the same trend as observed for Co-EH-catalyzed EL, also a sign that a lower rate for the ROOH decomposition reactions, which is probably the most important difference. Another major difference between the results for Co-EH and  $Mn(acac)_3$  is the amount of oligomers that are formed as observed in the SEC chromatograms. Although absolute amount of oligomers can not be obtained from SEC results, the levels of dimer, trimer and higher oligomers are clearly higher for the  $Mn(acac)_3$  catalyst. This observation can be explained by the high ROOH level that is generated through the cycle of reactions **2** and **3** and reaction **10**: each ROOH

that is formed results in the formation of a set of conjugated double bonds (see Chapter 2). A high ROOH concentration thus implies a high concentration of conjugated double bonds, which are especially prone to radical addition reactions<sup>13</sup>. Consequently, each time an alkoxy or especially a peroxy radical species is formed through decomposition of hydroperoxide, a probable reaction pathway for the radical is to react with a conjugated double bond to form a higher oligomer<sup>21</sup>.

As has been mentioned, the Mn(acac)<sub>3</sub>/bpy catalyst shows a very high rate for the oxidation of EL. The high oxidation activity is ascribed to the *in-situ* formation of the compound Mn<sup>II</sup>(acac)<sub>2</sub>(bpy) through reactions **8** and **11** (or **10** and **11**). The involvement of this species in the oxidation of EL by Mn(acac)<sub>3</sub>/bpy was already proposed<sup>3</sup>. The species Mn<sup>II</sup>(acac)<sub>2</sub>(bpy) has most probably a very high rate for reaction **12**, forming species [Mn<sup>III</sup>(acac)<sub>2</sub>(bpy)]<sup>+</sup>. Cyclic voltammetry (CV) measurements have shown that this complex has a reduction wave at 0.203 V (vs Ag/AgCl in CH<sub>3</sub>CN)<sup>3</sup>. This makes the species [Mn<sup>III</sup>(acac)<sub>2</sub>(bpy)]<sup>+</sup> a much more potent oxidizing agent than for example Mn<sup>III</sup>(acac)<sub>3</sub>, which has the corresponding reduction wave at -0.373 V (vs Ag/AgCl in CH<sub>3</sub>CN). Reactions **13** and **14** in Scheme 5.2 can thus proceed at a much higher rate than reactions **8** and **9**. The extremely high rate of oxygen uptake, coupled to the very low levels of detected hydroperoxides might be explained by the assumption that the oxidation most likely is dominated by reactions **12** and **14**, once the species Mn<sup>II</sup>(acac)<sub>2</sub>(bpy) is formed. The high amounts of hexanal and pentanal that are formed initially (Figures 5.7) as compared to Co-EH and Mn(acac)<sub>3</sub> is in agreement with the notion that reaction **12** is likely very rapid. The alkoxy radicals that are formed in reaction **12** have a tendency to undergo β-scission, thus forming hexanal and pentanal. An explanation for the complete end of uptake of oxygen once all hydroperoxides are decomposed after a reaction time of 35 h (Figure 5.3), could be that the complex [Mn<sup>III</sup>(acac)<sub>2</sub>(bpy)]<sup>+</sup> can probably only rapidly abstract C=CCH<sub>2</sub>C=C hydrogen atom. The SEC chromatogram for the oxidation of EL catalyzed by Mn(acac)<sub>3</sub>/bpy is similar to that for the Co-EH-catalyzed EL oxidation, except for the low intensity of the peak due to ROOH. A system, which predominantly generates alkoxy radicals, will have a lower extent of oligomerization, since these radicals generally have more pathways to form other products of low molecular weights<sup>21</sup>.

The Co-EH catalyst is the most widely used oxidative drier for alkyd paints. Judging only by the oxidation rate of the alkyd model compound EL, one is tempted

to say that the manganese catalyst system  $Mn(acac)_3/bpy$  would be an ideal replacement for cobalt as a drier. The results pertaining to the formation of higher oligomers show, however, that the slower catalyst  $Mn(acac)_3$  yields a much higher extent of oligomerization. It was also found in a separate study that the catalyst  $Mn(acac)_3$  shows better drying results in an actual alkyd paint formulation than the system  $Mn(acac)_3/bpy$ <sup>4</sup>. In real alkyd systems, cobalt-catalyst is never used as the only drier: so-called “secondary” and “auxiliary” driers are added, sometimes to *retard* the activity of the cobalt drier<sup>23</sup>. The lower performance for  $Mn(acac)_3/bpy$  in real alkyd paint might indeed be attributed to the fact that it is *too* active: the oxidation reactions yield predominantly alkoxy radicals, which result in less oligomerization.

## 5.8. Conclusions

$Mn(acac)_3$  is an efficient catalyst for the oxidation and the oligomerization of EL, which is proposed to proceed not only *via* hydroperoxide decomposition but also through substrate activation. The catalytic system  $Mn(acac)_3$  with bpy added has a very high activity for the oxidation of EL. *In-situ* formation of the species  $[Mn^{II}(acac)_2(bpy)]$  and  $[Mn^{III}(acac)_2(bpy)]^+$  and the high reactivities of these two species with ROOH and EL, respectively, are proposed as an explanation for the observed high oxidation rate. EL catalyzed by  $Mn(acac)_3/bpy$  shows relatively less oligomerization and a higher amount of volatile products (*via*  $\beta$ -scission reactions), probably due to the generation of predominantly alkoxy radicals in hydroperoxide decomposition.

## 5.9. References

1. Link G., et al., (1998) US6063841.
2. Wu J.-Z., et al., *Prog. Org. Coat.* 49 (2004) 103.
3. van Gorkum R., et al., *Inorg. Chem.* 43 (2004) 2456.
4. van Gorkum R., et al., (2004) EP1382648.
5. Muizebelt W.J., et al., *Prog. Org. Coat.* 40 (2000) 121.
6. Muizebelt W.J., et al., *Prog. Org. Coat.* 24 (1994) 263.
7. Warzeska S.T., et al., *Prog. Org. Coat.* 44(3) (2002) 243.
8. American Oil Chemists' Society, Cd 8b-53, (1990).



9. Ellis G., Claybourn M., *Spectrochimica Acta* 46A (1990) 227.
10. Oyman Z.O., Ming W., van der Linde R., *Prog. Org. Coat.* 48 (2003) 80.
11. Oyman Z.O., Ming W., van der Linde R., et al., *Polymer* 45 (2004) 7431.
12. Chapter 3 of this thesis (3a.3-3a.4).
13. Muizebelt W.J., et al., *J. Coat. Techn.* 70(876) (1998) 83.
14. Mallégol J., et al., *Prog. Org. Coat.* 41 (2001) 171.
15. Frankel E.N., Garwood R.F., et al., *J. Chem. Soc., Perkin Trans. I* (1982) 2707.
16. Bieleman J.H., “*Additives for Coatings*”, Wiley-VCH, Weinheim (2000) Chp. 7.
17. Mallégol J., et al., *Prog. Org. Coat.* 39 (2000) 107.
18. Tanase S., Bouwman E., Reedijk J., *Appl. Catal. A: General* 259 (2004) 101.
19. Hancock R.A., Leeves N.J., *Prog. Org. Coat.* 17 (1989) 321.
20. Chang J.C.S., Guo Z., *Atmosph. Environ.* 32 (1998) 3581.
21. Hubert J.C., et al., *Prog. Org. Coat.* 31 (1997) 331.
22. Reich L., Stivala S., “*Autoxidation of Hydrocarbons and Polyolefins*”, Marcel Dekker, Inc., New York (1969).
23. Middlemiss R.G., Olszanski D.J., *Am. Paint. Coat. J.* 78 (1993) 35.

## Chapter 6

### Oxidation of $^{13}\text{C}$ -labeled ethyl linoleate in the presence of various catalysts monitored by $^{13}\text{C}$ -NMR

#### Summary

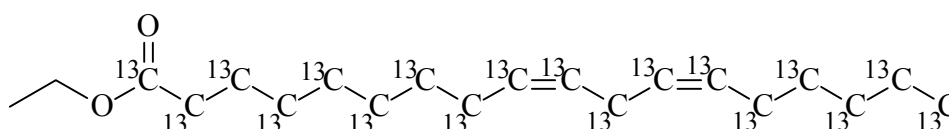
*The oxidation of  $^{13}\text{C}$ -labeled ethyl linoleate ( $^{13}\text{C}$ -EL), a model compound for alkyd coatings, is investigated in the presence of Co(II)-2-ethylhexanoate (Co-EH),  $\text{Mn}(\text{acac})_3$ , and  $\text{Mn}(\text{acac})_3$  in combination with 2,2'-bipyridine (bpy), respectively. The use of  $^{13}\text{C}$ -EL allows us to identify, in an unprecedented way, the oxidation intermediates during the oxidation. For the first time, the individual evolution of hydroperoxides (ROOH) and peroxy links (ROOR) is clearly revealed by  $^{13}\text{C}$ -NMR.  $\text{Mn}(\text{acac})_3$  appears to be less effective for ROOH decomposition than Co-EH and the  $\text{Mn}(\text{acac})_3/\text{bpy}$  combination. Quantitative analyses are attempted for a few major  $^{13}\text{C}$  peaks.*

## 6.1. Introduction

Understanding of metal-based catalyzed oxidation reactions during the drying of alkyd coatings is of great importance. Reactions during the drying of alkyd coatings such as hydroperoxide formation and decomposition, cross-linking, and other side reactions (*e.g.*,  $\beta$ -scission, Russell termination; see Chapter 2) are greatly influenced by the type of the catalyst used<sup>1-4</sup>.

It is known that alkyd resins catalyzed by Co-EH form R-R, R-O-R, and R-O-O-R cross-links via either radical recombination or radical addition to double bonds (see Chapter 2 for details)<sup>5</sup>. Consequently, these cross-links lead to the formation of networks that are insoluble in organic solvents, making it very difficult to analyze these networks with common techniques that are based on solutions. The drying of alkyd resins was demonstrated by Marshall *et al.* using solid-state NMR<sup>6,7</sup>, which is the only study, to the best of our knowledge, on the formation of the nature of cross-links in real alkyd coatings. Later on, model compounds such as ethyl linoleate (EL) were used to follow the extent of the cross-links<sup>5</sup>. EL-oligomers are soluble in organic solvents that are easy to characterize. Muizebelt *et al.*<sup>5</sup> studied the Co-EH catalyzed oxidation of EL by quantitative <sup>13</sup>C-NMR and MS. <sup>13</sup>C-NMR and MS studies revealed the formation of EL-oligomers (especially R-O-R and R-O-O-R). Besides, EL-oligomers, the formation of byproducts (nonvolatile acids, epoxies, endoperoxies, and aldehydes) from side reactions was demonstrated.

As also shown in the previous Chapters of this thesis, different catalysts have demonstrated different effects on the oxidation of EL, such as the rate of EL conversions *viz.* the oxygen uptake, the formation and decomposition of hydroperoxides, and the amounts of volatile byproducts. In this Chapter we further examine the oxidation of <sup>13</sup>C-labeled EL (<sup>13</sup>C-EL, Figure 6.1) catalyzed by various catalysts such as Co-EH, Mn(acac)<sub>3</sub>, and the Mn(acac)<sub>3</sub>/bpy combination. The use of <sup>13</sup>C-labeled EL makes <sup>13</sup>C signals easily distinguishable and allows more accurate quantitative analysis.



**Figure 6.1.** Structure of <sup>13</sup>C-labeled ethyl linoleate (<sup>13</sup>C-EL).

## 6.2. Experimental

### 6.2.1. Materials

Ethyl linoleate-U- $^{13}\text{C}$ 18 ( $^{13}\text{C}$ -EL, 98%) was obtained from Cambridge Isotope Laboratories. Mn(III)acetylacetonate ( $\text{Mn}(\text{acac})_3$ ) was obtained from Fluka. 2,2'-bipyridine (bpy) and Co(II)-2-ethylhexanoate (Co-EH) (65 w% solution in white spirit) were obtained from Sigma-Aldrich. Chemicals were used as received.

### 6.2.2. Oxidation of $^{13}\text{C}$ -EL

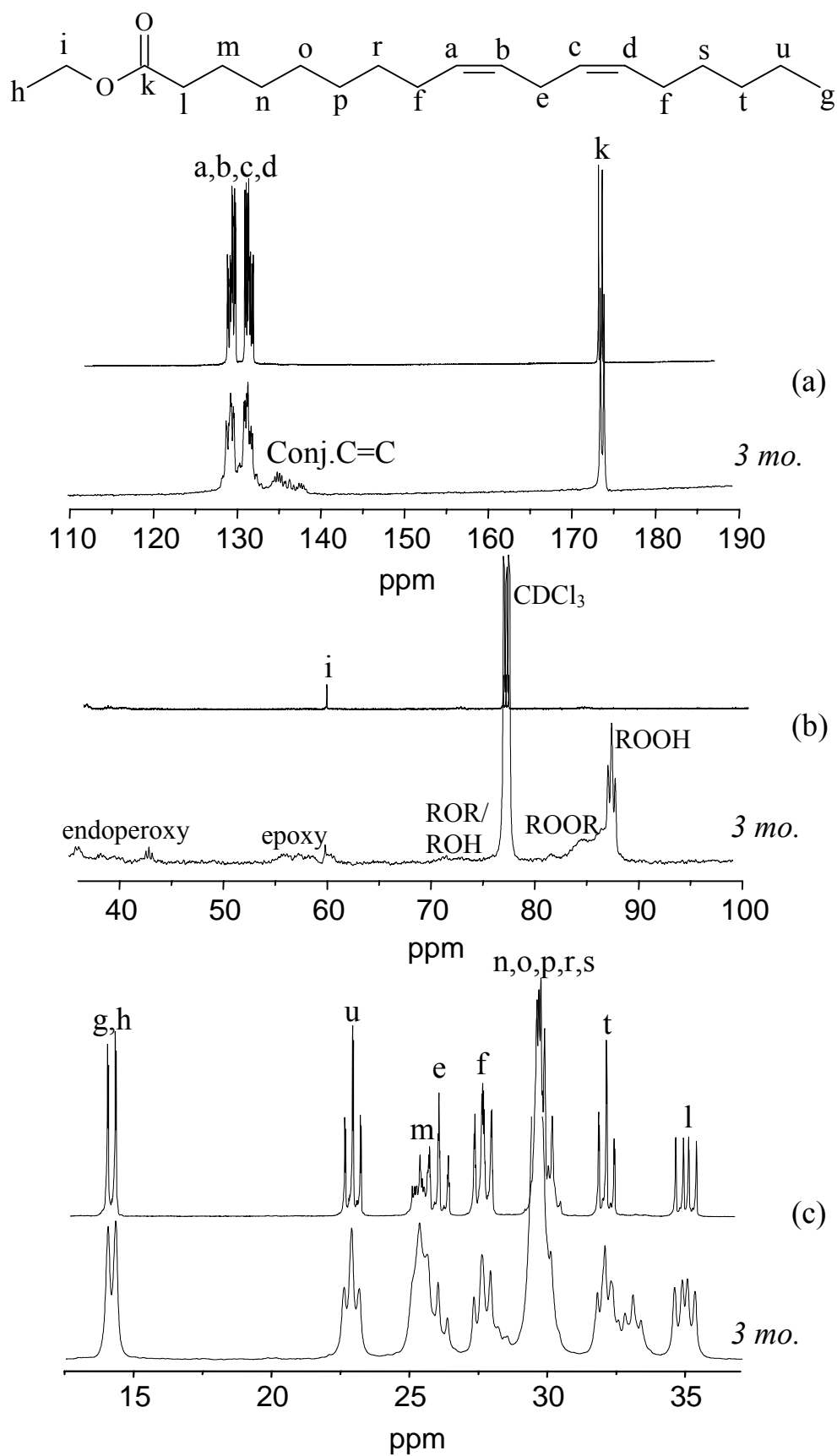
$^{13}\text{C}$ -EL was mixed with various catalysts (metal content: 0.07 w%, based on EL) and allowed to oxidize in air in Petri dishes at room temperature. When bpy was used, the molar ratio of  $\text{Mn}(\text{acac})_3$  over bpy was kept as 1.

### 6.2.3. Quantitative $^{13}\text{C}$ -NMR

During the oxidation of  $^{13}\text{C}$ -EL, samples were withdrawn at different time intervals and dissolved in  $\text{CDCl}_3$  (50 mg/mL) for quantitative  $^{13}\text{C}$ -NMR analysis on a Varian 500 MHz NMR spectrometer. Nuclear Overhauser effect was eliminated by inverse-gated decoupling method ( $\text{dm} = \text{nny}$ ) and a relaxation time ( $\text{d1}$ ) of 16 sec was used<sup>7</sup>. Acquisition time was at least 6 h that corresponds to the number of scans of  $> 300$  unless otherwise stated.

## 6.3. Advantage of using $^{13}\text{C}$ -EL

Non- $^{13}\text{C}$ -labeled EL has been used as a model compound for  $^{13}\text{C}$ -NMR analysis before and some useful information has been extracted<sup>5</sup>. However, as the oxidation of EL proceeds, a lot of reactions are involved; the complexity of these reactions results in the poor quality of  $^{13}\text{C}$ -NMR spectra if a conventional EL is used, making quantitative analyses extremely difficult, if not impossible. The use of  $^{13}\text{C}$ -EL without any doubt will enhance the intensity of  $^{13}\text{C}$ -NMR signals, thus makes  $^{13}\text{C}$  signals easily distinguishable and, consequently, allows more accurate quantitative analysis.



**Figure 6.2.**  $^{13}\text{C}$ -NMR spectra of  $^{13}\text{C}$ -EL at the beginning of oxidation and after 3 months without any catalyst added: (a) 110-190 ppm, (b) 37-100 pm, (c) 13-37 ppm.

$^{13}\text{C}$ -NMR spectra of  $^{13}\text{C}$ -EL at the beginning and after about 3 months of autoxidation are depicted in Figure 6.2. Although the autoxidation without any catalyst is a slow process, the decrease in the non-conjugated *cis*-C=C peaks (127-132 ppm) and the formation of conjugated -C=C (132-136 ppm) peaks during the oxidation of  $^{13}\text{C}$ -EL is clearly observed, as shown in Figure 6.2a. Furthermore, the formation of hydroperoxides (ROOH, 86.5 ppm) and peroxy links (ROOR, 82.0-86.0 ppm), ether (R-O-R) links and alcohols (67.0-76.0 ppm), epoxides (55.0-61.0 ppm), and endoperoxides (37.1-43.9 ppm) is also clearly seen (Figure 6.2b). The changes in the double allylic (~26 ppm) and monoallylic (~27.5 ppm) groups are also discernible. The  $^{13}\text{C}$ -NMR peak assignments of  $^{13}\text{C}$ -EL during the oxidation are summarized in Table 6.1.

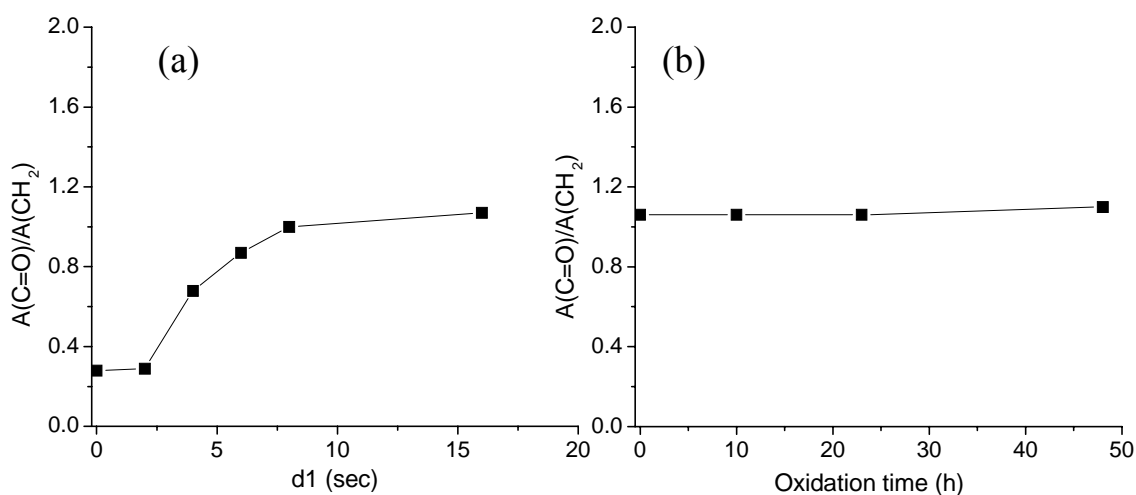
Table 6.1 Assignments of  $^{13}\text{C}$ -NMR signals of EL<sup>5,8-10</sup>.

ppm	Molecular unit
173.7	ester (-C=O)
142.8, 162.8	double bonds conjugated to aldehydes (-C=C-C=O)
159.4	double bonds conjugated to acids (-C=C-C=O)
145.7, 156.3	double bonds conjugated to ketones(-C=C-C=O)
124.3, 131.7-136.0	conjugated double bonds (-C=C-C=C-)
127.7-131.5	<i>cis</i> -non-conjugated double bonds (-C=C-C-C=C-)
86.5	hydroperoxides (-C-O-O-H) [8, 10, and THIS STUDY]
82.0-86.0	peroxy cross-links (-C-O-O-C-) [8,10, and THIS STUDY]
67.0-76.0	ether cross-links (-C-O-C-) and secondary alcohols (-C-O-H)
54.0-62.0	epoxides
60.4	-CH <sub>2</sub> -O-C=O
37.1-43.9	endoperoxides and/or C-C cross-links <sup>5</sup>
34.5	-CH <sub>2</sub> -C=O
31.5	-CH <sub>2</sub> -CH <sub>2</sub> -CH <sub>3</sub>
28.5-30	-CH <sub>2</sub> in EL chain (C4, C5, C6, C7, C15)
27.5	monoallylic -C-C=C- (C8, C14)
26.0	double allylic -C=C-C-C=C- (C11)
25.0	-CH <sub>2</sub> -C-C=O (C2)
22.5	-CH <sub>2</sub> -CH <sub>2</sub> -C=O (C3)
14.0	CH <sub>3</sub> -CH <sub>2</sub> -C-C- (C18)
14.0	CH <sub>3</sub> -CH <sub>2</sub> -O-C=O

As shown in Figure 6.2b, the  $^{13}\text{C}$  signals from ROOR and ROOH appear as two different peaks in the  $^{13}\text{C}$ -NMR spectra; this distinction is not observed if a non- $^{13}\text{C}$ -labeled EL is used. Even though these two peaks are not completely separated, the use of  $^{13}\text{C}$ -EL obviously offers an opportunity for us to further examine some of the unclear issues during the oxidation of EL, for instance, an in-situ monitoring on the individual evolution of ROOH and ROOR.

#### 6.4. Experimental setup for quantitative $^{13}\text{C}$ -NMR analysis

The relaxation time of  $^{13}\text{C}$  signals, C=O in particular, tends to be very long, so it normally needs a long relaxation delay time (d1) for the spectrum to be quantitatively analyzable. We tested the effect of the d1 value on the intensities of various signals. As shown in Figure 6.3a, d1 should be kept between 8 and 16 sec for the purpose of quantification. During the oxidation of  $^{13}\text{C}$ -EL, the ratio of the intensity of C=O (174 ppm, **k**)/ -CH<sub>2</sub>- (34.5 ppm, **l**) with d1 = 16 sec is close to 1 (Figure 6.3b), indicating it is reliable to perform quantitative analysis for those samples after about 50 h of oxidation (as the oxidation proceeds, the viscosity of the system increases, which may require an even longer d1 for quantitative analysis). The -CH<sub>2</sub>- (34.5 ppm, **l**) is supposed to remain unchanged during the oxidation, so it is used as an internal standard for the analysis below.



**Figure 6.3.** (a) The ratio of the intensity of C=O (173.7 ppm, **k**)/ -CH<sub>2</sub>- (34.5 ppm, **l**) for  $^{13}\text{C}$ -EL as a function of d1, and (b) the same ratio during the oxidation of EL catalyzed by Co-EH with d1 = 16 sec.

## 6.5. Quantitative analysis during the oxidation of $^{13}\text{C}$ -EL

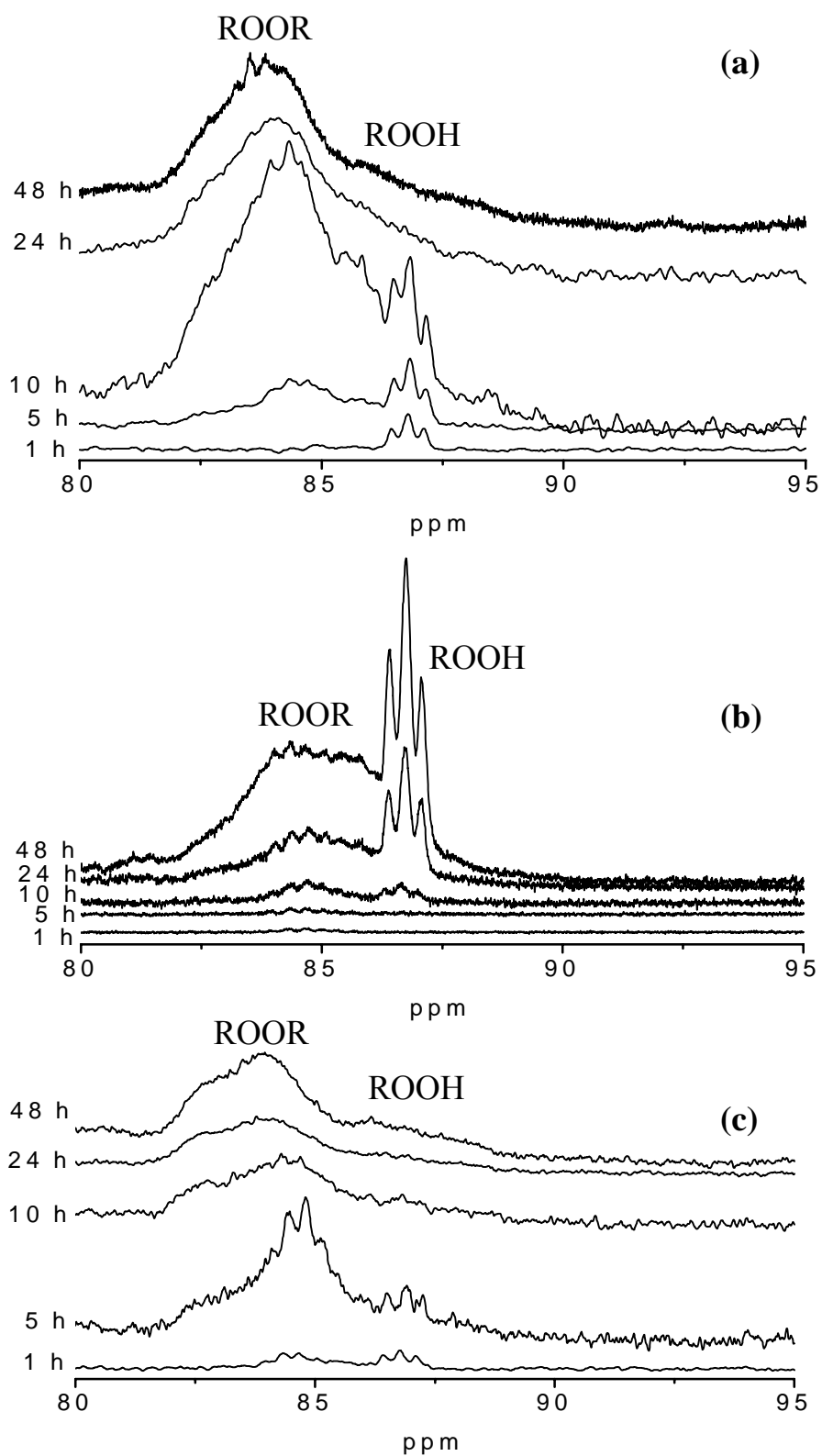
The  $^{13}\text{C}$ -NMR spectra of  $^{13}\text{C}$ -EL during the oxidation catalyzed by various catalysts will now be examined in details. Since the formation of carbonyl-containing species can be easily followed by other techniques (*e.g.*, FTIR, see Chapter 3b.5), the attention was not paid to the carbonyl peaks ( $> 170$  ppm).

### 6.5.1. Evolution of hydroperoxides (ROOH) and peroxy links (ROOR)

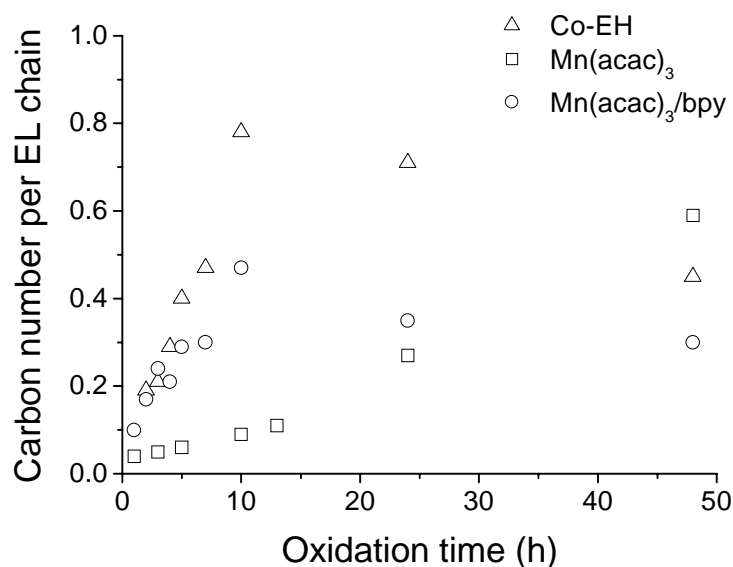
The  $^{13}\text{C}$ -NMR spectra (80-95 ppm) during the oxidation of  $^{13}\text{C}$ -EL catalyzed by Co-EH,  $\text{Mn}(\text{acac})_3$ , and  $\text{Mn}(\text{acac})_3/\text{bpy}$ , are shown in Figure 6.4. In this region the peaks corresponding to hydroperoxides (ROOH, 86.5 ppm) and peroxy links (ROOR, 82.0-86.0 ppm) can be distinguished. Therefore, the effect of various catalysts on the individual evolution of ROOH and ROOR can be monitored during the oxidation of  $^{13}\text{C}$ -EL.

As shown in Figure 6.4a, the appearance of the ROOH peak at 86.5 ppm is clearly observed after 1-h oxidation of  $^{13}\text{C}$ -EL in the presence of Co-EH. The ROOR peak also appears after 5-h oxidation. It is apparent from Figure 6.4a that the intensity of both ROOH and ROOR peaks increases during the first 10 h of oxidation. After that period, the intensity of the ROOH peak decreases to a low level. For ROOR, the intensity also decreases in the period of 10-48 h. For the first time, the observation on the individual variation of ROOH and ROOR signals is possible; the peroxide amount from titrations (see Chapters 3, 4 and 5) can only give a variation of the sum of ROOH and ROOR. During the oxidation of  $^{13}\text{C}$ -EL catalyzed by  $\text{Mn}(\text{acac})_3$ , the individual evolution of ROOH and ROOR is shown in Figure 6.4b, which appears to be very different with that in the case of Co-EH. The formation of ROOH and ROOR is much slower in the presence of  $\text{Mn}(\text{acac})_3$  than Co-EH, which contradicts what has been described in Chapter 5 (the reason is unclear at this moment). Once ROOH and ROOR are formed, their intensities keep increasing during the observed period (up to 48 h); the ROOH peak remains very pronounced at 48 h. When the  $\text{Mn}(\text{acac})_3/\text{bpy}$  combination is used as the catalyst, the ROOH/ROOR evolution (Figure 6.4c) appears to be similar to the Co-catalyst. It is also interesting to notice that, in Figure 6.4 (a) and (c), the ROOR peak broadens and shifts towards higher field as the oxidation proceeds. This is probably due to the change of neighboring environment of a C-O-O-C group; for instance, the disappearance of a double bond next to the C-O-O-C may cause this shift.





**Figure 6.4.** Evolution of hydroperoxides (ROOH) and peroxy links (ROOR) during the oxidation of  $^{13}\text{C}$ -EL followed by  $^{13}\text{C}$ -NMR in the presence of (a) Co-EH, (b)  $\text{Mn}(\text{acac})_3$ , and (c)  $\text{Mn}(\text{acac})_3/\text{bpy}$ .



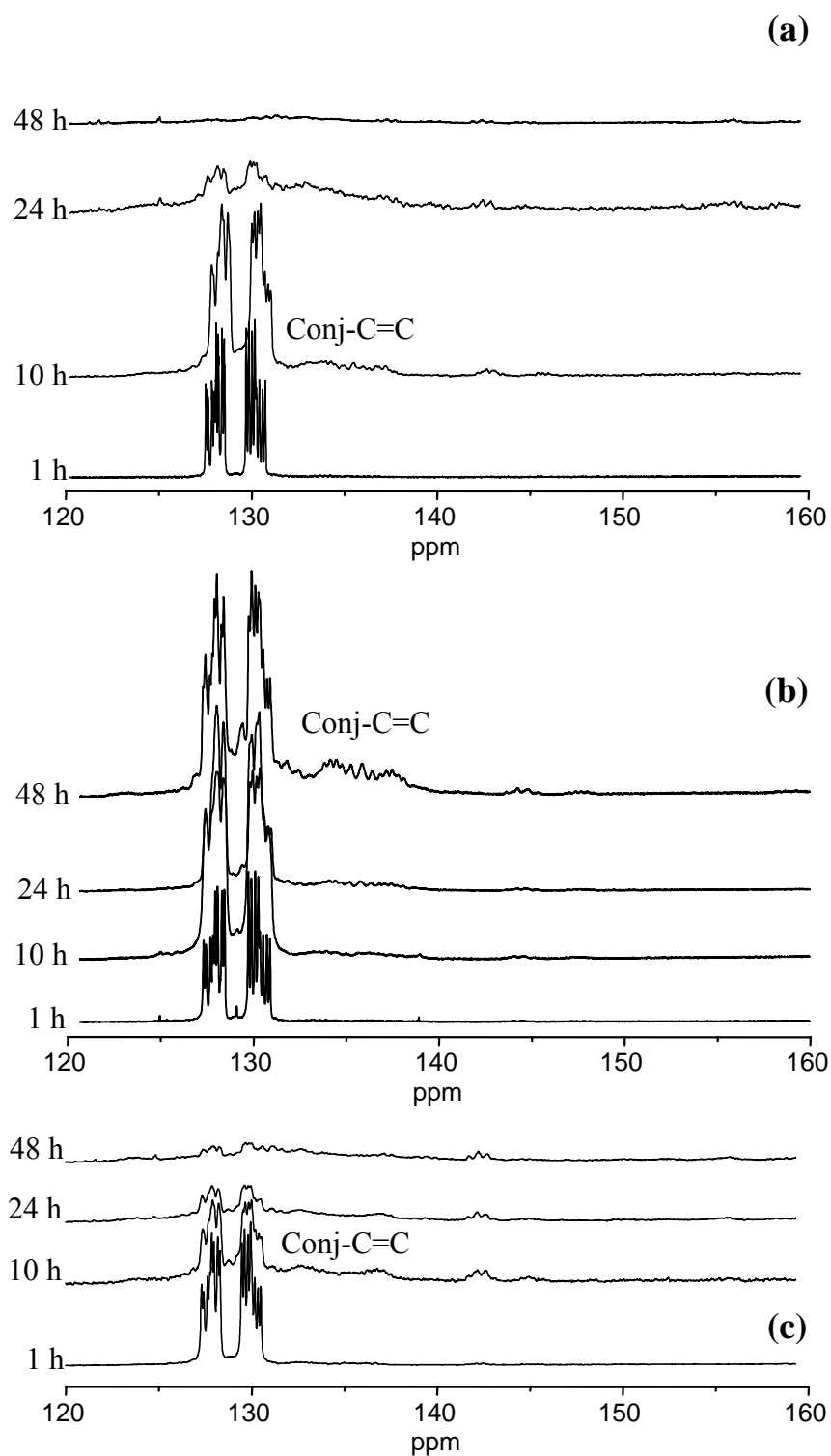
**Figure 6.5.** The evolution of the peroxide (ROOH and ROOR) during the oxidation of  $^{13}\text{C}$ -EL in the presence of various catalysts.

The quantification of the ROOH/ROOR change is tried. Unfortunately, the ROOR and ROOH peaks overlap, making the individual quantification very difficult. Instead, the overall amounts of ROOH/ROOR are quantified, as shown in Figure 6.5. In the presence of Co-EH, the peroxide amount increases during the early stage of the oxidation and reaches a maximum level, about 0.8 carbon per EL, at about 10 h, followed by a gradual decrease. A similar trend is observed for the Mn(acac)<sub>3</sub>/bpy combination; the only difference is that the highest peroxide level corresponds to a carbon number of about 0.5 per EL chain, in agreement with the peroxide titration results in Chapter 5. When Mn(acac)<sub>3</sub> is used alone, the peroxide amount during the early stage of EL oxidation is significantly lower than the other two cases, but increases rapidly from 24 – 48 h; it is anticipated that a much higher maximum level will be reached. Although the trend in the ROOH/ROOR evolution obtained from  $^{13}\text{C}$ -NMR does not appear to be exactly the same with the peroxide titration results in Chapter 5 (especially for Mn(acac)<sub>3</sub> alone), the  $^{13}\text{C}$ -NMR analysis on the  $^{13}\text{C}$ -EL does offer us an opportunity to examine the individual evolution of ROOH and ROOR during the oxidation.

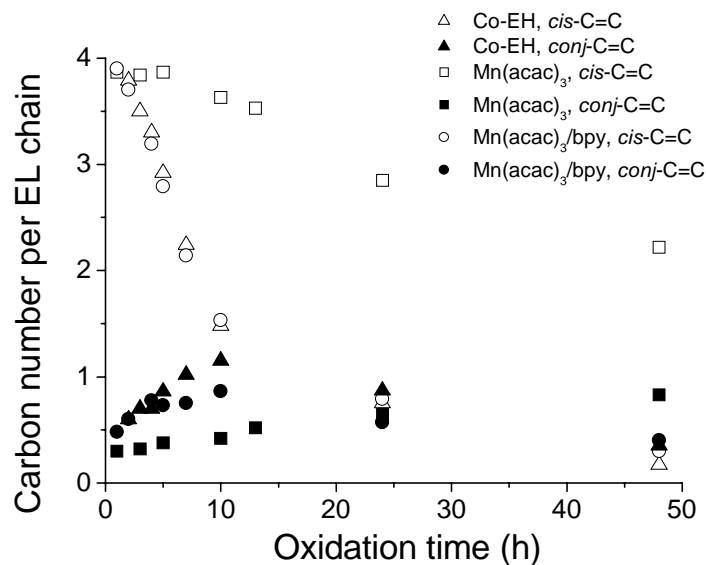
### 6.5.2. C=C variations during the oxidation of $^{13}\text{C}$ -EL

Similar to FTIR and Raman techniques, the variation of double bonds can also be followed by  $^{13}\text{C}$ -NMR during the oxidation of  $^{13}\text{C}$ -EL. As shown in Figure 6.6 (a) and (c), when the oxidation is catalyzed by either Co-EH or the  $\text{Mn}(\text{acac})_3/\text{bpy}$  combination, there is a significant decrease in the non-conjugated *cis*-C=C peaks at 127.7-131.5 ppm during the observation period (48 h). Meanwhile, a few small peaks corresponding to conjugated-C=C appear at 131.7-136.0 ppm emerge during the early stage of the oxidation and then decrease in intensity as the oxidation proceeds. Several other small peaks in the range of 142-160 ppm are believed to be due to the C=C conjugated to a carbonyl group<sup>5</sup>. The observation is in accordance to the generally accepted oxidation mechanism: first non-conjugated *cis*-C=C bonds are converted into *conj*-C=C during the formation of hydroperoxides, and then all double bonds are consumed as the oxidation continues<sup>11</sup>. During the  $\text{Mn}(\text{acac})_3$ -catalyzed oxidation of  $^{13}\text{C}$ -EL (Figure 6.6b), the decrease of the non-conjugated *cis*-C=C and the formation of conjugated-C=C is also observed. However, a significant amount of non-conjugated-*cis*-C=C still remains after 48 h.

The quantified results on the change of *cis*-C=C and *conj*-C=C are shown in Figure 6.7. It is clearly shown that the conversion of *cis*-C=C in the presence of  $\text{Mn}(\text{acac})_3$  is much slower compared to Co-EH and the  $\text{Mn}(\text{acac})_3/\text{bpy}$  combination, in agreement with FTIR<sup>12</sup> and Raman studies (Chapter 5). In the latter two cases *cis*-C=C has almost fully reacted after 48 h, indicating again that the combination of  $\text{Mn}(\text{acac})_3/\text{bpy}$  is a superior catalyst for the EL oxidation. Although the  $^{13}\text{C}$  peaks from *conj*-C=C are generally small, we try to analyze quantitatively the evolution of *conj*-C=C in the presence of various catalysts, as also shown in Figure 6.7. For Co-EH and the  $\text{Mn}(\text{acac})_3/\text{bpy}$  combination, the amount of *conj*-C=C first increases and then decreases during the oxidation of  $^{13}\text{C}$ -EL. For  $\text{Mn}(\text{acac})_3$  only a monotonic increase in the *conj*-C=C amount is observed in 48 h, due to the slow *cis*-C=C conversion.



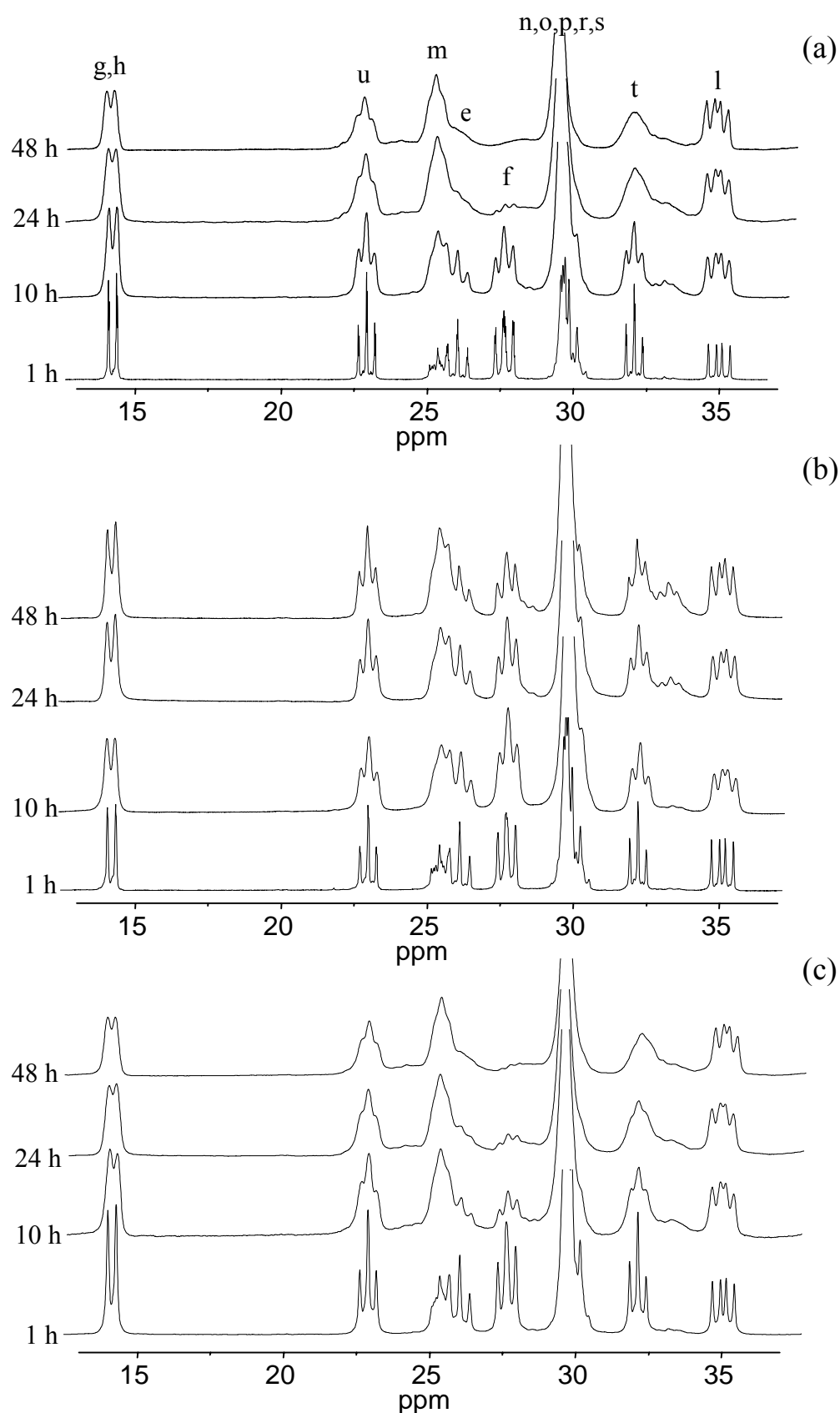
**Figure 6.6.** Variation of double bonds during the oxidation of  $^{13}\text{C}$ -EL followed by  $^{13}\text{C}$ -NMR in the range of 120-160 ppm in the presence of (a) Co-EH, (b)  $\text{Mn}(\text{acac})_3$ , and (c)  $\text{Mn}(\text{acac})_3/\text{bpy}$ .



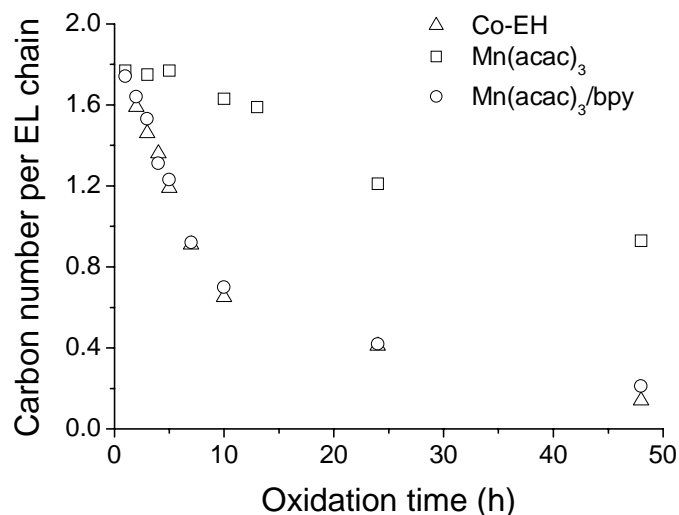
**Figure 6.7.** The conversion of *cis*-C=C and the evolution of *conj*-C=C during the oxidation of <sup>13</sup>C-EL in the presence of various catalysts.

### 6.5.3. Variation of allylic groups during the oxidation of <sup>13</sup>C-EL

Figure 6.8 illustrates the <sup>13</sup>C-NMR spectra (13-36 ppm) during the oxidation of <sup>13</sup>C-EL in the presence of various catalysts. The decrease in the double allylic C (26 ppm) and monoallylic C (27.5 ppm) is clearly visible. Unfortunately, the double allylic C peak overlaps with another peak, so the quantification is only made for the monoallylic C, as shown in Figure 6.9. Once again, the decrease in the monoallylic C peak is much more rapid for Co-EH and the Mn(acac)<sub>3</sub>/bpy combination than Mn(acac)<sub>3</sub> alone during the oxidation of <sup>13</sup>C-EL, very similar to the trend observed for non-conjugated *cis*-C=C in Figure 6.7.



**Figure 6.8.**  $^{13}\text{C}$ -NMR spectra (13-36 ppm) during the oxidation of  $^{13}\text{C}$ -EL in the presence of (a) Co-EH, (b)  $\text{Mn}(\text{acac})_3$ , and (c)  $\text{Mn}(\text{acac})_3/\text{bpy}$ .



**Figure 6.9.** The conversion of monoallylic C (27.5 ppm) during the oxidation of  $^{13}\text{C}$ -EL in the presence of various catalysts.

#### 6.5.4. Other oxidation products

Besides, the formation of *conj*-C=C, ROOR, and ROOH, other non-volatile oxidation products have been reported during the oxidation of EL<sup>5</sup>, such as epoxides, endoperoxides, alcohols and ROR links (as indicated in Figure 6.2), aldehydes, ketones, acids, and etc. Due to the low intensity of these peaks, quantification is not attempted in this study. Nonetheless, it appears that all these compounds are formed during the oxidation of  $^{13}\text{C}$ -EL, irrespective of the catalyst used.

#### 6.6. Conclusions

In summary, the use of  $^{13}\text{C}$ -EL enhances the intensity of  $^{13}\text{C}$ -NMR signals that provide a better identification of the oxidation products. The individual evolution of hydroperoxides (ROOH) and peroxy links (ROOR) is clearly revealed by  $^{13}\text{C}$ -NMR. Quantitative analysis on the changes in a few major peaks has been successfully attempted, and the results are generally in line with some early findings by other techniques given in Chapter 5.

## **6.7. References**

1. Oyman Z.O., Ming W., van der Linde R., et al., *Polymer* 45 (2004) 7431.
2. Bieleman J.H., "Additives for Coatings", Wiley-VCH, Weinheim (2000) Chp. 7.
3. Mallécol J., et al., *Prog. Org. Coat.* 39 (2000) 107.
4. Muizebelt W.J., et al., *Prog. Org. Coat.* 40(1-4) (2000) 121.
5. Muizebelt W.J., et al., *J. Coat. Techn.* 70(876) (1998) 83.
6. Marshall G.L., et al., *Polymer* 29(8) (1988) 1501.
7. Marshall G.L., et al., *Polymer* 28(7) (1987) 1093.
8. Assink R.A., et al., *Macromolecules* 33 (2000) 4023.
9. Zawadiak J., Danch M., *J. Appl. Polym. Sci.* 91 (2004) 15.
10. Fleming W.W., MacDonald S.A., *Anal. Chem.* 55 (1983) 1625.
11. Oyman Z.O., Ming W., van der Linde R., *Prog. Org. Coat.* 48(1) (2003) 80.
12. van Gorkum R., et al., *Inorg. Chem.* 43 (2004) 2456.





## **Chapter 7**

# **Oxidative drying of real alkyd coatings catalyzed by MnMeTACN\***

### **Summary**

*In this Chapter the application of MnMeTACN in real alkyd coatings is demonstrated to show the technological relevance of this catalyst. Preliminary results on the film properties (drying time and film hardness) for various solvent/water-borne alkyd coatings demonstrate that MnMeTACN is a potential alternative for commercially available Co- and Mn-based catalysts. MnMeTACN appears to be suitable for both water-borne and solvent-borne alkyd systems. Confocal Raman microscopy is used to study the depth profile of the drying of alkyd coatings catalyzed by different catalysts, and it is found that slow surface drying is somewhat compensated by relatively fast deep layer drying.*

---

\* Part of this Chapter was presented at XXVII FATIPEC Congress (April, 2004, Aix-en-Provence, France), and has been submitted for publication: Z.O. Oyman, W. Ming, R. van der Linde, J. ter Borg, A. Schut, J.H. Bieleman, submitted to *Surface Coatings International* (Dec. 2004).

## 7.1. Introduction

The ultimate aim of this research is to replace cobalt-based catalysts with environmentally friendlier alternatives for alkyd coatings. The alkyd coatings catalyzed by the new catalysts should have better or at least comparable film properties compared to those catalyzed by a cobalt catalyst. In this chapter, the technological relevance of the Mn-based catalysts, MnMeTACN<sup>1</sup> in particular, will be investigated by using MnMeTACN as the catalyst for real alkyd coatings.

Effects of various manganese-based catalysts on the oxidation of model compounds for alkyd resins have been demonstrated in the previous Chapters of this thesis<sup>1,2</sup>. Model compounds can mimic the chemical processes during the drying of alkyd coatings<sup>3-7</sup>. However, there are important differences between model compounds and real alkyds. For instance, for model compounds only oligomers are formed during the oxidation<sup>8</sup> while, for a real alkyd coating, a cross-linked network is formed during drying, leading to a large increase in viscosity and the subsequent immobilization of chains that may have a significant effect on further reactions. It is, therefore, necessary to study the drying of real alkyd coatings catalyzed by the Mn-based catalysts.

However, it is not trivial to follow cross-linking reactions during the drying of an alkyd coating with common analytical techniques, and due to its complexity the drying process has not been extensively studied. Among the very few studies, solid-state NMR was used to follow the oxidation reactions of alkyd coatings in the presence of a cobalt-based catalyst<sup>9,10</sup>, and FTIR<sup>11</sup> and Raman<sup>12</sup> spectroscopy techniques were also used. Raman spectroscopy in particular appeared to be a suitable technique studying the oxidative drying of alkyd resins due to the strong Raman intensity of double bonds<sup>13,14</sup>. These studies, however, only provided information on the bulk of the systems. On the other hand, it is known that cross-linking is not homogeneous along the depth of an alkyd film<sup>14-17</sup>. Confocal Raman Microscopy (CRM) was recently used to monitor the depth profiling chemical changes of polymeric films<sup>14-16</sup>.

In this Chapter we also use CRM to investigate the chemical changes during the drying of solvent/water-borne alkyd coatings catalyzed by MnMeTACN and other catalysts. Film properties such as drying time, hardness, whiteness index, and gloss will be investigated.

## 7.2. Experimental

### 7.2.1. Materials

The following alkyd resins were kindly provided by DSM Coating Resins, Zwolle, The Netherlands<sup>18</sup>: (a) a short oil alkyd resin based on soya bean oil, URALAC AK 429 WX-55, a 55 w% solution in white spirit/xylene (50/50, w/w) with an oil length of approximately 40; (b) a short oil alkyd emulsion based on also soya bean oil, URADIL AZ-554 Z-50 with an oil length of approximately 40; and (c) a long oil alkyd emulsion based on tall oil fatty acids, URADIL AZ-516 Z-60 with an oil length of approximately 63. A long oil alkyd resin dissolved in white spirit, SETAL 16 LV WS-70), was obtained from Akzo Nobel Resins, Bergen op Zoom, The Netherlands. Solvent/water-based paints were formulated from these alkyd resins separately. MnMeTACN was a gift from Unilever R&D, Vlaardingen. The Co(II)-2-ethylhexanoate (Co-EH) was obtained from Sigma-Aldrich. Two catalysts for solvent borne alkyd paints, Nuodex Combi BSR (containing 1.1% Co, 2.2% Ca, and 4.45% Sr) and Nuodex Mn (10 w% of Mn), and two catalysts for water-borne alkyd paints, Nuodex Web-Co (containing 6 w% Co) and Nuodex Web-Mn (9 w% Mn), were obtained from Sasol Servo B.V. (Delden, The Netherlands). Netherlands). Chemicals were used as received.

### 7.2.2. Confocal Raman Microscopy (CRM) for depth profiling

Drying of alkyd resins was followed *in-situ* by Confocal Raman Microscopy on a Dilor-Jobin Yvon-Horiba confocal dispersive Raman spectrometer (514 nm excitation wavelength, 100  $\mu\text{m}$  pinhole, and 10 mW laser intensity) with an Olympus MX40 microscope. Details about the CRM technique and the experimental set-up can be found in the Appendix. Alkyd resins were first vigorously mixed with 0.07 % (metal/resin, w/w) catalysts at room temperature for CRM analysis, and then deposited onto glass slides with a wet film thickness of  $\sim 200$   $\mu\text{m}$  using a doctor blade. After the solvent/water evaporation ( $\sim 30$  min), depth profiling analyses (each time 2.5  $\mu\text{m}$  deeper from the surface) of the films were performed automatically with a piezo-driven objective-positioning device using long working distance objective. Instead of a real depth, a nominal depth was used; depending on the refractive index of the material the real depth would be around twice of the nominal depth<sup>14</sup>. The measurement was repeated each hour.

### 7.2.3. Preparation of paint systems

Paints were formulated with alkyd resins containing pigment and dispersing agents. Materials were dispersed either on a pearl mill (solvent-borne) or on a high-speed dissolver (water-borne). Catalysts were added during the letdown stage of formulated paints and were stirred afterwards. Wet films were applied on glass substrates for drying time and hardness measurements 1 week after the siccation. When MnMeTACN was used for solvent-borne alkyd paints, a small amount of ethylene glycol was added to obtain homogeneous solutions.

### 7.2.4. Drying tests of alkyd resin-based paints

Drying time of the films (wet film thickness: 76  $\mu\text{m}$  at 23  $^{\circ}\text{C}$  and 50% humidity) was determined on a Braive recorder (30.5 $\times$ 2.5 cm) according to ASTM D5895-96.

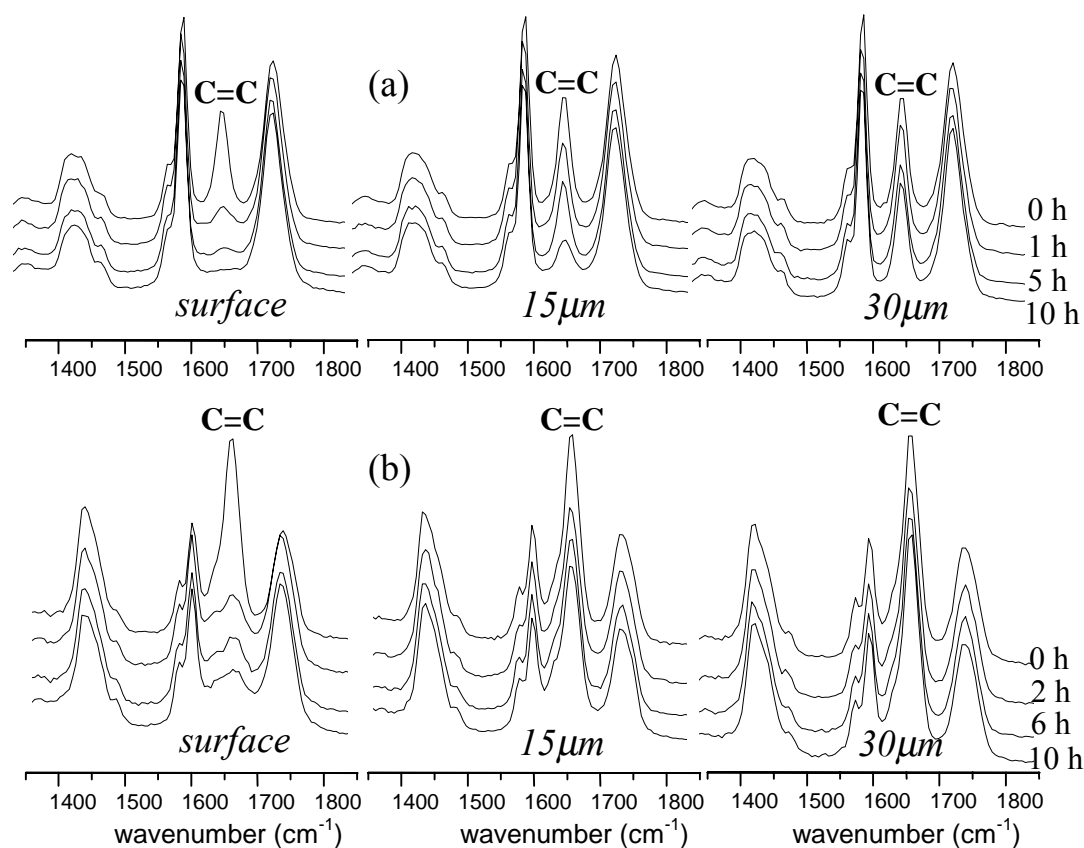
The drying mainly consists of four phases obtained from the trace pattern of the stylus in the film: stage a: solvent evaporation takes place, so-called “leveling”; stage b: a line is visible, and the paint begins to polymerize, so-called “sol-gel phase”; stage c: the stylus stops tearing or cutting the film, but only leaves a visible trace on the film, so-called “surface dry time”; and stage d: the film has solidified so completely that a large, twisting force can be applied without distorting the film, reaching so-called “through drying time”.<sup>19</sup>

Wet films (60  $\mu\text{m}$  in thickness at 23  $^{\circ}\text{C}$  and 50% humidity) were applied on glass slides, and the König hardness of the dried films was determined using the pendulum-damping test according to ASTM D4366-95. Whiteness index was measured with BYK Gardner Handheld Color guide according to ASTM E313. Gloss was measured with BYK Gardner Haze-Gloss meter according to ASTM D523 or DIN 67530.

## 7.3. Effect of various catalysts on the drying of alkyd resins followed by CRM

Typical depth profiling Raman spectra (1400-1800  $\text{cm}^{-1}$ ) during the drying of alkyd paints, a short oil alkyd emulsion and a long oil solvent-borne alkyd, are shown in Figure 7.1. In both cases, the intensity of the C=C stretch peak at 1650  $\text{cm}^{-1}$  decreases substantially at the film surface during the 10-h drying. However, in deeper layers (*e.g.*, 15  $\mu\text{m}$ ) the extent of the C=C conversion appears to be much less,

compared to the surface drying; this is especially true for the long-oil alkyd (Figure 7.1b). At a depth of about 30  $\mu\text{m}$ , virtually no C=C conversion is discerned for both alkyds. The different extents of the C=C conversion indicate that oxidation reactions are not homogeneous at different depths of the films.



**Figure 7.1.** Raman spectra (1400-1800  $\text{cm}^{-1}$ ) at different depths during the drying of (a) URADIL AZ554 Z-50, a short oil-alkyd emulsion, catalyzed by Web-Co, and (b) SETAL 16 LV WS-70, a long oil-alkyd in white spirit, catalyzed by Co-EH.

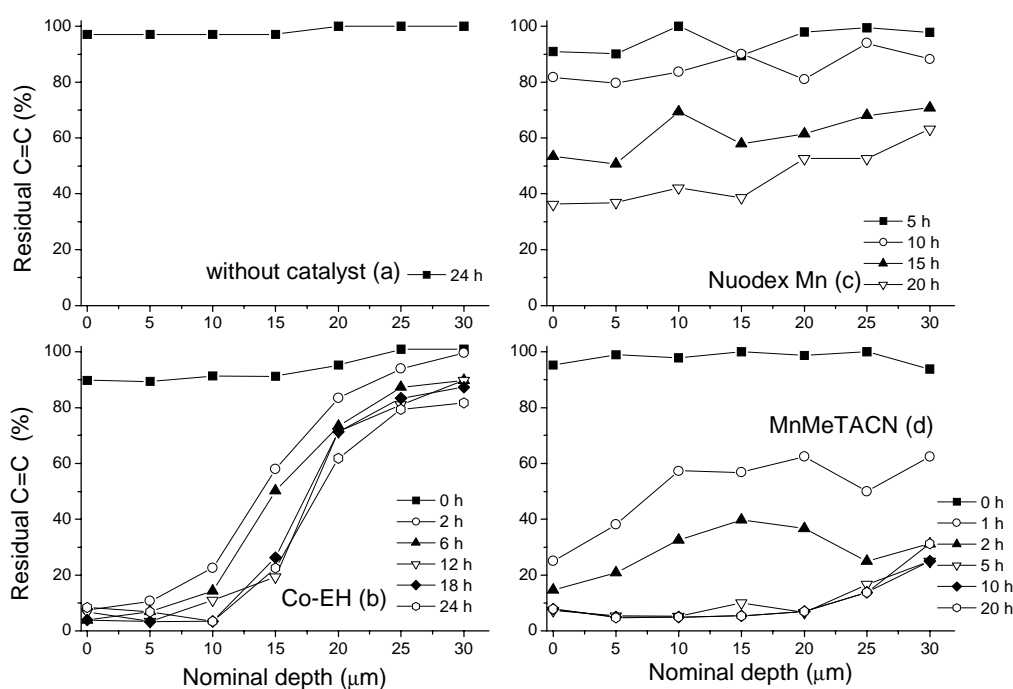
In the following we will examine the depth profiling C=C conversions for both solvent-borne and water-borne alkyds catalyzed by various catalysts, with the aromatic double bond peak at 1600  $\text{cm}^{-1}$  as an internal standard.

### 7.3.1. Depth profiling during the drying of solvent-borne alkyd resins

*Drying of a short oil alkyd resin.* Figure 7.2 illustrates the depth profiling C=C conversion during the drying of a solvent-borne short oil alkyd resin. First of all, in

the absence of a catalyst there is no double bond conversion after 24 h (Figure 7.2a), indicating the necessity of an effective catalyst to accelerate the oxidative drying of an alkyd.

When Co-EH is used as a catalyst, significant changes were observed during the oxidation. As shown in Figure 7.2b, around 90% of the double bonds have already disappeared at the surface after only 2 h. The conversion of double bonds after 18 h reaches 95% at the surface. Despite the very fast reaction at the surface, the conversion of double bonds is significantly lower in the deeper layers ( $> 15 \mu\text{m}$ ). Only around 20% of C=C disappeared at  $30 \mu\text{m}$  after 24 h. A very different trend in the conversion of C=C was observed in the presence of a commercial manganese based-catalyst (Nuodex Mn), as shown in Figure 7.2c. The C=C conversion at the film surface is much slower in the presence of Nuodex Mn: only ~65% of C=C has been converted after 20 h. Unlike Co-EH, however, there is almost no difference for the C=C conversion between the film surface and deep layers for Nuodex Mn.

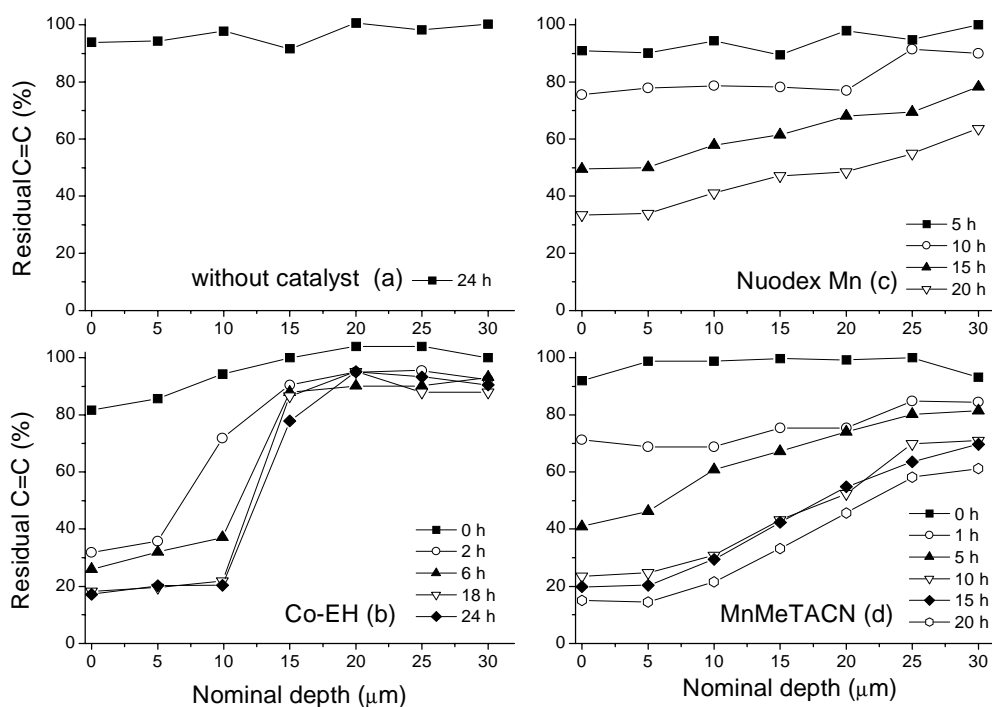


**Figure 7.2.** The depth profiling of the residual C=C amount during the drying of URALAC AK 429 WX-55 (a short oil-based alkyd) catalyzed by different catalysts followed by CRM.

When MnMeTACN was used as a catalyst for solvent-borne systems, a small amount of ethylene glycol was added to render the mixture homogeneous. As can be seen in Figure 7.2d, the extent of C=C conversion in the presence of MnMeTACN appears to fall in between that for Co-EH and Nuodex Mn. For MnMeTACN, the surface C=C conversion and the conversion in deeper layers is somewhat balanced: the reaction at the surface is not as fast as in the case of Co-EH but the deep layer conversion is far superior to the Co-catalyst. The performance of MnMeTACN is apparently much better than Nuodex Mn.

*Drying of a long oil alkyd resin.* Figure 7.3 shows the depth profiling C=C conversion during the drying of a solvent-borne long oil alkyd resin. Similar to the short oil alkyd resin, virtually no oxidation takes place in the absence of a catalyst after 24 h (Figure 7.3a). In the presence of various catalysts, the depth profiling C=C conversion appears to be very similar to what has been observed for the short oil alkyd (Figure 7.3): the surface C=C conversion in the presence of the Co-catalyst is the fastest, followed by MnMeTACN and Nuodex Mn; for the deep layer C=C conversion, both Mn-based catalysts are better than the Co-catalyst.



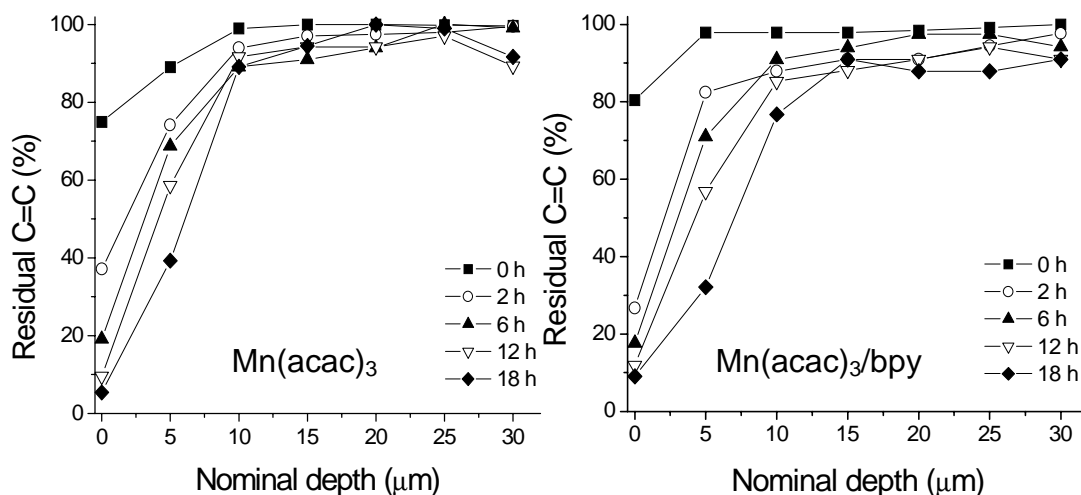


**Figure 7.3.** The depth profiling of the residual C=C amount during the drying of SETAL 16 LV WS-70 (a long oil-based alkyd) catalyzed by different catalysts followed by CRM.

*Drying of a long oil alkyd resin catalyzed by  $Mn(acac)_3$ -based catalyst.*

$Mn(acac)_3$ -based catalysts (details can be found in Chapter 5) are also tested for the drying of the long oil alkyd resin, as shown in Figure 7.4. When the alkyd is catalyzed by  $Mn(acac)_3$  alone, the C=C conversion profile seems to be similar to the alkyd catalyzed by the Co-catalyst (Figure 7.3): the double bonds at the surface react faster and in the deep layer (10-30 μm) the C=C conversion is less than 10%. In spite of this similarity, it seems that the Co-catalyst is more active in the first 10 μm of the film.

When bpy is combined with  $Mn(acac)_3$ , the depth profile of the C=C conversion does not differ much (Figure 7.4). A noticeable improvement lies in the conversion in the deeper layers (10-30 μm): a marginally higher C=C conversion (about 20%) can be seen, which is likely due to the higher catalytic capability of the  $Mn(acac)_3$ /bpy combination, as demonstrated in Chapter 5.

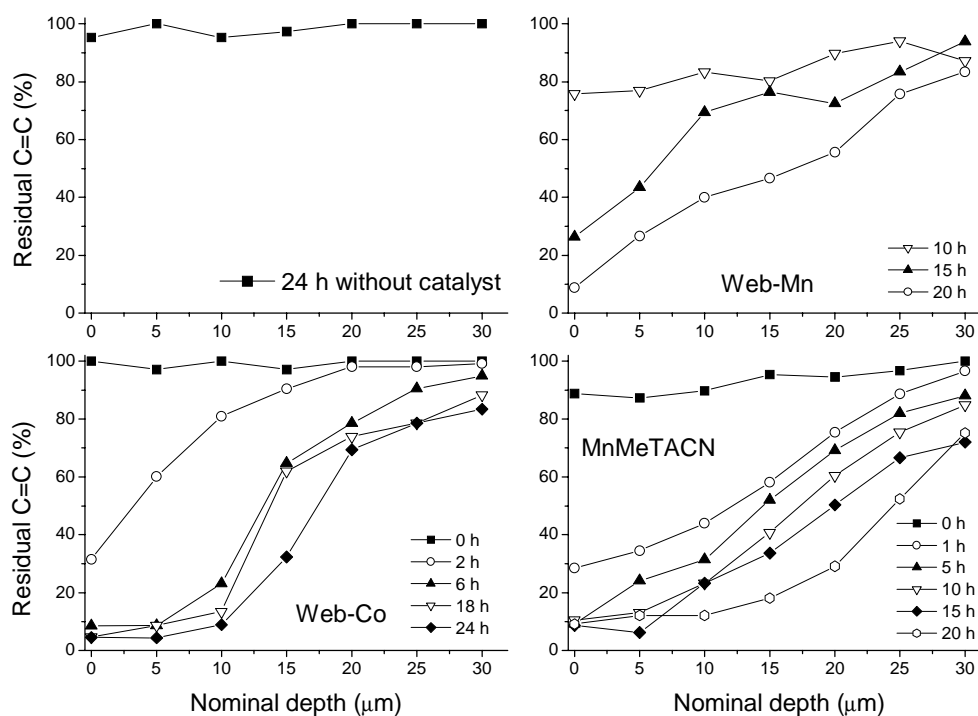


**Figure 7.4.** The depth profiling of the residual C=C amount during the drying of SETAL 16 LV WS-70 (a long oil-based alkyd) catalyzed by Mn(acac)<sub>3</sub>-based catalysts followed by CRM.

### 7.3.2. Depth profiling during the drying of water-borne alkyd resins

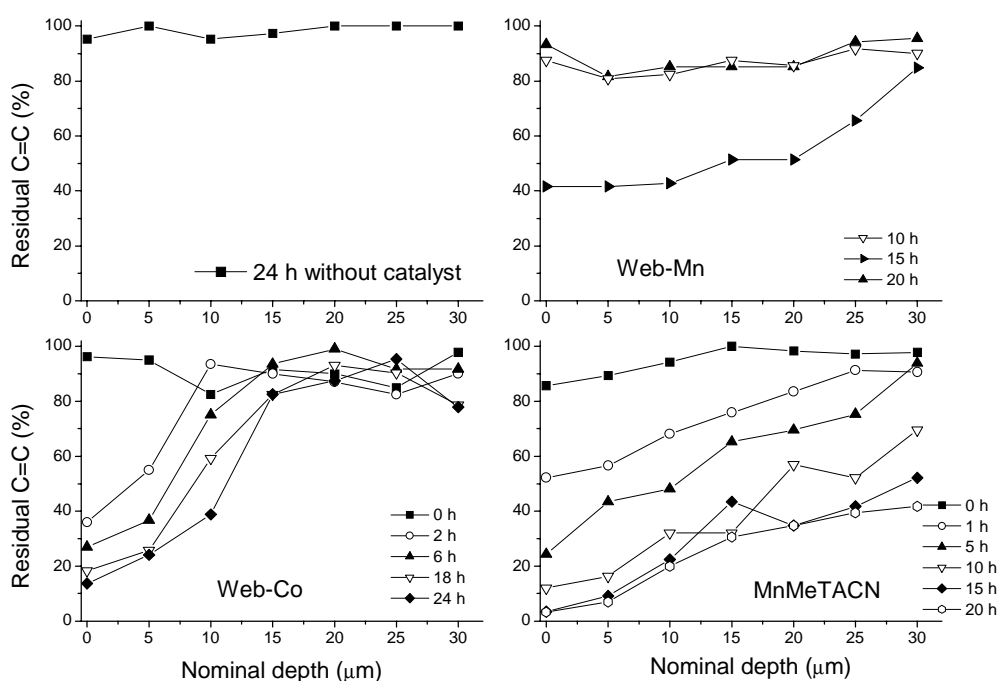
*Drying of a short oil alkyd emulsion.* The depth profiling C=C conversion during the drying of a short oil-based alkyd emulsion, URADIL AZ 554 Z-50, catalyzed by different catalysts is shown in Figure 7.5. In comparison with Figure 7.2, the depth profile for the oxidation of water-borne alkyds demonstrates a strong similarity with their solvent-borne counterparts, regardless of the catalyst used, even though for the water-borne alkyds water-emulsifiable Web-Co and Web-Mn catalysts are used. The Co- and Mn-based catalysts used for solvent-borne systems, Co-EH and Nuodex Mn, cannot be directly used in water-borne systems since the catalytic activity is lost due to the formation of metal hydrate complexes<sup>21</sup>. There is no such a problem for MnMeTACN; MnMeTACN is a water-soluble catalyst. The adaptability of MnMeTACN in both solvent-borne and water-borne systems is certainly an advantage over the other commercially available catalysts we have tested.

The MnMeTACN/HMTETA combination was also used for the drying of the alkyd emulsion, but no obvious difference was observed, compared to the system catalyzed by MnMeTACN alone.



**Figure 7.5.** The depth profiling of the residual C=C amount during the drying of URADIL AZ 554 Z-50 (a short oil-based alkyd emulsion) catalyzed by different catalysts followed by CRM.

*Drying of a long oil alkyd emulsion.* Drying of long oil alkyd emulsion was also investigated. Again, the similar depth profiles are observed when compared to the solvent-borne long oil-based alkyd, as shown in Figure 7.6. MnMeTACN seems to be a better catalyst than Web-Co and Web-Mn in terms of the C=C conversion both at the surface and in deeper layers.



**Figure 7.6.** The depth profiling of the residual C=C amount during the drying of URADIL AZ 554 Z-60 (a long oil-based alkyd emulsion) catalyzed by different catalysts followed by CRM.

### 7.3.3. Implications from surface versus deep-layer drying

It is clearly shown by CRM that the double bond conversion is not homogeneous along the depth of the alkyd coatings catalyzed by Co-based catalysts. This is probably due to the very high catalytic activity of the Co-catalysts. The C=C conversion at the surface is much higher than the deeper layers due to the presence of an ample amount of oxygen in air. The high C=C conversion to some extent corresponds to a high degree of cross-linking; consequently, a relatively dense solid film may form at the surface, possibly limiting the diffusion of oxygen to the deep layers<sup>14,15</sup>. The lack of oxygen may be the main reason that, for alkyd coatings catalyzed by the Co-catalysts, the C=C conversion is low in the deep layers. This may also partially explain the phenomenon that, under the skin that forms during storage of alkyd paint, the alkyd paint remains as a liquid; once the skin is removed, a new layer of skin will readily form.

The catalytic activity of commercially available Mn-based catalysts is much lower than the Co-based catalysts, therefore the surface cross-linking during the

drying of an alkyd would occur to a much lesser extent and the diffusion of oxygen to the deeper layers is less hindered. This may explain why for the commercially available Mn-based catalysts, Nuodex Mn and Web-Mn, there is not much difference between the surface drying and deeper-layer drying.

The catalytic activity of MnMeTACN falls in between the Co-catalysts and the commercially available Mn-catalysts, leading to the following scenario: the surface drying of an alkyd catalyzed by MnMeTACN is slower than by a Co-catalyst, but faster than by a commercially available Mn-catalyst; meanwhile, the deep-layer drying of an alkyd in the presence of MnMeTACN is better than in the presence of a Co-catalyst, but not as uniform as in the presence of a commercially available Mn-catalyst. In summary, it appears that slow surface drying is somewhat compensated by relatively fast deep-layer drying.

#### **7.4. Drying tests and film properties of alkyd coatings**

Drying tests for various solvent-borne and water-borne alkyd paints catalyzed by MnMeTACN were performed in comparison with commercially available Co- and Mn-based catalysts. Some film properties were measured as well. Drying tests of several solvent-borne alkyd paints in the presence of  $\text{Mn}(\text{acac})_3$  and  $\text{Mn}(\text{acac})_3/\text{bpy}$  can be found elsewhere<sup>21</sup>.

##### **7.4.1. Drying of solvent-borne alkyd paints**

*A short oil-alkyd paint.* In the absence of a catalyst, the paint dries very slowly (more than 20 h needed for total dry), as shown in Table 7.1, while the film hardness is far inferior to the coatings catalyzed by Co- or Mn-based catalysts. The total drying time of the film in the presence of Nuodex Mn is reduced to 16 h and the König hardness increases up to 100 s after 1 week drying. When a cobalt based-catalyst (Nuodex Combi BSR) is used, a much shorter total drying time (8 h) and a higher value of the hardness (118 s after 1 week) of the films are obtained. The performance of MnMeTACN (Table 7.1) appears to be very close to the Co-based catalyst and much better than Nuodex Mn. The gloss value for all four coatings is similar. Moreover, although MnMeTACN is reddish, the whiteness index of the coating catalyzed by MnMeTACN is acceptable.

Table 7.1. Drying tests and film properties of a solvent-borne short oil alkyd resin based paint (URALAC AK 429 WX-55).

Samples	Braive recorder 76 $\mu$ m at 23 °C	Whiteness Index	Gloss 60°	König hardness (s)	
	Total dry (h)			1 day	1 week
No catalyst	> 20.0	80.5	95.1	22.0	64.0
Nuodex Mn 0.03%	16.0	79.5	95.8	60.0	100.0
Nuodex Combi BSR 0.03%	8.0	76.4	95.9	80.0	118.0
MnMeTACN 0.03%	10.0	77.7	95.8	76.0	112.0

*A long oil-alkyd paint.* The long oil alkyd film without a catalyst does not dry after 24 h and remains tacky after 1 week. In the presence of Nuodex Mn, the improvement in the drying and film properties appears to be marginal (Table 7.2). A significant improvement is obtained when the film is catalyzed by the cobalt-based catalyst. The surface drying time is shortened to 4.1 h and the hardness value increases to 77 s after 1 week. Similar to the cobalt-based catalyst, MnMeTACN also demonstrates a substantial catalytic effect on the paint drying as well as film properties.

Table 7.2. Drying tests and film properties of a solvent-borne long oil alkyd resin based paint (SETAL 16 LV WS-70).

Samples	Braive recorder 76 $\mu$ m at 23 °C	Whiteness Index	Gloss 60°	König hardness (s)	
	Total dry (h)			1 day	1 week
No catalyst	> 20.0	- <sup>(1)</sup>	- <sup>(1)</sup>	11.0	13.0
Nuodex Mn 0.06%	> 20.0	73.0	88.0	12.0	25.0
Nuodex Combi BSR 0.06%	> 20.0 <sup>(2)</sup>	73.8	86.0	42.0	77.0
MnMeTACN 0.04%	5.0 <sup>(2)</sup>	78.1	91.7	39.0	67.0

<sup>(1)</sup> No data for gloss and whiteness index because film is tacky - does not dry.

<sup>(2)</sup> For Co-based catalyst, a = 1.0, b = 1.1, c = 4.1 (surface drying), d  $\geq$  20 (total drying); for MnMeTACN, a = 1.1, b = 1.30, c = 3.1 (surface drying), d = 5 (total drying). See section 7.2.4 for details.

### 7.4.2. Drying of water-borne alkyd paints

The drying tests on the water-borne alkyd (short and long oil) emulsions were also performed in the presence of various catalysts, as given in Tables 7.3 and 7.4. Among the three catalysts used, Web-Co appears to be the best. To our surprise, on the other hand, the performance of MnMeTACN (the film hardness in particular) is not better than Web-Mn, even though it has been shown that, from model compounds in emulsions (Chapter 5) and depth profiling analysis by CRM on water-borne alkyds (this chapter 7.3.2), MnMeTACN is a much more active catalyst than Web-Mn. The reason for this observation is currently unclear. Nevertheless, compared to Web-Mn, the paints catalyzed by MnMeTACN appear to dry a little faster, whereas the low whiteness index value may be due to the high amount of the catalyst.

Table 7.3. Drying tests and film properties of a short oil alkyd emulsion based paint (URADIL AZ 554 Z-50).

Samples	Braive recorder 76 $\mu$ m at 23 °C	Whiteness Index	Gloss 60°	König hardness (s)		
	total dry (h)			1 day	1 week	6 weeks
No catalyst	> 10.0	81.3	93.5	15.0	49.0	42.0
Nuodex Web-Mn 0.07%	> 10.0	74.3	93.1	28.0	43.0	52.0
Nuodex Web-Co 0.07%	2.0	76.6	93.5	38.0	63.0	80.0
MnMeTACN 0.07%	3.1	70.0	94.4	32.0	45.0	57.0

Table 7.4. Drying tests and film properties of a short oil alkyd emulsion based paint (URADIL AZ 516 Z-60).

Samples	Braive recorder 76 $\mu$ m at 23 °C	Whiteness index	Gloss 60°	König hardness (s)		
	total dry (h)			1day	1 week	6 weeks
No catalyst	> 20.0	80.4	88.0	8.0	14.0	17.0
Nuodex Web- Mn 0.07%	14.0	76.7	89.1	15.0	20.0	24.0
Nuodex Web- Co 0.07%	9.0	76.8	92.6	18.0	31.0	42.0
MnMeTACN 0.07%	10.0	68.7	93.2	14.0	17.0	22.0

## 7.5. Conclusions

In conclusion, MnMeTACN appears to be a promising catalyst for the oxidative drying of both solvent-borne and water-borne alkyd paints. The film properties in the presence of MnMeTACN lie between the coatings catalyzed by cobalt-catalysts and those by commercial manganese-based catalysts, in line with the fact that the catalytic capability of MnMeTACN also falls in between these two types of commercially available catalysts.

## 7.6. References

1. Chapter 4 of this thesis.
2. Chapter 5 of this thesis.
3. Muizebelt W.J., et al., *Prog. Org. Coat.* 24(1-4) (1994) 263.
4. Mallégol J., et al., *Prog. Org. Coat.* 39 (2000) 107.
5. Muizebelt W.J., Hubert J.C., Nielen M.W.F., Klaasen R.P., Zabel K.H., *Prog. Org. Coat.* 40(1-4) (2000) 121.
6. Frankel E.N., et al., *Lipids* 12(11) (1977) 901.
7. Porter N.A., et al., *Lipids* 30(4) (1995) 277.
8. Muizebelt W.J., Nielen M.W.F., *J. Mass. Spec.* 31 (1996) 545.
9. Marshall G.L., et al., *Polymer* 29(8) (1988) 1501.
10. Marshall G.L., et al., *Polymer* 28(7) (1987) 1093.
11. Hartsthon J.H., *J. Coat. Techn.* 54(687) (1982) 53.
12. Ellis G., Claybourn M., *Spectrochimica Acta* 46A(2) (1990) 227.
13. Agbenyega J.K., Claybourn M., Ellis G., *Spectrochimica Acta* 47A(9/10) (1991) 1375.
14. Laven J., et al., *Proceedings of the International Conference of Coatings Science and Technology*, Athens, Greece, (2003) 205.
15. Marton B., *A depth resolved look at the film formation and properties of alkyd-based coatings*, thesis, U. Twente (2004).
16. Mirone G., Marton B., Vancso G.J., *Eur. Polym. J.* 40(3) (2004) 549.
17. Froud C.A., Hayward I.P., Laven J. et al., *Appl. Spec.* 57 (2003) 12.
18. [www.dsmcoatingresins.com](http://www.dsmcoatingresins.com).
19. Koleske J.V., “*Paint and Coating Testing Manual*”, ASTM manual series (1995) 439.



20. Bieleman J.H., "*Additives for Coatings*", Wiley-VCH, Weinheim (2000) Chp. 7.
21. van Gorkum R., et al. (2004) EP1382648.

## Chapter 8

### Epilogue

Alkyd paints have been the workhorses of the coatings industry for more than 50 years. The possibility to obtain versatile, low cost, renewable, and low VOC emission products makes alkyd paints very attractive materials in the modern society.

Today, it is well known that chemical drying of alkyds occurs via the oxidation of the unsaturated fatty acid ester chains in the alkyd resin, catalyzed by metal-based catalysts, known as “driers”. These catalysts are the inevitable ingredients in typical alkyd paint formulations. Cobalt-based compounds are very effective primary catalysts in these oxidation reactions at room temperature.

In Chapter 3 of this thesis we showed that cobalt-catalyzed chemical drying of model systems from emulsions occurs similarly to the solvent-borne systems. In addition, a clear distinction between the oxidation mechanism of conjugated drying oils and non-conjugated drying oils has been made. Several mechanisms of the cobalt compounds involved in catalyzing oxidation reactions were already proposed in the literature. No study so far, including this study, is able to demonstrate the exact active species involved in the cobalt-catalyzed oxidations of alkyd resins. Further research should continue towards finding these active species to provide a fundamental understanding of the drying processes.

Cobalt compounds were recently reported as potentially carcinogenic to tissues and lungs. In this thesis two environmentally friendlier manganese-based complexes are demonstrated as the promising alternatives to cobalt-based catalysts.

A significant catalytic activity of  $[\text{Mn}^{\text{IV}}_2(\mu\text{-O})_3\text{L}_2](\text{PF}_6)_2$  (MnMeTACN) (L = 1,4,7-trimethyl-1,4,7-triazacyclononane) is observed during the oxidation of EL from emulsions even though MnMeTACN is barely soluble in ethyl linoleate (EL). Catalytic activity of MnMeTACN is further improved by the addition of polyamines such as 1,1,4,7,10,10-hexamethyl triethylenetetramine (HMTETA). We showed that hydroperoxides are the necessary ingredients for MnMeTACN. A tentative catalytic cycle is proposed based on the reversible transition between Mn(IV) and Mn(III). However, the catalytic activity in the absence of polyamines is still lower than the cobalt-based catalysts in EL oxidation. We demonstrated that MnMeTACN is an

effective catalyst when it is molecularly mixed with EL. Further research should continue with the lipophilic derivatives of MnMeTACN, which may provide much higher catalytic activities than MnMeTACN in emulsions.

Mn(acac)<sub>3</sub>, particularly in combination with 2,2'-bipyridine (bpy) is also shown to be a promising catalyst in Chapter 5 of this thesis. [Mn<sup>II</sup>(acac)<sub>2</sub>(bpy)] and [Mn<sup>III</sup>(acac)<sub>2</sub>(bpy)]<sup>+</sup> are proposed as the active species involved in the catalytic cycle. The Mn(acac)<sub>3</sub>/bpy combination is found to be *too* active at decomposing the formed hydroperoxides, which leads to uncross-linked oxidation products. Instead of bpy other ligands that have slightly slower hydroperoxide decomposing performance than bpy may lead to a good balance between high oxidation rate and effective cross-linking.

It is shown that manganese-based complexes can reach the catalytic activities similar to the cobalt carboxylates during the chemical drying of alkyd coatings. Catalytic activity of other metal-based catalysts such as vanadium or bismuth compounds as oxidation catalysts may be the topic of further research.

The use of <sup>13</sup>C-labeled EL gives more insights on the oxidation reactions, particularly the evolution of hydroperoxides and peroxy links as demonstrated in Chapter 6. On the other hand, it is expected that labeling exclusively double-bond carbon atoms may give much better understanding on the oxidation mechanism of the unsaturated fatty acids.

The ultimate goal of the research should be the creation of environmentally friendly organic-based catalysts, which may totally replace metal-based catalysts for the formulations of alkyd coatings.

## Appendix

### General overview of the analytical techniques and methods

#### Summary

*Basic principles of analytical techniques and methods used in this thesis are briefly described.*

#### A.1. General overview of the characterization methods used on the oxidation of unsaturated fatty acid derivatives

In the previous studies on the oxidation of unsaturated fatty acid derivatives and alkyd coatings, many techniques have been used such as FTIR<sup>1-5</sup>, solid-state NMR<sup>6,7</sup> and solution NMR<sup>8</sup>, Raman spectroscopy<sup>9-12</sup> and Confocal Raman Microscopy<sup>13,14</sup>, size exclusion chromatography (SEC),<sup>8,15</sup> mass spectrometry<sup>16</sup>, various hyphenated techniques such as gas chromatography (GC)-MS including head-space GC-MS<sup>17</sup> and liquid chromatography (LC)-MS<sup>18</sup>, atomic force microscopy (AFM)<sup>14</sup>, magnetic resonance imaging (MRI)<sup>19</sup>, and differential scanning calorimetry (DSC)<sup>20</sup>.

In the next section a general introduction on techniques and methods used in this thesis is given. Experimental details and other techniques that are not mentioned here can be found in the respective Chapters.

#### A.2. Raman spectroscopy

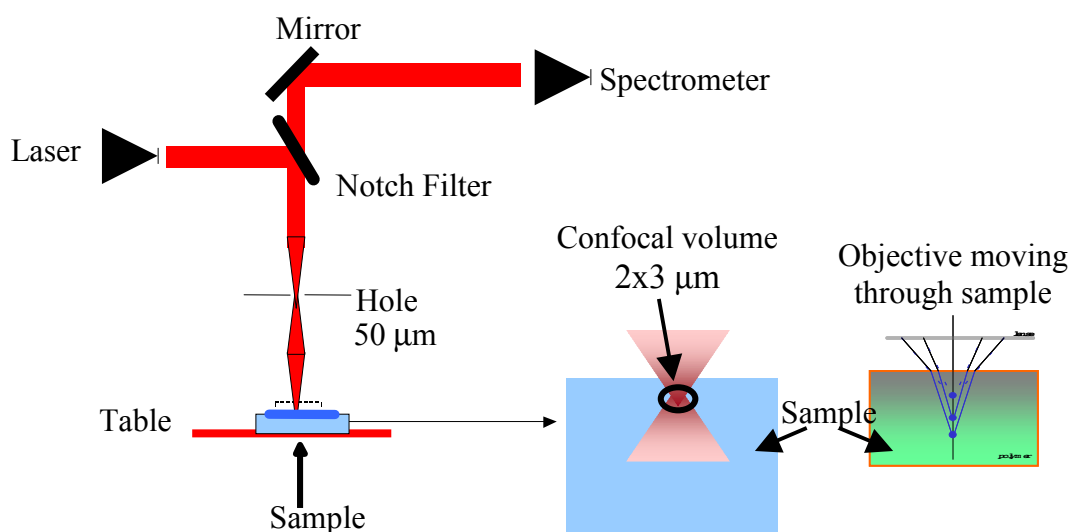
Sample handling for Raman spectroscopy measurements is simpler than for transmission infrared spectroscopy because glass can be used for windows, lenses, and other optical components instead of more fragile and less stable crystalline halides.

Fiber optics can be used to bridge large distances (as much as 100 m or more) and online non-invasive monitoring of the reactions can be performed<sup>21-24</sup>. Since the technique is based on scattered light instead of light that passes through the sample,

transparency of the samples is not required. Therefore, Raman spectroscopy can be applied to turbid dispersions and solid organic/inorganic materials with no sample pretreatment. Since the intensity of water peaks is quite low in Raman spectra, measurements can be performed in the presence of water.

Raman spectra yield more information about certain types of organic compounds than their infrared counterparts. For example double bond stretching vibration for olefins ( $\sim 1600\text{ cm}^{-1}$ ) is intense and its position is sensitive to the nature of substituents as well as to their geometry. Thus, Raman studies are likely to yield great information about olefinic functional groups that may not be revealed by infrared spectra<sup>12</sup>.

The use of Raman depth profiling to determine the structural changes of polymeric layers is increasing<sup>13,14</sup>. By using a confocal pinhole the scattering that arrives in the analyzer is restricted to a volume with very small focus depth, which gives information on the local chemical composition of a sample. A schematic representation of a general set-up for the Confocal Raman Microscope is given in Figure A.1. Laser radiation passes through a notch filter (to filter most of the Rayleigh scattering) and a pinhole (the smaller the size of the pinhole, the smaller the confocal volume). Chemical composition on the different layers of the medium can be examined by a movable objective in the Z-direction (through the sample).



**Figure A.1.** A general set-up of confocal Raman Microscopy.

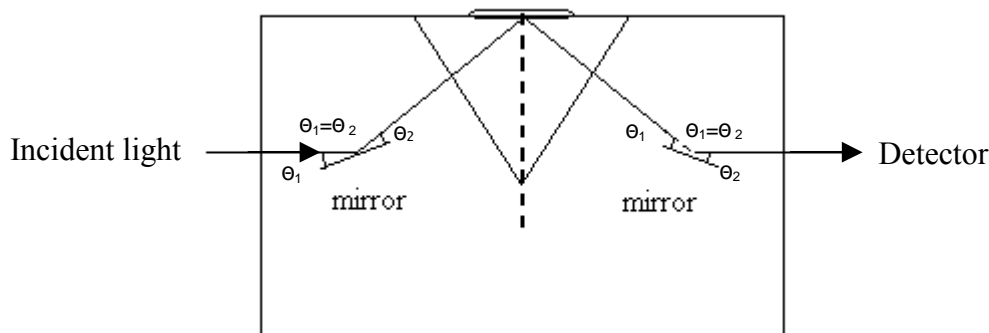
Drying of alkyd resins was followed *in-situ* by confocal Raman microscopy on a Dilor-Jobin Yvon-Horiba confocal dispersive Raman spectrometer (514 nm excitation wavelength, 100  $\mu\text{m}$  pinhole, and 10 mW laser intensity) with an Olympus MX40 microscope. Samples were deposited onto glass slides with a wet film thickness of  $\sim 200 \mu\text{m}$  using a doctor blade. After the water evaporation (30-40 min), depth profiling measurements (each time 2.5  $\mu\text{m}$  deeper from the surface) of the films were performed automatically with a piezo-driven objective-positioning device using long working distance objective. Instead of a real depth, a nominal depth was used; the real depth would be around twice of the nominal depth<sup>13</sup>. The measurement was repeated each hour. Experimental results are shown in Chapter 7 of this thesis.

### **A.3. Attenuated total reflectance (ATR)-infrared spectroscopy**

One of the most frequently used surface infrared techniques nowadays is attenuated total reflectance (ATR)-infrared spectroscopy. With ATR technique, non-destructive in-situ monitoring of the surfaces of solid powders, liquids, films and coatings can be obtained.

#### ***Principle***

When electromagnetic radiation strikes an interface between media of two different refractive indices, refraction and reflection can occur. The fraction of radiation that is reflected becomes larger with increasing differences in refractive index and may be reflected totally at the interface<sup>25</sup>. A small part of this reflected radiation actually penetrates on the low refractive index material near the interface. Low refractive index material absorbs specific frequencies of radiation resulting in an absorption spectrum. This penetration depth basically depends on the angle of the incident light and the refractive indices of two media. A schematic representation of a fixed angle ATR accessory is depicted in Figure A.2.



**Figure A.2.** An ATR accessory for single reflection with a fixed angle prism at  $45^\circ$ .

There are various ATR accessories with possibilities of multiple reflections of the radiation and variable angle. The latter option allows depth profiling of the materials. Several optical materials used in internal reflection spectroscopy (such as diamond, germanium, zinc selenide, zinc sulfide) are available. They are transparent for infrared radiation and their refractive indices are quite high (2.0 to 4.0), where the refractive indices for organic substrates are usually around 1.5. More detailed information about ATR can be found elsewhere<sup>25</sup>.

The oxidation of model compounds was followed *in-situ* by time-resolved ATR-FTIR on a Bio-Rad Excalibur FTS3000MX infrared spectrophotometer (30 scans per spectrum with a resolution of  $4\text{ cm}^{-1}$ ) equipped with an ATR diamond unit (Golden Gate).

#### A.4. Fiber-optic oxygen meter

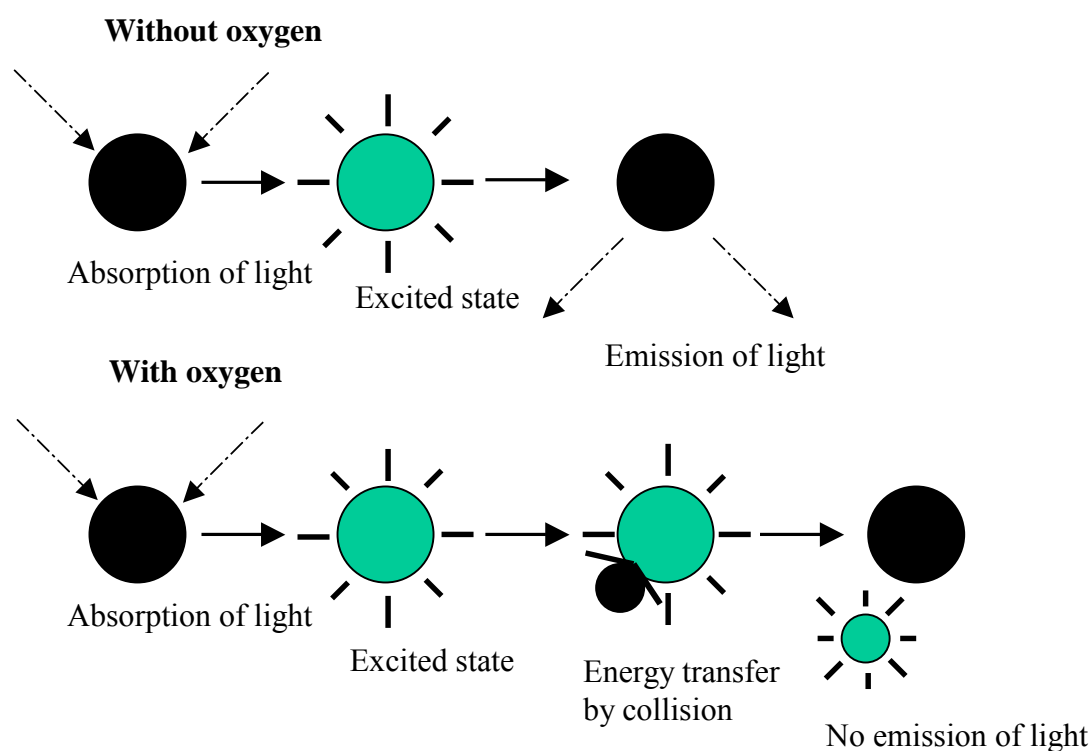
The principle of the fiber-optic oxygen meter is based on the quenching of luminescence caused by collision between molecular oxygen and luminescent dye molecules in the excited state. The collision between the luminophore in its excited state and the quencher (oxygen) results in radiationless deactivation, which is called 'collisional or dynamic quenching'. After collision, energy transfer takes place from the excited indicator molecule to oxygen, which is subsequently transferred from its ground state (triplet state) to its excited singlet state. As a result, the indicator molecule does not emit luminescence and the measurable luminescence signal decreases. A schematic representation of the dynamic quenching of luminescence is given in Figure A.3.

The relation between the oxygen concentration and the luminescence intensity and lifetime is described by the Stern-Volmer equation:<sup>26</sup>

$$\frac{I_0}{I} = \frac{\tau_0}{\tau} = 1 + K_{sv}[\text{O}_2]$$

$\tau_0$  and  $\tau$  are the luminescence decay times in the absence and the presence of oxygen,  $I_0$  and  $I$  are the luminescence intensities in the absence and the presence of oxygen,  $[\text{O}_2]$  is the oxygen concentration, and  $K_{sv}$  is the overall quenching constant (Stern-Volmer constant, quantifies the quenching efficiency therefore the sensitivity of the sensor). The concentration of oxygen molecule can be calculated by measuring the luminescence intensities or decay times.

### Dynamic Quenching of Luminescence



**Figure A.3.** A schematic representation of the dynamic quenching of luminescence<sup>26</sup>.

A Fibox fiber-optic oxygen meter (Precision Sensing GmbH) was used to measure the oxygen uptake of model compounds in the presence of catalysts during the oxidation reactions. The oxygen meter consists of an oxygen sensor probe (PSt3). The tip of the probe is coated with a Pt(II) indicator dye embedded in a silicone



matrix, which is connected to a LED (excitation wavelength: 505 nm) through a fiber optic cable, a photomultiplier detector (PMT). A PT 100 type temperature sensor is used for temperature compensation. More detailed information about the working principle and the measurement ranges of the oxygen meter can be found elsewhere<sup>26</sup>. Experimental details are given in the respective Chapters.

#### **A.5. Head-space gas chromatography-mass spectrometry (HSGC-MS)**

Head-space gas chromatography (HSGC) is an indirect method of analysis for the rapid determination of volatile components of liquid and solid samples. The principle of the operation of this technique is based on gas chromatographic analysis of the sample in gas-vapor phase in thermodynamic equilibrium with the sample in a closed vial. Under these conditions, the quantity of volatile components is proportional to their concentration in the sample<sup>27</sup>.

HSGC eliminates all the disadvantages connected with the sample preparation requiring tedious and time-consuming procedures to concentrate the trace components, and it avoids possible interference with non-volatile components. The technique is particularly suitable for the determination of traces in samples, which cannot be injected through gas chromatography because of column overloading or contamination, decomposition or dissociation problems. The sample is not vaporized in the GC, therefore its partial decomposition is avoided and interference of other components eliminated<sup>27</sup>.

HSGC generally consists of 6 components: sampling unit, control module, revolving turret, injection assembly, sample tray, and incubation oven. Incubation oven incorporates a motor to shake the sample during the incubation period. Sample tray can accommodate up to 32 vials numbered for identification. Revolving turret consists of a vertical, moving structure that houses the injection assembly and performs movements necessary to transfer vials from the sample tray to the incubation oven, to draw and inject headspace gas. In the injection assembly, a high precision gas withdrawal from the vial and subsequent injection of the headspace vapors takes place through a gas tight syringe installed on a movable sliding plate located inside the revolving turret. The gas tight syringe is housed in a thermostatic holder (temperature range 40 to 150 °C).

EL (1 g) was first mixed with different catalysts (0.07% w/w, metal/oil). An aliquot of 10 mg was placed in a 20-mL head-space vial for each measurement,

followed by the addition of 1  $\mu\text{L}$  of cyclohexane solution (0.37 M in xylene) as an internal standard. Vials were then sealed with silicon rubber Teflon<sup>®</sup> caps using a crimper. EL was oxidized in the sealed vials in the presence of catalysts. Several vials were prepared and, at different time intervals, volatile byproducts were determined on a Thermoquest CE 2000 series trace GC-MS equipped with static head-space autosampler (HS 2000 model). Trace GC was equipped with a capillary column (based on silica, length 60 m  $\times$  0.25 mm, 0.25  $\mu\text{m}$  thickness, Alltech). Helium was used as a carrier gas, and ionisation mode of the trace MS was electron impact (EI+). All of the intricate operations of establishing an equilibrium in static head-space analysis was performed by the HS 2000 robotic autosampler through a local controller using Windows<sup>®</sup>-based software. After reaching equilibration, the heated gas-tight head-space syringe (45  $^{\circ}\text{C}$ ) was moved over the incubator by a turret and a sample was withdrawn. The turret was turned to the position over the inlet, and the injection was made. The syringe was then automatically cleaned with a purged carrier gas (He). For the programmable temperature vaporisation (PTV) injector method, the base temperature was 43  $^{\circ}\text{C}$  with a split flow of 50 mL/min. The transfer temperature to the column was 325  $^{\circ}\text{C}$ . The GC column was programmed with an initial hold of 4 min at 45  $^{\circ}\text{C}$  and then the temperature was raised to 330  $^{\circ}\text{C}$  at a rate of 10  $^{\circ}\text{C}/\text{min}$ . Peak areas for the volatiles (e.g. hexanal, pentanal) were integrated and normalized with the peak area of cyclohexane using characteristic mass ranges. The amounts of hexanal and pentanal formed during the oxidation of EL were calculated by using pure compounds of hexanal, pentanal as references. The typical experimental error for the GC-MS analysis was found to be 6%. Other experimental details are given in the respective Chapters.

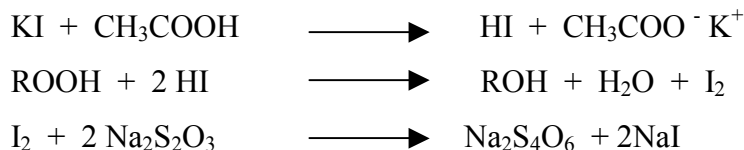
#### **A.6. NMR**

Chemical changes during the oxidation of unsaturated fatty acid derivatives were followed by  $^1\text{H}$  and  $^{13}\text{C}$  NMR. NMR spectra were recorded on Varian 400 and 500 MHz spectrometers. Experimental details are given in the respective Chapters.

#### **A.7. Peroxide Value**

An American Oil Chemists' Society (AOCS)-approved method for determining peroxide value (PV, Cd 8b-53)<sup>28</sup> is used with some modifications.

Peroxide value calculations are based on the reactions shown below.



Peroxide values are calculated using the following equation expressed as mmol/kg unless otherwise stated.

$$\text{PV} = [1000 \cdot (V - V_0) \cdot c] / 2m$$

Where

V = volume of sodium thiosulfate solution in mL

V<sub>0</sub> = volume of sodium thiosulfate solution for blank sample in mL

c = concentration of sodium thiosulfate solution, in mol/L

m = mass of the sample

The accuracy of the method was checked by the titration of H<sub>2</sub>O<sub>2</sub> and cumene hydroperoxide, and it was found that typical experimental error was less than 2%.

Other methods and experimental considerations are discussed in the related Chapters of this thesis.

## A.8. References

1. Muizebelt W.J., Van Velde J.W., Van Wijk F.G.H., *Adv. Org. Coat. Sci. Techn Ser.* 13 (1991) 57.
2. Muizebelt W.J., et al., *Prog. Org. Coat.* 40(1-4) (2000) 121.
3. Hartsthon J.H., *J. Coat. Techn.* 54(687) (1982) 53.
4. Mallégol J., et al., *Prog. Org. Coat.* 39(1-3) (2000) 107.
5. Muizebelt W. J., et al., *J. Coat. Techn.* 69(869) (1997) 59.
6. Marshall G.L., et al., *Polymer* 29(8) (1988) 1501.
7. Marshall G.L., et al., *Polymer* 28(7) (1987) 1093.
8. Muizebelt W.J., et al., *J. Coat. Techn.* 70(876) (1998) 83.
9. Davies J.E.D., et al., *J. Chem. Soc., Perkin Trans.* 2(11) (1972) 1557.

10. Agbenyega J.K., Claybourn M., Ellis G., *Spectrochimica Acta* 47A(9/10) (1991) 1375.
11. Ellis G., Claybourn M., *Spectrochimica Acta* 46A(2) (1990) 227.
12. Oyman Z.O., Ming W., van der Linde R., *Prog. Org. Coat.* 48 (2003) 80.
13. Laven J., et al., *Proceedings of the International Conference of Coatings Science and Technology*, Athens, Greece (2003) 205.
14. Marton B., et al., *Polym. Mater. Sci. Eng.* 88 (2003) 445.
15. Muizebelt W.J., et al., *Prog. Org. Coat.* 24(1-4) (1994) 263.
16. Muizebelt W.J., Nielen M.W.F., *J. Mass. Spec.* 31 (1996) 545.
17. Frankel E.N., et al., *Lipids* 12(11) (1977) 901.
18. Steven Q.Y., et al., *Free Rad. Bio. Med.* 34(8) (2003) 1017.
19. Mallegol J., et al., *J. Coat. Techn.* 74(933) (2002) 113.
20. Mallegol J., et al., *Prog. Org. Coat.* 41(1-3) (2001) 171.
21. van den Brink M., *On-line monitoring of polymerization reactions by Raman spectroscopy*, thesis, TU Eindhoven (2000).
22. Pepers M. L. H., *On-line monitoring and control of co polymerizations*, thesis, TU Eindhoven (2004).
23. van der Maas J., “*Raman Spectroscopy Course Manual*”, University of Utrecht, 15-16 Oct. (2001).
24. [www.jobinyvin.co.uk](http://www.jobinyvin.co.uk).
25. Urban W.M., “*Attenuated Total Reflectance Spectroscopy of Polymers*”, ACS Publ. (1996) 6.
26. Fibox fiber-optic oxygen meter instruction manual ([www.presens.de](http://www.presens.de)).
27. Manual of Thermoquest CE 2000 series head-space GC-MS (<http://www.thermoquest.com>).
28. American Oil Chemists’ Society, Cd 8b-53 (1990).



## Summary

The objective of this research was to obtain a deep understanding of the catalytic activities and reaction mechanisms during the chemical drying of alkyd resins in the presence of cobalt-based and potential manganese-based catalysts. These Mn-based catalysts are promising alternatives to the conventional, carcinogenic cobalt-based compounds that are currently widely used in alkyd coatings. Instead of alkyd resins, model compounds such as (m)ethyl esters of fatty acids and drying oils, were mostly used in this study.

Oxidations of model compounds in the presence of Co-based catalysts are described in the first part of the thesis. The great loss of the formed conjugated double bonds after the initial formation suggests that radical addition to the double bonds also plays a major role during the oxidation of non-conjugated systems. The oxidation of drying oils containing non-conjugated double bonds is compared with drying oils containing conjugated double bonds. The rationale of their mechanistic differences during the oxidation is examined. It is found that for the oil containing non-conjugated double bonds, more oxygen is consumed and more hydroperoxides and  $\beta$ -scission byproducts are formed as compared to the oil containing conjugated double bonds. The free radical addition to conjugated double bonds is predominant for conjugated system leading to higher molecular weight oligomers. The oxidation of model compounds from emulsions, after the water evaporation, is found to be similar to the oxidation of solvent-borne model compounds.

In the second part of the thesis an environmentally-friendly dinuclear manganese-based complex,  $[\text{Mn}^{\text{IV}}_2(\mu\text{-O})_3\text{L}_2](\text{PF}_6)_2$  (MnMeTACN) (L = 1,4,7-trimethyl-1,4,7-triazacyclononane), is described as a potential catalyst for alkyd paints. The catalytic activity of MnMeTACN is further improved by the addition of polyamines such as 1,1,4,7,10,10-hexamethyl triethylenetetramine (HMTETA) during the oxidation of ethyl linoleate in emulsions. The main role of polyamines is proposed as increasing the miscibility between MnMeTACN and EL (MnMeTACN is barely soluble in EL), and decomposing the formed hydroperoxides. However, the existence of HMTETA leads to the formation of a high amount of volatile byproducts and less oligomerization. When MnMeTACN is molecularly mixed with EL in a co-solvent (*i.e.*, methanol), with the assistance of existing hydroperoxides, MnMeTACN alone is

found to be a very active catalyst for EL oxidation. A tentative catalytic cycle for MnMeTACN on the decomposition of hydroperoxides is proposed, which is based on the reversible transition between Mn(IV) and Mn(III) containing species. It is shown that hydroperoxides are necessary for the fast initiation of the catalytic cycle for MnMeTACN. The use of MnMeTACN in both solvent-borne and water-borne systems is an advantage over other commercially available catalysts.

The oxidation of EL is also examined in the presence of Mn(III)acetylacetonate ( $\text{Mn}(\text{acac})_3$ ) as a promising catalyst and the possible role of 2,2'-bipyridine (bpy) ligand on  $\text{Mn}(\text{acac})_3$  is explained. The catalytic system  $\text{Mn}(\text{acac})_3$ , particularly in combination with bpy, has a very high activity for the oxidation of EL. *In-situ* formation of the species  $[\text{Mn}^{\text{II}}(\text{acac})_2(\text{bpy})]$  and  $[\text{Mn}^{\text{III}}(\text{acac})_2(\text{bpy})]^+$  and the high reactivity of these two species with ROOH and EL, respectively, are proposed as the main reason for the observed high oxidation rate. The lower performance for  $\text{Mn}(\text{acac})_3/\text{bpy}$  in real alkyd paint might be attributed to the fact that  $\text{Mn}(\text{acac})_3/\text{bpy}$  is *too* active: the oxidation reactions yield predominantly alkoxy radicals, which results in less oligomerization and more volatile byproducts. A good oxidative drying should be based on a proper balance between the fast oxidation (formation of hydroperoxides and their subsequent decomposition into free radicals) and the effective formation of higher oligomers.

Furthermore, the oxidation of  $^{13}\text{C}$ -labeled ethyl linoleate, a model compound for alkyd coatings, is investigated in the presence of various catalysts. For the first time, the individual evolution of hydroperoxides (ROOH) and peroxy links (ROOR) is clearly revealed by  $^{13}\text{C}$ -NMR.

In the final part of the thesis the application of MnMeTACN in real alkyd coatings is demonstrated. Results on the film properties (drying time and film hardness) demonstrate that MnMeTACN is a potential alternative for commercially available Co- and Mn-based catalysts for various solvent/water-borne alkyd coatings. Confocal Raman Microscopy is used to study the depth profile of the drying of alkyd coatings catalyzed by different catalysts, and it is found that slow surface drying is somewhat compensated by relatively fast deep layer drying in the presence of Mn-based catalyst.

## Samenvatting

Het doel van dit onderzoek is het verkrijgen van diepgaand inzicht in de katalytische activiteit en de reactiemechanismen tijdens de droging van alkydharsen in de aanwezigheid van katalysatoren op basis van cobalt of mangaan. De katalysatoren op basis van mangaan zijn veelbelovende alternatieven voor de conventionele, carcinogene verbindingen op basis van cobalt, die momenteel veel gebruikt worden in alkydcoatings. In plaats van alkydharsen zijn in deze studie veelal modelverbindingen zoals (m)ethylesters van vetzuren en drogende oliën gebruikt.

Het eerste deel van dit proefschrift gaat over de oxidatie van modelverbindingen in aanwezigheid van katalysatoren op basis van cobalt. De sterke afname van het aantal gevormde geconjugeerde dubbele bindingen na aanvankelijke vorming ervan doet veronderstellen dat radicaaladditie aan de dubbele bindingen ook bij de oxidatie van verbindingen zonder geconjugeerde bindingen een grote rol speelt. Verder zijn drogende oliën met geconjugeerde dubbele bindingen qua drooggedrag vergeleken met oliën met niet-geconjugeerde dubbele bindingen. Oliën van de laatstgenoemde soort vertonen een hoger zuurstofverbruik en een hogere productie van hydroperoxides en  $\beta$ -scission-bijprodukten. Bij oliën van de eerste soort is de vrij-radicaaladditie aan geconjugeerde bindingen overheersend; dit leidt tot met hoger molecuul gewicht oligomeren. Het oxidatiegedrag in een dunne laag van modelverbindingen aangebracht op een substraat is vergelijkbaar met dat van een dunne laag van een waterige emulsie van die modelverbinding waaruit het water na aanbrenging verdampt cq is verdampt. De gevonden verschillen in reactiemechanisme worden besproken en verklaard.

In het tweede deel van dit proefschrift wordt een milieuvriendelijk dinucleair complex op basis van Mn,  $[\text{Mn}^{\text{IV}}_2(\mu\text{-O})_3\text{L}_2](\text{PF}_6)_2$ ; (MnMeTACN) (L = 1,4,7-trimethyl-1,4,7-triazacyclononaan), beschreven. Dit blijkt een potentiële katalysator te zijn voor alkydverven. De katalytische activiteit van MnMeTACN tijdens de oxidatie van films op basis van ethyllinoleaat(EL)-emulsie kan verder verbeterd worden door toevoeging van polyamines zoals 1,1,4,7,10,10-hexamethyl triethyleentetramine (HMTETA). Als belangrijkste rol van polyamines wordt voorgesteld dat het de mengbaarheid van MnMeTACN en EL verhoogt (MnMeTACN zelf is nauwelijks oplosbaar in EL), en dat het de gevormde hydroperoxides ontleedt. De aanwezigheid



van HMTETA leidt echter ook tot de vorming van grote hoeveelheden vluchtige bijproducten tengevolge van  $\beta$ -scission; een te hoog gehalte aan HMTETA zou leiden tot bijproducten die niet kunnen crosslinken en tot minder oligomerisatie. Indien MnMeTACN moleculair wordt gemengd met EL in een co-solvent (methanol), blijkt MnMeTACN, in combinatie met de aanwezige hydroperoxiden, een zeer actieve katalysator te zijn voor de oxidatie van EL. Een mogelijk schema voor een katalytische reactiecyclus van MnMeTACN bij de ontleding wordt voorgesteld; het is gebaseerd op de reversibele overgang tussen de Mn(IV) en de Mn(III) variant van de verbinding. Aangetoond wordt dat de aanwezigheid van hydroperoxides noodzakelijk is voor de snelle initiatie van de katalytische reactiecyclus van MnMeTACN. Het gebruik van MnMeTACN in plaats van commercieel verkrijgbare katalysatoren is voordelig, zowel in oplosmiddel-gebaseerde als in watergedragen systemen.

De oxidatie van EL is ook onderzocht in de aanwezigheid van Mn(III)acetylacetaat ( $\text{Mn}(\text{acac})_3$ ). Ook Deze verbinding is veelbelovend als katalysator. De mogelijke rol van de 2,2'-bipyridine (bpy) ligande van  $\text{Mn}(\text{acac})_3$  wordt verklaard. Het katalytische systeem  $\text{Mn}(\text{acac})_3$  heeft, vooral in combinatie met bpy, een zeer hoge activiteit voor de oxidatie van EL. Voorgesteld wordt dat de *in-situ* vorming van de verbindingen  $[\text{Mn}^{\text{II}}(\text{acac})_2(\text{bpy})]$  en  $[\text{Mn}^{\text{III}}(\text{acac})_2(\text{bpy})]^+$  en hun hoge reactiviteit met ROOH en EL de belangrijkste oorzaken zijn voor de waargenomen hoge oxidatiesnelheid. De slechtere "performance" van  $\text{Mn}(\text{acac})_3/\text{bpy}$  in echte alkydverf zou veroorzaakt kunnen zijn door het feit dat  $\text{Mn}(\text{acac})_3/\text{bpy}$  te actief is: de oxidatiereacties leveren vooral alkoxyradicalen hetgeen leidt tot minder oligomerisatie en tot meer vluchtige bijproducten. Goede oxidatieve droging vereist een juiste balans tussen de snelle oxidatie, waarbij hydroperoxides ontstaan die vervolgens ontleden in vrije radicalen, en de effectieve vorming van relatief lange oligomeren.

De oxidatie van EL, een modelverbinding voor alkydverven, is bovendien onderzocht met een  $^{13}\text{C}$  gelabelde variant, in aanwezigheid van verschillende katalysatoren. Dit onderzoek is het eerste waarin, met behulp van  $^{13}\text{C}$ -NMR, het te gelijktijd ontstaan van hydroperoxides (ROOH) en peroxies (ROOR) kon worden onderscheiden.

In het laatste deel van dit proefschrift wordt de toepassing van MnMeTACN in echte coatings gedemonstreerd. Resultaten van filmeigenschappen (droogtijd en

filmhardheid) tonen aan dat MnMeTACN potentieel een alternatief is voor commercieel verkrijgbare katalysatoren op basis van Co en Mn, voor diverse oplosmiddel-gebaseerde en watergedragen alkydverven. Confocale Raman Microscopie is gebruikt om diepteafhankelijk de mate van droging van alkydfilms te bepalen, bij gebruik van uiteenlopende katalysatoren. Bij gebruik van Mn drogers blijkt de langzame droging dicht bij het oppervlak in zekere mate samen te gaan met een relatief snelle droging in diepere lagen.



## Özet

Bu çalışma kobalt ve yeni geliştirilmiş mangan esaslı kurutucuların alkid reçinelerinin kimyasal kuruma sırasındaki etkisine derin bir anlayış getirmesini amaçlamaktadır. Kimyasal kuruma sırasındaki katalitik aktiviteleri ve reaksiyon mekanizmalarına bir ışık tutulmaya çalışılmıştır. Mangan esaslı bu kurutucular, şu anda alkid boyalarında sıkça kullanılan ve kansorejen olduğu iddia edilen kobalt esaslı bileşiklere alternatiflerdir. Alkid reçineleri yerine çoğunlukla yağ asitlerinin (m)etil esterleri gibi model sistemler kullanılmıştır.

Model sistemlerin kobalt esaslı kurutucuların etkisi altındaki oksitlenmesi bu tezin ilk kısmında tanımlanmıştır. Oluşan konjüğe çifte bağların büyük bir bölümü oksitlenme sırasında reaksiyona girmiştir. Bu sonuç konjüğe olmayan sistemlerin oksitlenmesi sırasında radikallerin çifte bağlara katılma reaksiyonunun da önemli bir rol oynadığını göstermektedir. Ayrıca konjüğe ve konjüğe olmayan çifte bağlar içeren bitkisel yağların oksitlenmeside karşılaştırılmıştır. Konjüğe olmayan çifte bağların oksitlenme sırasında konjüğe çifte bağlar içeren yağlara oranla daha fazla oksijen harcadığı ve daha fazla hidroperoksit ve  $\beta$ -scission ürünleri oluşturduğu bulunmuştur. Serbest radikallerin konjüğe çifte bağlara katılma reaksiyon mekanizması konjüğe sistemler için daha baskın gözükmemektedir ve bu mekanizma daha yüksek molekül ağırlıklı oligomerlerin oluşmasına yol açmaktadır. Emülsiyon esaslı model sistemlerin oksitlenmesi suyun buharlaşmasından sonra solvent esaslı model sistemlerin oksitlenmesiyle benzer olduğu saptanmıştır.

Tezin ikinci kısmında alkid reçineleri için çevreye kobalt a oranla daha dost mangan esaslı bir kompleks olan  $[Mn^{IV}_2(\mu-O)_3L_2](PF_6)_2$  (MnMeTACN) (L = 1,4,7-trimethyl-1,4,7-triazacyclononan) tanımlanmıştır. MnMeTACN in katalitik aktivitesi etil linoleate emülsiyonunun oksitlenmesinde 1,1,4,7,10,10-hexametil trietilenetetramin (HMTETA) gibi poliaminlerle daha da arttırılmıştır. Poliaminlerin ana görevi MnMeTACN ve EL in karışabilirliğini arttırmak (MnMeTACN EL içinde çok az çözünmektedir) ve hidroperoksitleri serbest radikallere ayırmak olarak önerilmiştir. Fakat HMTETA daha fazla uçucu ürünlerin oluşmasına yol açmaktadır. Fazla miktarda HMTETA kullanıldığında ise çapraz bağlamaya yol açmayan ürünler ve daha az oligomerizasyon ortaya çıkmaktadır. MnMeTACN kosolvent (metanol gibi) sayesinde moleküler olarak EL ile karıştığında hidroperoksitlerin yardımıyla

MnMeTACN in poliaminler olmaksızın EL oksitlenmesi için çok aktif bir katalizör olduğu bulunmuştur. MnMeTACN için geri dönüşümlü ve hidroperoksitlerin serbest radikallere çevrildiği Mn(IV) ve Mn(III) içeren maddelerin olduğu bir katalitik mekanizma önerilmiştir. Katalitik mekanizmanın hızlı başlayabilmesi için hidroperoksitlerin gerekli olduğu gösterilmiştir. MnMeTACN in hem solvent esaslı hem de su esaslı sistemlerde kullanılabilirliği endüstride kullanılan diğer katalizörlere göre bir avantaj teşkil etmektedir.

Mn(III)asetilaseton ( $Mn(acac)_3$ ) etkisi altındaki EL oksitlenmesi ve 2,2'-bipyridin (bpy) in  $Mn(acac)_3$  e olan etkiside araştırılmıştır.  $Mn(acac)_3$  katalitik sisteminin özellikle bpy etkisi altında EL oksitlenmesinde çok aktif olduğu saptanmıştır. Oksitlenme sırasında oluşan  $[Mn^{II}(acac)_2(bpy)]$  and  $[Mn^{III}(acac)_2(bpy)]^+$  bileşiklerinin ROOH ve EL ile olan yüksek reaktivitesi oksitlenme reaksiyonlarının hızının yüksek olmasının nedeni olarak gösterilmiştir.  $Mn(acac)_3/bpy$  sisteminin gerçek alkid sistemlerinde daha az performans göstermesinin sebebi bu sistemin gereğinden fazla aktif olmasından dolayı oluşan alkoksi serbest radikallerinin daha az oligomerizasyon ve daha fazla uçucu ürünleri oluşturmasına bağlanmaktadır. Alkid reçineler için iyi bir oksitlenme hızlı hidroperoksit oluşumuna ve serbest radikallere etkili dönüşümüne ve yüksek oligomer oluşumunun dengesine bağlıdır.

$^{13}C$ -izotopu arttırılmış etil linoleat ın oksitlenmesi çeşitli katalizörlerin etkisi altında araştırılmıştır.  $^{13}C$ -NMR yardımıyla ilk defa hidroperoksitlerin (ROOH) ve peroksi (ROOR) bağlarının oluşumu gözlenmiştir.

Tezin en son kısmında MnMeTACN gerçek alkid boyalarda uygulanabilirliği test edilmiştir. Solvent/su esaslı alkid boyaları için MnMeTACN in endüstride sıklıkla kullanılan Co ve Mn esaslı kurutuculara potansiyel bir alternatif olduğu film özelliklerindeki (kuruma zamanı ve film sertliği) sonuçlarla gösterilmiştir. Alkid reçinelerinin kuruması sırasındaki reaksiyonların filmin derinliğine göre değişimi Confocal Raman Mikroskopi yardımı ile araştırılmıştır. Mn esaslı kurutucunun yavaş yüzey kuruması biraz olsun filmin hızlı dip kurumasıyla telafi edilmiştir.

## **Acknowledgements**

There are lots of things to say after four years of experience in Eindhoven and in The Netherlands. I will never forget my PhD period and most importantly people I met here and people who helped me creating this thesis. First of all, I would like to thank my promoter Prof.dr. Rob van der Linde for his support and professional guidance during my PhD period in his research group. His optimism and encouragement always impress me during our meetings and discussions. I also would like to thank my co-promoter Dr. Marshall Ming for his great efforts and recommendations for the thesis. Within the long working hours, you were the one closest to me. I always feel that Marshall is more a friend than my co-promoter. In my good and bad days in Eindhoven you were there. With all my deep gratitude to Marshall, he is the perfect example how a good guidance and friendship should be performed. I enjoyed the freedom of doing research with you and Rob.

I also would like to thank Prof.dr. Bert de With, Prof.dr.ir. Anton German, and Prof.dr. Rolf van Benthem for the valuable discussions and their support.

I greatly acknowledge Dr. Jos Laven for useful discussions and introducing me with the Raman technique. I would like to thank Wieb Kingma, Rajan and Bas Staal for SEC analysis, Marion van Straten for LC-MS, Marco Hubers from TNO for head-space GC-MS, Dr. Marcel van Genderen for NMR, Otto van Asselen for FTIR.

I would like to thank our collaborators, Remy van Gorkum, Dr. Elisabeth Bouwman and Prof.dr. J. Reedijk from Leiden University and Dr. Jacco van Haveren, Dr. Eef Oostveen and Fabrizio Micciché from ATO-DLO in Wageningen. I acknowledge the financial support for the alkyd project to SENTER-IOP heavy metals and many thanks to the IOP committee members for their interests in our project meetings. Particularly, I would like to thank Dr. Ad Hofland from DSM Coating Resins, Zwolle for fruitful discussions and accepting me for a provisional training about the alkyd synthesis, emulsification and paint preparation. Moreover, I acknowledge, Arno Schut, J. ter Borg, and Dr. J.H. Bieleman from Elementis specialties (formerly known as Sasol Servo B.V.) in Delden for the fruitful discussions and for testing MnMeTACN catalyst in real alkyd coatings. I would like to thank Barbara Breimer from SENTER for organizing the IOP committee meetings.

I greatly acknowledge Dr. Ronald Hage from Unilever R&D Vlaardingen for providing me the MnMeTACN catalyst. Chapter 4 and 7 will never be created without his help. I also would like to thank my former mentor Dr. Wim Muizebelt at Akzo Nobel in Arnhem for introducing me with the chemistry of coatings and alkyds.

I would like to thank the former members of the group Robert, Chouaib, Willem, Viktor (I will never forget the Salsa nights and dinners), Aloke, and Maru for their friendship. I would like to thank the SMG group members Tamara, Daniela, Francesca, Dennis, Dennis2, Olavio, Srdjan, Talal, Vincent, Willem-Jan, Dirk-Jan, Przemyslaw, and Alex for their friendship.

I always remember Sasha when I am listening to him, Niek with a smiling face, Marco with his changing hairstyle. I am very much thankful to Imanda, Huub, and Anneka for their support during my stay. My former office mates Luc, Swapan, Usha, Nathalie (Boris) you are the ones that will always be remembered.

Thank you for the quite and kind atmosphere Di Wu, Zhe Chen, and Amir (special thanks for serving me coffee all the time). I would like to thank Peter Bruin for the nice discussions and “explosive” tests.

Romy; I will never forget Kruisstraat 132. Thank you Jan and Toon for the very kind environment in Tweelingenlaan.

Eindhoven'daki yaşamımı biraz olsun renklendiren Mustafa, Ulaş, Barış, Aslı, Sandra, Tarkan, Müge, Fransız Özgür, Ceren, Şeniz ve Bülent hepiniz benim için çok değerlisiniz burada yaşadıklarımı ve sizi hiç unutmayacağım. Yaşam boyu dostlarım Burak, İrem, Okay ve Ebru'ya bana her zaman destek oldukları için çok çok teşekkürler. Sizin yeriniz benim için hep ayrı olacak bunu hiç unutmayın. Binnur, Hasan, Güliz, Aslıhan, Pınar, Erdem, Serkan, Alper Ünver, Alper İşleyen, Merttaş, Cem İnan, Bora ve ismini burada belirtmediğim bir çok arkadaşım hepinize gösterdiğiniz destekten ötürü sonsuz teşekkürler.

Her zaman yanımda olan aileme, abime, ablama, Mahinur ablaya, Destina Meral'e, Yaşar Omay'a sonsuz teşekkürler. Son olarak nişanlım Özlem'e; Senin desteğin olmasaydı yaptıklarımın hiç bir anlamı olmazdı. Seni çok seviyorum ve seninle varım tatlım.

Emeği geçen herkese teşekkürler. Sevgilerle...

Okan.

## **Curriculum Vitae**

Zahit Okan Oyman was born in Silifke, Turkey, on the 24<sup>th</sup> of January 1976. In 1993, he graduated from Gazi Anatolian high school in Ankara, Turkey. He obtained his B.Sc. degree in Chemistry in June 1998 and M.Sc. degree in Polymer Chemistry in June 2000 at Middle East Technical University (METU-ODTÜ) in Ankara, Turkey. He studied melt blending of recycled poly (ethylene terephthalate)(PET) with polypropylene (PP) in the presence of silane coupling agents to improve the mechanical properties of polymer blends. His supervisor was Prof.Dr. Teoman Tinçer (1998-2000). On the 15<sup>th</sup> of January 2001, he joined the group of Coatings Technology at Eindhoven University of Technology as a PhD student under the supervision of Dr. W. Ming and Prof.Dr. R. van der Linde, which has resulted in this thesis.